Approaching Mosaicism for the Genomic Odyssey of Rare and Undiagnosed Diseases

by

Ece Çepni

A Dissertation Submitted to the

Graduate School of Health Sciences in
Partial Fulfillment of the Requirements
for the Degree of

Doctor of Philosophy

in

Cellular and Molecular Medicine

KOÇ ÜNİVERSİTESİ

August 28, 2025

Approaching Mosaicism for the Genomic Odyssey of Rare and Undiagnosed Diseases

Koc University

Graduate School of Health Sciences

This is to certify that I have examined this copy of a doctoral dissertation by

Ece Çepni

and have found that it is complete and satisfactory in all respects,

and that any and all revisions required by the final

examining committee have been made.

Committee Members:

_____

Prof. Hülya Kayserili Karabey (Advisor)

_____

Prof. Mehmet Kaya

_____

Prof. Yasemin Gürsoy Özdemir

_____

Prof. Zehra Oya Uyguner

_____

Prof. Hans van Bokhoven

Date: August 28, 2025

“Her eğitimli kadının Cumhuriyete borcu var!”

To my beloved family.

For their endless encouragement and support.

ABSTRACT

Approaching Mosaicism for the Genomic Odyssey of Rare and Undiagnosed Diseases

Ece Çepni

Doctor of Philosophy in Cellular and Molecular Medicine

August 2025

Mosaicism is a fundamental biological phenomenon with broad implications for human health and disease. This thesis firmly establishes that postzygotic genetic variation arising at distinct developmental stages can lead to a diverse array of phenotypes, ranging from subtle pigmentary changes to severe multisystem disorders. The difficulties and limitations in detecting somatic mosaicism hinder definitive diagnosis of the affected individuals, yet the knowledge and data regarding its genetic basis remain limited. With a particular focus on selected syndromes/cases that exhibit segmental and/or cutaneous findings, we aimed to address these challenges by confirming clinical diagnoses of individuals in this patient group at the genomic level using advanced molecular and cytogenetic diagnostic techniques.

The study is structured around two key components: a cohort presumptive for *PIK3CA*-related overgrowth spectrum syndromes and a series of single-case studies involving diverse mosaic phenotypes. We evaluated patients with clinical findings suggestive of mosaicism using a multimodal diagnostic approach. By integrating thorough clinical phenotyping with genomic analyses, we identified, characterized, and redefined the molecular basis of various rare mosaic disorders. These findings encompass variants in crucial biological pathways, including the PI3K-AKT-mTOR and RAS-RAF-MAPK pathways, along with the components of cell-cycle regulation, mitochondrial dynamics, and chromosomal architecture.

This study highlights the significant impact of timing and distribution of postzygotic mutations on phenotypic expression, thereby challenging conventional genotype-phenotype paradigms. The findings support the implementation of comprehensive clinical-genomic workflows and suggest that mosaicism can be viewed as a unifying framework for interpreting rare syndromes and complex phenotypes. Ultimately, this work reinforces our understanding of mosaicism as a fundamental, yet poorly understood and poorly explored concept in medical genetics, demonstrating the importance of personalized diagnosis for improved genetic counseling and care for patients and their families. The unsolved cases provide valuable resources for future research and fuel our continued desire to explore the unknown in cell and human biology.

Keywords: somatic mosaicism, postzygotic variants, PI3K-AKT-mTOR pathway

ÖZETÇE

Nadir ve Tanısı Konulamamış Hastalıkların Genomik Yolculuğunda Mozaisizme Yaklaşım

Ece Çepni

Hücresel ve Moleküler Tıp Doktoru

Ağustos 2025

Mozaisizm, insan sağlığı ve hastalıkları üzerinde geniş kapsamlı etkileri olan temel bir biyolojik durumdur. Bu tez, farklı gelişimsel aşamalarda ortaya çıkan postzigotik genetik varyasyonun, hafif pigment değişikliklerinden ağır multisistem bozukluklarına kadar çeşitli fenotiplere yol açabildiğini ortaya koymaktadır. Somatik mozaisizmin tanımlanmasındaki zorluklar ve sınırlamalar, etkilenen bireylerin kesin tanı almasını zorlaştırmaktadır, ayrıca, somatik mozaisizmin genetik temeline ilişkin bilgi ve veriler hala sınırlıdır. Segmental ve/veya kutanöz bulguları olan sendromlara/olgulara odaklanarak, bu hasta grubundaki bireylerin klinik tanılarını gelişmiş moleküler ve sitogenetik tanı teknikleri ile genomik düzeyde doğrulayarak bu zorlukları ele almayı amaçladık.

Çalışma iki ana bileşen olmak üzere, *PIK3CA*-ilişkili aşırı büyüme spektrumu sendromlarını düşündüren bir kohort ve çeşitli mozaik fenotipleri içeren bir dizi tek olgu çalışması etrafında yapılandırılmıştır. Mozaisizmi düşündüren klinik bulgulara sahip hastaları multimodal bir tanı yaklaşımı ile değerlendirdik. Kapsamlı klinik fenotiplemeyi genomik analizler ile entegre ederek, birçok farklı nadir mozaik sendromun moleküler ve sitogenetik etyopatogenezini belirledik, fenotip-genotip ilişkisine katkıda bulunarak, yeni temel tanımlamalar yaptık. Tanımlamalar PI3K-AKT-mTOR ve RAS-RAF-MAPK gibi temel biyolojik yolaklardaki değişimler ile, hücre döngüsü düzenlemesini, mitokondriyal dinamikleri ve kromozom yapı bileşenlerini etkileyen değişimleri içermektedir.

Çalışma, postzigotik değişimlerin zamanlaması ve dağılımının fenotip üzerindeki etkisini vurgulamakta ve geleneksel genotip-fenotip paradigmalarını sorgulamaktadır. Bulgular, kapsamlı klinik-genomik iş akışlarının uygulanmasını desteklemekte ve mozaisizmin, nadir sendromları ve karmaşık fenotipleri yorumlamada birleştirici bir kavram olabileceğini önermektedir. Sonuç olarak, bu tez çalışması mozaisizmin tıbbi genetik alanında temel ama iyi bilinmeyen ve iyi irdelenmeyen bir kavram olduğunu göstermekte ve kişiselleştirilmiş tanının tedavi ve genetik danışmadaki önemini pekiştirmektedir. Tez çalışmasında yer alan ve henüz çözüme ulaşmayan olguların varlığı ise ileri zamanlardaki araştırma çalışmaları için değerli bir kaynak oluştururken, hücre ve insan biyolojisinde bilinmeyeni araştırma isteğimizin sürekliliğini sağlamaktadır.

Anahtar kelimeler: somatik mozaisizm, postzigotik değişimler, PI3K-AKT-mTOR yolağı

ACKNOWLEDGEMENTS

First and foremost, I would like to thank my advisor, *Prof. Hulya Kayserili*, for mentoring and inspiring me not only academically but throughout my life. She was my idol before beginning my doctoral work. After working eight years closely with her, I have changed and grown as a scientist and as a person, but my idol remains the same. Thank you for believing in me and giving me the freedom to pursue my passion in medical genetics.

I cordially thank all patients and their families for their support and collaboration over the years.

I would like to thank all the past and current members of the *Genetic Diseases Evaluation Center* at Koç University Hospital for fostering a supportive work environment. I am grateful to *Serpil Eraslan, PhD* & *Gul Leyla Kılıç, PhD* & *Şahin Avcı, MD* & *Umut Altunoglu, MD* for sharing their years of knowledge and experience with me whenever I needed. Special thanks to *Nergiz Kar, Meltem Batıbay, Merve Çelik, Dicle Ballıkaya, Fatma Aydın,* and *Elanur Yılmaz* for sharing their expertise in wet-lab and for all their help during my thesis. I do thank Didem Özer and Şeymanur Tur for the plenty of laughter we've shared.

I have made great friends along the way… and found sisters. *H. Pırıl Saraçoğlu* has been one of the most significant gains of my life. The bond we share is special, and it's just the beginning… *Manar Kaptan*, thank you for your soul-healing friendship. I know that we will continue to cherish life together…

I would like to express my deepest appreciation to my committee members. I would like to thank *Prof. Mehmet Kaya* and *Prof. Yasemin Gürsoy Özdemir* for their support and motivation throughout my study at Koç University. I do thank Prof. Zehra Oya Uyguner for her support and for valuable feedback. I would also like to say "dank je wel" to my former mentor, *Prof. Hans van Bokhoven*, whose guidance and support will have a lasting impact on my career.

I want to express my deepest gratitude to my family, which I consider myself lucky to be born into.

My parents, *Berrin & Özcan Çepni*, always supported my dreams and goals. Thank you for your endless love and patience.

My brother, *Alp Çepni,* is my great source of joy. I know that he will achieve all the great things he deserves in life. Thank you for being my rock.

My grandmother, Nüket Leyla Çekirge, has believed in me from day one. Thank you for raising me to be a strong, independent woman.

My aunt, *Şermin Bulut*, I am proud to be your emergency contact. Thank you for always having my back, even when I don't ask you to.

I would have ended this section with the lyric "*Nobody said it was easy, no one ever said it would be so hard*"; if my uncle *Bulent Bulut* had not warned and encouraged me about all aspects of the grad life. Thank you for being an example of hard work to me, my brother, and my cousins.

Last but not least, I want to thank *myself*…

TABLE OF CONTENTS

LIST OF TABLES

LIST OF FIGURES

ABBREVIATIONS

BUB1B	BUBR1 Mitotic Checkpoint Serine/Threonine Kinase B
DNA	Deoxyribonucleic acid
FFPE	Formalin-Fixed Paraffin-Embedded
FGFR2	Fibroblast growth factor receptor 2
GoF	Gain-of-function
IUGR	Intrauterine growth restriction
LoF	Loss-of-function
MFN2	Mitofusin-2
MSL	Multiple Symmetric Lipomatosis
MTOR	Mammalian target of rapamycin
NF	Neurofibromatosis
NGS	Next-generation sequencing
OFC	Occipital Frontal Circumference
PIK3CA	Phosphatidylinositol-4,5-bisphosphate 3-kinase catalytic subunit alpha
PROS	*PIK3CA*-related overgrowth spectrum
RASA1	RAS p21 protein activator
SNP	Single-nucleotide polymorphism
TSC	Tuberous sclerosis complex
VAF	Variant allele frequency

Chapter 1

INTRODUCTION

1.1. MOSAICISM

Mosaicism is a recognized mechanism underlying many partial and generalized overgrowth disorders, skin disorders, cancer, and neurodevelopmental disorders with or without central nervous system malformations.

The *Oxford English Dictionary* defines the word "mosaic" as "a picture or pattern made by placing together small pieces of glass, stone, and other materials of different colors" (Oxford University Press, n.d.). In biology, the term "mosaicism" denotes the presence of at least two populations of cells with distinct genotypes in an individual, that are derived from a single fertilized egg. Generation of genetically distinct cells from a single zygote underlies *de novo* mutational events, which usually arise postzygotically in subsequent mitotic cell divisions after fertilization and zygote formation (Figure 1.1).

Throughout a human's lifespan, from fertilization and zygote formation to death, approximately 10^{16} mitotic divisions occur. With each cell division, the risk of genetic change increases. These spontaneous postzygotic mutations can lead to multiple cell lineages with different genomes, all originating from a single progenitor cell. The presence of mutation-positive cells alongside non-mutated cells results in a mosaic individual, with different DNA sequences in various cells throughout the body. Therefore, benign mosaic variation is universal, and genetic/genomic/epigenetic variants are no exception in any multicellular organism.

Mosaicism becomes a concern when it is associated with phenotypic consequences. Signs of genetic mosaicism are streaky or patchy pigmentary skin findings and disproportionate body growth (either overgrowth or undergrowth) resulting

in asymmetry with unilateral hypoplasia and/or hemihypertrophy (Hall, 1988). However, as will be discussed later, predicting the clinical effects of mosaicism is challenging because the patterns and distribution of abnormal cells depend on the type of mutation, the percentage of cells with the mutation, and how the genetic change is spread across tissues. In some cases, mosaicism may not be visible as a distinct phenotype but instead acts as a modifier to an existing phenotype. Yet, in some mosaic individuals, the phenotype may appear normal, similar to wildtype, and only through molecular genetic or cytogenetic testing mosaicism is detected.

Identifying the causative postzygotic variant in those disorders is another challenge, as the variant may not be detectable in the DNA sample obtained from routine peripheral blood samples, but only in affected tissue. Moreover, in most cases, mosaicism is identified in one tissue, and much remains unknown about the distribution of normal and abnormal cells in other tissues throughout the body.

This thesis provides a comprehensive overview of the current understanding of somatic mosaicism, with a particular focus on selected syndromes/cases that exhibit segmental and/or cutaneous findings suggesting mosaicism. By presenting a cohort of clinically well-defined mosaic syndromes and unique examples of mosaicism, the overall aim is to enhance the understanding of mosaicism as an underlying genetic mechanism in rare genetic disorders and to improve genetic counseling and patient care.

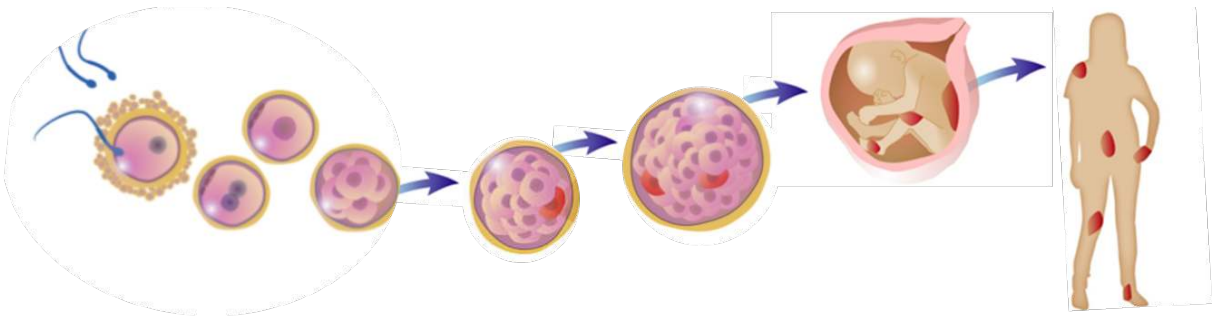

Figure 1-1. **Schematic representation of somatic mosaicism**. A spontaneous mutation occurs during early embryonic development in one cell. As the zygote undergoes further mitotic division, the mutation-positive cells (in red) continue to proliferate alongside wild-type cells (in purple), leading to the coexistence of genetically distinct cell populations within the individual.

1.2. MOSAICISM IN HUMAN HEALTH AND DISEASE: HISTORICAL CONTEXT

Mosaicism also finds rich metaphorical resonance in myths, art, and literature. Across cultures, numerous mythological figures such as *chimeras*, *centaurs*, or *hybrid deities*, embody the concept of an organism composed of genetically distinct cell populations. It is important to note, however, that while the terms *chimera* and *mosaic* are sometimes used interchangeably in metaphorical contexts, they refer to distinct biological phenomena: chimeras arise from the fusion of genetically different cell populations originating from separate zygotes, whereas mosaics result from genetic variation occurring within the cells of a single zygote.

Overgrowth is a relatively easily recognizable mosaic phenotype, which has been historically portrayed in myths and artistic works across diverse cultures, frequently referred to as divine or semi-divine creatures, such as *titans* or *giants*. Notable examples include Prometheus and Atlas in Greek and Latin mythology, the Daityas in Hindu tradition, Ymir in Norse mythology, Gilgamesh in Mesopotamian epics, and the Nephilim, Og, and Goliath in biblical narratives (Figure 1.2 A). Over time, the connotations of the terms "giant" and "gigantism", which originated from Greek mythology, have evolved from signifying superhuman attributes linked to divine or semi-divine lineage to referring to individuals characterized by easily distinguishable physical features (Boccuto & Neri, 2021).

Overgrowth has historically been regarded as an indicator of good health, likely due to prevailing social and cultural beliefs. A famous example depicting overgrowth as a positive attribute is Michelangelo's sculpture of *David*, in which the head and hands were deliberately rendered disproportionately large relative to the rest of the body, symbolizing his intellect and actions (Figure 1.2 B). In the 19th century, however, individuals with overgrowth and/or other striking physical differences were described as "*freaks of nature*" and presented as objects of public fascination and disdain. One of the earliest and most tragic examples was Saartjie Baartman (1789-1815), known as the "*Hottentot Venus*[1]" who was exhibited across Europe for her pronounced steatopygia, a common and culturally valued trait among Khoisan women characterized by an excessive accumulation of adipose tissue in the buttocks (Figure 1.2 C). Today,

[1] "*Hottentot'* is a colonial-era term historically used by European settlers to refer to the Khoisan people of Southern Africa. It is now recognized as a derogatory and offensive term.

Baartman's is often cited as a striking example of how race, gender, and colonial science intersected in the objectification and exploitation of the human body.

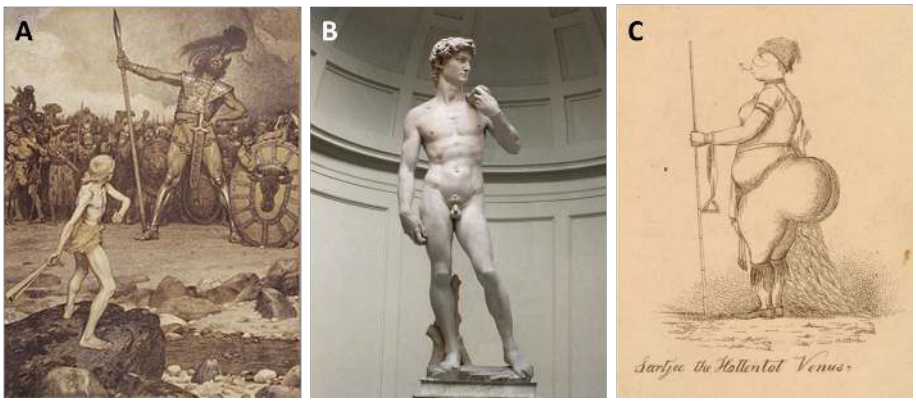

Figure 1-2. **Historical Examples of Mosaicism. (A)** *David und Goliath* (1888) by Osmar Schindler. (A) Goliath's Giant size can be easily noticed. Adapted from Wikimedia Commons. **(B)** *David* by Michelangelo (1501-1504), with head and hands sculpted slightly out of proportion compared to the rest of the body. Image Source: Galleria Dell'accademia, Florence, via Museums in Florence Website. **(C)** Historical Etching of Saartjie Baartman with the exaggerated focus on steatopygia. Adapted from *The Hottentot Venus* (1811), British Museum, Museum Number: 1851,0308.638. Image Courtesy of The Trustees of The British Museum.

The interest in physical abnormalities and deformities reached its peak and became an 'industry' in Victorian Britain from the 1840s until around 1914. Exploitative sideshows, or so-called "*freak shows*," were organized to exhibit individuals with excessive height, skeletal dysplasia, or other unusual features as spectacles of monstrosity, and were one of the few sources of employment available to such individuals. One of the best-known figures of that era was Joseph Carey Merrick (1862–1890), remembered as "The Elephant Man" (Figure 1.3).

Merrick's clinical features were first recognized and documented by Dr. Frederick Treves, whose care and advocacy helped Merrick to spend his final years in relative comfort and dignity (Treves, 1923; The "Elephant-Man," 1886; Death Of The "Elephant Man," 1890). At 21 years of age, he had a relatively short stature (height: 157 cm). His skull was markedly enlarged (OFC: 91 cm) and asymmetrical due to extensive osteochondromas involving the frontal bone, the posterior parietal regions, and the occipital bone. Facial bone malformations on the right maxillary bone and palate were lowering the right upper teeth compared to the left. The nose was deviated to the left, the lips were prominent, and a soft-tissue mass beneath the upper lip further contributed

to the resemblance to an elephant's trunk, which inspired his stage name (Figure 1.3 A-B). Papillomas and pendulous folds predominantly involved the right side of his body, extending from the neck and chest to the abdomen and gluteal area (Figure 1.3 C-D). Notably, the eyelids, ears, entire left arm, most of the anterior abdomen, both thighs, the left leg, the posterior right leg, and the penis and scrotum were not affected (The "Elephant-Man," 1886; Boccuto & Neri, 2021).

His condition presented a diagnostic challenge lasting for years. Initially, von Recklinghausen's disease (Neurofibromatosis type 1) was proposed due to the bone lesions and subcutaneous masses, although key diagnostic features of NF1 [will be discussed in detail in Study 6] were absent. In 1986, the diagnosis was reestablished as Proteus syndrome, based on the presence and mosaic distribution of the papillomatous lesions, asymmetric overgrowth, sporadic occurrence, and progressive course with symptoms initiating after five years of age (Tibbles & Cohen, 1986; Howell & Ford, 1980; Huntley et al., 2015). As such, Merrick's case remains one of the most well-known historical examples of somatic mosaicism manifesting as striking segmental overgrowth.

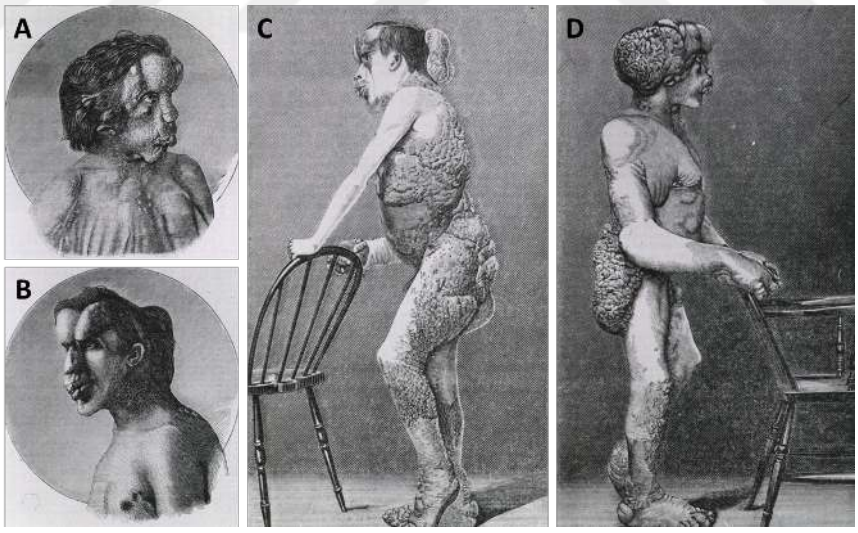

Figure 1-3. **Historical engravings of Joseph Carey Merrick**, illustrating the extent and asymmetry of his overgrowth and cutaneous lesions. Portraits from the **(A)** right and **(B)** left profiles highlight facial deformities and soft-tissue masses. **(C)** Left and **(D)** right full-body profiles show the mosaic distribution of skin papillomas, pendulous folds, and skeletal malformations predominantly affecting the right side of the body. Adapted from *The "Elephant-Man."* (1886). *The British Medical Journal*, 2(1354), 1188–1189. http://www.jstor.org/stable/25270008. Image courtesy of the U.S. National Library of Medicine: Images from the History of Medicine (Local Identifiers: 101434390, 101434391, 101434392, 101434393).

1.2.1. Mosaicism as a Biological Concept: Early Biological Observations

The concept of mosaicism was first appreciated by zoologists and plant biologists in the early 20th century. Häcker introduced the term "mosaic bastards [*Mosaikbastarde*]" to describe animals showing patchy distributions of traits across their bodies (Häcker, 1904). In the years that followed, the terms "mosaic" (Collins, 1913; Wright & Eaton, 1926) and "somatic segregation" (Kraus, 1916; Serebrovsky, 1925) were used interchangeably to describe this phenomenon (Happle, 2017).

Experimental studies in model organisms further advanced the biological understanding of mosaicism. In 1914, Morgan reported rare cases of gynandromorphism[2] in *Drosophila melanogaster* (Morgan, 1914). Building on this, Sturtevant generated mosaic flies having both XX (female) and XO (male) cells (Sturtevant, 1929). Later, in 1936, Stern demonstrated that genetic recombination in meiosis, crossover, can also occur in mitosis and lead to mosaicism in *Drosophila melanogaster* (Stern, 1936). 15 years later, McClintock demonstrated the phenotypic importance of somatic transposition in maize (McClintock, 1951). Despite these early and foundational biological observations in animals and plants, the concept of mosaicism in humans however remained largely overlooked and was not initially connected to the genetic mechanisms described in experimental models.

1.2.2. Patterns of Mosaicism: Blaschko's Lines and Other Cutaneous Phenomena

[Here, special credit must be given to Prof. Rudolf Happle, who systematically categorized the cutaneous patterns of mosaicism through extensive research and insightful analyses over many years.]

The recognition of visible patterns in the human body, especially in the skin, has played a crucial role in uncovering the biological phenomenon of mosaicism. Among them, the most notable observation is the lines of Blaschko, first described by the German dermatologist Alfred Blaschko in 1895. *"...If we assume that, during the months when differentiation takes place, a disturbing factor would interfere, then it would easily be possible that only particular territories are involved, whereas*

[2] Gynandromorphism refers to an organism that contains both male and female tissues, often with a distinct bilateral or mosaic distribution of sex-specific characteristics.

intervening regions are healthy" (Alexander & Blaschko, 1895). At that time, the concepts of genes and mutations were not yet established. Blaschko proposed that a "disturbing factor" might arise during embryonic development, thus only some parts of the body are affected. He postulated that linear nevoid skin lesions resulted from developmental "disturbances" occurring at the boundaries of metameres. With this statement, he not only reflected an early intuition of mosaicism but also revealed the underlying metameric (segmental) organization of the human body.

In the following years, Blaschko examined over 140 patients with linear skin lesions and meticulously documented the intricate and often asymmetric patterns of linear skin markings that he observed across a diverse range of dermatological conditions, including genetic skin disorders, such as incontinentia pigmenti and focal dermal hypoplasia, inflammatory skin diseases like lichen planus and psoriasis, and even in healthy individuals, where the lines may be present without any associated pathology. In 1901, he presented a composite diagram of the distribution patterns of these lines, typically exhibiting inverted U-shaped arcs from the chest to the upper arms, V-shaped configuration on the trunk and S-shaped arrangement on the abdomen, and vertically down the front and back of the lower limbs (Blaschko, 1901). In his schematic drawing, he left the scalp blank due to a lack of informative cases, and the lines were drawn in a cursory manner on the face and the anterior of the neck (Figure 1.4).

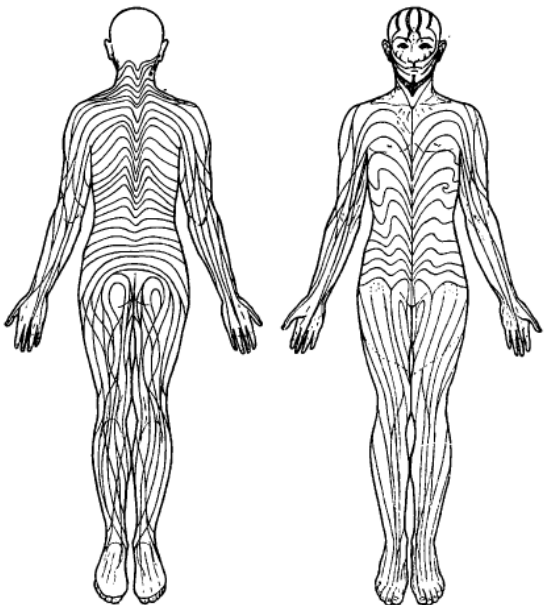

Figure 1-4. **Blaschko's original depiction of "nevus lines"**, now known as Blaschko's lines, follow a characteristic pattern: inverted U-shaped from the chest to the upper arms, V-shaped over the trunk (which do not cross the anterior midline but instead run parallel to it), S-shaped on the abdomen, and vertically down the front and back of the lower limbs. The head was mapped only superficially and left partially blank due to limited data at the time.

A century later, the blank areas were filled in by Happle and Assim by reviewing 187 figures showing skin lesions following Blaschko's lines on the head and neck from dermatologic journals, monographs, and patient files (Happle & Assim, 2001). On the forehead, the lines run in a sandglass-like arrangement from the scalp to the eyebrows and converge on the nasal root; with a definite crossing of lines, sometimes even at an angle of 90°, in the temporal area, on the cheek, and in the retroauricular region. From the nasal root the lines run in (1) a perpendicular direction to the tip of the nose and the philtrum; (2) along the lateral aspects of the nose in the direction of the nasolabial folds, surround the mouth, and run to the point of the chin; (3) following the margin of the lower lid to the earlobe; (4) parallel to the margin of the lower lid and subsequently form a large bend on the cheek to converge at the labial commissure. On the ventral aspect of the neck the lines run from the craniolateral areas to the midline, forming a V from the chin they likewise run to the anterior midline of the neck (Figure 1.5 A). In the lateral view, starting from the upper margin of the ear, lines run horizontally to the external canthus of the eye. In the preauricular area, they are crossed by lines that run downwards almost straight and then form large bends curving towards the back and converging at the mouth. Close to the preauricular area, some of the perpendicular lines curve towards the lateral aspect of the neck while others run horizontally from the bottom of the earlobe to the nape. In the retroauricular region, these lines are crossed by lines that show an almost vertical arrangement and subsequently follow the mandibula to reach the lower lip, whereas another part curves towards the back to form a V shape in the anterior midline of the neck, as described above (Figure 1.5 B). In the dorsal view, lines run vertically down the middle of the nape and then bend towards the ears. On the scalp, the lines form a spiral pattern that culminates on the vertex. The direction of the spiral usually does not match the direction of the hair whorl (Figure 1.5 C) (Happle & Assim, 2001).

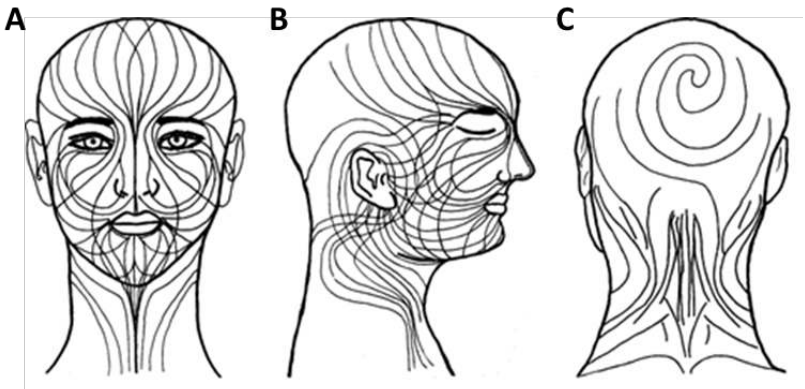

Figure 1-5. **Happle's illustration of Blaschko's lines on the head and neck**. Definitive patterns of Blaschko's lines as shown from three perspectives: **(A)** frontal, **(B)** lateral, and **(C)** dorsal view.

Today, the diagram of the distribution pattern of the nevus lines is widely accepted and referred to as the "**lines of Blaschko**". Although normally invisible, many inherited and acquired skin disorders manifest along these lines, making them visible through the distribution of lesions. Moreover, the intriguing nature of the Blaschko lines has led to their investigation into other mammalian species, with studies indicating that similar patterns can be observed in the brindle[3] coat color in dogs (Lewis et al.,1998) and mares[4] (Towers et al., 2013; Murgiano et al., 2016) (Figure 1.6). However, except for being mentioned in a handful of textbooks (Carol, 1944; Siemens, 1948; Siemens, 1952), Blashko's foundational work was neglected for nearly half a decade. Probably since the title of his presentation "*The distribution of nerves in the skin and its relationship to skin diseases* [*Die Nervenverteilung in der Haut in ihrer Beziehung zu den Erkrankungen der Haut*]" was misleading, even though he concluded that there is no relationship between the "nevus lines" and the nervous system (Blaschko, 1901).

Figure 1-6. **Examples of Blaschko's lines in other species**. **(A)** *Köpke*, a stray dog with a brindle coat pattern, showing irregular stripes of lighter and darker hair. Photograph by the author (KUH Open Parking Lot, 5 May 2025). **(B)** *DA Remote Control*, a mare with segmental hypopigmentation along Blaschko's lines, appearing as broad bands. Adapted from a non-peer-reviewed hobbyist website for illustrative purposes only (White Horse Productions, n.d.). **(C)** Mare with Incontinentia Pigmenti due to a nonsense mutation in the *IKBKG* gene. Brindled pigmentation and patches of alopecia pattern follow the lines of Blaschko. Adapted from Towers et al., 2013.

In 1901, American dermatologist Montgomery also supported Blaschko's ideas on the "disturbing factor" and hypothesized that linear streaks reflect "streams" of tissue growth and adaptation of the embryonic sutures. He further argued that linear nevi do not follow the lines of nerves or blood vessels, Voigt's lines, the lines of skin cleavage,

[3] In brindle coats, stripes of red-yellow hair alternate with black-brown hair, typically forming a "V" shape over the back and an "S" shape along the sides and belly.
[4] Mare is an adult female horse or other equine.

or the metameres of the body; instead, *"... a nevus linearis originates at an early stage in the development of the fetus, when the embryonic layers are still a plastic mass.... Imagining the affected cells or groups of cells to lie in the plastic mass like currants in dough, one can see that such a group lying in the region which will afterwards become the back of the neck might be pulled toward the median line when the skin closes over the neural canal, and its individual constituents become scattered along this line as the fetus elongates..."* (Montgomery, 1901).

In 1962, Mary Lyon discovered that one of the two X chromosomes in female embryos is randomly and irreversibly inactivated between 12 and to 16 days of development, resulting in females exhibiting varying X-inactivation ratios, ranging from balanced (50:50) to highly skewed (e.g., 0:100) patterns in which one X chromosome is preferentially active in most cells. The clinical significance of this process, now known as X-inactivation or lyonization, is dosage compensation, variable gene expression, and mosaicism in heterozygous females (Lyon, 1962; Happle, 2006).

German dermatologist Haensch documented a case of eczema [now recognized as blaschkitis[5]] that followed a strictly segmental distribution and concluded that a disturbance in the spinal roots, likely due to polyneuroradiculitis, was the determining factor (Haensch, 1961). Similarly, in 1964, Swiss anatomist Töndury claimed that, except for a brief segmentation in the corium of the embryonic back, the skin does not exhibit segmentation during development; however, its vascularization and innervation reflect the original segmental organization of the vascular and nervous systems (Töndury, 1964). While both authors attributed these unique skin patterns to nerve-related segmentations, if such claims were accurate, the existence and consistent patterning of Blaschko's lines would remain unexplained. Nevertheless, even today, linear skin lesions and nevi that follow Blaschko's lines are often mistakenly described as exhibiting 'dermatomal' or 'zosteriform' patterns.

In 1965, unaware of Blaschko's work, Curth and Warburton argued that the mechanism of X-inactivation does not adequately explain incontinentia pigmenti, as the pigmentation is consistently confined to specific regions, follows a distinct pattern rather than a random patchy distribution, and the same pattern is observed in a few

[5] Blaschkitis is an acquired dermatosis that presents as grouped or lined pruritic papules following Blaschko's lines.

affected males (Curth & Warburton, 1965). In 1969, again unaware of Blaschko's work, Macdonald and Sims comprehensively reviewed the literature. Based on the observations on a total of 101 cases with linear lesions, they concluded that the epidermis does not exhibit inherent segmentation, suggesting that linear lesions arise from factors other than the skin's anatomical segmentation (Macdonald & Sims, 1969).

Blaschko's lines were later independently redefined in the late-70s by Happle and Jackson (Happle, 1976; Jackson, 1976). In 1976, Canadian dermatologist Jackson pointed out the uncertainty of the embryological explanation of Blaschko's lines. Further, he discussed the need for additional extracutaneous findings to determine the underlying change's time and nature. In his words, he has been *"…unable even to make a guess at what stage of development the changes occur which could provide a mechanism by which the localization of Blaschko's lines is determined. It would be helpful to tie in Blaschko's lines with some other dateable embryological event…*." (Jackson, 1976).

Happle then proposed lyonization as such a "dateable embryologic event" to explain the nature and origin of Blaschko lines, knowing other mechanisms such as somatic mutations, gametic half chromatid mutations, or chimerism can give rise to the same cutaneous patterns. By reviewing the pattern of the Blaschko lines observed in X-linked disorders at the heterozygous state, such as incontinentia pigmenti, focal dermal hypoplasia, X-linked dominant chondrodysplasia punctata, X-linked hypohidrotic ectodermal dysplasia, and Menkes syndrome; he stated that these lines are independent from the metameric structure of the human body and represent a marker of the normal embryogenesis of the skin, contrary to Blaschko's early assumptions (Happle, 1985).

It was just in 2020 that Happle brought an utmost important article published in the *Journal of Heredity* in 1945, entitled "*A human mosaic: bilaterally asymmetrical noevus pigmentosus pilosus et mollusciformis unilateralis*" to light (Happle, 2020). The author, Russian physician Zlotnikoff, was from the former Soviet Union and unaware of Blaschko's work. Zlotnikoff reported on a 24-year-old woman with a congenital linear epidermal nevus on the left side of her body in a systematized and strictly unilateral arrangement. He proposed that the disorder occurred due to a mutation that occurred "at the stage of the blastomere", and explained the condition as "*If we assume that at the stage of two blastomeres a somatic mutation had taken place, i.e., one of these blastomeres underwent some mutation, then the development of these blastomeres*

would proceed in accordance with this mutation, i.e., the difference between the 'normal' and the mutated blastomere would exist in all stages of development of the organism. If we assume that in our case one of the blastomeres (at the two-blastomere stage) namely, the left underwent a mutation then we can easily understand from what has already been said that the left side of the organism would reflect all the features resulting from the mutation, that took place at the stage of the blastomeres, and the pathology of the organism would be strictly symmetrical…. Assuming that this explanation is the most probable one, we are inclined to apply it in the present case, as it is impossible to give any other explanation to this one-sided asymmetry of mosaic mutation in our patient ..." (Zlotnikoff, 1945). To the best of our knowledge, M. Zlotnikoff was the first to describe linear epidermal nevus as "a human mosaic" and explain it by the concept of mosaicism, reflecting the effect of a postzygotic mutation occurred at an early developmental stage (Happle, 2020).

1.2.3. The Recognition of Mosaicism in Human Genetics

The concept of mosaicism gained biological significance in the early 20th century. In 1914, Theodor Boveri proposed that a mutation within the nuclear chromatin of a single cell could initiate tumor development, establishing an early conceptual link between somatic mosaicism and cancer (Boveri, 1914).

By the mid-20th century, mosaicism was formally recognized in immunology and genetics. The term "somatic mosaicism" was introduced by Cotterman in 1956 in the context of antigenic variation (Cotterman, 1956). Soon later, Burnet proposed the clonal selection theory of acquired immunity, suggesting that somatic mutations in early lymphoid differentiation might underlie autoimmune responses (Burnet, 1959).

From the perspective of human genetics, the concept of mosaicism took on a new significance with the beginning of the human cytogenetics era. In 1956, the correct number of human chromosomes was established as 46 (Tjio & Levan, 1956). Shortly thereafter, the first descriptions of human mosaics were published in patients with sex chromosome aneuploidies (Danon & Sachs, 1957), including Klinefelter's syndrome (Ford et al., 1959) and Turner syndrome (Fraccaro et al., 1960; Hirschhorn et al., 1960; Jacobs et al., 1961), followed by mosaicism in autosome chromosome aneuploidies including trisomy 21 (Clarke et al., 1961), 18 (Koulischer et al., 1963), 13 (Forteza et

al., 1964) and double trisomy of chromosome pairs 13-15 and 17-18 (Bain et al., 1965; Baikie et al., 1965; Garson et al., 1969).

In the late 1970s, Pagon et al. (1979) documented the first report of tissue-specific mosaicism in four patients who had normal lymphocyte karyotypes but chromosomal mosaicism confined to fibroblasts. Chemke et al. (1983) provided one of the earliest cytogenetic demonstrations of cutaneous mosaicism by identifying trisomy 18 mosaicism in cells derived from a lesion of linear hypermelanosis in a patient with intellectual disability. This case marked a pivotal example of somatic chromosomal mosaicism with visible cutaneous manifestations, highlighting the important intersection of dermatologists' observations with genetic insights. In the years that followed, molecular analyses provided further evidence of mosaicism underlying a variety of skin disorders exhibiting segmental distribution patterns (Hall, 1988; Moss & Savin, 1995; Paller et al., 1994). Since then, the understanding of mosaic skin disorders has expanded, and it is broadly accepted that many, if not all, nevi are the result of somatic mosaic events (Happle, 2017).

The relationship between somatic mutations and monogenic diseases was further clarified with the demonstration of mosaicism in single-gene diseases showing Mendelian inheritance. The first molecular evidence was the detection of postzygotic activating *GNAS1* mutations in patients with McCune-Albright syndrome (Weinstein et al., 1991), which was originally described in 1936 as a triad of fibrous dysplasia of bone (FD), café-au-lait skin macules, and precocious puberty (McCune, 1936). Followed by identification of postzygotic *FGFR3* mutations in García-Hafner-Happle syndrome (García-Vargas et al., 2008), *IDH1* and *IDH2* in Ollier disease/Maffucci syndrome (Pansuriya et al., 2011), *HRAS* and *KRAS* in nevus sebaceus/Schimmelpenning syndrome (Groesser et al., 2012) and phacomatosis pigmentokeratotica (Groesser et al., 2013), and *NRAS* in large congenital melanocytic nevi (Kinsler et al., 2013).

The recognition of mosaicism in overgrowth syndromes during the 2010s was another breakthrough, as it not only redefined the clinical significance of somatic mutations but also drove significant advances in molecular diagnostics. A key milestone was the identification of a postzygotic gain-of-function (GoF) mutation [c.49G>A, p.Glu17Lys] in the *AKT1* gene, which is involved in the etiopathogenesis of Proteus syndrome, over three decades after its first clinical description (Cohen & Hayden, 1979; Lindhurst et al., 2011). Following the identification of *AKT1* as the cause of Proteus

syndrome, with the introduction of NGS technologies, many mosaic overgrowth syndromes and neurocutaneous disorders have been associated with postzygotic mutations in other members of the PI3K-AKT-mTOR and RAS/RAF/MAPK pathways, which will be further pointed out throughout this thesis (Happle, 2017; Moog et al., 2020).

Today, somatic mutations are recognized as a widespread phenomenon encompassing a broad range of syndromic and non-syndromic conditions, ranging from rare developmental and neurocutaneous disorders to cancer, aging, and an increasing number of Mendelian conditions.

1.3 CLASSIFICATION OF MOSAICISM

Mosaicism can be classified in multiple aspects, such as the distribution of affected body parts and the kind of underlying mechanism. Additionally, there have been numerous attempts to categorize skin genetic mosaicism. Recently, a new classification of mosaicism was proposed, considering the affected tissue, the pattern and distribution of the mosaicism, the pathogenicity of the variant, the direction of the change (benign to pathogenic vs. pathogenic to benign), and the postzygotic mutational mechanism (Martínez-Glez et al., 2020). Accordingly,

A. Depending on the distribution of affected cell populations within the body, mosaicism may be divided into four classes: somatic, germinal (gonadal), gonadosomatic, and confined placental mosaicism (Figure 1.7).

A1. Somatic mosaicism refers to mosaicism caused by postzygotic mutations that occur in the soma, affecting any tissue/cell type in the body except the germinal cells. Somatic mosaicism is more abundant and pervasive in human disease and is the emphasis of this thesis.

A2. Germline mosaicism, also termed **gonadal mosaicism,** refers to mosaicism caused by postzygotic mutations that occur in germinal cells of the gonads. Germline mosaicism can be identified by pedigree analysis, a phenotypically normal parent with gonadal mosaicism may transmit the very same variant of the gene to offspring and may have more than one affected child.

A3. Gonadosomatic mosaicism, also termed **somatogonadal mosaicism,** is used to describe mosaicism present in both the germinal cells within the gonads and other extragerminal tissues.

A4. Confined placental mosaicism implies mosaicism limited to the placental tissues, and does not affect the fetus. CPM is often detected incidentally during prenatal testing, in approximately 2-3% of all chorionic villus sampling analyses. Based on the placental membrane localization of the genetic or chromosomal abnormality/variant, CPM can be further classified into three subtypes: type 1, 2 and 3 (Figure 1.8) (Reilly et al., 2023; Raymond et al., 2024).

- Type 1 CPM: This variation is exclusively present in the cytotrophoblast and is detectable following cytogenetic or genetic/genomic testing of short-term cultured villi derived from the cytotrophoblast.
- Type 2 CPM: The variation is restricted to the mesenchymal core of the chorionic villi and is identifiable only after cytogenetic or genetic/genomic testing of long-term cultured villi.
- Type 3 CPM: This type denotes the presence of a variation in both the cytotrophoblast and the mesenchymal core of the chorionic villi, detectable after analyzing both short- and long-term cultured villi.

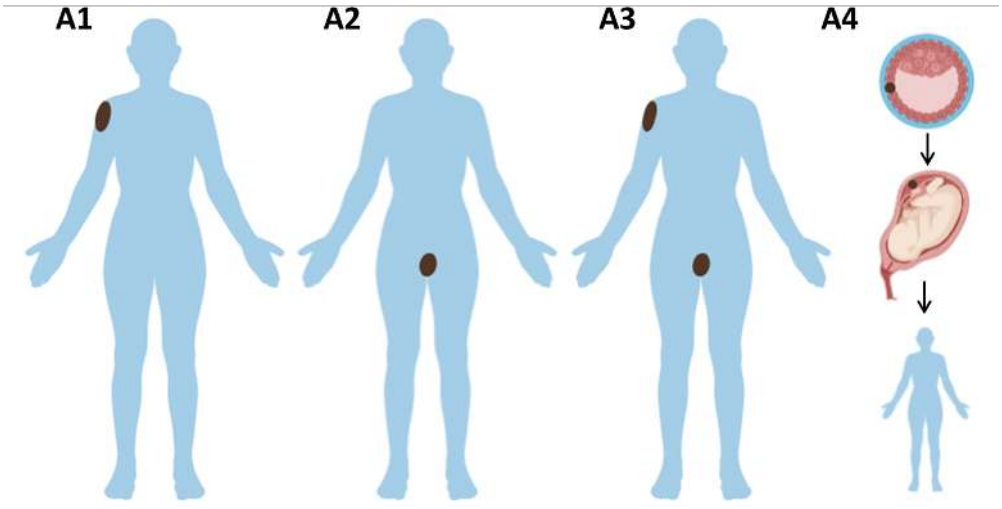

Figure 1-7. **Types of affected tissues in mosaicism**. **(A1)** Somatic mosaicism, mutation present in somatic cells only. **(A2)** Germinal (gonadal) mosaicism, a mutation confined to germ cells that can be passed to offspring. **(A3)** Gonadosomatic mosaicism, mutation present in both germ cells and some somatic cells. **(A4)** Confined placental mosaicism, mutation restricted to placental tissue. The mutant cell is indicated as a brown spot, blue color indicates wild-type cell(s).

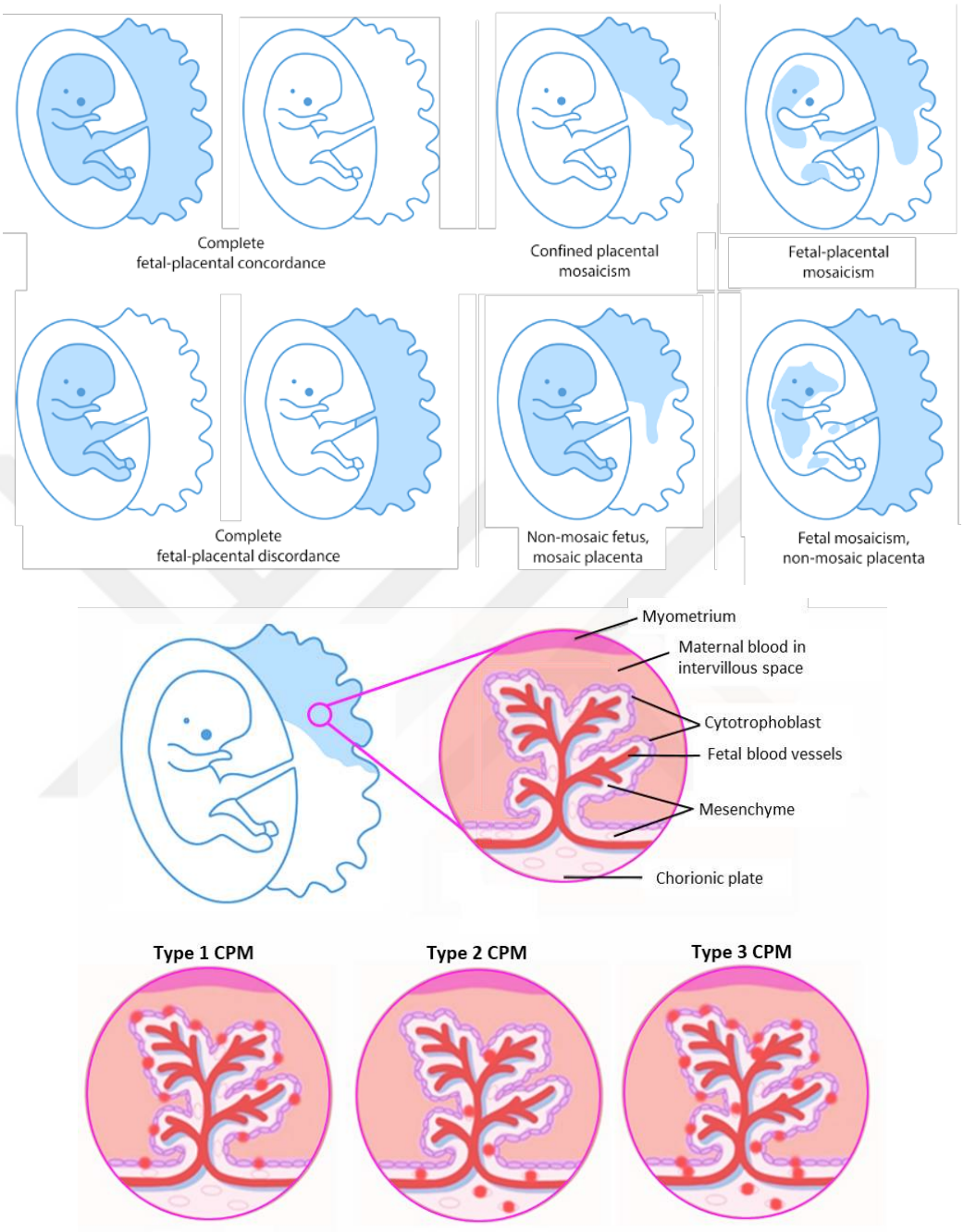

Figure 1-8. **Illustration of placental and fetal mosaicism patterns**. The top panel shows possible configurations of placental mosaicism and fetal–placental concordance or discordance. The placental cross-section on the bottom panel shows the three subtypes of CPM: Type 1 (mutation confined to the cytotrophoblast), Type 2 (confined to the mesenchyme), and Type 3 (involving both cytotrophoblast and mesenchyme). Mutated cells within chorionic villi are indicated by red dots. Adapted from Reilly et al., 2023 and Raymond et al., 2024.

B. Depending on the extent and distribution pattern(s) of the mosaic clinical manifestations through the body, mosaicism can be classified under two major classes: nonsegmental and segmental mosaicism. This is an anatomic classification to define cutaneous mosaicism, and only possible to define when the skin is affected.

The **nonsegmental patterns** include mosaicism confined to only one location in the body (single point), disseminated mosaicism, and patchy mosaicism without midline separation or no pattern (Figure 1.9).

B1. Single point mosaicism is recognized in the presence of lesions or abnormalities in one location.

B2. Disseminated mosaicism is used to explain the presence of two or more lesions in the body. This is seen mostly in genodermatoses with skin manifestations and all autosomal dominant disorders with multiple tumors may be classified under this category.

B3. Patchy without midline separation is observed when the distribution of lesions is due to large plaques that do not respect the dorsal or ventral midline pattern.

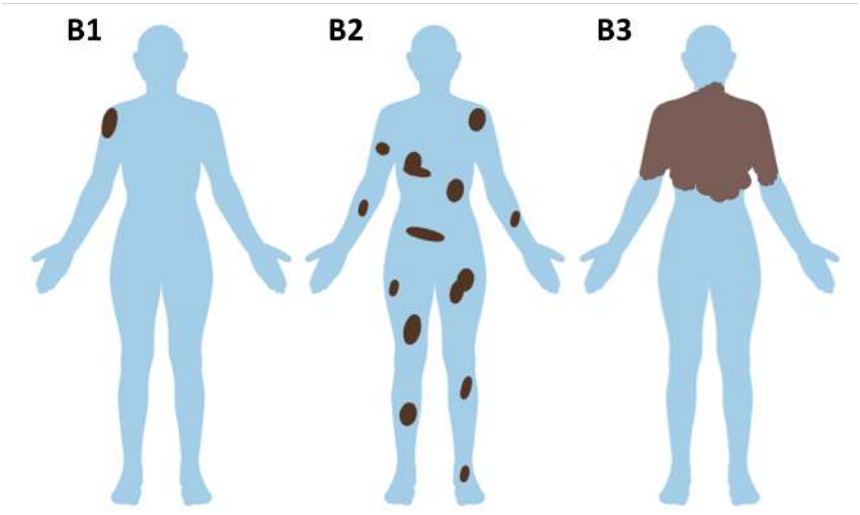

Figure 1-9. **Body patterns of nonsegmental mosaicism**. **(B1)** Single-point mosaicism, a localized, well-defined area of affected cells. **(B2)** Disseminated mosaicism, multiple affected spots scattered across the body. **(B3)** Patchy mosaicism without midline separation, irregular patches of affected cells crossing the midline. Brown color indicates the mutant cell(s), blue color indicates wild-type cell(s).

The **segmental patterns** denote that a skin lesion involves one or more separate body areas, usually in an asymmetric configuration and respecting the midline. This category includes Blaschko lines in narrow or broad bands, Checkerboard, Phylloid, and Lateralization/half-body distribution (Figure 1.10).

B4. Blaschko lines in narrow bands: lesions in this pattern follow the Blaschko lines and are distributed in narrow bands. X-linked incontinentia pigmenti and pigmentary disorders such as hypomelanosis of Ito are typical examples.

B5. Blaschko lines in broad bands: lesions distributed along the Blaschko lines, in "broad" bands that are wider than 2 cm in size. Typically, it is seen in McCune-Albright syndrome.

B6. Checkerboard, also called a block or flag-like pattern, involves cutaneous lesions of large squares with a clear midline separation with less defined lateral borders. These block-like skin lesions are usually located on the trunk and extremities and are observed as multiple, bilateral lesions in different areas on each hemibody, resembling a checkerboard. Rarely, the face and neck are also involved. Many vascular anomalies, such as port-wine stains (nevus flammeus) and cutis marmorata telangiectatica congenita, and epidermal naevus, such as Becker nevus, nevus spilus, are examples of this pattern.

B7. Phylloid pattern is characterized by skin lesions showing a "leaf-like" appearance. Usually involves pear-shaped, round/oval/oblong patches, asymmetrical and elongated macules in an arrangement reminiscent of a floral ornament. Phylloid hypomelanosis due to 13q trisomy is the classic example of this pattern.

B8. Lateralization/half-body pattern is characterized by a diffuse lesion on only one side of the body with a sharp midline demarcation. This pattern is uniquely seen in CHILD syndrome (**C**ongenital **H**emidysplasia with **I**chthyosis form nevus and **L**imb **D**efects), a rare X-linked dominant, male-lethal disorder. The unique pattern of the CHILD nevus is unilateral and follows the Blaschko lines. Contralateral minor skin lesions may be observed along with ipsilateral limb, brain, and visceral anomalies.

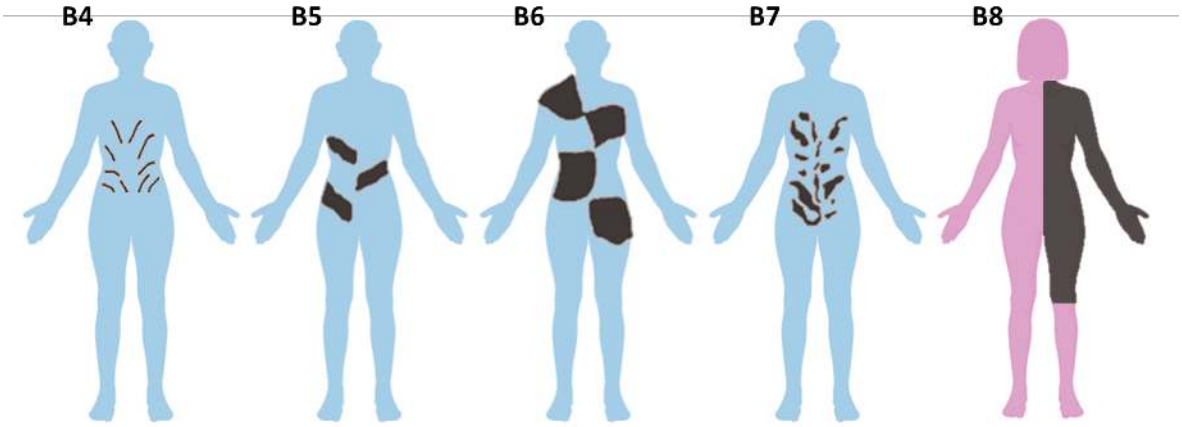

Figure 1-10. **Body patterns of segmental mosaicism**. **(B4)** Blaschko's lines appearing as narrow bands. **(B5)** Blaschko's lines appearing as broad bands. **(B6)** Checkerboard pattern, characterized by sharply demarcated patches. **(B7)** Phylloid pattern, resembling leaf-like shapes. **(B8)** Lateralization or half-body involvement, where one side of the body is affected.

C. Depending on the directional change in the mutational event, mosaicism can convert from benign to pathogenic, pathogenic to benign (revertant) or normal to more than one pathogenic variant (didysmosis) (Figure 1.11).

C1. Healthy (normal) to pathogenic: In this form of mosaicism, a wild-type cell changes to a mutant cell, so the direction of the mutational event is from normal (benign) to pathogenic. This is the most common form and the fundamental explanation of postzygotic mosaicism, where disease-causing mutations arise at an early developmental stage in an otherwise "healthy" embryo.

C2. Pathogenic to normal (revertant mosaicism): In this case, a disease-causing mutation is spontaneously corrected/reverted by somatic mutational events, so there is a conversion from pathogenic to normal (benign). Affected individuals may show one or more areas of healthy skin, as some cells may genetically normalize, reverting the affected tissue to unaffected. Representing a potential "natural gene therapy", this phenomenon is relatively common in several blistering skin diseases such as ichthyosis with confetti and epidermolysis bullosa.

C3. Didymosis/twin spotting: Twin-spot phenomenon refers to paired mutant tissue patches that differ genetically from each other and the background tissue. Typically, mutant patches are homozygous for either of two different recessive mutations on a background tissue that is heterozygous for those two mutations. The mutations may involve the same gene locus (allelic didymosis) or affect different loci (nonallelic didymosis). While molecular proof for both mechanisms is lacking so far, allelic twin spotting is the only confirmed concept in humans as different types of patches/lesions/phacomatoses originate from different mutations. Skin disorders, cutis tricolor, keratinopathic ichthyosis of Brocq, Darier disease, phacomatosis pigmentovascularis and phacomatosis pigmentokeratotica are considered as examples of didymosis (Happle & Torrelo, 2022a).

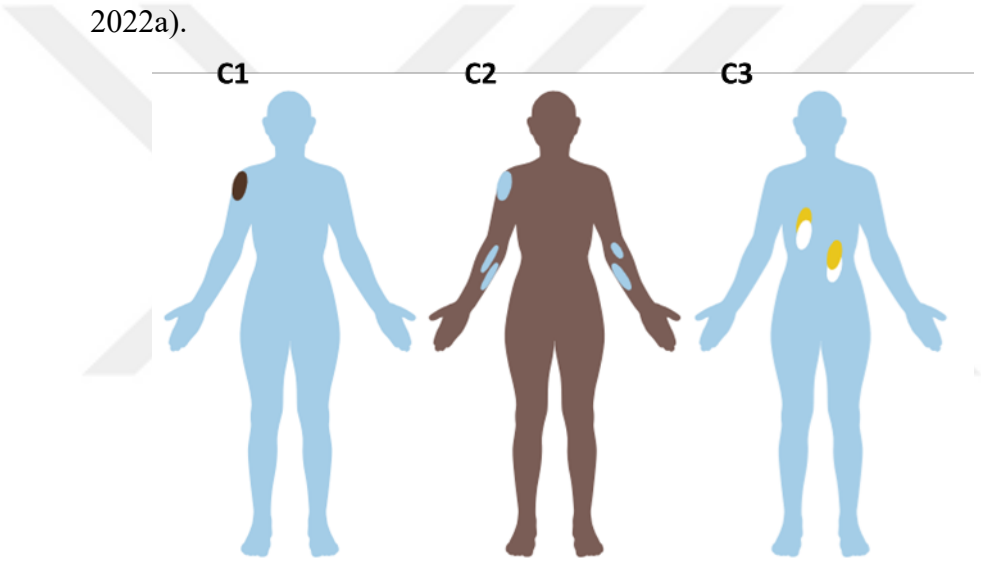

Figure 1-11. **Directional changes in mosaicism**. **(C1)** Transition from benign (wild-type) to pathogenic — a postzygotic mutation results in disease-causing cells within an otherwise healthy background. **(C2)** Transition from pathogenic to benign (wild type), known as revertant mosaicism, where spontaneous correction of a disease-causing mutation restores normal gene function in some cells. **(C3) Didymosis**, the presence of two adjacent but genetically distinct cell populations, each carrying a different postzygotic mutation. Brown color indicates the mutant cell(s), blue color indicates wild-type cell(s), yellow and white colors on C3 represent different mutations.

D. Depending on the developmental mechanism of the mutant cells, mosaicism can be stratified in three main groups: mosaicism in non-lethal autosomal dominant diseases, functional X-chromosome mosaicism and mosaicism in lethal autosomal dominant diseases (Figure 1.12).

Mosaicism in non-lethal diseases:

D1. Type 1 segmental mosaicism, also referred to as **simple segmental mosaicism**, originates from a *de novo* postzygotic mutation in a single cell that was wild type for that specific locus, before the mutational event. In other words, it reflects heterozygosity for a postzygotic new mutation on a normal genetic background. Examples of type 1 segmental mosaicism include tuberous sclerosis (TSC), neurofibromatosis type 1 (NF1), Gorlin syndrome and Darier disease.

D2. Type 2 segmental mosaicism originates from a second-hit mutation in a single cell that was constitutionally heterozygous for that specific locus, before the postzygotic mutational event. It reflects heterozygosity for a postzygotic second mutation on a heterozygous germline background. This category is thus also referred to as '**superimposed mosaicism**'. In monogenic skin disorders, early postzygotic mutational events may give rise to the loss of heterozygosity on the corresponding wild-type allele; while in polygenic disorders, it may cause heterozygosity at another predisposing gene locus. Type 2 segmental mosaicism has been described in many skin disorders including Buschke-Ollendorff syndrome, Hailey-Hailey disease, PTEN hamartoma syndrome, and TSC, NF1 and Darier's disease.

D3. Functional X-chromosome mosaicism is no exception in any female embryo, due to random postzygotic inactivation of one of the two X chromosomes. This process, regulated by differential expression of the X-inactive-specific transcript (*XIST*), occurs at an early developmental stage and results in a mosaic distribution of cells. In X-linked skin disorders, heterozygous females are often clinically unaffected with rare instances of severe manifestations resembling those seen in hemizygous males. However, they may have mild cutaneous findings that follow Blaschko lines, which may remain unnoticed unless a pigmentary skin disorder is present.

Female carriers of X-linked disorders with male lethality, such as focal dermal hypoplasia (Goltz–Gorlin syndrome), incontinentia pigmenti, Conradi–Hünermann–Happle syndrome, oral-facial-digital syndrome type 1 and MIDAS (microphthalmia, dermal aplasia and sclerocornea) syndrome, as well as X-linked non-lethal diseases such as IFAP (ichthyosis follicularis, atrichia, and photophobia) syndrome, hypohidrotic ectodermal dysplasia of Christ-Siemens-

Touraine, X-linked dyskeratosis congenita, and male-sublethal Menkes syndrome may show variable mosaic skin involvement. Distinct segmental patterns can also be seen, as the lateralization in CHILD (congenital hemidysplasia with ichthyosiform nevus and limb defects) syndrome, and the chequerboard pattern in X-linked congenital hypertrichosis. On the other hand, some X-linked skin disorders are caused by genes that escape X-inactivation. Consequently, female carriers typically do not exhibit clinical manifestations. A classic example is X-linked ichthyosis caused by variations in steroid sulphatase (*STS*) gene, located at Xp22.31 the distal end of the X chromosome's short arm and is not inactivated through lyonization (Happle, 2006).

Mosaicism in lethal diseases:

D4. Disorders that manifest only as mosaics

Some Mendelian disorders exist solely in mosaic form and are incapable of vertical germline transmission. In these cases, the causing mutations are incompatible with embryonic development, resulting in early intrauterine death when present in all cells of the embryo. The existence of these disorders was hypothesized based on the observation of *de novo* (non-familial) cases with affected individuals manifesting cutaneous findings in a segmental pattern. Furthermore, this class of disorders has also been seen in discordant monozygotic twin pairs, implying the occurrence of mutational events in somatic cells of one twin but not in the parental germline or in the shared embryo pre-twinning. Cases in this group can be named "obligate mosaics" as the genetic variant is only seen in the context of mosaicism and would be lethal otherwise. Well-known examples of obligate mosaic syndromes have been listed in Table 1.1.

- **Type 4a. Disorders that manifest only as mosaics (D4a: autosomal)**

The most well-characterized examples of this class of disorders include McCune–Albright syndrome, Proteus syndrome, Schimmelpenning–Feuerstein–Mims syndrome and *PIK3CA*-related overgrowth spectrum. Also, some chromosomal syndromes including Pallister–Killian syndrome and trisomy 8, 9, 14 are compatible with life when only in mosaic form.

- **Type 4b. Disorders that manifest only as mosaics (D4b: X-linked)**

"Developmental and epileptic encephalopathy 9 (MIM #300088)" is caused by mutations in the protocadherin-19 gene (*PCDH19*; 300460) on chromosome Xq22. Also known as "epilepsy and mental retardation restricted to females (EFMR)", pathogenic germline variants in the *PCDH19* affect females only, whereas hemizygous males are unaffected but transmit the disease to all their daughters. However, somatic mosaicism was also reported in rare cases of affected males with a similar phenotype to EFMR.

The findings pointed to a mechanism of pathogenesis in which the development of disease involves the requirement for two cell populations, mutant and wild-type, while a homogeneous population, either mutant or wild-type, cells does not contribute to the development of the disease. Therefore, cellular mosaicism, due to either X-chromosome inactivation in heterozygous females or postzygotic pathogenic variants in hemizygous males, underscores this class of disorders.

Table 1-1. **Well-known examples of obligate mosaic syndromes**. Adapted from Waldvogel et al., 2024.

Gene	Disorder	Mutation Detection Rate
PIK3CA	CLOVES	Highest in the affected tissue
FGFR1	Encephalocraniocutaneous lipomatosis	Highest in the skin fibroblasts
MTOR	Focal cortical dysplasia	Higher in brain, seldom detection in blood
IDH1	Maffucci syndrome	Highest in the affected tissue
GNAS1	McCune–Albright syndrome	Highest in the affected tissue
EPAS1	Pacak–Zhuang syndrome	High in tumours, low elsewhere
Tetrasomy 12p	Pallister–Killian syndrome	Detected in skin fibroblasts, seldom detection in lymphocytes
AKT1	Proteus syndrome	Not detected in blood
HRAS, KRAS, NRAS	Schimmelpenning-Feuerstein-Mims syndrome	Not detected in lymphocytes and non-lesional skin
GNAQ	Sturge–Weber syndrome	Detected in affected brain and skin
UBA1	VEXAS syndrome	Detected in myeloid lineage, but not in mature lymphocytes

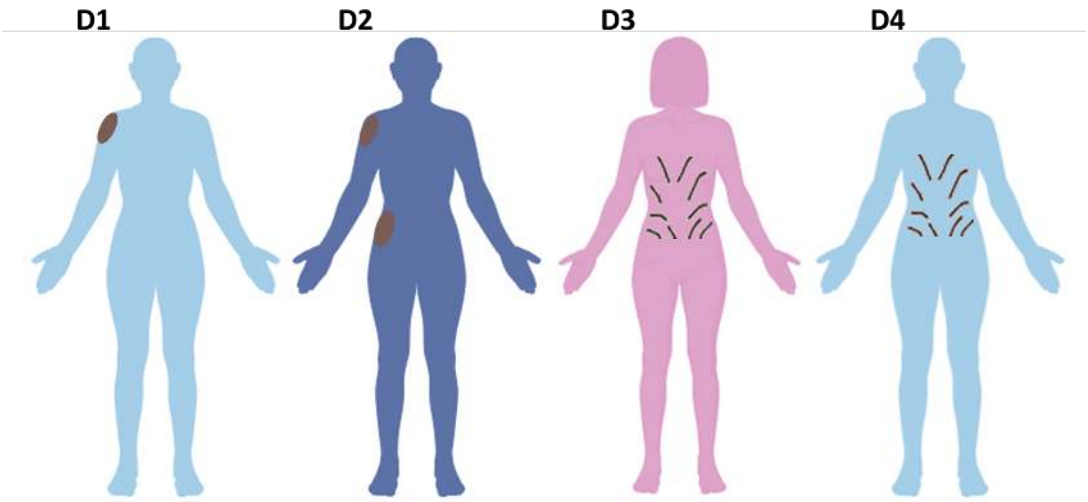

Figure 1-12. **Developmental mechanisms underlying mosaicism**. **(D1)** Type 1 segmental mosaicism caused by a mutation occurring after fertilization, resulting in a mix of normal and mutated cells. **(D2)** Type 2 segmental mosaicism where a second mutation affects the normal copy of a gene that was already in a heterozygous state, leading to complete loss of normal gene function in affected cells. **(D3)** X-chromosome mosaicism, where differences in gene activity between X chromosomes lead to a visible pattern in females; in some cases, the condition is only seen in mosaic males due to male lethality. **(D4)** Disorders caused by mutations that are lethal unless present in a mosaic state.

E. Depending on the underlying genetic alterations, mosaicism can be caused by variants spanning whole chromosomes, copy-number variants (CNVs), structural variants, indels, single-nucleotide variants (SNV), small insertions and deletions and epigenetic changes. Thus mosaicism may be divided into four major classes: genomic variants, genetic changes, epigenetic changes, and positional effects (Figure 1.13).

E1. Genomic changes (large variations)

The mosaicisms in this group are caused by genomic aberrations, which can be classified as follows:

- **Large losses or gains of chromosomes** (>100 Mb), including chromosomal aneuploidies that are usually visible under the light microscope (e.g., Down syndrome).
- **Medium-sized losses or gains of part of chromosomes** (4–100 Mb), typically deletions and duplications visible under the light microscope (e.g., Wolf–Hirschhorn syndrome).

- **Losses or gains of small parts of a chromosome** (0.1–4 Mb), which are not visible under light microscope but detected by cytomolecular techniques such as fluorescence in situ hybridization (FISH), multiplex ligation-dependent probe amplification (MLPA), chromosome microarrays (e.g., Smith-Magenis syndrome); molecular combing, optical genome mapping (e.g., Facioscapulohumeral muscular dystrophy).
- **Long interspersed nuclear elements (LINE or L1) retrotranspositions** (1–100 Kb) that can only be interrogated by molecular techniques such as L1 reporter assays and high-throughput sequencing (e.g., some cases of colonic cancer due to *APC* gene variants).
- **Short interspersed nuclear elements (SINE or Alu element) retrotranspositions** (100 bp–1 Kb) that can only be detected by molecular techniques (e.g., congenital cataracts due to a fraction of patients with *GCNT2* variants).
- **Copy-neutral genomic variants** of any size, including whole chromosome, genomic inversions, and segmental uniparental disomies of non-imprinting regions without epigenetic consequences.

E2. Genetic changes (Small Nucleotide Variants and Indels)

It is estimated that the fidelity and repair capacity of DNA polymerase results in approximately one error for every 109 nucleotides replicated per cell division. Mosaicisms in this group represent relatively small changes and variations due to DNA damage, replication errors and erroneous DNA repair mechanisms. For example, errors in base excision repair, nucleotide excision repair and transcription-coupled repair can lead to mosaic genetic changes; DNA damage induced by ultraviolet radiation, environmental carcinogens and X-ray radiation can lead to somatic genetic changes.

The most common variants observed in this group are single nucleotide variants and small indels (<50bp), including DNA polymerase slippage and trinucleotide repeat expansions affecting a short DNA segment (10–100 bp, e.g. in Huntington's disease).

E3. Epigenetic changes

Epigenetic mosaics refer to the presence of different epigenetic patterns due to “epimutations” within a single organism. The term "epimutations" describes alterations in the epigenetic state of a gene, leading to changes in its expression without altering the underlying DNA sequence. These changes can result in alternative monoallelic expression, meaning that only one of the two inherited alleles is expressed. This altered expression can be attributed to the methylation or demethylation of nearby regulatory regions, impacting gene function and potentially leading to phenotypic variation within the organism.

For instance, Beckwith-Wiedemann Syndrome (BWS) is linked to the disruption of gene expression regulation in two key domains - imprinting control region 1 (ICR1 = *H19*/*IGF2*:IG-DMR) and imprinting control region 2 (ICR2 = *KCNQ1OT1*:TSS-DMR) at the 11p15.5 chromosomal region. Partial increase (partial hypermethylation) in the ICR1 methylation pattern and partial decrease (partial hypomethylation) in the ICR2 methylation pattern adresses mosaic paternal 11p15 UPD, causing an imbalance among imprinted genes that either stimulate or restrict growth. Similarly, epigenetic mechanisms involved in functional X-chromosome mosaicism are also part of this category.

E4. Positional effect variants

These variants do arise from disturbances in gene(s) or their regulatory elements as a result of translocations, inversions, or changes in topological domains. While positional effects are not common in skin mosaicism; a notable example of this etiology is the mosaic Philadelphia chromosome found in leukemia cells. Caused by the reciprocal translocation t(9;22)(q34;q11),the fusion gene *BCR-ABL1* produces a hybrid protein (a tyrosine kinase signaling protein) that causes uncontrolled cell division by disrupting genome stability and interfering with various cell cycle signaling pathways.

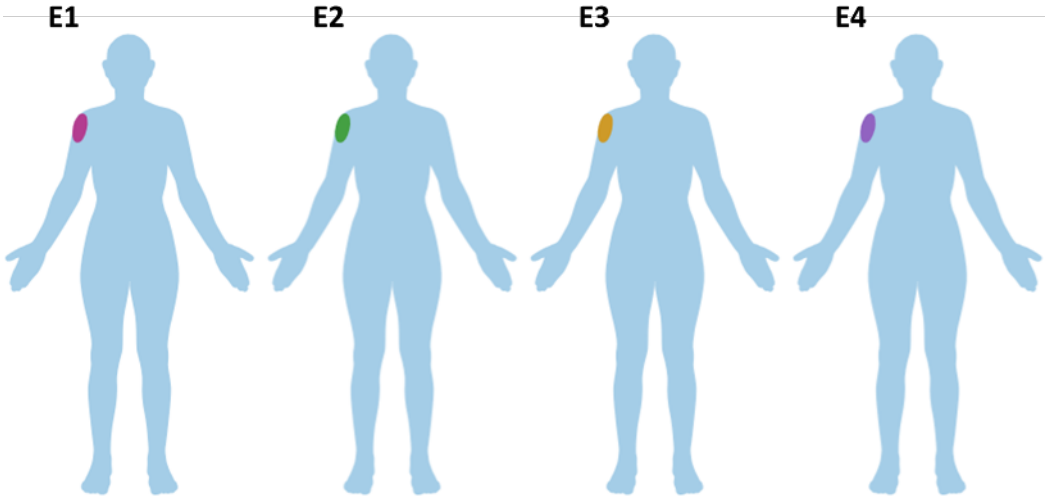

Figure 1-13. **Etiological mechanisms underlying mosaicism**. **(E1)** Genomic changes, such as deletions, duplications, or translocations, arising postzygotically and affecting only a subset of cells (indicated with pink). **(E2)** Genetic changes involving point mutations or small insertions/deletions occurring after fertilization, leading to a mosaic distribution of affected cells (indicated with green). **(E3)** Epigenetic changes, including altered DNA methylation or chromatin remodeling, resulting in variable gene expression across different cell populations (indicated with orange). **(E4)** Positional effects, where changes in the genomic context or regulatory environment postzygotically impact gene expression in a mosaic pattern (indicated with purple).

F. Depending on the percentage of the affected tissue in comparison with normal tissue, there are four subcategories (Figure 1.14):

F1. Mild involvement, less than 10% of body surface (<5% VAF);

F2. Moderate involvement, 10–30% of body surface (5–15% VAF);

F3. Severe involvement, 30–50% of body surface (15–25% VAF);

F4. Very severe involvement, >50% of body surface (>25% VAF).

In the context of somatic mutations, VAF describes the percentage of sequencing reads at a given location with the variant of interest. For instance, if 5% of the sequencing reads at a given position harbor the variant, the VAF is calculated as 0.05 (or 5%). While the variant allele frequency (VAF) can theoretically be used for quantification, it's important to note that molecular testing typically assesses variants

rather than cells. Given that all genes are diploid, reported VAF values generally correspond to half the fraction of mutant cells.

For skin disorders, the fraction of affected tissue is estimated by measuring the affected body surface area, as it is challenging to accurately quantify depth and volume. This approach with or without VAF can also be used to quantify other mosaic disorders with similar anatomic or morphologic attributes that are easily quantifiable (vascular or bone disorders). However, if there's a discrepancy between the two, the VAF value takes precedence over the percentage of affected tissue determined by clinical examination.

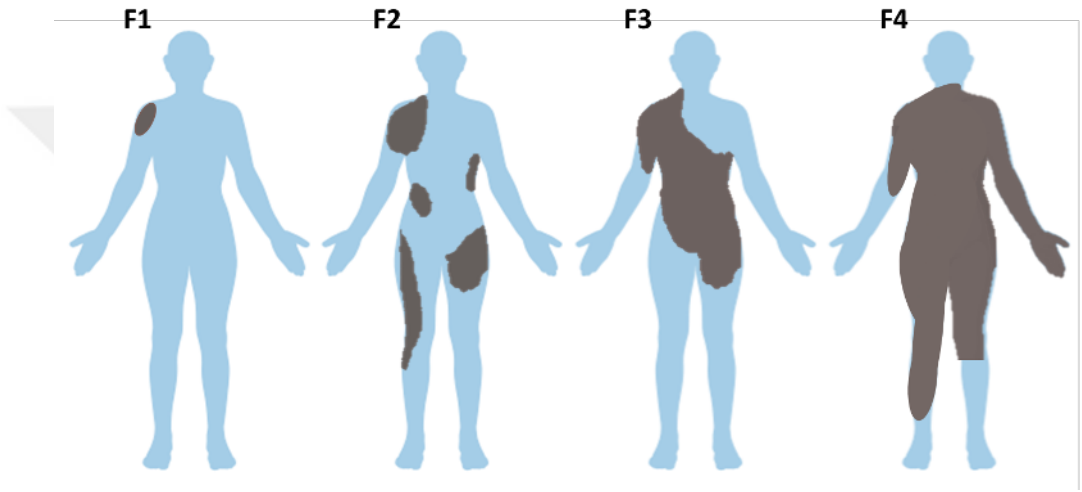

Figure 1-14. **Fraction of tissue affected in mosaicism**. **(F1)** Mild involvement: a small portion of tissue is affected, often with subtle or localized changes. **(F2)** Moderate involvement: a larger but still limited area is affected, with more noticeable clinical features. **(F3)** Severe involvement: extensive tissue is affected, often with significant functional or structural impact. **(F4)** Very severe involvement: widespread or nearly complete tissue involvement, potentially mimicking non-mosaic form(s) of the disorder.

1.4 DEVELOPMENTAL TIMING OF MOSAICISM

Mosaicism occurs throughout the human lifespan. While the genetic alterations usually involve key genes in cell survival and proliferation pathways, some variants can be a “hotspot” and associated with both congenital malformations and oncogenesis. The severity and clinical symptoms of mosaicism depend on the time of the mutational event, the type of cell in which the mutation takes place, the expansion of cells with mutations, the mutated gene, and the mutation.

1.4.1. The Timing and Lineage of Variant Acquisition Characterize the Extent of Mosaicism

The initiating mutational event can occur in any cell type at any time during development, leading to significant variation in the distribution and phenotypic effects and thus resulting in highly variable clinical expressivity. Variants acquired during early stages of the embryonic development could have the propensity to impact large proportions of cells in various tissues in the body and may lead to serious consequences (Waldvogel et al., 2024). That is:

- If the variant is acquired at or before fertilization, it will be present in all cells of the individual and be transmitted to the offspring following the rules of Mendelian genetics (germline mosaicism) (Figure 1.15 A).

- If the mutational event occurs up to 12 days post-fertilization between the 2-cell to 4-cell stage and gastrulation, i.e., before specification of the primordial germ cells, the variant will be present in both somatic and germ cell tissue (gonadosomatic mosaicism) (Figure 1.15 B). Depending on the affected tissues and degree of mosaicism, the mosaic individual may be phenotypically affected and can transmit the variant to their offspring.

- If the mutational event occurs after 12 days post-fertilization in a primordial germ cell, it will be confined to the germ cells (gonadal mosaicism), and the variant can be passed to offspring, but the mosaic individual is unlikely to exhibit a phenotype (Figure 1.15 C).

- If the mutational event arises between 14-21 days post-fertilization, i.e., during gastrulation, the variant will be confined to the tissues derived from that specific germ layer, but it may be seen in multiple cell types from that germ layer depending on the timing of acquisition (Figure 1.15 D). The mosaic individual may be phenotypically affected, depending on the variant and the affected organ.

- If the mutational event arises after 21 days post-fertilization, i.e., after the onset of organogenesis, it is likely limited to one organ (Figure 1.15 E). Depending on the variant and the affected organ, the mosaic individual may be phenotypically affected.

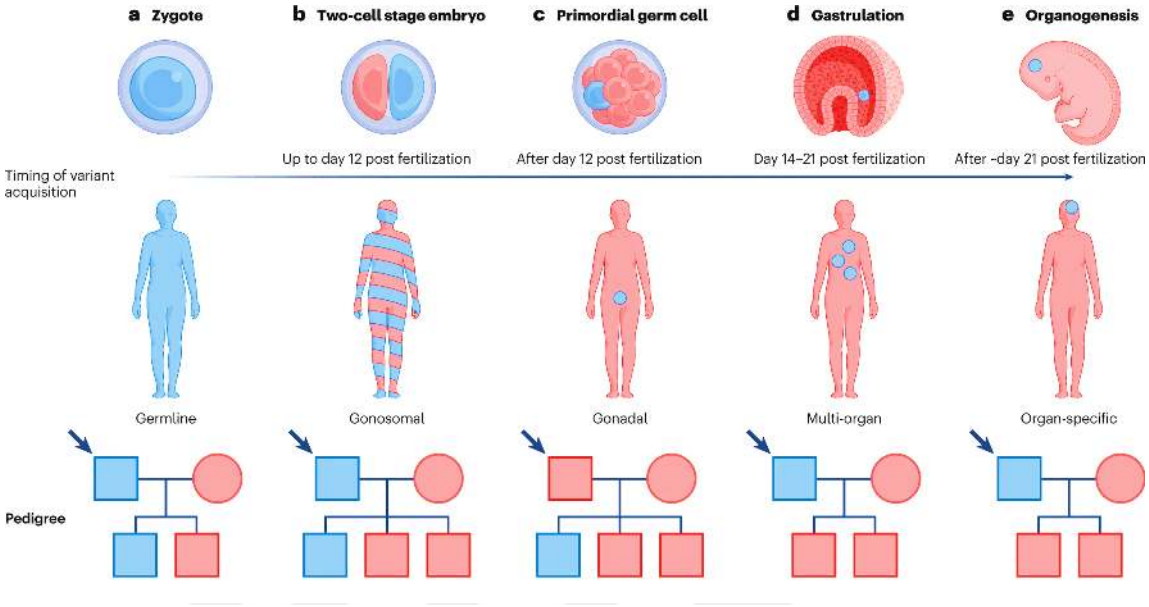

Figure 1-15. **Transmission of a heterozygous variant acquired at different stages of embryonic development influences the distribution and extent of mosaicism**. Affected cells and/or individuals are shown in blue. Adapted from Waldvogel et al., 2024.

1.4.2. Variants Acquired at Different Stages of Embryogenesis Exhibit Distinct Genetic Features

The estimated average rate of germline *de novo* mutations for SNVs is 1-1.8×10^{-8} per nucleotide per generation, resulting in ~44-82 new SNVs in each individual (Shadrina et al., 2025). The first few cell divisions in the early embryogenesis are the most prone to mutation.

Genetic variations acquired before gastrulation are more likely to be present in a larger percentage of cells and across different tissues compared to those acquired after gastrulation. As a result, mosaic variants acquired during early embryogenesis generally have higher VAFs. They also tend to have a lower proportion of non-synonymous variants that lead to protein-coding changes and a higher proportion of synonymous (silent) variants. This lower ratio of non-synonymous to synonymous variants (dN/dS) indicates that early embryonic variants are under stronger negative selection against harmful variants, which likely reduces embryo survival. Therefore, early embryonic variants found in living individuals are more likely to be present in

genes where LoF is tolerated (Waldvogel et al., 2024). By contrast, mosaic variants acquired later in embryonic development are generally found at lower VAFs and are confined to a smaller number of tissues. These variants exhibit a higher dN/dS ratio and are deleterious at the organismal level or damaging if they are present in a very high proportion of embryonic cells. Despite this, they are subject to positive selection in the embryonic context and are favorable in mosaic state with low VAF (Figure 1.16).

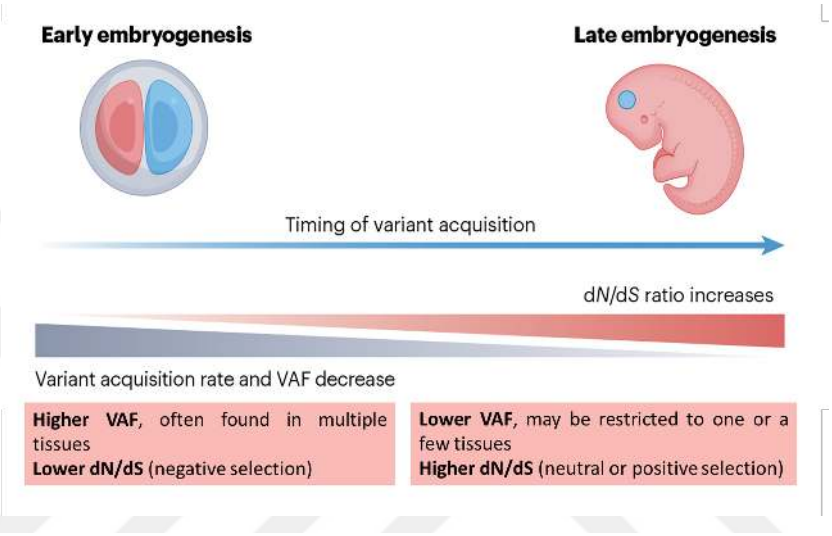

Figure 1-16. **Timing of variant acquisition during embryogenesis affects mosaicism characteristics**, including variant allele frequency, tissue distribution, and selective pressures. Modified from Waldvogel et al., 2024.

1.5. APPROACHES TO INVESTIGATE GENETIC MOSAICISM: CHALLENGES IN THE DIAGNOSIS

In genetics, the term "mosaicism" applies fully when a certain percentage of cells in a tissue contain a genetic variant that was not present in the germline. This can be identified through routine cytogenetic, genetic, or genomic testing.

Rapid advances in sequencing and analysis technologies have enabled the precise detection of diverse genomic variants. Especially in the last decade, the increasing efficiency and reduced cost of molecular diagnostic technologies have enabled the genome-wide identification of postzygotic mutations. Consequently, numerous congenital and childhood-onset developmental anomalies and syndromes have been linked to mosaic mutations. For example, the genetic etiopathogenesis of Proteus syndrome (*AKT1*), CLOVES and MCAP syndromes (*PIK3CA*), nevus

flammeus/Sturge-Weber syndrome (*GNAQ*), epidermal nevus and linear nevus sebaceous syndrome (*HRAS, KRAS, PIK3CA*), encephalocraniocutaneous lipomatosis (*FGFR1*), and neurocutaneous melanosis (*NRAS*) and oculoectodermal syndrome (*KRAS)* has been identified with the introduction of NGS methods (Lindhurst et al., 2011; Kurek et al., 2012; Mirzaa & Doybns, 2013; Shirley et al., 2013; Kinsler et al., 2013; Bennett et al., 2016; Happle et al., 2017). Moreover, in the last 15 years, with NGS techniques that facilitate the detection of low-rate mosaic changes in related genes in affected tissues, postzygotic mosaic mutations have been shown to play a role in the etiopathogenesis of different entities including overgrowth syndromes (Riviere et al., 2012), structural brain malformations (Poduri et al., 2012; Lee et al., 2012; Jamuar et al., 2014), epilepsy (Stosser et al., 2018), autism spectrum disorders (Lim et al., 2017; Krupp et al., 2017; Dou et al., 2017).

The diagnostic algorithm to enlighten the molecular pathogenesis of a genetic disease is guided by clinical examination findings. An accurate clinical diagnosis can direct the choice of appropriate test(s) to be performed and ultimately lead to a definitive diagnosis. However, as previously mentioned, “mosaic” phenotypes are influenced by various factors, and findings are often nonspecific and indistinguishable, which complicates making the preliminary diagnosis. Additionally, diagnosing mosaicism poses challenges in both sampling and methodological approach. It is important to carefully consider the appropriateness of the sampled tissue and chosen diagnostic test, as the quality of the sample and detection threshold of the technique are crucial for the detection. Currently, a combination of traditional laboratory techniques and NGS approaches is routinely employed for rare disease diagnosis. Table 1.2 summarizes the specifications of existing and emerging technologies for genomic variant identification.

Karyotyping remains the first-line chromosomal analysis for patients presenting with multiple congenital anomalies. If the chromosomal analysis of peripheral blood is normal, then skin tissue should be examined to assess the possibility of mosaicism. If karyotyping from both blood and skin tissues reveals normal results, but clinical suspicion of a chromosomal abnormality persists, the next step is to conduct microarray analyses by SNP array or array-CGH.

If clinical findings suggest a specific diagnosis, single-gene testing may be considered. Sanger sequencing analysis is performed as the first molecular test to detect small intragenic deletions/insertions and/or missense, nonsense, and splice site variants.

Depending on the size of the gene(s) and targeted exon(s), single-exon, multi-exon, or whole-gene deletions/duplications can also be ruled out by Sanger sequencing. However, if no pathogenic variant is detected through sequencing and large deletions/duplications have been reported in previous cases associated with the suspected phenotype/disease/syndrome, gene-targeted MLPA analysis should be considered as the next step.

When there is locus heterogeneity or when the size of the related gene and its exons make Sanger sequencing impractical, it is sensible to use panel testing with second-generation sequencing methods. In cases involving syndromes with unidentified causative genes or when a specific diagnosis cannot be established through clinical evaluation alone, targeted gene panels and/or whole exome and/or genome sequencing that include all genes with an elucidated phenotype-genotype relationship can be utilized.

Emerging approaches such as long-read sequencing and optical genome mapping are shifting from research applications to clinical diagnostics to identify complex genomic alterations more effectively. Additionally, various omic platforms, including RNA sequencing (RNA-seq), proteomics, epigenomics, lipidomics, and metabolomics, have been developed. Although these technologies were initially intended to identify disease-causing genetic variations, they have been primarily successful as secondary functional assays. Nevertheless, when integrated with DNA sequencing, multi-omics approaches hold the potential for identifying disease mechanisms.

Table 1-2. **Existing and emerging technologies for genomic variant identification.**

Method	Detectable DNA Variants	Advantages	Disadvantages
Karyotyping	CNVs, SVs, Aneuploidy, Mosaicism	• Inexpensive • Whole-genome survey	• Low resolution • Low throughput
FISH	CNVs, SVs, Aneuploidy, Mosaicism	• Inexpensive • Targeted	• Practical for targeted analysis • Limited resolution • Low throughput
MLPA	CNVs, Aneuploidy	• Inexpensive • Targeted	• Practical for targeted analysis
Microarray	CNVs, Aneuploidy, Mosaicism	• Inexpensive • Whole-genome survey	• Limited resolution

Triplet primed PCR	STRs	• Inexpensive • Targeted	• Practical for targeted analysis
Southern blotting	STRs	• Inexpensive • Targeted	• Time-consuming • Low throughput
Real-time PCR	SNVs	• Inexpensive • Targeted	• Practical for targeted analysis
Sanger sequencing	SNVs, mtDNA, Mosaicism	• Inexpensive • Targeted	• Practical for targeted analysis • Secondary findings are unlikely
Exome sequencing	SNVs, CNVs, mtDNA, Mosaicism	• Higher coverage than WGS • Sequencing reads placed where diagnoses are most probable • Secondary findings are possible	• Uneven coverage across exons • Unable to align to repetitive regions • Limited detection of CNVs • No detection of SVs
Short-read genome sequencing	SNVs, CNVs, SVs, STRs, Mosaicism, mtDNA	• Even coverage across genome • Improved CNV calling over WES • Secondary findings are possible	• Expensive • Unable to detect repeat expansions and repeat-rich regions • Low sensitivity for SVs, STRs • Decreased read depth, limited detection of mosaicism as low VAF variants might be missed
Long-read genome sequencing	SNVs, CNVs, SVs, STRs, Mosaicism, mtDNA	• Even coverage across genome including repetitive regions, • Improved CNV and SV calling over short-read WGS • Secondary findings are possible	• Very Expensive • Requires a special DNA isolation protocol • Low sensitivity for mosaicism • Algorithms are still being developed
Optical genome mapping	CNVs, SVs, STRs, Aneuploidy, Mosaicism	• Better CNV and SV calling than short-read WGS • Higher resolution than microarray and karyotyping • Unbiased screen across genome possible	• Requires a special DNA isolation protocol • Limited resolution in some regions • Triploidies, polyploidies, and whole-arm translocations including Robertsonian translocations are not detected • Lower potential resolution than WGS

1.5.1. Detecting Mosaicism: Tissue Type Matters

Although mosaicism is often categorized based on origin and cell lineage (e.g., somatic, germline), these classifications are not always conclusive due to practical limitations in tissue sampling. Postzygotic mutations typically affect multiple cell populations to varying degrees, meaning that a mutation may be undetectable in certain tissues while being present in others. This variability complicates diagnostic efforts, particularly in distinguishing germline or gonosomal mosaicism. For example, diagnosing a patient with germline mosaicism is typically based on finding a mutation in germ cells (e.g. sperm) while not detecting it in peripheral blood or skin fibroblasts. However, this analysis may not completely rule out the presence of the mutation in other somatic cells.

For disorders caused by postzygotic mutations, particularly those showing cutaneous mosaicism, it is widely recognized that relying on a single tissue for analysis may lead to false negatives. Due to the uneven distribution of mosaic variants across tissues, molecular diagnosis might be challenging and not straightforward. It is important to carefully choose what and where to sample to find detectable levels of the pathogenic variant. In many cases, blood samples may fail to reveal pathogenic variants (Rivière et al., 2012; Keppler-Noreuil et al., 2015; Mirzaa et al., 2016; Kuentz et al., 2017). Higher VAFs are consistently observed in samples from skin and affected tissues, compared to blood and buccal samples. Moreover, an essential factor in analyzing tissue samples is the precision of tissue selection and dissection, as sample purity directly influences the accuracy of variant detection.

Current diagnostic guidelines recommend prioritizing DNA sequencing from tissues showing clear clinical involvement. Fresh tissue samples from clinically affected areas are the most suitable samples for optimal molecular diagnosis. It is further recommended to test uncultured tissues due to potential shifts in mosaic levels for an activating variant that may arise during culturing (Mirzaa et al., 2016). If fresh tissue is unavailable, formalin-fixed, paraffin-embedded (FFPE) samples can be used only if the latter is unavailable, though the quality of extracted DNA may be compromised, reducing the diagnostic yield.

Another challenge is the tissue availability, as some tissues are and can not be typically sampled in a routine diagnostic setting. For instance, surgical resection or postmortem biopsy is crucial to detect mosaicism of the brain, as direct testing of

malformed brain tissue has been reported to provide the highest diagnostic yield (Lee et al., 2012; Lim et al., 2017). However, it is not only generally infeasible in standard clinical practice but may also be unnecessary. For example, patients with cortical malformations who do not have epilepsy will therefore not require surgery to resect the epileptogenic lesions. When brain tissue is inaccessible and clinical suspicion remains high (e.g., for *MTOR* mutations), testing alternative tissues like saliva or skin using high-depth exome or targeted sequencing is advisable, especially when blood-based results are inconclusive.

1.5.2. Detecting Mosaicism: Methodological Considerations

Patients presenting with highly localized or tissue-specific features are reported to have a lower diagnostic yield (Mirzaa et al., 2016), as certain pathogenic variants may only exist at very low allele fractions, due to the mosaic nature of the disease. Low-level mosaics (<5%–10%) may be below the detection threshold of conventional molecular diagnostic approaches, i.e., Sanger sequencing must be used if the pathogenic variant allele fraction is relatively high (>10-15%). The minimum number of observations required to reliably confirm a variant depends on the platform used and its capacity to distinguish true mutation peaks or signals from background noise. High sensitivity is therefore required; more specific and sensitive methods that can detect mosaic variants with allele frequencies as low as 5% or even lower at 1%, should be applied.

Several techniques have been validated for the detection of low-level mosaicism, which include but not limited to Sanger sequencing, digital droplet PCR (ddPCR), SNaPshot assay, qBiomarker array, MassARRAY system, NGS, and custom restriction fragment length polymorphism (RFLP) (Table 1.3). Digital droplet PCR (ddPCR), with a theoretical sensitivity down to 0.001%, routinely detects mosaicism at 0.1%. Targeted amplicon-based NGS, with approximately 1,000× coverage, can detect mutation rates as low as ~1%, although high sequencing error rates present challenges to its utility in a clinical setting. Hybridization-based NGS platforms, with a minimum 350x and mean 500x coverage, has been shown to reliably detect mosaic variants at ~5% VAF. SNaPshot, qBiomarker arrays, MassARRAY, and custom RFLP analyses are also utilized, though their sensitivity may vary. Yet, real-time PCR (qPCR) remains a promising method for detecting mosaicism and warrants further investigation for its diagnostic efficiency. Additionally, while standard-depth exome or genome sequencing

(100×–200×) may uncover mosaic variants at higher VAFs (≥5%–10%), most low-level mosaics may remain undetected at such depths.

Considering the limitations of orthogonal methods (e.g., Sanger sequencing for VAFs ≥10%, pyrosequencing for VAFs ≥5%), ddPCR and NGS-based sequencing are favored methods available for the molecular diagnosis of low-level mosaicism. However, ddPCR can typically screen only a few variants at a time, so it is mainly limited to hotspot detection or confirming results from NGS. Given the allelic heterogeneity in many mosaic diseases, false negatives are likely (Kuentz et al., 2017). Additionally, interpreting the biological significance of very low VAFs (e.g., 0.001%) can be challenging.

Table 1-3. **Comparison of Common Molecular Techniques for the Detection of Mosaic Variants**

Method	Depth / Sensitivity	Suitability for Mosaic Detection
ddPCR	0.001% theoretical; 0.1% routine	Ideal for ultra-low mosaicism on targeted hotspots, requires a custom assay for each variant, no multiplexing
Targeted Amplicon-based NGS	~1,000×; ~1%, can reach <0.5% with UMI/error correction	Sensitive but affected by error rates, thus requiring careful bioinformatic analysis. Requires panel design but is more scalable for large sets. High throughput, broad detection, supports novel variant discovery.
Hybridization-based NGS	350–500×; ~5% VAF	Robust for detecting ≥5% VAF, broad panel coverage, commonly used in exploratory variant detection in diagnostics, lower sensitivity without deep coverage
SNaPshot Assay	≥1–5% VAF	Good for targeted hotspots; sensitivity depends on assay design
qBiomarker Array	1% typical; best ~0.01% VAF	High sensitivity and multiplexed qPCR platform, effective even on FFPE samples, limited to known variants
MassARRAY System	1–5% VAF	Mass spectrometry-based genotyping; good for multiplexed hotspot detection; sensitivity depends on the sample content
Custom RFLP Analysis	5–10% VAF	Cheap and simple, but sensitivity is limited
qPCR	Standard: ≥5–10% VAF; Specialized: ~0.4% VAF	Cheap and fast turnaround for known CNVs and/or variants. Low sensitivity unless specialized, design-dependent, needs more validation in mosaic settings
Standard short-read WES/WGS	100–200×; ≥5–10% VAF	Limited for low-level mosaics. Useful for higher mosaic fractions or exploratory diagnosis.
Sanger Sequencing	≥10% VAF	Cheap and simple, not suitable for low-level mosaicism
Pyrosequencing	≥5% VAF	Better than Sanger sequencing but still misses <5% VAF

Chapter 2

MATERIALS AND METHODS

2.1. PARTICIPANTS

The patients and/or the families were consulted and followed up at the Medical Genetics Department of Koç University School of Medicine (KUSoM) and the Genetic Diseases Evaluation Center at Koç University Hospital.

2.1.1. Ethical Approval and Informed Consents

All procedures were performed in accordance with the institutional and national ethical standards. All bio-specimens were obtained after written informed consents were signed by the participants or their legal guardians. Studies were reviewed and approved by the Koç University Ethical Committee, Istanbul, Turkey (2015.120.IRB2.047 & 2021.009.IRB2.003). The study on the PROS cohort (Study 1) was partially funded by TUBITAK, with project number 220S492.

2.1.2. Sampling of the Bio-Specimens

- **Blood Samples**: 5-ml peripheral blood sample from each patient and their available family members was collected using vacutainers containing K_2EDTA and/or heparin (BD Vacutainer® or Greiner Bio-One VACUETTE® Blood Collection Tubes).

- **Buccal swap/saliva Samples:** Patients were asked to provide buccal swab samples using a sterile tongue depressor and/or saliva samples using self-guided instructions. In children, the swab was scraped firmly against the inside of each cheek multiple times to collect a sample.

- **Skin Samples:** Following the standard incisional "punch" biopsy procedure, a full-thickness cylindrical tissue sample was taken from the lesioned/affected skin of the patient(s).

- **Formalin-fixed, paraffin-embedded (FFPE) Tissue Samples:** Serial sections of 5 µm (from paraffin blocks) were prepared using a microtome and the resulting sections were placed on glass slides. Excess paraffin around the tissue was scraped off using a sterile scalpel and transferred to a microcentrifuge tube.

2.2. METHODS

2.2.1. Molecular Genetic Analyses

2.2.1.1. DNA isolation

DNA was extracted using either QIAamp DNA Blood Mini Kit, QIAamp DSP Circulating Nucleic Acid Kit, AllPrep DNA/RNA FFPE Kit, or QIAamp DSP DNA FFPE Tissue Kit (Qiagen, Germany) and/or manually, depending on the sample type.

- **Genomic DNA Isolation from Blood Samples** was performed following the manufacturer's instructions using the spin protocol of QIAamp DNA Blood Mini Kit (Qiagen, 2023).

- **Genomic DNA Isolation from Buccal swab and saliva Samples** was established following the manufacturer's instructions using the spin protocol of QIAamp DNA Blood Mini Kit (Qiagen, 2010) with an additional initial centrifugation step at 2500 rpm for 5 minutes.

- **Genomic DNA Isolation from Skin Samples (obtained from Punch Biopsy)** was performed manually by an in-house phenol/chloroform protocol. The tissue was cut into small pieces and placed in a 1.5 mL microfuge tube. 650 µl nuclear lysis buffer (10mM Tris-HCl pH 7.5, 10 mM EDTA pH 7.8, 10 mM sodium citrate, 0.5% Na Deoxycholate, 0.1% sodium dodecyl sulfate (SDS)) was added and vortexed. The sample was incubated overnight at 37°C. After incubation, 175 µl sodium chloride and 950 µl chloroform were added. The mixture was vortexed and centrifuged at full speed (14.500 rpm) for 2 minutes. 650 µl of the upper phase was placed in a clean 2 mL microcentrifuge tube. 1300 µl ice-cold 100% Ethanol was added and mixed by

inverting. Following the centrifugation at full speed (14.500 rpm) for 2 minutes, the supernatant was discarded, and the pellet was air-dried for 2-5 minutes. The pellet was eluted with an appropriate volume (20-30 µL) of Buffer AE (containing 10 mM Tris-Cl; 0.5 mM EDTA; pH 9.0) (Qiagen, USA).

- **Genomic DNA Isolation from Cultured Fibroblasts (derived from Punch Biopsy)** was performed manually by an in-house protocol. Fibroblast cells were scraped from culture flasks, and pellets were obtained by centrifuging the samples at 1500 rpm for 5 minutes. The supernatant was carefully removed, and the cell pellet was resuspended in 250 µL of freshly prepared lysis buffer (400 mM NaCl, 100 mM Tris-HCl pH 8.5, 5 mM EDTA pH 7.8, 0.20% SDS, 0.5 mg/ml Proteinase K). The mixture was then incubated overnight at 37°C to allow complete cell lysis and protein digestion. After incubation, 500 µL of isopropanol was added to the lysate to precipitate the DNA. The mixture was gently vortexed until the DNA formed visible strands. By centrifugation at 14,000 rpm for 3 minutes, the DNA was precipitated to the bottom of the tube. The upper phase was removed, and the tube was air-dried. The pellet was then resuspended in 25-100 µL of TE buffer. If precipitation was not evident, the sample was incubated at room temperature for up to 1 hour and then centrifuged at 13,000 rpm for 30 seconds. The upper phase was again removed, and the final DNA pellet was eluted in an appropriate volume (50-60 µL) of Buffer AE.

- **Genomic DNA Isolation from FFPE tissue samples** was performed following the manufacturer's instructions using the AllPrep DNA/RNA FFPE Kit (Qiagen, 2020) or QIAamp DSP DNA FFPE Tissue Kit (Qiagen, 2017).

- **Circulating DNA isolation from blood plasma samples** was established using the QIAamp Circulating Nucleic Acid Kit with modifications (Figure 2.1), due to the lack of additional instruments specified in the manual (Qiagen, 2019). **Plasma Separation:** Blood samples were centrifuged for 10 min at 1900 x g (3000 rpm) at 4°C setting. Plasma supernatant was aspirated without disturbing the buffy coat layer and transferred into fresh 2 ml centrifuge tubes. Plasma samples were then centrifuged for 10 min at 16,000 x g and 4°C to remove additional cellular nucleic acids attached to cell debris. Supernatants are collected in 15 ml centrifuge tubes. **Purification of Circulating Nucleic Acids from Plasma:** 2 ml serum sample is

added onto 200 µl QIAGEN Proteinase K. Secondly, 1.6 ml Buffer ACL (containing 1.0 µg carrier RNA in Buffer AVE) is added and vortexed for 30 seconds. The mixture is then incubated at 60°C for 30 minutes. 3.6 ml Buffer ACB is added to the lysate in the tube and mixed thoroughly by pulse-vortexing for 30 seconds and incubated for 5 min on ice. Then, 500 ul of the mixture was applied to the QIAamp Mini spin column and centrifuged at 5000 rpm for 5 minutes and the filtrate was discarded. This step is repeated until all the lysate is filtrated. 600 µl Buffer ACW1 was applied to the QIAamp Mini column, centrifuged at 5000 rpm for 5 minutes, and then the lysate in the collection tube was discarded. 750 µl Buffer ACW2 was applied to the QIAamp Mini column, centrifuged at 5000 rpm for 5 minutes, and then the lysate in the collection tube was discarded. 750 µl of 100% ethanol was applied to the QIAamp Mini column, centrifuged at 5000 rpm for 5 minutes, and then lysate in the collection tube was discarded and centrifuged at 14,000 rpm for 3 minutes. QIAamp Mini Column was placed into a new 2 ml collection tube, assembly was air-dried at 56°C for 10 minutes. QIAamp Mini column was placed in a clean 1.5 ml elution tube, and 20 µl of Buffer AVE was added to the center of the QIAamp Mini membrane and incubated at room temperature for half an hour. Finally, DNA is eluted by centrifugation at 14,000 rpm for a minute.

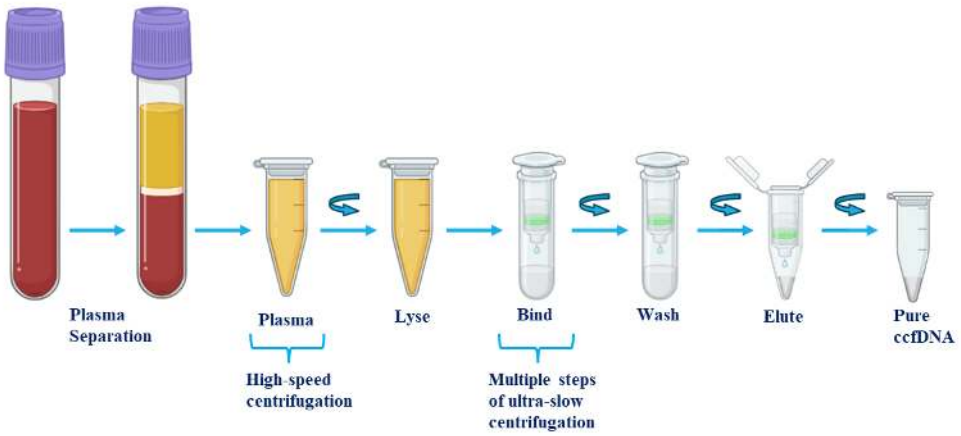

Figure 2-1. **Modified in-house protocol for purification of circulating nucleic acids from plasma** with QIAamp Circulating Nucleic Acid Kit (QIAGEN, Germany).

2.2.1.2. Sample Quality and Storage

Sample quality was checked using NanoDrop™ 2000c microvolume spectrophotometer (Thermo Fisher Scientific, USA). DNA materials with an A260/280 absorbance value of 1.8–2.0, A260/A230 of 2.0–2.2, and a minimum amount of 5 ng/µl were processed. If needed, the DNA isolation procedure was repeated. Blood and plasma samples are kept frozen at –80°C. DNA samples were stored at +4°C (short term) and -20°C (long term).

2.2.1.3. Sanger DNA Sequencing

Specific primer pairs were designed using the NCBI Primer-BLAST tool (Ye et al., 2012) to amplify the variant/region of interest by polymerase chain reaction (PCR). Primer pairs used in this thesis, including forward and reverse primer sequences (5′ to 3′), and their respective TD-PCR annealing temperature (A_T) values are shown in Table 2.1. 100µM stock primers diluted with dH2O to working concentrations of 10µM and 8µM.

Table 2-1. **List of primer pairs designed and used in this thesis**

Study	Gene & NCBI Accession Number	Exon	Primer Pairs (5'to 3')	A_T (°C)
1	*PIK3CA* NM_006218	7	F:AAGGAAAGAATGGGCTTAAACC R: GAGAAGGTTTGACTGCCATAAAA	60-52
2	*PTPN11* NM_002834	1	F: GTCGCGAGCGGTGACATCAC R: TCGGGGAGGCAGGAAATGAATGG	72-55
		2	F: ACTCTGCTCATAATGCGTCTTAGCTG R: GAAATGCAGGCAGCAAGCTATCC	72-55
		3	F: CTTGCCTCCCTTTCCAATGGAC R: GCATTTCTGACACTCAGGGCAC	72-55
		4	F: GAAAGAACAACATGAACCCATAGTAGAGC R: CACCCAAAGGTAACATCTTGCCAG	72-55
		5	F: CTGCACCCAGCCTATTATCTGTC R: CTACCTCTGTATGTTTGCAAAATTCTCTATTAGG	72-55
		6	F: CTATGAACCCTCTGTCCGTGC R: GTTTCAAGTCTCTCAGGTCCAATTCC	72-55
		7	F: CCTTAAAGAAGTAATGCTGATCCAGGC R: CCCTGAGGAAAGGTACAGAGG	72-55
		8	F: GACTAGGCTGGGGAGTAACTG R:GCTAGAAATTTAGGAAGAAAATCCTTCAAACACC	72-55
		9	F: CAGTGTTTTCTGACCATACATTTCTAGCC R: CATGGCCAATCTGACATGTCTGATAC	72-55
		10	F: GCCATTTTCCATGTTGGTGGTTATTAAGC R: GTTCACAATGTACCAGTACTGCTTAAACTG	72-55
		11	F: GCTTAGAACCGGGTGATTCCTC R: CTACAGTTAAAGAGCTAGGAGTGGG	72-55
		12	F: GCTGACTCCAAAGCCCTATGC R: CCCAGACTGTTTTCGTGAGCAC	72-55
		13	F: GTCTCTGAGTCCACTAAAAGTTGTGC R: AGCGTATCCAAGAGGCCTAGC	72-55
		14	F: GTCAATGTATCAGTATTCTCAACCCGTC R: CACCAGTGAAAGGCATGTGCTAC	72-55
		15	F: CCATATCTGGTGCCCAAAGAATGTAG R: CTAAAACATTCCCAAATTGCTTGCCTGC	72-55
3	*BUB1B* NM_001211	21	F:GCAGCTTCTTTCATGGCCTA R: TGGGTGGTAGGCAGTAGGAG	60-52
		1-4	F: TCAAGGCTAGTCCCCTGAAG R: TGGGTGACAGAGTGAGACCTT	60-52
4	*MTOR* NM_004958.3	43	F: AGCCCCTTCCTGGTAGTCTC R: GTCAGAGGAAGTGCACAGCA	60-52
5	*RASA1* NM_002890.2	9	F: GCCATGTATTCTGGCCTGT R: TACCTTCCTCCACGACTGCT	60-52
7	*MFN2* NM_001127660.1	17	F: GCTGCTGGCAGGGATATAGA R: TTTGTGTCCACACCCAAGAC	60-52

8	*TWIST2* NM_001271893.4	1-2	F: AAGGCCCCAGAACTTGTCC R: AGCGTGGGGATGATCTTGC	60-52
			F: GAAGATGGCAGCCCGACC R: CTAAGAGGAAAAGCGCACGG	60-52
			F: GGGCTCTGTTCTCACCACA R: GCGAGATACTGAATGAGCCC	60-52
	FGFR2 NM_000141.5	9	F: TGCGTCAGTCTGGTGTGCTAAC R: AGGACAAGATCCACAAGCTGGC	72-55
		14	F: CTGGCGGTGTTTTGAAATTAG R: CCTTTCTTCCTGGAACATTCTG	60-52
	FGFR3 NM_000142.5	5-7	F: TCCTACACAGGACGGGAAAC R: AACCCCTAGACCCAAATCCTC	60-52
	KRAS NM_004985.5	2	F: GTCCGCTCCGTACCTCTCTC R: GGCCTGCTGAAAATGACTG	60-52
	AKT1 NM_005163.2	2	F: GTTTTCAGACACAGCTCGGG R: CCCAAATCTGAATCCCGAG	60-52
	HRAS NM_005343.4	2	F: GGCAGGAGACCCTGTAGGA R: AGCCCTATCCTGGCTGTGT	72-55
9	*NF2* NM_000268.3	1	F: GCTAAAGGGCTCAGAGTGCAG R: CAAAACCCAAAAGTCCTATGAAAA	60-52
		2	F: AGTCCTCATCAGCTGTCTTAGTGTC R: GCCCCCTTCTCTACTATACAGCTAC	60-52
		3	F: CACAACTTTCAGGAAATGTGATAAA R: AATACAAAGGTGTTTGTGGTCAACT	60-52
		4	F: CATAGCCGTCATACCAGTAACTTCT R: AAACCCAAAGAAAGAGAAGATAGGA	60-52
		5	F: CCATCTCTTACAGGATTATGCAACT R: CCTTTGGTTAGCTTTCTTTTAGACC	60-52
		6	F: TGCATAATTATAAAAGTGGCAAACA R: CGTACTAGAAAAGGACACACACAAA	60-52
		7	F: TGCTTGACCTCAGTGTGTTTAATAG R: ATAAAAGAGTCTATCGCCTTGGAAT	60-52
		8	F: CAGATTCTTTGGAAGGTTGAATAAA R: GTAAAGACTTCGAAAATCAACAACC	60-52
		9	F: GCTCCTAATTCCCTGAGGTTTAGT R: CGCCAAGTGAGATACCATTCTATAC	60-52
		10	F: ATTCATCTTCACGTTTACTGCTACC R: ATAAAACAAGAGCAGGTATGTCCAC	60-52
		11	F: AATAAGAATGACCCTGGCTACCTAA R: GCTAACTCATGGTTTTCAGGAGAC	60-52
		12	F: GTTTGTCCCATCTCAGTGTTCA R: AGCTTGAGGACAACTGCTGTAGA	60-52
		13	F: GTGGTGTCTTTTCCTGCTACCT R: GACAACTAACTAGTCCAAAGCCAAA	60-52
		14	F: ACAGTAGTGTCCTTCTGTGCTTGTA R: TGATTAAGGAAATTCTTCCTCCAG	60-52
		15	F: CTCAAACCCTAGATCGCACAC R: CTAGTGACTTGGCTACTGAGGAAAC	60-52
		16	F: CCAACTTCTTGAGCATCTATTTGA R: GAAATCTCTACAGGGTCGTAGTTCA	60-52

F: forward, R: reverse complement.

2.2.1.3.1. PCR Conditions

Reactions were performed using GoTaq® G2 Flexi DNA Polymerase (Promega, USA), 5X Green GoTaq® Flexi Buffer (Promega, USA), Thermo Scientific dNTP Mix (Thermo Fisher Scientific, USA), MgCl2 Solution (Promega, USA), to amplify genomic DNA. Touchdown PCRs (TD-PCR) were carried out on BioRad T100 and/or Applied Biosystems Veriti thermal cycler in two stages, with annealing performed at the optimal temperatures specific to each primer pair. Reagents and cycling conditions are shown in Tables 2.2 and 2.3, respectively.

Table 2-2. **Reagents for PCR Amplification**

Reagents	Stock Conc.	Final Conc.	Volume (µl) per reaction
5X Green GoTaq® Flexi Buffer	5X	1X	5
Deoxynucleotide triphosphate (dNTP) mix	10 mM each	0.1 mM each	0,25
Forward primer	10 µM	0.2 µM	0,5
Reverse primer	10 µM	0.2 µM	0,5
GoTaq DNA Polymerase	5 U/µl	1.25 U	0,25
MgCl2	25 mM	2 mM	2
Dimethyl sulfoxide (DMSO)	100%	4%	1
DNA			1,5
Deionized water (RNase/DNase-free)			14
Total volume (µl)			**25**

Table 2-3. **Thermal Cycling Conditions for PCR Amplification**

Stage	Step	Temperature	Time	Number of Cycles
1	Initial Denaturation	95°C	3 min	x1
2	Denaturation	93°C	20 sec	x16
	Annealing	60 or 72°C *	25 sec	
	Extension	72°C	50 sec	
3	Denaturation	95°C	15 sec	x20
	Annealing	52 or 55°C *	20 sec	
	Extension	72°C	40 sec	
4	Final Extension	72°C	5 min	x1
	Hold	4°C	Indefinite	x1

*Annealing temperature was optimized for each primer set based on the primer A_T in Table 2.1.

2.2.1.3.2. Agarose Gel Electrophoresis

The amplification reactions were visualized by agarose gel electrophoresis and ethidium bromide (EtBr) staining. 2% agarose gel was

prepared with 0.5X TBE (Tris-borate-EDTA) buffer and EtBr. GeneRuler 1 kb DNA Ladder (Thermo Fisher Scientific, USA) and PCR products were loaded onto the gel. The gel was run at 100-110V for 15-30 minutes [depending on the expected amplicon size] and visualized under UV light using ChemiDocTM MP Imaging System (Bio-Rad, USA).

2.2.1.3.3. Purification of PCR Products

PCR products were purified using ExoSAP-IT™ PCR Product Clean-up Reagent by following the manufacturer's instructions (Thermo Fisher Scientific, 2017).

2.2.1.3.4. Sequencing PCR Conditions

The sequencing reactions were performed using BigDye® Terminator v3.1 Cycle Sequencing Kit with minor modifications to the manufacturer's instructions (Thermo Fisher Scientific, 2024). A 20 µL reaction mixture was prepared as indicated in Table 2.4, and sequencing PCRs were carried out under the conditions described in Table 2.5.

Table 2-4. **Reagents for the Sequencing Reaction**

	Volume per reaction	
Reagents	Forward reaction	Reverse reaction
BigDye™ Terminator 3.1 Ready Reaction Mix	2 µl	2 µl
BigDye™ Terminator v3.1 5X Sequencing Buffer	3 µl	3 µl
Forward primer (8 µM)	4 µl	-
Reverse primer (8 µM)	-	4 µl
Purified PCR product	3 µl	3 µl
Deionized water (RNase/DNase-free)	9 µl	9 µl
Total volume	**20 µl**	**20 µl**

Table 2-5. **Thermal Cycling Conditions for the Sequencing Reaction**

Stage	**Step**	**Temperature**	**Time**	**Number of Cycles**
1	Incubation	96°C	1 min	x1
2	Denaturation	96°C	10 sec	x25
	Annealing	50°C	5 sec	
	Extension	60°C	4 min	
3	Hold	4°C	Indefinite	x1

2.2.1.3.5. Purification of Sequencing PCR Products

Sequencing PCR products were purified using the ZR-96 DNA Sequencing Clean-Up Kit (Zymo, USA), according to the manufacturer's instructions (Zymo Research, 2021).

3.2.1.3.6. Capillary Electrophoresis

Sequencing was performed by Applied Biosystems™ 3500xL Genetic Analyzer (ThermoFisher Scientific, USA).

2.2.1.3.7. Sanger Sequencing Data Analysis

The ABI chromatogram files were analyzed by FinchTV software (Geospiza, Inc., USA). FASTA sequences were aligned by Nucleotide BLAST tool (Altschul et al., 1990) and annotated by Ensembl genome browser (Dyer et al., 2025).

2.2.1.4. Targeted NGS Panel (Oncopanel)

Oncopanel testing was carried out with Illumina TruSight Hereditary Cancer Panel, which targets 113 genes and 125 SNPs (Illumina, Inc., San Diego, CA, USA) associated with genetic predisposition to cancer. The complete list of targeted genes is available online (Illumina, n.d.). Targeted genomic DNA regions were enriched using hybrid capture probes, and indexed libraries were prepared according to the manufacturer’s instructions. Sequencing was conducted on the Illumina MiSeq platform with the MiSeq Reagent Kit v2 (Illumina, Inc., USA). Raw reads were mapped against the human reference genome GRCh37/hg19, and variant calling was performed using Illumina BaseSpace DRAGEN Enrichment App. Quality-filtered single nucleotide variants (minimum of ×20 coverage) were annotated using QIAGEN Clinical Insight (QCI) Interpret software. Intronic variants located outside the boundaries of 10 bp from the exons and synonymous exonic ones were filtered out. Putative splicing variants were analyzed using Human Splicing Finder (HSF).

2.2.1.5. Targeted NGS Panel (VANSeq)

Targeted NGS panel targeting 13 genes associated with lymphatic/venous/arteriovenous malformations (*ACVRL1, ARAF, BRAF, ELMO2,*

ENG, EPHB4, GDF2, GLMN, HRAS, KRAS, MAP2K1, MAP3K3, NRAS, PIK3CA, PTEN, RASA1, TEK (TIE2) genes) was performed at Seattle Children's Hospital Molecular Genetics Laboratory, USA. Sequencing was performed using NextSeq (Illumina Inc., USA), aiming for all coding exons and at least 10 bp of intronic sequence flanking each coding exon of the genes tested. Target enrichment is performed using a custom-designed panel (Integrated DNA Technologies Inc, USA). Informatics tools (Novoalign v2.08.02, samtools (mpileup) v0.1.19, Freebayes v0.9.21, GATK v1.2, Pindel v0.2.4d) and the databases (GRCh37.p13, NCBI RefSeq v105, NHLBI ESP v.0.0.30, dbSNP 149, ClinVar 20190307, dbNSFP 3.5c, ExAC v1.0) were used to perform and evaluate the sequence data with pipeline version 1.0.11.

2.2.1.6. Whole Exome Sequencing (WES)

WES was performed at CENTOGENE GmbH (Rostock, Germany). Genomic DNA was enzymatically fragmented, and target regions were enriched using DNA capture probes. These regions included approximately 41 Mb of the human coding exome (targeting > 98% of the coding RefSeq from the human genome build GRCh37/hg19), as well as the mitochondrial genome. The generated library was sequenced on an Illumina platform to obtain at least 20x coverage depth for > 98% of the targeted bases (Trujillano et al., 2017). An in-house bioinformatics pipeline, including read alignment to Genome Reference Consortium Human Build 37 (GRCh37/hg19) and Revised Cambridge Reference Sequence (rCRS) of the Human Mitochondrial DNA (NC_012920), variant calling, annotation, and comprehensive variant filtering was applied. Investigation for relevant variants is focused on coding exons and flanking +/-10 intronic nucleotides of genes with clear gene-phenotype evidence (based on OMIM® information).

2.2.1.7. Whole Genome Sequencing (WGS)

WGS was performed at CENTOGENE GmbH (Rostock, Germany). Genomic DNA was enzymatically fragmented, and libraries were generated by PCR-mediated addition of Illumina-compatible adapters. The libraries are paired end sequenced on an Illumina platform to yield an average coverage depth of ~30x. An in-house bioinformatics pipeline was applied. The sequencing reads were aligned to

the GRCh37/hg19 genome assembly, as well as the rCRS of the Human Mitochondrial DNA (NC_012920). Structural variant calling was based on the DRAGEN pipeline from Illumina. The complete gene region was interrogated for candidate variants with plausible association to the phenotype, although the evaluation is focused on coding exons and flanking +/-20 intronic regions.

2.2.1.8. SNP-array

The SNP array adopted was 300K HumanCytoSNP-12v2-1 (Illumina Inc., USA). Genomic positions were based on the human reference genome GRCh37/hg19. The raw data were processed and analyzed using Illumina GenomeStudio, Illumina KaryoStudio, and/or BlueFuse Multi software packages. The resolution threshold was set at 200 Kb for copy number gains and 100 Kb for losses. Detected variants were included in the analysis if identified by at least 25 oligonucleotide probes on the array matrix.

2.2.1.9. Multiplex Ligation-Dependent Probe Amplification (MLPA)

MLPA and methylation-specific MLPA (MS-MLPA) reactions were performed according to the manufacturer's instructions (MRC Holland, 2024; 2025) with SALSA® MLPA® probe mixes (MRC Holland, Netherlands). Probe-mixes used are listed in Table 2.6. Fragmentation analyses were performed on Applied Biosystems™ 3500xL Genetic Analyzer (ThermoFisher Scientific, USA). *.fsa files were analyzed using Coffalyser.Net™ software (MRC Holland, Netherlands).

Table 2-6. **List of probe-mixes used in MLPA reactions**

Study	Probemix	Targeted Genes/Region	Targeted Syndrome	Techniq ue
1 (only for patient PIK3CA2)	P043-E1	*APC* 5q22.2; *MUTYH* 1p34.1; *GREM1* 15q13.3	Hereditary Cancer Susceptibility	MLPA
	P002-D1	*BRCA1* 17q21.31		
	P045-D1	*BRCA2* 13q13.1; *CHEK2* 22q12.1		
2	ME030-C3	*H19, IGF2, CDKN1C, KCNQ1* 11p15 region	RSS	MS-MLPA
6	P081-C1 P082-C1 P122-C2	*NF1* 17q11.2	NF1	MLPA
10	P081-D1 P082-C2			

2.2.1.10. Real-Time PCR (qPCR)

Real-time PCR analysis was performed for the qualitative detection of hotspot mutations of the *PIK3CA* gene on (i) gDNA extracted from FFPE tissue and/or skin biopsy and/or (ii) gDNA extracted from buccal swap or saliva samples; and (iii) ccfDNA isolated from plasma derived from K_2EDTA anticoagulated peripheral venous whole blood.

The *therascreen* PIK3CA RGQ PCR Kit (QIAGEN, Germany) is comprised of six reaction mixes; one control reaction targeting exon 15 and five hotspot mutation-specific reactions were utilized to detect 11 mutations in exons 7, 9 and 20 of the *PIK3CA* gene [Exon 7: C420R; Exon 9: E542K; E545A, E545D (1635G>T only), E545G, E545K, Q546E, Q546R; and Exon 20: H1047L, H1047R, H1047Y] (Table 2.7).

qPCR reactions were set up according to the manufacturer's instructions (Qiagen, 2020) on the Rotor-Gene Q MDx 5plex HRM instrument. Analysis was performed manually using Rotor-Gene AssayManager® version 2.1, Gamma Plug-in version 1.0.0, PIK3CA_Tissue_RUO Assay Profile version 1.0.1 and PIK3CA_Plasma_RUO Assay Profile version 1.0.0 (QIAGEN, Germany) by examining high-resolution melting (HRM) curves and CT values.

Table 2-7. **Targeted *PIK3CA* hotspot mutations by qPCR**

Exon	Nucleotide Change	Amino Acid Change	
7	c.1258 T>C	C420R	p.Cys420Arg
9	c.1624 G>A	E542K	p.Glu542Lys
	c.1634 A>C	E545A	p.Glu545Ala
	c.1635 G>T	E545D	p.Glu545Asp
	c.1634 A>G	E545G	p.Glu545Gly
	c.1633 G>A	E545K	p.Glu545Lys
	c.1636 C>G	Q546E	p.Gln546Glu
	c.1637 A>G	Q546R	p.Gln546Arg
20	c.3140 A>T	H1047L	p.His1047Leu
	c.3140 A>G	H1047R	p.His1047Arg
	c.3139 C>T	H1047Y	p.His1047Tyr

2.2.1.11. Pathogenicity Evaluation and Reporting of the Variants

Detected variants were interpreted under five categories, as pathogenic (P), likely pathogenic (LP), uncertain significance (VUS), likely benign (LB), and benign (B) according to the ACMG/AMP guidelines and ClinGen recommendations. Each pathogenic criterion is weighted as very strong (PVS1), strong (PS1–4); moderate (PM1–6), or supporting (PP1–5) and each benign criterion is weighted as stand-alone (BA1), strong (BS1–4) or supporting (BP1–6) (Richards et al., 2015).

Minor allele frequency (MAF) filter (< 0.01) was set based on ExAC, dbSNP, gnomAD, and 1000G data. Pathogenicity evaluation was performed based on the inheritance mode, database entries (HGMD, ClinVar), commercial services (Genoox Franklin, Varsome) *in silico* prediction tools (SIFT, Polyphen2, MutationTaster). The clinical information and family history were used to evaluate identified variants for their pathogenicity and disease-causality. All potential modes of inheritance are considered. Human Phenotype Ontology (HPO) terms were also adopted to classify the patient phenotypes. All relevant P/LP/VUS variants related to the phenotype of the patient are reported.

In line with the ACMG/AMP variant interpretation guidelines, the terms "pathogenic variant" and "likely pathogenic variant" were considered synonymous, and both are disease-causing. Identification of a VUS was not regarded as sufficient to establish or rule out a diagnosis (Richards et al., 2015).

2.2.2. Cytogenetic Analyses

Cytogenetic studies were performed on cultured fibroblasts from skin biopsy samples in parallel to the peripheral blood lymphocyte cultures using standard cytogenetic methods at the 400-550 band level. Cells were grown in two independent cultures for each cell type to distinguish true mosaicism from Level II pseudomosaicism. Cytogenetic analyses and the karyotypic designation were done according to the recommendations of the International System for Chromosomal Nomenclature (ISCN) (McGowan-Jordan et al., 2020).

2.2.2.1 Cell Culturing

2.2.2.1.1. Fibroblast Cultures

The skin biopsy samples were cut into small pieces (0.5-1 mm) by using sterile surgical razor blades. 3-5 ml Collagenase IV was added to the minced tissue and incubated at 37°C for an hour. After incubation, the cells were collected in a Falcon tube and washed with filtered Dulbecco's Modified Eagle Medium/Nutrient Mixture F-12 (DMEM/F12) (5 ml medium was added, cells were resuspended and centrifuged at 1,200 rpm for 10 minutes, supernatant was discarded). The cells were resuspended with medium and transferred onto a petri dish. Then, 3-5 ml of trypsin was added, and the cells were incubated at 37°C for an additional 1,5 hours. Following incubation, cells were washed with medium twice. Then, the cells were seeded onto the T25 flask to be expanded in culture. Fibroblast cells were incubated at 37°C with 5% CO_2 and treated with DMEM/F12 (Thermo Fisher Scientific, USA) supplemented with 10% fetal bovine serum (FBS, Heat Inactivated) (GE Healthcare, USA) and 1% penicillin/streptomycin (Thermo Fisher Scientific, USA). Cell lines were routinely tested for Mycoplasma contamination using the MycoAlert Mycoplasma Detection Kit (Lonza, Switzerland). The growth of fibroblasts was observed under the microscope daily, and the medium was changed once every two days. When the cells reached greater than 70% confluency, they were either passaged or cryopreserved, and, if planned, were also prepared for karyotyping and/or DNA isolation.

For passaging, cells were washed with medium, and 2 ml of 0.05% Trypsin/0.53mM EDTA (Wisent Inc, Canada) was added. The cultures were then incubated for 5 minutes at 37 °C to detach the cells, which were then resuspended with fresh medium and transferred to a 15 ml conical tube. The cell suspension was centrifuged at 300 × g for 5 minutes at room temperature, and the supernatant was discarded. The cell pellet was resuspended in fresh medium and passaged at a 1:3 ratio to new culture flasks.

For cryopreservation, cells were suspended in freezing medium containing 90% DMEM/F12 and 10% DMSO and then transferred into cryovial tubes (Corning, USA). The vials were placed and stored in a

controlled-rate freezing container filled with isopropyl alcohol (Mr. Frosty™ Freezing Container, Thermo Fisher Scientific, USA) and stored at −80 °C overnight before being transferred to liquid nitrogen for long-term storage.

For karyotyping, Colcemid Solution (10 µg/ml in DPBS; Capricorn Scientific, Germany) was added directly to the culture medium at a final concentration of 0.1 µg/ml, and cultures were incubated for 2–3 hours at 37 °C. Cells were washed with DPBS and detached using 0.05% trypsin–EDTA (Wisent Inc., Canada) for 5 minutes at 37 °C. The subsequent steps are described in Section 2.2.2.2.

2.2.2.1.2. Lymphocyte Cultures

Peripheral blood lymphocytes were cultured with ChromosomeSynchro Kit (EuroClone, Italy) for subsequent chromosome analysis. 0,3-0,5 ml of heparinized blood sample was cultured in 15 ml Falcon tubes containing 5 ml of complete Chromosome P medium and incubated at 37°C with 5% CO_2 for 72 hours. To synchronize cells at the prometaphase to obtain longer chromosomes suitable for analysis, solution A (containing methotrexate) was added at the 48th hour, and solution B (containing thymidine) was added at the 68th hour. For karyotyping, at the 72nd hour, 0.1 ml of Colcemid Solution (10 µg/ml in DPBS, Capricorn Scientific, Germany) was added to arrest cells at the metaphase stage. The cells were incubated at 37°C for 30 minutes and then harvested. The subsequent steps are described in Section 2.2.2.2.

2.2.2.2. Harvesting and Fixation of Cells

The cell suspensions were collected, transferred to conical tubes, and centrifuged at 300 × g for 5 minutes at room temperature. The supernatant was discarded, and the pellet was gently resuspended in pre-warmed (37 °C) hypotonic 0.075 M potassium chloride (KCl) solution. Following incubation at 37 °C for 25-30 minutes, the cells were centrifuged again at 1200 × g for 10 minutes. The supernatant was removed, and the pellet was carefully agitated by adding 5-10 ml of fresh, ice-cold fixative solution (one part acetic acid to three parts methanol) drop by drop while gently mixing. The suspensions were kept at 4 °C for 10 minutes and centrifuged once more. Fixation was repeated at least twice to ensure optimal

chromosomal preservation. Finally, the fixed cell suspensions were resuspended in a small volume (0.5–1 ml) of fresh fixative, and several drops were placed onto clean microscope slides. The slides were allowed to air-dry in Optichrome Plus® humidity chamber (Erma Inc., Japan) at 22°C with 48% relative humidity and stored at 36°C overnight.

2.2.2.3. Karyotyping

Following the overnight incubation, slides were aged by UV-treatment for one minute with ChemiDocTM MP Imaging System (Bio-Rad, USA). Slides were then treated with pancreatine at 42°C for 15-17 seconds and stained for 3 minutes with Leichmann's stain, with two dH2O washing steps in between. Slides were air-dried, and metaphase images were captured and then analysed using CytoVision GSL120 platform (Leica Microsystems, Germany). The general protocol for karyotyping is summarized in Figure 2.2.

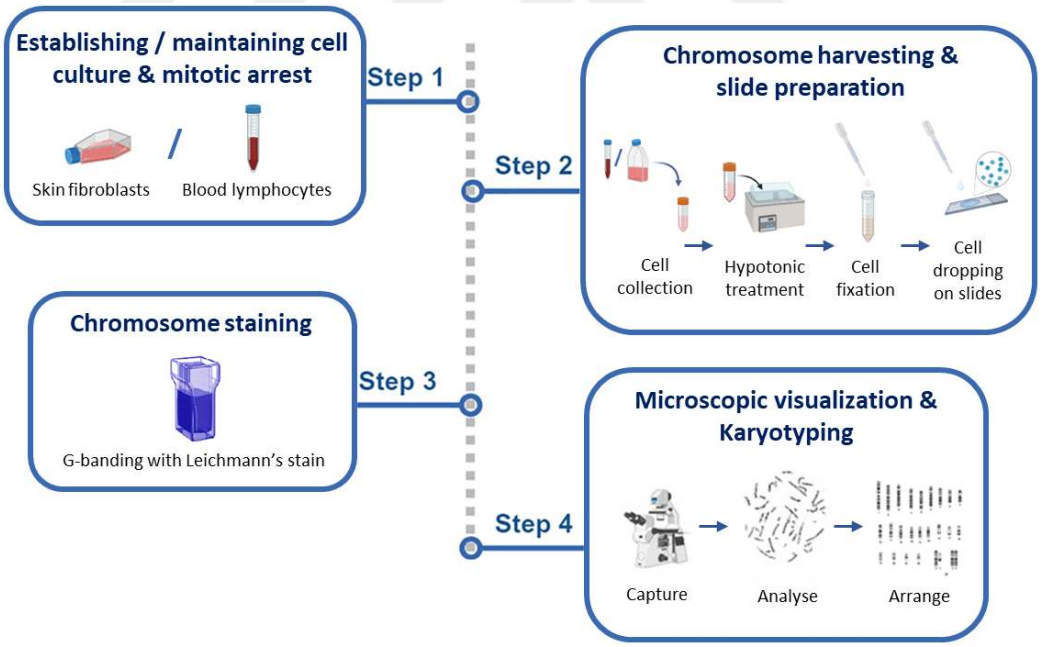

Figure 2-2. **Overview of the karyotyping workflow**, involving four main steps. Step 1: Establishment and maintenance of cell cultures from either skin fibroblasts or peripheral blood lymphocytes, followed by mitotic arrest with Colcemid. Step 2: Chromosome harvesting and slide preparation, which includes cell collection, hypotonic treatment, fixation, and slide preparation. Step 3: G-banding with Leichmann's stain to visualize distinct chromosomal banding patterns. Step 4: Microscopic visualization and karyotyping to analyze structural or numerical chromosome abnormalities.

2.2.2.4. Fluorescent In Situ Hybridization (FISH) on Fibroblast Metaphases

Fibroblast cells were prepared for metaphase FISH as previously described in sections *2.2.1.1* and *2.2.2.2.* The general protocol for iFISH is illustrated in Figure 2.3.

The slides were incubated in 2× standard saline citrate (SSC) for 5 minutes and then dehydrated by immersion in a graded ethanol series (70%, 85%, and 100%) for 2 minutes each and allowed to air-dry completely (Thermo Fisher Scientific, USA). 7 µl of probe solution (Cytocell, UK) was applied to the target area on each slide (with a minimum of two replicates for each probe). The samples were covered with 22×22 mm coverslips, ensuring that no air bubbles were trapped, and sealed with Fixogum rubber cement. The slides were then denatured at 75 °C for 3 minutes on a heat block, then incubated in a light-protected, humidified chamber overnight (16–18 hours) at 37 °C for hybridization. After hybridization, the coverslips were carefully removed, and the slides were washed in preheated 0,4×SSC at 71.5 °C for 40-45 seconds. A second wash was performed in freshly prepared 2× SSC with 0,005 ml Tween 20 for 2 minutes. The slides were then briefly dried using absorbent paper. 8-10 µl of DAPI (Cytocell, UK) was applied to each target area, and a 22×22 mm coverslip was placed on top without trapping air bubbles. Finally, the slides were incubated at -20 °C for 20 minutes and then analyzed under a fluorescence microscope.

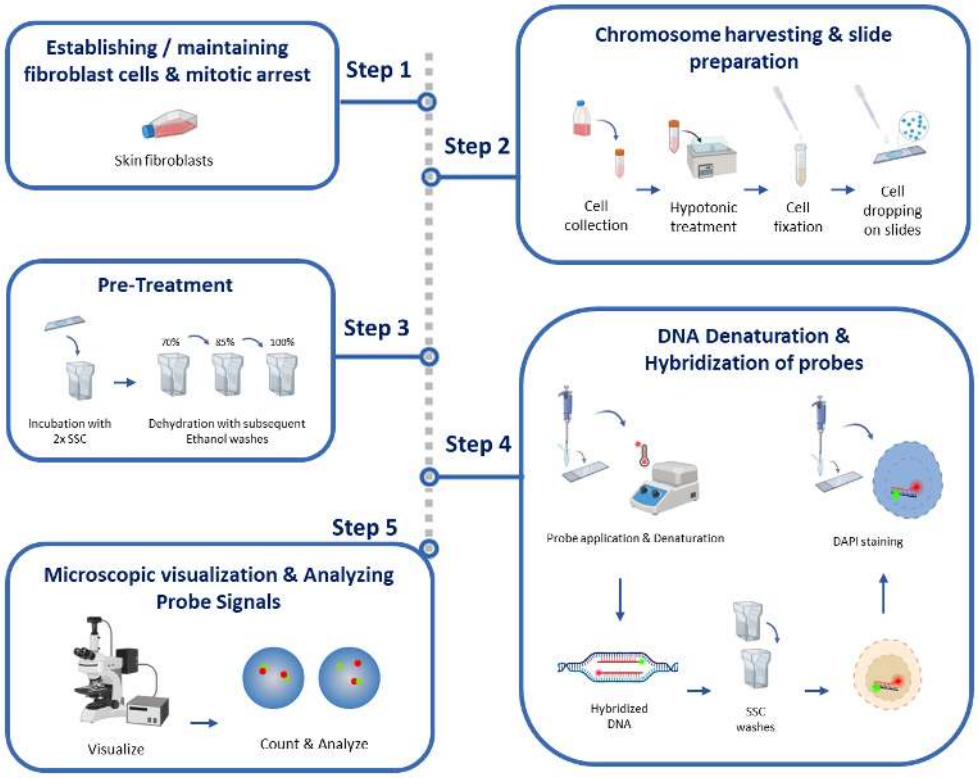

Figure 2-3. **Overview of the iFISH workflow**, involving five main steps. Step 1: Maintenance of fibroblast cell cultures, followed by mitotic arrest; Step 2: Chromosome harvesting and slide preparation, Step 3: Pre-treatment with 2xSSC and dehydration with graded ethanol washes; Step 4: DNA denaturation and hybridization of fluorescently labeled FISH probes to targeted loci, followed by counterstaining with DAPI; Step 5: Fluorescent microscopy and signal analysis to count and interpret probe binding patterns, in order to detect chromosomal abnormalities.

Chapter 3

RESULTS & DISCUSSION

STUDY 1

PIK3CA-Related Overgrowth Spectrum Syndromes: Well-Defined Yet Underdiagnosed Mosaicism

Background

Tissue proliferation is a tightly regulated process from embryonic development through the adult life. One of the main regulators of cell proliferation is the PI3K/AKT/mTOR signaling pathway. Phosphoinositide 3-kinase (PI3K), one of the three primary components of the PI3K/AKT/mTOR pathway, are members of a highly conserved lipid kinase family that phosphorylate the 3β-hydroxyl group of the inositol ring on phosphatidylinositol (Paplomata & O'Regan, 2014), and play a crucial role in facilitating the activation of downstream effectors such as Protein Kinase B (AKT) and the mammalian target of rapamycin (mTOR).

PI3Ks are classified into three main groups based on sequence homology, substrate specificity, and tissue distribution (Class I-III) (Mukohara, 2015). Class I PI3Ks are the most studied group, as they are activated directly by cell surface receptors. Although there is no clear idea about the specific cellular functions of class II, it is known that class III is an important regulator of membrane traffic, cell growth and autophagy processes. Class I phosphoinositide 3-kinases (PI3Ks) are further divided into IA and IB subclasses and function as heterodimers composed of a p85 regulatory subunit and a p110 catalytic subunit (Cantley, 2002; Ligresti et al., 2009). The genes

PIK3CA, *PIK3CB*, and *PIK3CD* encode three highly homologous class IA catalytic isoforms: p110α, p110β, and p110δ, respectively. These isoforms associate with one of the five regulatory subunits: p85α (along with its splicing variants p55α and p50α, encoded by *PIK3R1*), p85β (*PIK3R2*), and p55γ (*PIK3R3*).

Upon binding of growth factors, such as epidermal growth factor (EGF) or insulin-like growth factor 1 (IGF-1), receptor tyrosine kinases (RTKs) or G protein-coupled receptors (GPCRs) become activated and recruit the p85-p110 PI3K complex to the plasma membrane. The p85 regulatory subunit binds phosphorylated tyrosine residues on activated receptors, facilitates the activation of the p110 catalytic subunit. Subsequent activation of the catalytic p110 subunit converts phosphatidylinositol-4,5-bisphosphate (PIP2) to phosphatidylinositol-3,4,5-trisphosphate (PIP3) (Zhao & Vogt, 2008). PIP3 then becomes a binding target for the pleckstrin homology (PH) domains of the 3-phosphoinositide-dependent protein kinase 1 (PDPK1) and AKT at the plasma membrane. PDK1 phosphorylates and partially activates AKT at the catalytic phosphorylation site (Thr308). Full activation of AKT is achieved upon additional phosphorylation at serine 473 (Ser473), typically mediated by the mTOR complex 2 (mTORC2). Activated AKT inhibits the tuberous sclerosis protein complex (TSC1/TSC2), allowing the Rheb GTPase to bind and directly activate mTOR complex 1 (mTORC1). As a result, various cellular functions such as cell proliferation, protein translation and autophagy occur with the activation of ribosomal protein S6 kinase 1 (S6K1) and 4E binding protein 1 (4E-BP1), which stimulate the onset of protein biosynthesis and ribosome biogenesis (Engelman, 2009).

Hyperactivation of the PI3K/AKT/mTOR pathway, which is regulated by multiple feedback mechanisms and cross-talks with the RAS/MAPK pathway, leads to significant dysregulation of cellular functions, leading to a competitive growth advantage and angiogenesis. Gain or loss-of-function mutations in genes involved in the pathway have been associated with many different solid and hematological tumors. It is estimated that 70% of all breast carcinomas are activated due to genetic alterations in the PI3K/Akt/mTOR signaling pathway (Miller et al., 2011). Common alterations include p110 alpha activating mutations (*PIK3CA*), *PTEN* loss, and *AKT* mutations (Ligresti et al., 2009; Madsen et al., 2018).

The *PIK3CA* gene encodes the p110 alpha subunit of class IA PI3K. Pathogenic alterations in *PIK3CA*, the most frequently mutated gene after *TP53* in human somatic cancers, have been associated with more than 12 types of solid cancer: primarily breast cancer (>30% in all cases), endometrial cancer (>30%), bladder cancer (>20%), colorectal carcinoma (>17%), and head and neck squamous cell carcinoma (>15%) (Madsen et al., 2018; Alqahtani et al., 2019). In addition to the well-characterized role of *PIK3CA* in cancer, postzygotic somatic variants in *PIK3CA* are associated with a group of benign skin lesions and overgrowth disorders. Driver mutations in the *PIK3CA* gene, which have been linked to conditions such as epidermal nevi and seborrheic keratosis, have also been found in cases of segmental overgrowth (Hafner et al., 2007; Keppler-Noreuil et al., 2014; Luks et al., 2015). These GoF mutations lead to hyperactivation of the PI3K signaling pathway, as well as the downstream AKT1 and RAS/RAF/MAPK pathways, and result in segmental, often asymmetric overgrowth of various tissues, including fat, nerve, muscle, skin, bone, and both blood and lymphatic vessels. Since the primary determinant of the phenotype is the timing and location of the pathogenic mutation during the postzygotic process, the patients present with heterogeneous clinical manifestations (Figure 3.1).

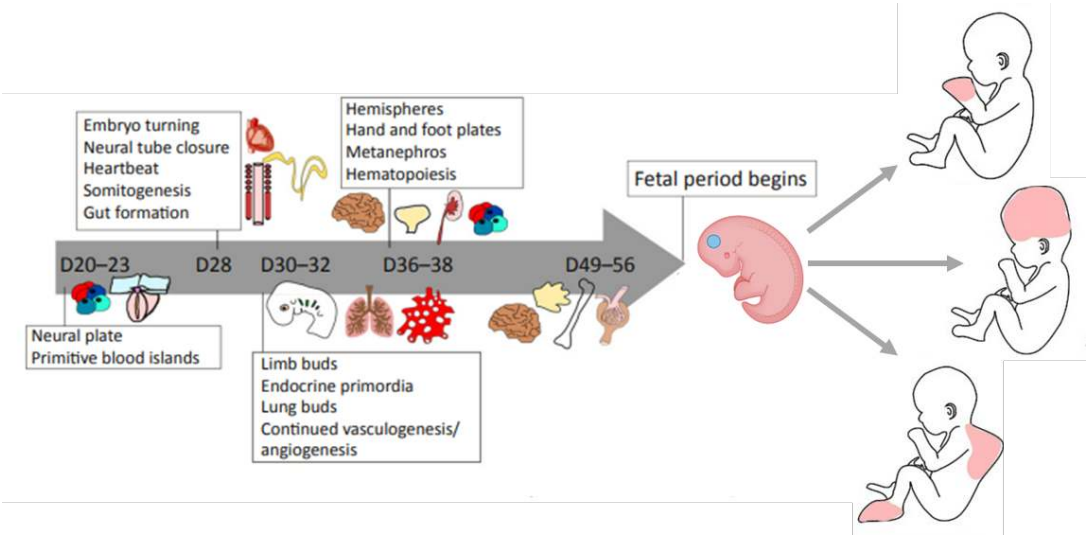

Figure 3-1. **Developmental timing and anatomical location of postzygotic *PIK3CA* variant determine the phenotype.** Modified from Madsen et al., 2018.

Prior to the identification of the molecular nature, clinically distinct but overlapping phenotypes were described. Given the significant variability among patients, disagreements in classifications, and the absence of established diagnostic

criteria, has often led to the misdiagnosis of cases within this group, with many being simplistically classified as "Proteus/Proteus-like" syndromes. Since 2014, the umbrella term of "***PIK3CA*-Related Overgrowth Spectrum (PROS)"** has been used to encompass both the known and emerging clinical entities associated with postzygotic somatic mutations in the *PIK3CA* gene (Keppler-Noreuil et al., 2014).

It is difficult to estimate the prevalence of PROS due to its relatively recent characterization in the literature, rarity, broad phenotypic spectrum, and atypical/mild phenotypes that can lead to misdiagnosis (Mirzaa et al., 2013; Keppler-Noreuil et al., 2014). Based on the number of patients seen in the clinic, the incidence rate is estimated to be approximately 1 in 70,000. The estimated prevalence of the following five combined PROS conditions is about 14 per million patients: MCAP syndrome, hemihyperplasia multiple lipomatosis, macrodactyly, fibroadipose hyperplasia, and KTS. Moreover, technical challenges and limitations in molecular diagnosis often prevent affected individuals from receiving a definitive diagnosis.

Clinical Spectrum and Diagnostic Criteria of PROS

The clinical spectrum of PROS includes, but not limited to: Megalencephaly-capillary malformation (MCAP) syndrome (Rivière et al., 2012), Congenital lipomatous overgrowth, vascular malformations, epidermal nevi, scoliosis/skeletal and spinal (CLOVES) syndrome (Sapp et al., 2007; Alomari, 2009; Kurek et al., 2012), Dysplastic megalencephaly (DMEG), hemimegalencephaly (HMEG) (Lee et al., 2012), focal cortical dysplasia (FCD) (Jansen et al., 2015), capillary malformation of the lower lip, lymphatic malformation of the face and neck, asymmetry and partial/generalized overgrowth (CLAPO) syndrome, KTS (Klippel-Trenaunay syndrome) (Kurek et al., 2012; Luks et al., 2015), Fibroadipose hyperplasia or overgrowth (FAO) (Lindhurst et al., 2012), Hemihyperplasia multiple lipomatosis (HHML) (Biesecker et al., 1998), Macrodactyly, Fibroadipose infiltrating lipomatosis / facial infiltrative lipomatosis and isolated tissue dysplasia-overgrowth phenotypes (lymphatic malformations, vascular malformations, venous malformations, lipomatosis) (Figure 3.2).

Although defined as different clinical entities, these syndromes share broad and overlapping features. They are primarily characterized by congenital or early childhood-

onset of segmental or focal overgrowth with or without cellular dysplasia, often accompanied by vascular malformations, skin lesions, and acral anomalies in various body parts and tissues. Asymmetric, segmental overgrowth usually starts in infancy and progresses, predominantly on the brain, limbs (including fingers and toes), trunk (including abdomen and chest), and face. In some lesions, overgrowth can be limited to childhood. Yet, in some cases, intrauterine overgrowth has been reported (Keppler-Noreuil et al., 2014; Mirzaa et al., 2016).

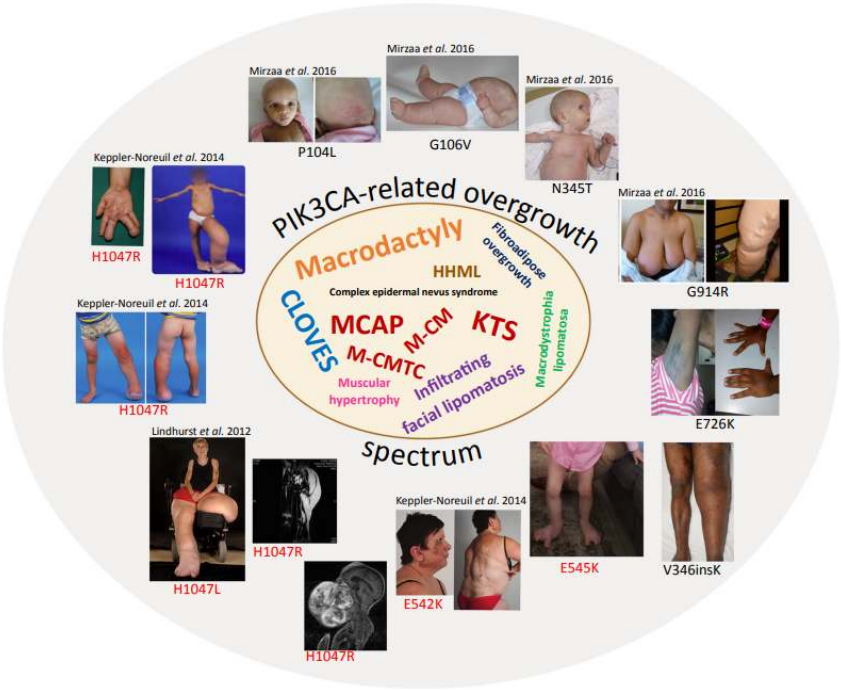

Figure 3-2. **Clinical presentations within PROS**. Representative images showing various phenotypes. The causal *PIK3CA* mutation identified in each case is listed below each image, with hotspot mutations highlighted in red. Adapted from Madsen et al., 2018.

Tissues in the affected overgrowth can include all or some of these types: fibrous, adipose, vascular, nervous and skeletal. Vascular malformations may be capillary, venous, and less frequently, arterial or mixed (capillary-lymphatic-venous or arteriovenous) malformations. Lymphatic malformations may be internal and/or external and can be associated with problems, including swelling, pain, and occasionally localized bleeding secondary to trauma. Lipomatous overgrowth may occur ipsilateral or contralateral to a vascular malformation, if present. Generalized brain overgrowth may be accompanied by secondary overgrowth of specific brain structures, resulting in

ventriculomegaly, thick corpus callosum, and cerebellar tonsillar ectopia with crowding of the posterior fossa.

Complications associated with PROS depend on the anatomical site and extent of overgrowth, but may include functional impairment (e.g., of walking or swallowing), pain, cardiac dysfunction, pulmonary hypertension, seizures, impaired neurological development, recurrent superficial infections, thromboembolism and/or hemorrhage, amongst other manifestations. These complications can be debilitating and may contribute to early mortality.

Table 3-1. **Clinical Diagnostic Criteria for PROS.** Adapted from Keppler-Noreuil et al., 2015.

Required findings	- Presence of somatic *PIK3CA* mutation* - Congenital or Early Childhood Onset - Sporadic and Mosaic (Patchy, Irregular) Overgrowth - Features as described in either A or B
A. Spectrum findings (two or more features)**	- Overgrowth: Adipose, Muscle, Nerve, Skeletal - Vascular Malformations: Capillary, Venous, Arteriovenous, Lymphatic - Epidermal Nevus
B. Isolated findings (one isolated and more tissue-specific feature)	- Large Isolated Lymphatic Malformation - Isolated Macrodactyly*** or Overgrown Splayed Feet/ Hands, Overgrown Limbs - Truncal Adipose Overgrowth - Hemimegalencephaly (bilateral)/ Dysplastic Megalencephaly/ Focal Cortical Dysplasia - Epidermal nevus - Seborrheic Keratoses - Benign Lichenoid Keratoses

* If no mutation is identified, considered as presumptive PROS.
** Typically Progressive. Can manifest as: Scoliosis (Kyphosis), Limb overgrowth, CNS (HC, Cerebellar tonsillar ectopia, Chiari, Megalencephaly, Mega corpus callosum, Regional lipomatous undergrowth with overgrowth, Infiltrating lipomatosis, Wilms tumor/ovarian cystadenoma.
*** Other terms: macrodystrophia lipomatosa, macrodactylia fibrolipomatosis and gigantism.

The diagnostic criteria for PROS include a spectrum of disease features and identification of a mosaic pathogenic variant in *PIK3CA* (Table 3.1). While the spectrum of findings is broad, **required findings** are deemed as comprehensive as possible across all related clinical entities and include the presence of a mosaic *PIK3CA* mutation, congenital or early childhood onset, and patchy/irregular overgrowth (Keppler-Noreuil et al., 2015). Although most patients experience a progressive course, this is not universally required, as individuals may present with **isolated features** (focal lesion that affects only

one tissue or location, such as lymphatic malformation or macrodactyly) and/or a range of **syndromic features** (at least two of the following: segmental overgrowth, vascular malformation, and epidermal nevus).

Treatment/Therapy

Historically, the management of PROS has been limited to supportive and surgical interventions, which frequently yield only temporary benefits and are associated with significant morbidity. Treatment options primarily rely on debulking surgery or amputation, sclerotherapy, endovascular occlusive procedures, and symptomatic treatment. However, regrowth of the tissue after surgery is common and often necessitates repeated surgical interventions. The mTOR inhibitor sirolimus was used off-label in PROS patients as a therapeutic approach, but its clinical benefit was limited, with partial or no response in some cases. Moreover, adverse effects such as immunosuppression, increased infection risk, and impaired wound healing was observed (Parker et al., 2019). Thus, there was a need for targeted, novel therapeutic approaches and more effective treatments.

Development of PI3K/AKT/mTOR Inhibitors in PROS

The efficacy and safety of the mTOR inhibitor Sirolimus were initially tested in patients with complex vascular anomalies and later in those with PROS. The treatment demonstrated clinical benefits in reducing overgrowth; however, it also presented notable side effects, necessitating careful consideration of the risks and benefits (Adams et al., 2016; Parker et al., 2019).

The pan-AKT inhibitor, miransertib (ARQ 092), has also showed preliminary signs of clinical activity in patients with PROS and Proteus Syndrome, with generally manageable safety concerns (Leoni et al., 2019). Similarly, the identification of GoF mutations in PI3K pathway has generated interest in targeting this pathway through the inhibition of *PIK3CA.* The trial of Taselisib, a selective class I PI3K inhibitor targeting the p110α isoform, was terminated early due to safety concerns (ClinicalTrials.gov, 2017). Overall, these early results supported the need for further investigation into targeted therapies for these rare overgrowth disorders.

Overview of Alpelisib: Preclinical Studies

Alpelisib (BYL719) is an oral PI3K inhibitor from the 2-aminothiazole class that selectively targets the p110α subunit (IC50 = 4.6 nM), showing ≥50-fold higher potency for p110α than other class I PI3K isoforms (e.g. p110β IC50 = 1156 nM, p110δ IC50 = 290 nM, p110γ IC50 = 250 nM) and minimal activity against most other kinases (Fritsch et al., 2014). Alpelisib has demonstrated potent antitumor activity in cancer models harboring *PIK3CA* mutations (Keegan et al., 2018) and has shown efficacy with a favorable safety profile in clinical trials involving tumors with *PIK3CA* alterations (Juric et al., 2018; Hoste et al., 2018). Moreover, Alpelisib was approved to be used in combination with the endocrine therapy fulvestrant, to treat postmenopausal women and men with hormone receptor (HR)-positive, human epidermal growth factor receptor 2 (HER2)-negative, *PIK3CA*-mutated, advanced or metastatic breast cancer following progression on or after an endocrine-based regimen by the U.S. FDA (2019).

Given the shared somatic *PIK3CA* mutations driving cell proliferation in PROS, Alpelisib was hypothesized as a promising therapeutic candidate. For this, a PROS/CLOVES mouse model (PIK3CACAGG-CreER) was used, and treatment with alpelisib significantly improved survival and reduced tissue overgrowth and vascular malformations. Histological analysis showed preserved tissue structure and decreased cell proliferation in treated mice, whereas untreated mice died within 15 days. Stopping treatment led to rapid disease progression, indicating the need of continuous therapy. Compared to rapamycin, alpelisib better blocked critical AKT phosphorylation sites (on both Thr308 and Ser473), suggesting its potential as a more effective therapeutic option for patients with PROS (Venot et al., 2018).

Alpelisib in PROS Patients: Clinical Outcomes

Alpelisib (BYL719) was administered to 19 PROS patients under a compassionate use program at a single center, improving symptoms in all cases, with treatment periods extending beyond 18 months in some (Venot et al., 2018). Initially, two patients, a 29-year-old male and a 9-year-old girl both with severe PROS/CLOVES syndrome and *PIK3CA* H1047R mutation, received Alpelisib. Treatment led to rapid and marked improvements, including reductions in vascular malformations, limb

hypertrophy, and organ dysfunction, along with improved performance scores. Based on these promising outcomes, 17 additional patients, including 14 children and three adults with life-threatening complications and history of debulking surgeries were treated with daily oral alpelisib (50 mg for children and 250 mg for adults). Within three to six months of treatment, all patients demonstrated significant clinical and radiological improvements, including decreased lesion volumes, improved skin and vascular abnormalities, resolution of severe complications (e.g., chronic gastrointestinal bleeding, opioid dependence), and improvements in scoliosis and cognitive function in some cases. Treatment was well tolerated, with only minor adverse events, including transient mouth ulcers in three patients and manageable hyperglycemia in one obese patient, and no evidence of significant organ toxicity as assessed by heart, liver, kidney function, and blood testing. These findings were supported by the subsequent EPIK-P1 study (ClinicalTrials.gov, 2020), which retrospectively evaluated alpelisib treatment in 57 pediatric and adult patients with severe manifestations of PROS (Canaud et al., 2023). Altogether, these results, supported by preclinical data, reinforced Alpelisib as an efficient and safe PI3Kα inhibitor, providing a promising therapeutic option for patients with PROS. In April 2022, in recognition of these findings, the U.S. FDA (2022) approved alpelisib as the first and only treatment for adults and children (≥2 years) with severe PROS requiring systemic therapy.

Between 2019 and 2022, our department [Medical Genetics Department of Koç University School of Medicine (KUSoM) and the Genetic Diseases Evaluation Center at Koç University Hospital] was involved to the "EPIK-P2: A Phase II double-blind study with an upfront, 12-week randomized, placebo-controlled period, to assess the efficacy, safety and pharmacokinetics of alpelisib (BYL719) in pediatric and adult patients with *PIK3CA*-related overgrowth spectrum (PROS)" trial led by of Novartis Pharma AG as the only clinical site in Asia, Middle East, Africa region, among 43 sites across 12 countries worldwide. However, due to regulatory factors and delays caused by the COVID-19 pandemic, the study was discontinued in Turkey in 2022 as part of a global site reduction. As of 2025, the study remains active and is estimated to be completed in 2031 (ClinicalTrials.gov, 2021). Current research continues to focus on elucidating optimal dosing regimens, long-term safety profiles, and the potential expansion of therapeutic indications for alpelisib within this patient population.

Molecular Spectrum and Diagnostic Approaches

All PROS cases have been sporadic and represent simplex cases within their families. *De novo* pathogenic *PIK3CA* variants are typically somatic and exhibit mosaic distribution. However, germline variants in *PIK3CA* have been reported in 20 patients who were diagnosed as MCAP, Cowden syndrome, pulmonary vein stenosis and cancer (Rivière et al., 2012; Orloff et al., 2013; Di Donato et al., 2016; Yeung et al., 2017; Zollino et al., 2019; Yung et al., 2022; D'Alfonso et al., 2021; Sylvester et al., 2022; Cooley Coleman et al., 2023).

To date, 2,155 *PIK3CA* variants are listed in the Catalogue of Somatic Mutations in Cancer (COSMIC, v85, on August 2024). About 80% of the somatic driver mutations of *PIK3CA* cluster at three hotspots: two glutamic acid residues at codons 542 and 545 (E542K, E545K); and a histidine residue at codon 1047 (H1047R) (Cancer Genome Atlas Network, 2012; Kandoth et al., 2013; Hoadley et al., 2014). Other common *PIK3CA* mutations are C420R in exon 7; E545A E545D, E545G, Q546E, Q546R in exon 9; and H1047L and H1047Y in exon 20. These hotspot mutations confer strong oncogenic activity by disrupting normal regulatory interactions within the PI3K complex. Specifically, substitutions in exon 9 are believed to enhance PI3K activity by enabling the p110α catalytic subunit to evade inhibition by the p85 regulatory subunit, mediated through the SH2 domain (Mukohara et al., 2015). Functionally, these alterations have been shown to drive tumorigenesis, as evidenced by mammary tumor development in transgenic mouse models, as well as cell transformation and tumor formation *in vitro* and *in vivo* human mammary epithelial cells. These hotspot mutations are also frequently observed in PROS syndromes, especially in focal phenotypes where brain overgrowth is not typically present (Lindhurst et al., 2012; Lee et al., 2012; Kurek et al., 2012; Keppler-Noreuil et al., 2014). MCAP syndrome, on the other hand, is primarily associated with a broad range of rare nucleotide substitutions and less commonly linked to the *PIK3CA* mutational hotspots (Rivière et al., 2012; Mirzaa et al., 2016).

Genetic heterogeneity accounts for the majority of the reported cases, i.e., the same mutation can often be detected in individuals with different clinical features (Figure 3.2). Mirzaa et al. detected 29 different *PIK3CA* mutations in 33% (60/131) of 131 patients with MCAP phenotype, 19 of whom showed extensive brain overgrowth

and 31 of whom showed somatic overgrowth and vascular malformations, by NGS (Mirzaa et al., 2016). Kuentz et al. reported disease-causing mutations in 108 of 162 patients in whom they performed clinical NGS; all but one mutation was postzygotic and 22 of 40 alterations, most of which were missense, were shown in more than one patient. Thus, diagnostic efforts have been widely limited to hotspot screening (Kuentz et al., 2017).

Same as all mosaic conditions, technical considerations also apply to PROS, and the applied technique must be able to detect mosaic variants with low VAFs. Targeted NGS-based deep sequencing is the recommended technique for detecting *PIK3CA* variants with low VAFs; however, other common techniques have also been widely used (page 35, *Detecting mosaicism: Methodological considerations*). Again, the limitations of each technique must be taken into consideration.

Following the identification of a candidate mosaic *PIK3CA* variant, secondary testing by orthogonal methods such as Sanger sequencing, pyrosequencing, ddPCR or an independent NGS analysis may be needed to confirm the variant. Additionally, exons 10 to 14 of *PIK3CA* share 95% sequence identity with a pseudogene located on chromosome 22. Therefore, not only the initial testing type but the validation assay should be carefully designed to discriminate between these loci, e.g., using long-range PCR instead of standard PCR in Sanger sequencing (Rodriguez-Laguna et al., 2018). However, additional validation may be unnecessary when the same variant is identified in multiple distinct tissues from the same individual (Douzgou et al., 2022).

As discussed in the Introduction chapter (page 36, *Detecting mosaicism: Tissue type matters*), testing in at least two different tissue types is a must. *PIK3CA* mutations are usually not detectable in DNA material obtained from peripheral blood or saliva samples, except in individuals with MCAP syndrome (Rivière et al., 2012; Keppler-Noreuil et al., 2015; Mirzaa et al., 2016; Kuentz et al., 2017). In highly focal PROS disorders (e.g., CLOVES syndrome or FAO), pathogenic *PIK3CA* variants can be detected in affected tissues, often with varying VAFs. Moreover, affected tissue could be inaccessible, especially in localized/tissue-specific clinical presentations. In such cases, the most effective approach for molecular diagnosis would be obtaining affected tissue during reduction surgery for macrodactyly or debulking of ectopic accessory muscle. Overall, the current recommendation for non-MCAP PROS suggests

prioritizing targeted NGS analysis of DNA derived from fresh, uncultured tissue samples and/or FFPE tissues from clinically affected areas for genetic testing, while for MCAP testing peripheral blood or saliva samples is enough, although the diagnostic yield is lower (Mirzaa et al., 2016; Kuentz et al., 2017; Douzgou et al., 2022).

The usage of circulating cell-free DNA (ccfDNA) for molecular profiling has gained considerable momentum, with studies highlighting its potential as a marker for diagnosis, prognosis, and disease monitoring in cancer patients, including those with *PIK3CA* mutations. It employs liquid biopsy techniques to identify mutations in circulating tumor DNA (ctDNA) within ccfDNA, and has advantages over traditional biopsies, such as being less invasive and more accessible (Diehl et al., 2008; Heitzer et al., 2019).

ccfDNA mainly originates from cell degradation via apoptosis or necrosis in hematopoietic cells, leading to the release of genomic DNA into the bloodstream. ccfDNA released by apoptosis consists of short fragments (<1000 bp), while ccfDNA released from necrosis, often via exosomes or tumor cells, is generally longer and highly fragmented (>1000 bp) (Elazezy & Joosse, 2018; Leest et al., 2020). Thus, cancer patients usually exhibit higher levels of ccfDNA compared to healthy individuals (0 to 100 ng/ml vs 0 to >1000 ng/ml in plasma) (Schwarzenbach et al., 2011). Within the total ccfDNA, ctDNA accounts for less than 1% in general, but fractions may vary among patients and can range from 0.01% to 90% based on the location, size, and vascularity of the tumor (Diehl et al., 2008; Haber & Velculescu, 2014; Buedts & Vandenberghe, 2016; Elazezy & Joosse, 2018).

As interest in ccfDNA-based diagnostics grows, the number of extraction kits and methods has increased significantly in recent years (Warton et al., 2018; van Dessel et al., 2019). Blood-based detection of *PIK3CA* variants is now a routine, non-invasive approach used in cancer diagnostics, especially for breast cancer (Leest et al., 2020; Ma et al., 2024). However, the diagnostic yield in PROS may be lower than in cancer because the likelihood of cffDNA carrying the mutation can vary based on clinical factors like the presence of vascular malformations [there is likely less neovascularization in PROS compared to cancer], and the VAF in cffDNA can be very low, necessitating sensitive techniques or special pipelines for detection. More

systematic studies and larger datasets are needed before definitive recommendations can be made regarding its routine use in diagnostics (Douzgou et al., 2022).

Sampling and Performed Tests

For each patient, a clinical diagnosis was established through a detailed physical examination and evaluation of radiological findings (if available and applicable). Genetic testing was performed on at least two samples: buccal swab/saliva, blood plasma, and/or affected tissue. Circulating DNA was isolated from blood plasma samples, and genomic DNA was isolated from skin biopsy and/or FFPE tissue samples.

In 2019, with the limited research budget (TUBİTAK 1002 project), the existing machines and equipment we had in our lab, we searched for the most suitable and cost-effective FDA-approved method to detect *PIK3CA* mutations. We opted to use a qPCR-based diagnostic approach, using the *therascreen* PIK3CA RGQ PCR Kit.

Based on the qPCR results, available patients were subjected to secondary testing:

- If a *PIK3CA* mutation was detected by qPCR, the variant was confirmed with an NGS-based test (targeted panel/WES).
- If no mutation was identified by qPCR, available patients were subjected to NGS-based testing (targeted panel/WES) (Figure 3.3).

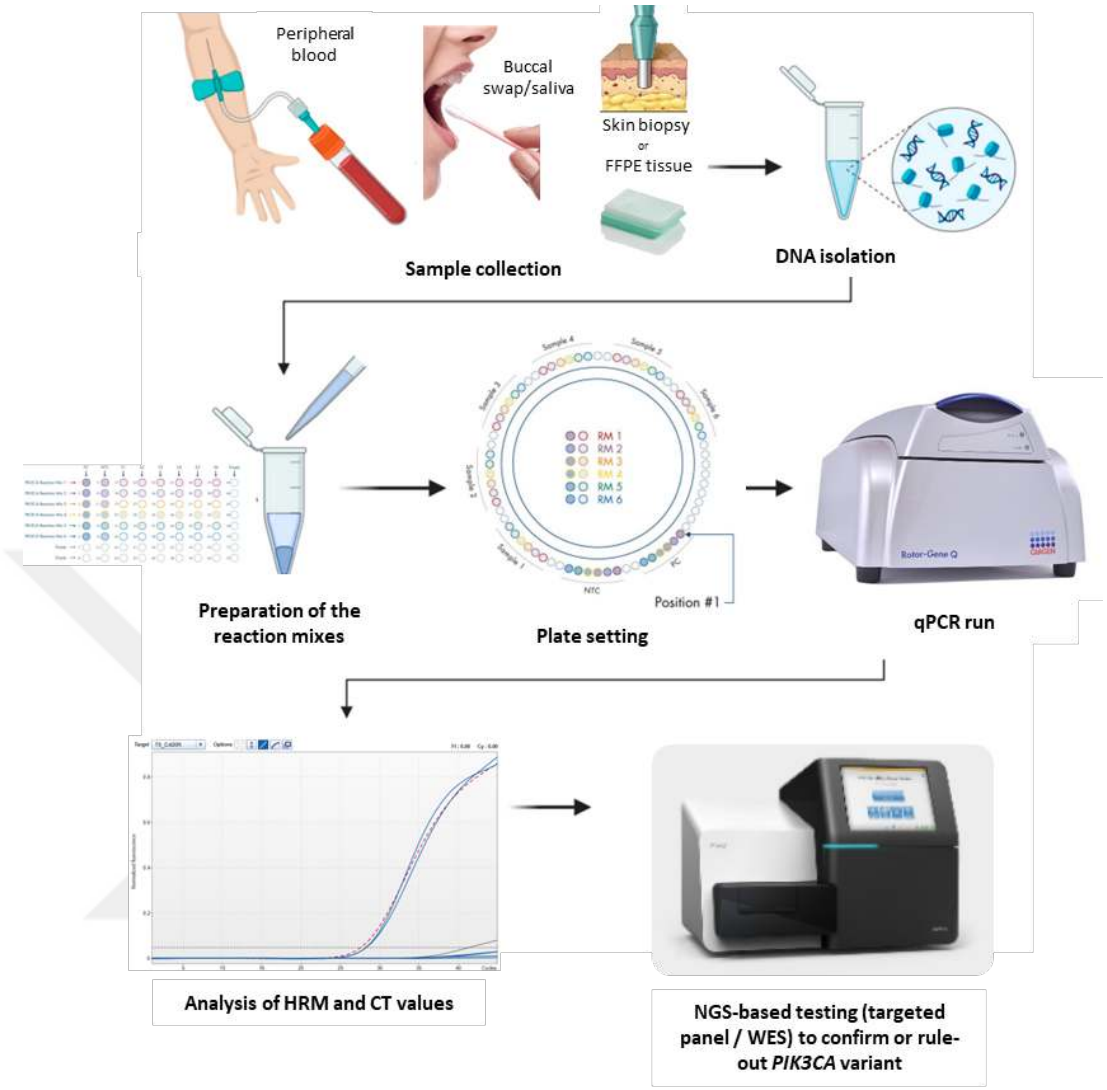

Figure 3-3. **Diagnostic workflow in Study 1**. DNA was isolated from peripheral blood, buccal swab/saliva, and/or tissue (fresh or FFPE). qPCR analysis was performed first to screen for *PIK3CA* hotspot variants, followed by NGS, either targeted gene panels or WES, to confirm or rule out *PIK3CA* variants.

Results and Discussion

A total of fifteen patients with clinical features suggestive of PROS were evaluated in the study, including three with a clinical diagnosis of CLOVES syndrome, four with Klippel-Trenaunay syndrome (KTW), five with fibroadipose overgrowth (FAO), one with hemimegalencephaly (HHML), and two with other isolated or atypical presentations within the PROS spectrum (Figure 3.4). Clinical findings along with the molecular testing results are shown in Table 3.2.

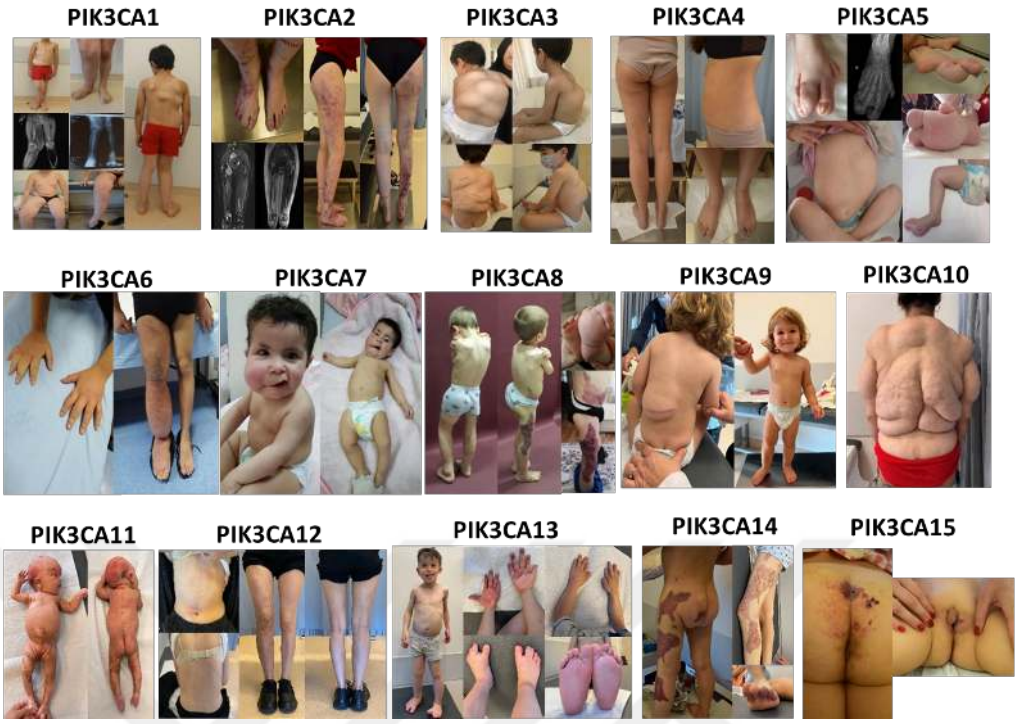

***Figure 3-4*. Clinical images of 15 patients included in the Study 1 cohort**. The images highlight the variability in tissue involvement, distribution, and severity among affected individuals.

Initial screening using real-time PCR targeting hotspot PIK3CA mutations identified pathogenic variants in three patients (3/15) (Figure 3.5). In patient **PIK3CA3**, c.1258T>C (p.C420R) mutation was detected by qPCR on DNA extracted from the lipomatous tissue on the back which was sampled during debulking surgery, and the presence of the PIK3CA C420R variant was confirmed with a VAF of 15% (?/? reads not reported) by NGS at an outer center using the same DNA sample (Intergen Genetic Diseases Evaluation Center, report date: 13.01.2020). In patient **PIK3CA7**, c.1258 T>C (p.C420R) mutation was detected on DNA derived from the buccal swab and skin biopsy from the upper leg. Sanger sequencing was attempted to confirm the variant but was not successful. In patient **PIK3CA9**, c.3140A>G (p.H1047R) mutation was detected in the DNA from the FFPE lipomatous tissues obtained during debulking surgery on the back. WES confirmed the presence of the *PIK3CA* H1047R variant at an outer center, VAFs were 11% (20/190 reads) in the tissue sections from the first FFPE block (P1), 16% (37/227 reads) in the second (P2), and 25% (47/191 reads) in the third (P3) (Aalborg University Hospital Department of Molecular Diagnostics, report date: 25.05.2023).

Importantly, all three mutations were detected in affected tissue samples but not in blood, underscoring the necessity of testing lesional DNA in mosaic disorders.

Given the possibility of low-level mosaicism and the limitations of qPCR, targeted NGS panel or WES was planned in ten patients with negative qPCR results. Testing has been completed in four of these patients: three cases have been resolved (PIK3CA5, PIK3CA10 and PIK3CA12), and one remains inconclusive (PIK3CA2). The analyses of the remaining six patients (**PIK3CA1, PIK3CA6, PIK3CA8, PIK3CA12, PIK3CA13, PIK3CA15**) are ongoing [in collaboration with Prof. Pablo Lapunzina, Institute of Medical and Molecular Genetics, Hospital Universitario La Paz, Madrid, Spain].

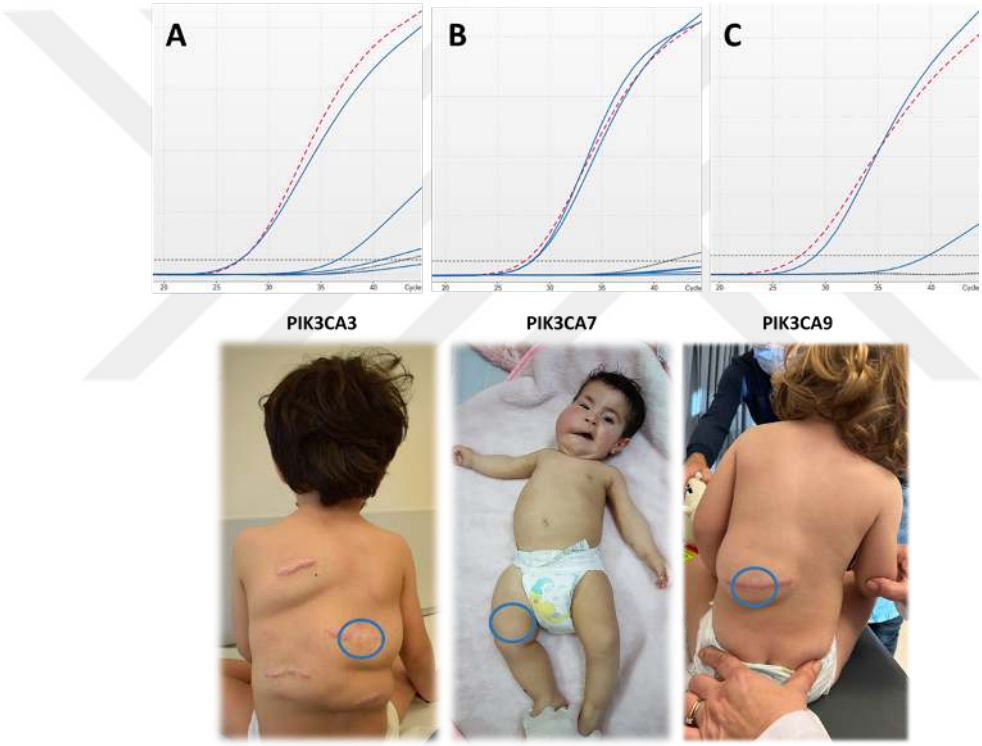

Figure 3-5. **HRM curve images** of **(A)** PIK3CA7 buccal swab sample showing C420R positivity, **(B)** PIK3CA3 and PIK3CA7 tissue samples showing C420R positivity, **(C)** PIK3CA9 tissue sample showing H1047R positivity. Locations of the tested tissue samples of each case are shown in the lower panel.

Notably, in patient **PIK3CA5**, the H1047R variant was subsequently identified by targeted NGS testing (VANSeq). VAFs were depending on the tissue type analyzed, which were 0.82% in gDNA derived from peripheral blood, 7.24% in buccal swab, 4.62% in tissue obtained from the plantar surface of the foot, and 6.58% in lipomatous tissue from the abdomen. Although VAFs are relatively large (as >5%), prior negative

qPCR result is explained by the detection threshold of the qPCR kit used (see Appendix). This finding highlights the importance of assay sensitivity and sampling strategy.

In P**IK3CA2**, no molecular diagnosis could be established. No *PIK3CA* hotspot mutation was detected in blood ccfDNA, blood gDNA, buccal swab gDNA, skin biopsy gDNA and desmoid tm FFPE gDNA by qPCR. Targeted NGS (VANSeq) on skin biopsy gDNA, which covers not only *PIK3CA* but 12 other genes associated with lymphatic/venous/arteriovenous malformations, revealed no variants associated with the phenotype. Moreover, due to the presence of desmoid tumor on the breast and familial cancer history, hereditary cancer panel (Oncopanel) and MLPA for *BRCA1/2* and *APC* were performed on blood gDNA, which revealed no causative variant. This case illustrates the ongoing challenge of genetic diagnosis in mosaic disorders and suggests the potential role of yet unidentified genes and/or regulatory variants that cannot be detected by current assays.

In two patients (**PIK3CA10** and **PIK3CA11**) where no *PIK3CA* mutation was detected despite overlapping clinical features, broader genetic analyses by WES identified variants in two different genes, *MFN2* and *FGFR2*. These two patients will be discussed in detail in Study 8 (page 126) and Study 9 (page 141). In the remaining two KTW patients (**PIK3C4** and **PIK3CA14**) with no tissue samples, secondary testing was not planned as the diagnostic yield was expected to be low.

Our findings support the crucial role of molecular diagnosis in patients with PROS. Confirming the presence of a pathogenic *PIK3CA* variant not only establishes a definitive diagnosis but also provides an opportunity for targeted therapy. Although it is a prerequisite, not all mutation-positive patients are eligible or suitable for therapy. Clinical factors such as disease progression, symptom severity, and risk–benefit assessment must also guide therapeutic decisions. For example, patient PIK3CA3 has been followed up in our center with a diagnosis of FAO since the age of four. His initial presentation included an atypical skin lesion on the right hypochondrium observed at 14 days of age, which was biopsied and diagnosed as a lymphangioma. By age one, he had developed multiple lipomatous masses on his back, along with progressive enlargement of the lymphangioma. Between the ages of two and three, he underwent several surgical procedures to debulk the growing lipomas. Currently, at 8 years 11 months of age, he

continues to exhibit progressive lipomatous overgrowth on his back, with worsening symptoms of fatigue, pain, and limited mobility. In his case, the presence of progressive overgrowth and functional impairment, along with molecular confirmation of the C420R variant, led to the decision to start alpelisib treatment [personal communication with Dr. Guillaume Canaud]. Similarly, patient PIK3CA9 has been followed up with FAO diagnosis since 1 year 8 months of age. She had debulking surgery at 13 months of age for the removal of a single lipomatous lesion on her back, which was noticed at birth. At consultation, seven months after surgery, she had an isolated voluminous lipoma with possible hypertrophy of the left paravertebral muscle. She is currently 4 years 2 months old and had a stable clinical course without significant progression. Despite harboring the H1047R variant, the lack of ongoing growth, pain, or functional limitations led to a decision to monitor her clinically with MRI, without immediate treatment [personal communication with Dr. Guillaume Canaud]. These two cases emphasize that the presence of a pathogenic mutation alone does not necessitate treatment and highlight the importance of integrating both molecular and clinical data in decision-making.

Besides its clinical importance, this study offers methodological insight into the diagnostic use of qPCR for detecting *PIK3CA* mutations in mosaic overgrowth syndromes. The qPCR assay used here was originally developed and validated for identifying *PIK3CA* hotspot mutations in a cancer setting. Tissue samples remain the gold standard for mutation detection; however, non-invasive sampling methods, such as buccal swab/saliva and ccfDNA from plasma, may provide valuable alternatives, especially in cases where tissue biopsy is not feasible. Our results show that, when used carefully and with proper sample selection, preferably from the affected tissue, qPCR can be a useful initial screening tool for diagnosing PROS at the molecular level. However, a negative qPCR result should not rule out the diagnosis, especially when clinical signs strongly suggest it. Because of its limited sensitivity, particularly for detecting low-level mosaicism, follow-up testing with more sensitive methods such as targeted NGS should be considered. Additionally, identification of non-*PIK3CA* pathogenic variants in two patients by WES indicates molecular heterogeneity and underlines the need for high-sensitivity techniques and proper sampling.

In conclusion, the diagnostic yield of genetic testing in our cohort highlights the diagnostic challenges associated with detecting mosaic *PIK3CA* variants, particularly when VAFs are low or when sampling is suboptimal. Accurate and reliable molecular testing is crucial for providing a definitive diagnosis and enabling effective therapy/treatment to enhance clinical outcomes and patient care. Ongoing testing in the remaining patients is expected to further inform the mutation spectrum and refine diagnostic strategies for PROS.

Table 3-2. **Summary of clinical and molecular findings of patients included in Study 1.**

Patients	PIK3CA1	PIK3CA2	PIK3CA3	PIK3CA4	PIK3CA5	PIK3CA6	PIK3CA7	PIK3CA8	PIK3CA9	PIK3CA10	PIK3CA11	PIK3CA12	PIK3CA13	PIK3CA14	PIK3CA15
Sex	M	F	M	F	F	M	F	M	F	F	F	F	M	M	F
Required findings															
Congenital or Early Childhood onset	+	+	+	+	+	+	+	+	+	+	+	+	+	+	+
Sporadic and Mosaic Overgrowth	+	+	+	+	+	+	+	+	+	+	+	+	+	+	+
Spectrum findings															
Vascular Malformations: Capillary / Venous / Lymphatic / Arteriovenous	-	+	-	+	-	-	-	+	-	-	-	+	+	+	+
Overgrowth: Adipose / Muscle / Nerve / Skeletal	+	+	+	+	+	+	+	+	+	+	+	+	+	+	+
Epidermal Nevus	-	-	-	-	+	-	-	-	-	-	+	-	-	-	-
Isolated findings															
Large Isolated Lymphatic Malformation	-	+	-	+	-	-	-	-	-	+	+	-	-	-	-
Isolated Macrodactyly or Overgrown Splayed Feet / Hands, Overgrown Limbs	+	+	-	+	+	+	+	+	-	-	-	-	+	-	-
Truncal Adipose Overgrowth	-	-	-	-	-	-	-	-	-	+	-	-	-	-	-
Hemimegalencephaly (bilateral) / Dysplastic Megalencephaly / FCD	-	-	-	-	+	-	-	-	-	-	-	-	-	-	-
Seborrheic Keratoses	-	-	-	-	-	-	-	-	-	-	-	-	-	-	-
Benign Lichenoid Keratoses	-	-	-	-	-	-	-	-	-	-	-	-	-	-	-
Clinical diagnosis	FAO	KTW	FAO	KTW	FAO	CLOVES	HHML	CLOVES	FAO	FAO / FML	KEN	KTW	CLOVES	KTW	Isolated vascular malformation
Tested sample type for *PIK3CA* by qPCR analysis	K, P, BS	K, D, BS	K, D, BS	K, BS	K, BS	K, F, D, BS	K, D, BS	K, D, BS	K, P, BS	K, D, BS	K, D, BS	K, D, BS	K, D, BS	K	P
qPCR analysis results	-	-	**C420R in D**	-	-	-	**C420R in D & BS**	-	**H1047R in P**	-	-	-	-	-	-
Secondary test planned to rule-out / confirm	Targeted NGS panel	Targeted NGS panel	*PIK3CA* by NGS	n/a	Targeted NGS panel	Targeted NGS panel	n/a	Targeted NGS panel	WES	WES	WES	Targeted NGS panel	Targeted NGS panel	n/a	Targeted NGS panel
Tested sample type for targeted NGS panel / WES	G, P	D	D	n/a	K, D, BS	G, D	n/a	G, D	P	D	D	G, D	G, D	n/a	G, P
Targeted NGS panel / WES results	*ongoing*	-	**C420R 15% in D**	n/a	**H1047R 0.82% in K 4.62% in D1** (plantar surface of the foot) **6.58% in D2** (lipomatous tissue from abdomen) **7.24% in BS**	*ongoing*	n/a	*ongoing*	**H1047R 11% in P1 16% in P2 25% in P3**	***MFN2*** NM_001127660.1: c.2119C>T p.(Arg707Trp)	***FGFR2*** NM_022970.3: c.1979A>T p.(Lys660Met)	*ongoing*	*ongoing*	n/a	*ongoing*

(K) blood plasma, (P) FFPE tissue sample from the affected area, (D) fresh tissue from the skin biopsy, (F) cultured fibroblast cells from the skin biopsy (BS) buccal swap/saliva, (+) present, (-) absent.

STUDY 2

Postnatal Diagnosis of Trisomy 22 Mosaicism Limited to the Skin Fibroblasts

Clinical Findings

In Study 2, an 8-year-old girl with multiple congenital anomalies, mild cognitive retardation, right hemiatrophy involving face and extremities, hyperpigmentation and facial dysmorphism is reported (Figure 3.6). She had been followed up since two months of age with differential diagnoses including Russell-Silver syndrome (RSS), Weill-Marchesani syndrome 1, Pallister-Killian Syndrome, autosomal dominant Robinow syndrome 1, Emanuel syndrome and RASopathy/Noonan syndrome.

Antenatal findings included cystic hygroma, single umbilical artery, hyperechogenic intestine, thickening of the heart walls and intrauterine growth retardation (IUGR). She was born via c-section at 32^{+5} GW with a weight of 1430 g, height of 34 cm, and OFC of 28 cm. In the first week of life, atrial septal defect (ASD: 3-4 mm) and ventricular septal defect (VSD: 1-2 mm) were detected, and she was admitted to the NICU for 43 days.

Physical examination at two months 20 days of age revealed brachycephaly and facial dysmorphism comprising of ptosis, low-set ears, bilateral pre-auricular pit. She had short-webbed neck, disproportionate short stature, right hemiatrophy, Duane anomaly, and bilateral clinodactyly of the 5^{th} fingers. Her growth parameters were significantly below the 3rd centile, weight being 3120 g (-3.48 SDS), height: 47 cm (-4.83 SDS), span: 43.5 cm, and OFC: 34 cm (-4.53 SDS).

At 22 months of age, she had a weight of 8100 g (-2.81 SD), height of 72 cm (-3.91 SD), span of 67 cm, and OFC of 43.2 (-3.26 SD) cm. She had neurodevelopmental

delay, cubitus valgus, and short 4th-5th toe metacarpals. She had asymmetric limbs, measurements of feet being 9.2 cm on the left, 10 cm on the right; and hands being 8.5 cm on the left, 7.6 cm on the right.

At five years seven months of age, she had a weight of 13.95 kg (-2.38 SDS), height of 106 cm (-1.33 SDS), and OFC of 46 cm (-2.99 SDS). Right hemiatrophy and limb length discrepancy had become more prominent. Measurements of feet being 13.8 cm on the left, 12.5 cm on the right. The mother had reported slower hair and nail growth on the right side. Moreover, she had hypopigmented lesions following Blaschko lines on the right upper arm.

Performed Tests and Results

At the first visit at two months 20 days of age, peripheral blood and buccal smear samples were collected. SNP array analysis performed on DNA sample derived from peripheral blood and chromosome analysis of cultured blood lymphocytes revealed normal female karyotype with no numerical and structural chromosome anomalies. Pallister-Killian Syndrome was ruled out by FISH analysis on buccal smear sample.

At the second visit at 22 months of age, Silver-Russel syndrome was ruled out with MLPA analysis and *PTPN11*-related Noonan syndrome was ruled out by whole gene sequencing on DNA sample derived from peripheral blood. Skin biopsy was recommended and planned for the next visit. However, due to the COVID-19 pandemic, her annual visit had to be postponed for three years.

At the last visit five years seven months, skin biopsy was obtained from the affected area and further genetic analyses were planned. Karyotype analysis from fibroblast cells revealed an additional 22nd chromosome (trisomy 22) in 16/20 (80%) metaphases and normal karyotype in the 4/20 (20%). No structural chromosomal anomaly was detected. Trisomy 22 mosaic state has been confirmed by FISH using *BCR*/*ABL1* translocation, dual fusion probe (LPH 007, Cytocell, Cambridge, UK).

These results lead to the **diagnosis of mosaic trisomy 22 syndrome** in the proposita with 47,XX,+22(16)/46,XX(4) karyotype (Figure 3.7).

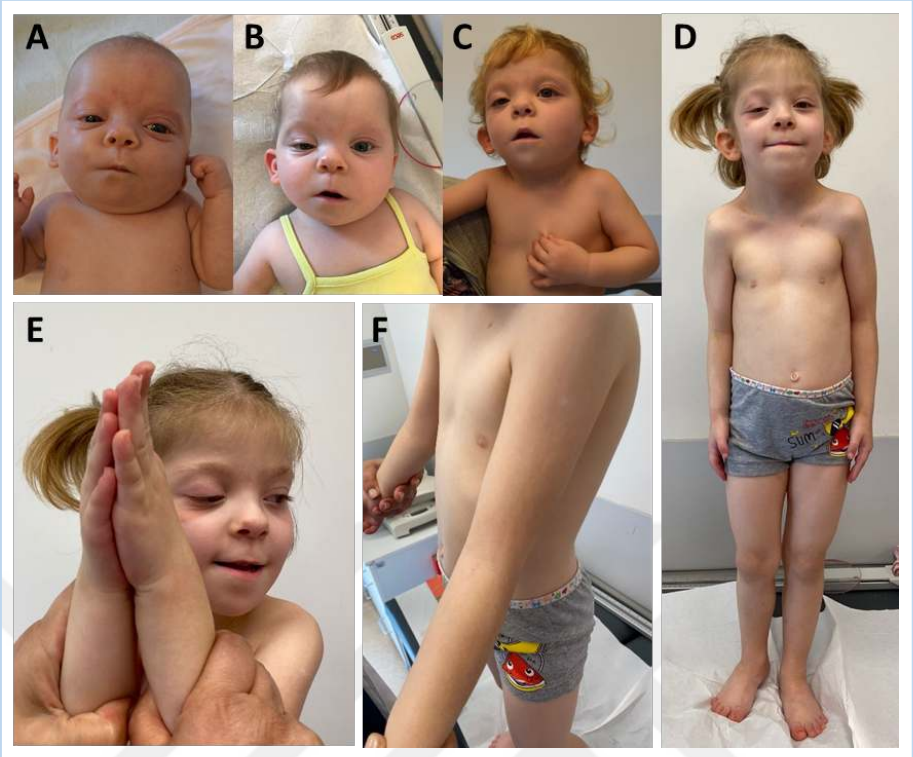

Figure 3-6. **Clinical findings of index 2, (A)** at two months 20 days of age **(B)** at one year of age **(C)** At 22 months of age **(D)** at five years seven months of age, showing distinct facial dysmorphism, right hemiatrophy, **(E)** hand asymmetry, and **(F)** hypopigmented lesions.

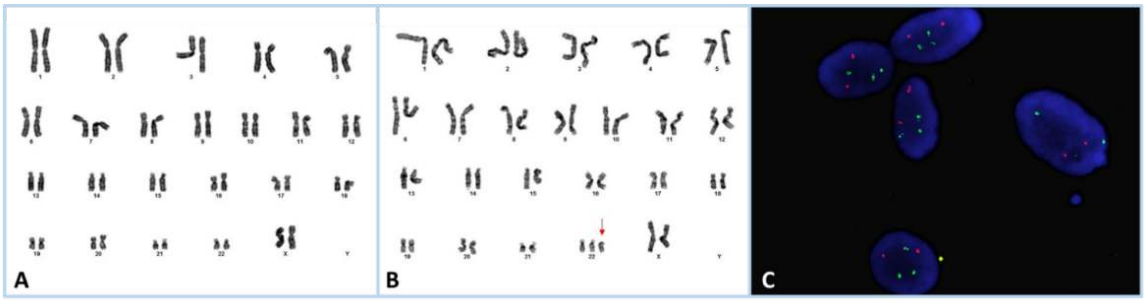

Figure 3-7. **Chromosome analysis results of index 2.** Karyotype images showing **(A)** Normal female karyotype, **(B)** Normal female karyotype with additional 22nd chromosome (trisomy 22), **(C)** FISH image confirming trisomy 22 mosaicism. Red signal indicates chr 9 (*ABL1*, 9q34.11-q34.12), green signal indicates chr 22 (*BCR*, 22q11.22-q11.23).

Discussion

Trisomy 22, the second most common chromosomal aneuploidy, accounts for approximately 2.9% of spontaneous abortions and is lethal during the neonatal period with an average survival of four days (Wang et al.,2007; Kehinde et al., 2014). Mosaic trisomy 22 (mT22), characterized by the coexistence of normal and trisomic cell lines within an individual, is an exceptionally rare aneuploidy compatible with extended postnatal survival. The incidence of trisomy 22, including both mosaic and non-mosaic forms, is estimated at 9–20 cases per 100,000 miscarriages (Florez et al., 2005). To date, there have been only 18 prenatal and 26 postnatal cases of mosaic trisomy 22 reported (reviewed by Trevisan et al., 2024; Khalid & Fadl-Elmula, 2024).

The phenotypic presentation of mosaic trisomy 22 (mT22) is highly variable. Schinzel first described the syndrome in 1981, and reported characteristic findings as growth restriction, webbed neck, facial dysmorphism, body asymmetry, cardiac defects, delayed puberty, and varying degrees of neurodevelopmental delay (Schinzel et al., 1981).

As an attempt to define possible phenotype correlation in index, all reported cases were reviewed. At the prenatal stage, fetuses may develop IUGR, and exhibit facial and auricular dysmorphisms, heart defects, digit anomalies and/or the urogenital anomalies. In the postnatal period, growth delay (16/26, 61.5%) and failure to thrive (9/26, 34.6%) were the predominant findings. Neurodevelopmental outcomes ranged from normal to severe intellectual disability. Among 12 patients whose neurodevelopmental data were available, three had normal intellect, five mild ID, three moderate ID, and one severe ID. Other common postnatal clinical features were cardiac defects (14/26, 53.8%), skeletal defects (19/26, 73.1%), and genital anomalies (11/26, 42.3%). Atrial and ventricular septal defects were the most common cardiac malformations. Facial dysmorphism comprised craniofacial asymmetry (8/26, 30.8%) commonly associated with midface hypoplasia (6/26, 23.1%), frontal bossing (8/26, 30.8%), microcephaly (7/26, 26.9%), hypertelorism (11/26, 42.3%), epicanthal folds (10/26, 38.5%), unilateral or bilateral ptosis (7/26, 26.9%), flattened nasal bridge (10/26, 38.5%), anteverted nostrils (5/26, 19.2%), long philtrum (6/26, 23.1%), thin lips (4/26, 15.4%), micro/retrognathia (6/26, 23.1%), low set ears (12/26, 46.2%), dysmorphic ears (11/26, 42.3%), pre-auricular pits/tags (15/26, 57.7%), low posterior airline (7/26,

26.9%), cleft palate (3/26, 11.5%) and webbed neck (8/26, 30.8%). More than half of the affected individuals displayed body asymmetry, manifesting as hemiatrophy, limb length discrepancy, and one hand being noticeably smaller than the other. 5th finger clinodactyly (11/26, 42.3%) and cutaneous or partial syndactyly (7/26, 26.9%) were also reported. Vertebral anomalies (4/26, 15.4%) and foot deformities of talipes equinovarus, and hallux varus were seldom reported. Terminal transverse limb reduction and thumb hypoplasia have also been reported in one case each, respectively. Among ectodermal anomalies, nail dysplasia and hypoplasia were the most common findings (12/26, 46.2%). Additionally, pigmentary changes (8/26, 30.8%) either along Blaschko lines, hypomelanosis of Ito, hyperpigmentation, or hypopigmentation have been reported. Dental anomalies (7/26, 26.9%) as malposition, delayed dentition, aplasia, and notched incisors have been reported (Trevisan et al., 2024; Khalid & Fadl-Elmula, 2024).

The index patient exhibited the majority of previously reported findings, including facial dysmorphism, pre- and postnatal growth delay, mild developmental delay, bilateral 5th finger clinodactyly, hypopigmentation, nail hypoplasia, and complex congenital heart anomalies of ASD and VSD. Due to its rare occurrence at the postnatal period, the phenotype associated with mT22 is only partially delineated. And as most findings are nonspecific, clinical diagnosis is difficult to establish. As reported for the index, non-specific findings had led to the differential diagnoses of Pallister-Killian Syndrome, Silver-Russell syndrome and *PTPN11*-related Noonan syndrome, which have all been ruled out.

The diagnosis of mT22 is further challenging due to the variability in mosaicism levels across different tissues, the presence or absence of detectable mosaicism in blood, and the potential influence of paternal or maternal uniparental disomy. In the review by Abdelgadir et al., approximately 30% of patients exhibited a mosaic karyotype in blood lymphocytes, whereas nearly 90% demonstrated mosaicism in skin fibroblasts (Abdelgadir et al., 2013). The diagnosis of mT22 in our patient was “delayed” by the presence of mosaicism among different tissues. Chromosome analysis of blood by karyotyping and SNParray analysis showed a normal female karyotype. However, a definitive diagnosis of mT22 was only established through a skin biopsy, which had to be performed five years after the first consultation. In cases where mosaicism is suspected because of body asymmetry and skin lesions such as hypo- or

hyperpigmentation, analysis of skin fibroblasts should be considered when peripheral blood samples or saliva reveal a normal karyotype. This case further supports previous studies and emphasizes the importance of testing multiple tissue types for a definitive diagnosis.

Given the scarcity of comprehensive data on mT22, especially regarding its natural history and developmental outcome, there is a need for detailed case studies to enhance our understanding of this entity.

STUDY 3

Mosaic Variegated Aneuploidy Syndrome 1 Caused by a Novel Gross Deletion and a Monoallelic Variant in *BUB1B* Results in Premature Centromere Division Without Accompanying Aneuploidies

Clinical Findings

The index was the second born of non-consanguineous parents of Turkish descent. Antenatal findings included oedema of the umbilical cord and IUGR. He was born via cesarean section at 30th gestational weeks due to bradycardia with a weight of 850 g (-1.84 SDS), length of 34 cm (-2.35 SDS) and head circumference of 23 cm (-3.43 SDS). He was followed up at the neonatal intensive care unit for postnatal 87 days. The neonatal period was further complicated by jaundice. Cardiological examination revealed patent foramen ovale with left-to-right shunt and peripheral pulmonary stenosis at 3 months of age. Computed tomography (CT) imaging of the brain and metabolic screening tests were reported as normal. Karyotype analysis at an outer center was reported as normal.

First outpatient clinical genetic consultation at 10 months of age revealed a weight of 4 kg (-6.21 SDS), height of 52 cm (-7.49 SDS) and OFC of 34 cm (-8.4 SDS). Dysmorphic findings included high forehead, bilateral microphthalmia, strabismus, nystagmus, long philtrum, micrognathia, low-set ears and short neck. He had cutis marmorata, capillary hemangiomas and edema on the dorsum of hands and feet (Figure 3.8 A-D). A detailed, multisystemic evaluation was carried out. Pulmonary assessment revealed atelectasis and cardiovascular evaluation showed peripheral pulmonary stenosis, bradycardia and pericardial effusion necessitated immediate pericardiocentesis. Routine lab workup and urinalysis revealed proteinuria and glucosuria. Thyroid function tests were suggestive for hypothyroidism, and he was put on levothyroxine treatment.

Between one to three years of age, he was hospitalized for long periods due to feeding difficulties, electrolyte imbalances and recurrent pericardial effusion. At 1 year 10 months of age, he had a height of 58 cm (-7.62 SDS), weight of 4.140 kg (-10.25 SDS), OFC of 34 cm (-9.94 SDS) (Figure 3.8 E). At one year 11 months of age, cranial magnetic resonance imaging (MRI) revealed severe cerebral atrophy and pachymacrogyric areas mainly on parietal lobes (Figure 3.8 G). Spinal colon MRI findings were within normal limits.

At 2 years 7 months of age, he had a height of 60 cm (-8.69 SDS), weight of 3.950 kg (-14.38 SDS), OFC of 34.8 cm (-9.74 SDS). Lymphoscintigraphy revealed no flow issues in bilateral upper and right lower extremities. Although it is not typical for lymphedema, following the radiopharmaceutical injection of the left lower extremity, only one delayed low-level lymph node visualization was observed at the inguinal region. Arterial system Doppler USG on lower extremities revealed no other findings that could underlie the persistent edema. He had hypokalemia (venous potassium: 2.42 mmol/L, ref: 3.5-4.5 mmol/L), hypocalcemia (total calcium: 8.1 mg/dL, ref: 8.8-10.8 g/L) and hypoalbuminemia (serum albumin: 15.1 g/L, ref: 38-54 g/L), necessitating intravenous infusions to recover the metabolic parameters. He had respiratory distress, thorax US revealed pleural effusion necessitating IV treatment.

Recent hospitalization at 3 years 4 months of age was due to a mass on the right upper eyelid, and conjunctival redness of the right eye (Figure 3.8 F). He had a height of 67 cm (-7,96 SDS) and weight of 6.470 kg (-8,53 SDS). Orbital MRI revealed an extraconal mass of 30x26x21 mm in size that surrounds the anterior and lateral parts of the right bulbus oculi and extending to the preseptal area. The described mass infiltrates the superior rectus and levator palpebrae muscles and the lacrimal gland (Figure 3.8 H). Histopathological evaluation was compatible with embryonal rhabdomyosarcoma with Ki67 levels being 50-60% and reaching 70% in some regions. *PAX3-FOXO1* fusion, a marker for alveolar rhabdomyosarcoma, was also ruled-out. He started receiving multiple combination chemotherapy with dactinomycin (1x160 mg), vincristine (1x0,16 mg) and cyclophosphamide (1x250 mg).

At 3 years 5 months of age, abdominal CT without contrast revealed a soft tissue of 17x12 mm in size in the mediobasal segment of the left lung lower lobe and increased thickness of the distal wall of the esophagus. Thorax CT without contrast revealed

bilateral pleural effusion (8 mm on right, 14 mm on left), increased left pleural thickness and a 4 mm nodule on the left upper lobe anterior segment. Parathyroid lesions were ruled out by neck USG. ^{18}F-fluorodeoxyglucose (FDG) PET/CT further revealed increased soft tissue density in the mediobasal segment of the left lung lower lobe, with no significant FDG uptake in the paraoesophageal area and mild hypermetabolism (physiological? pathological?) of the spinal cord at the T11-12 vertebra level. He died at the ICU at 3 years 7 months of age.

Performed Tests and Results

WGS on DNA sample obtained from EDTA blood; karyotype analysis on peripheral blood lymphocyte and fibroblast cells were performed.

Molecular Findings

WGS revealed a heterozygous variant c.2791C>T in the *BUB1B* gene (NM_001211.5) that causes a missense change of arginine to tryptophan at codon 931 (p. Arg931Trp). Located on the protein kinase domain of BUB1B, the identified variant is reported in population databases (rs766052877, gnomAD:0.0000040, 1000 G:0.0000041, CentoMD:0.000044); predicted to be 'deleterious' by SIFT and 'possibly damaging' by Polyphen-2; and classed as a variant of unknown significance (VUS, class 3) based on ACMG criteria.

Secondly, by CNV analysis, a heterozygous 9985bp deletion spanning exons 1 to 4 (chr15:40452846-40462831) of the *BUB1B* gene (NM_001211.5) was detected. While gross deletions are not yet described for *BUB1B*, these exons encode a part of the BUB1 N-terminal domain, the highly conserved region that maintains the kinetochore localization and binding to BUB3 (Bolanos-Garcia & Blundell, 2011). Thus, this deletion is classified as likely pathogenic (class 2) based on ACMG criteria. The percent of targeted nucleotides covered at ≥10x depth was 99.77 (CENTOGENE GmbH, Rostock, Germany).

Segregation analyses by Sanger sequencing revealed that the 9985 bp deletion is maternally inherited while the missense variant, VUS, is paternally inherited (Figure 3.9 A). The parents had normal karyotypes.

After the development of embryonal rhabdomyosarcoma in the index, FFPE tumor sample was obtained to pursue further chromosomal and genetic analyses. SNP array of E-RMS revealed gain of chromosome 8.

Additionally, a hemizygote variant in *DMD* gene (c.1049A>T), heterozygote variant in *F13A1* gene (c.1829C>T) and heterozygote variant *POGZ* gene (c.3287A>T) were detected in WGS analysis. Since he has normal CK levels, DMD was ruled out. White-Sutton syndrome related *POGZ* variant was also present in the mother, so it was considered benign. Both mother and the index have the *F13A1* gene VUS variant, considered as carrier state.

Cytogenetic Findings

Banding of chromosomes obtained from peripheral blood lymphocyte culture, premature centromere division was detected in 57% (34/60) of the analyzed metaphases, and normal karyotype was seen in the remaining 26 metaphases (Figure 3.9 B). Banding of chromosomes obtained from fibroblast cell culture revealed premature centromere division in 10% (10/100) of analyzed metaphases while normal karyotype was seen in the remaining 90 metaphases (Figure 3.9 C). No aneuploidies were observed in either of the cell types.

As a result, chromosome analysis from the peripheral blood lymphocyte and fibroblast cells showed abnormal male karyotype of pcd 46,XY(34)/46,XY(26) and pcd 46,XY(10)/46,XY(90), respectively. Parental karyotype analysis on peripheral lymphocyte cultures revealed normal constitutions with no PCS.

These results were **compatible with the diagnosis of Mosaic variegated aneuploidy syndrome 1 (MVA1).**

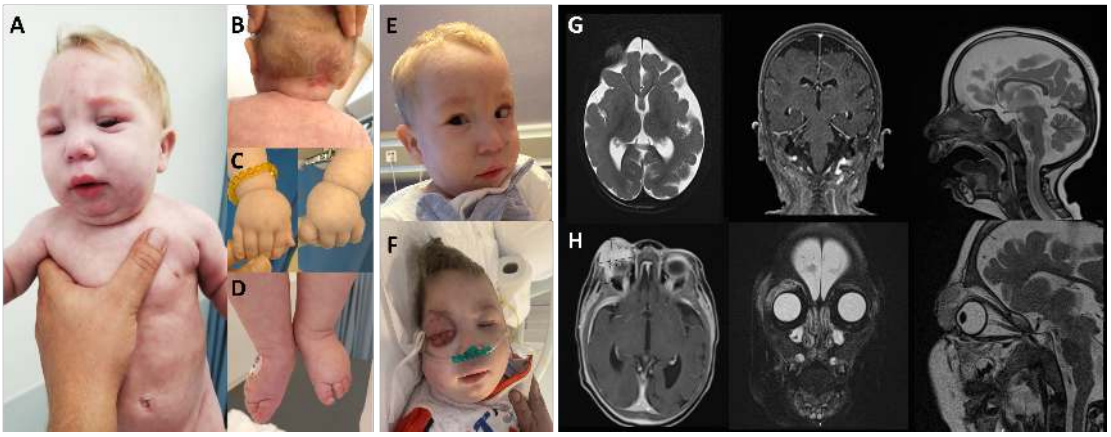

Figure 3-8. **Clinical findings of index 3** at 10 months of age show **(A)** mild facial dysmorphism comprising high forehead, bilateral microphthalmia, strabismus, nystagmus, long philtrum, micrognathia, low-set ears and short neck, **(B)** cutis marmorata, capillary hemangiomas, **(C-D)** edema on the dorsum of hands and feet. Phenotype of the index at **(E)** at 1 year 8 months of age, **(F)** at 3 years 4 months of age, further shows the mass on the right upper eyelid. **(G)** cranial MRI at 1 year 11 months of age showed severe cerebral atrophy and pachymacrogyric areas mainly on parietal lobes. **(H)** orbital MRI at 3 years 4 months of age demonstrated an extraconal mass of 30x26x21 mm in size that surrounds the anterior and lateral parts of the right bulbus oculi and extending to the preseptal area.

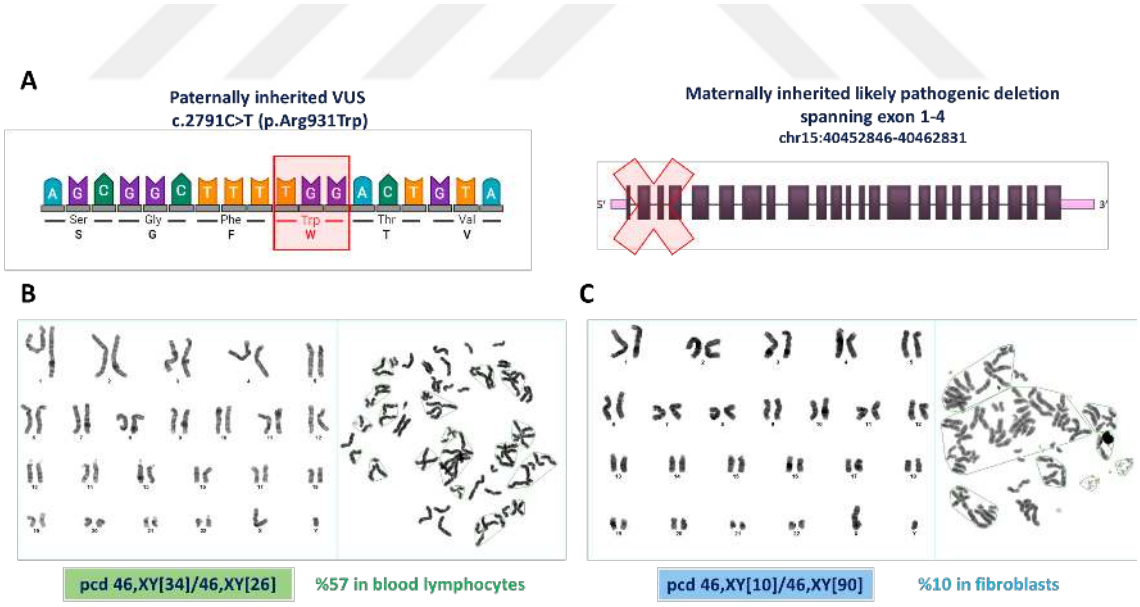

Figure 3-9. **Schematic illustration of the detected variants/aneuploidies in index 3 (A)** Paternally inherited c.2791C>T variant results in a missense change of arginine to tryptophan at codon 931, and maternally inherited 9985 bp deletion spans exons 1 to 4 of BUB1B. **(B)** Premature centromere division was detected in 57% (34/60) of the analyzed metaphases from peripheral blood lymphocyte culture and **(C)** premature centromere division in 10% (10/100) of analyzed metaphases from fibroblast cell culture with no accompanying aneuploidies.

Discussion

Chromosome segregation is a fundamental process across all life forms, from unicellular organisms to complex multicellular species. It ensures the accurate and timely distribution of duplicated sister chromatids to nascent daughter cells during cell division. Errors that disrupt this process can lead to disastrous consequences at both the cellular and organismal levels. In eukaryotic cells, the spindle assembly checkpoint (SAC) is a crucial surveillance mechanism that mitigates segregation errors and maintains genome stability by monitoring the interactions between kinetochores and the mitotic spindle. A key player in the SAC is the BUBR1 Mitotic Checkpoint Serine/Threonine Kinase B (BUB1B), also known as BUBR1 (Budding Uninhibited by Benzimidazoles-related 1), which plays a pivotal role in maintaining centromeric cohesion (Elowe & Bolanos-Garcia, 2022) (Figure 3.10).

Biallelic mutations in its encoding gene, *BUB1B*, are associated with mosaic variegated aneuploidy syndrome 1 (MVA1, MIM #257300). MVA is an ultra-rare autosomal recessive disorder characterized by various chromosomal abnormalities involving different and multiple chromosomes and/or tissues. Affected individuals present with severe pre/postnatal growth retardation, microcephaly and neurological impairment. Patients have a high cancer predisposition for rhabdomyosarcoma, Wilms tumor and leukemia being the most common malignancies leading to short disease-free survival and short life span (Hanks et al., 2004; Pavone et al., 2022).

Although the MVA phenotype has been well-characterized, a clear genotype-phenotype association is missing. Along with novel findings, we reviewed all molecularly confirmed MVA1 cases in the literature and provided the second detailed report of the *BUB1B*-related MVA1 phenotype. Clinical findings are highly variable across individuals, severe intrauterine and postnatal growth retardation, microcephaly and neurologic impairment are the characteristic findings of the syndrome. Common dysmorphic features reported are micrognathia, frontal bossing, triangular face, epicanthic folds, hypertelorism, low-set ears and broad nasal bridge. Cardiovascular, skeletal, genitourinary anomalies and additional congenital abnormalities have also been described. Pericardial effusion has been reported antenatally in one MVA1 patient. Index, the second case, had recurrent pericardial effusion necessitating multiple rounds of pericardiocentesis along with bradycardia and peripheral pulmonary stenosis (Lin et

al., 2020). To the best of our knowledge, this is the second report of *BUB1B*-related MVA1 with hypothyroidism and immunodeficiency (García-Castillo et al., 2008).

MVA1 is an ultra-rare autosomal recessive entity characterized by biallelic variations in the *BUB1B* gene along with multiple and variable chromosomal abnormalities. Disrupted BUB1B expression represents the causal mechanism leading to defective cell division. Likewise, the identified VUS is predicted to affect the catalytic function of the encoded protein, and possibly cause impaired signaling among SAC and its components due to decreased BUB1B kinase activity, while the gross deletion spanning exons one to four, likely to interfere with kinetochore localization and binding to its targeting adaptor BUB3 (Bolanos-Garcia & Blundel, 2011). To date, 60 different disease-causing *BUB1B* variants have been reported to be associated with mosaic variegated aneuploidy syndrome 1 and/or premature chromatid separation trait in ClinVar database (on March 06, 2024). The majority are single nucleotide variants (62%) and small deletion (23%) variants. Additionally, two small insertions (3%), two microsatellite variants (3%) and five duplications (8%) have been reported. To the best of our knowledge, this is the first association of a gross intragenic deletion in the *BUB1B* gene with MVA1 phenotype.

The majority of the published cases of MVA1 were based on conventional cytogenetic methods, yet only 29 molecularly confirmed cases reported till now. Various mosaic aneuploidies with/without premature chromatid separation (PCS) in metaphase cells are the cytogenetic hallmark of MVA. PCS manifests as separate and splayed, rod-like sister chromatids with detectable centromeres in metaphase and may involve all or most chromosomes. Mosaic aneuploidies predominantly observed, but not limited to, are trisomies and monosomies. The proportion of metaphase cells with chromosomal abnormalities varies but is usually >10-25%, and is greater than healthy individuals (Kajii et al., 1998). In general, PCS presents as an accompanying feature. Uncommonly in our case, chromosome analysis from the blood lymphocyte and fibroblast cells showed mosaic male karyotype with premature centromere division in independent cultures without any additional aneuploidies. Moreover, heterozygous parents were cytogenetically normal, and their cells did not show PCS trait. This novel observation further adds to the cytogenetic findings of MVA1.

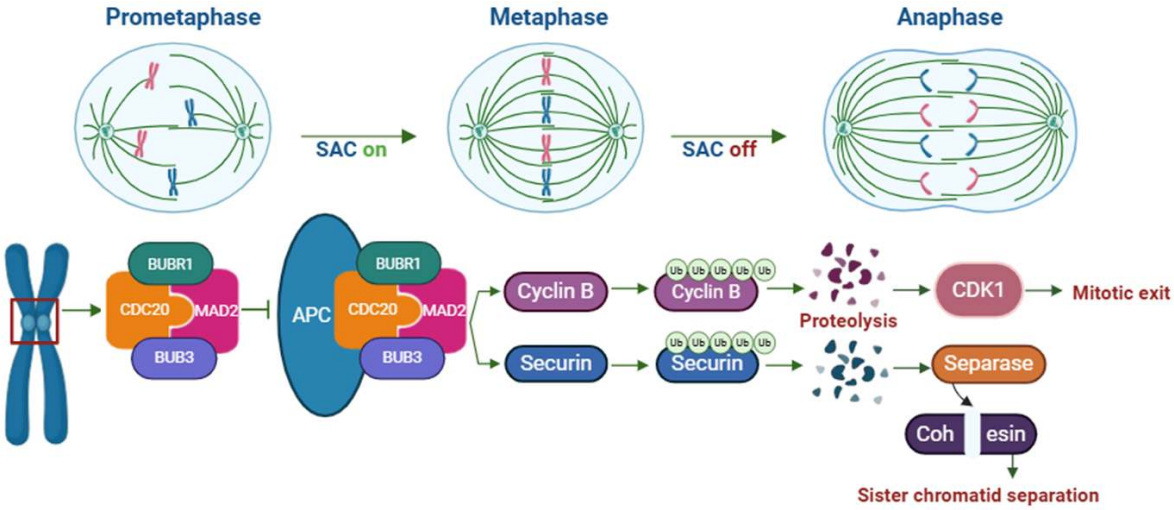

Figure 3-10. **The SAC ensures accurate chromosome segregation during mitosis**. During prometaphase, if kinetochores are not properly attached to microtubules, SAC components, [BUB1, BUBR1, BUB3, MAD1, MAD2, CDC20] are recruited to the unattached kinetochores. A conformational change in MAD2 from an inactive open to an active closed form enables it to bind CDC20, facilitating the formation of the mitotic checkpoint complex (MCC) with BUBR1 and BUB3. The MCC inhibits the anaphase-promoting complex/cyclosome (APC/C) by sequestering CDC20, thereby halting premature progression to anaphase. Once all chromosomes are correctly aligned at the metaphase plate, the SAC is silenced, APC/C is activated, and the cell progresses into anaphase. During this transition, securin and cyclin B1 are ubiquitylated by APC/C^{CDC20} and targeted for degradation by the proteasome. Degradation of securin activates separase, a caspase-like protease that cleaves cohesin, allowing sister chromatids to separate and move toward opposite poles. Concurrently, cyclin B1 degradation leads to the inactivation of CDK1, initiating mitotic exit.

Previous CGH analyses have shown that gains and losses of whole chromosomes are common in sporadic E-RMS. Gain of chromosome 8 is the most common aneuploidy in a wide variety of malignancies, as well as in E-RMS. Hanks et al. reported gain of chromosomes 3, 8, 13 and loss of chromosomes 9, 14, X on embryonal rhabdomyosarcoma sample from an MVA1 patient (Hanks et al., 2006). Consistently, SNP array on E-RMS revealed a gain of chromosome 8 in the index. This observation supports that E-RMS in MVA cases follow a similar oncogenetic pathway to sporadic E-RMS (Martin-Giacalone et al., 2021).

Due to the nature of the syndrome, patients have a high cancer predisposition and a short life span. Rhabdomyosarcoma, Wilms tumor, nephroblastoma, Sertoli-Leydig cell tumor and leukemia are the reported malignancies [Jacquemont et al., 2002;

Lin et al., 2020; MIM #257300]. The patient who has been reported with the longest life span in the literature was a 22-year-old female, who had been followed up since the antenatal period (Lin et al., 2020). After establishing the diagnosis, all relevant radiological and laboratory investigations should be planned to detect malignancies at an early stage. It is indeed important to provide genetic counselling to the parents/guardians/caretakers about all aspects of the disorder and discuss the surveillance plan. Effective communication among the family and health professionals is mandatory for facilitating the close follow-up and screening of the infants and young children for possible malignancies.

Although additional genetically -both molecularly and cytogenetically- confirmed cases are necessary to further delineate the *BUB1B*-related disease, we herein reported a complete case report, which favors a genotype-phenotype association in MVA1. This report highlights the importance of definite genetic diagnosis at early stages for timely clinical management of the patients for fair prognosis. Further reports with comprehensive data along with follow-up studies are needed to have a better insight for the natural history of this ultra-rare disorder.

STUDY 4

Recurrent Mosaic *MTOR* Variant Causing Hypomelanosis of Ito Without Accompanying Brain Malformations or Epilepsy

Clinical Findings

The index was the secondborn of non-consanguineous parents of Turkish descent. He was large for gestational age (LGA), and pregnancy was complicated by preeclampsia. He was born via normal spontaneous delivery at 41st GWs with a birth weight of 3980g (SDS 0.16), length and OFC were not recorded. The mother reports that she had noticed the difference between the two lower extremities at three months of age. Although his motor milestones were reported as age-appropriate, he had mild language delay. He had single words by 24 months but started combining two-word phrases around the age of five. He has been receiving speech therapy since the age of 4.5 due to language delay and articulation disorder. He learned to read and write in first grade. His mother reports temper tantrums and a short attention span. He has been followed up with the clinical diagnosis of Beckwith-Wiedemann syndrome at an outer center and referred for genetic consultation and further testing.

At six years four months of age, he had a weight of 31.3 kg (2.31 SDS), height of 124.7 cm (1.41 SDS), and OFC of 50 cm (-1.28 SDS). Minor dysmorphic findings included macroglossia and prognathia (Figure 3.11 A-F). He had unilateral (left) hemihypertrophy and hypopigmented streaks on the left side of the trunk, back, and left upper arm following Blaschko lines. He had asymmetry of the fingers/hands and feet/toes, having a smaller right hand (13.7 cm R;15 cm L) and right foot (19.2 cm R; 19.8 cm L). He was cooperative but his verbal communication was poor. He had 10 + 10 teeth with a single permanent tooth in the lower jaw.

Family history was non-informative, the parents were clinically evaluated for similar features. His father had prognathia and diastema of lower incisors along with a hypopigmented patch (3 x 3 cm with white body hair) on his left calf. A few colorless hairs were observed emerging from the hypopigmented area, leukotrichia.

At eight months eleven months of age, he had a weight of 42,.5 kg (2.31 SDS), height of 143.5 cm (1.41 SDS), and OFC of 52 cm (-1.28 SDS). Left hemihypertrophy was notable on the lower limbs with a smaller right leg (circumferential limb volume measurement of the right ankle 21,5 cm R; 24 cm L), and a smaller right foot (21 cm R; 22,5 cm L). No volume/length difference was observed on upper limbs (23,5 cm L-R), but he had a smaller right hand (15,3 cm R; 16,3 cm L) (Figure 3.11 G-K). Bone age was consistent with 10 years 10 months of age. He was much social and talkative compared to his last visit. His mother reports normal school performance with low achievement in mathematics, necessitating educational support. Cranial MRI at 9 years 6 months of age revealed no anomalies (Figure 3.11 L-M).

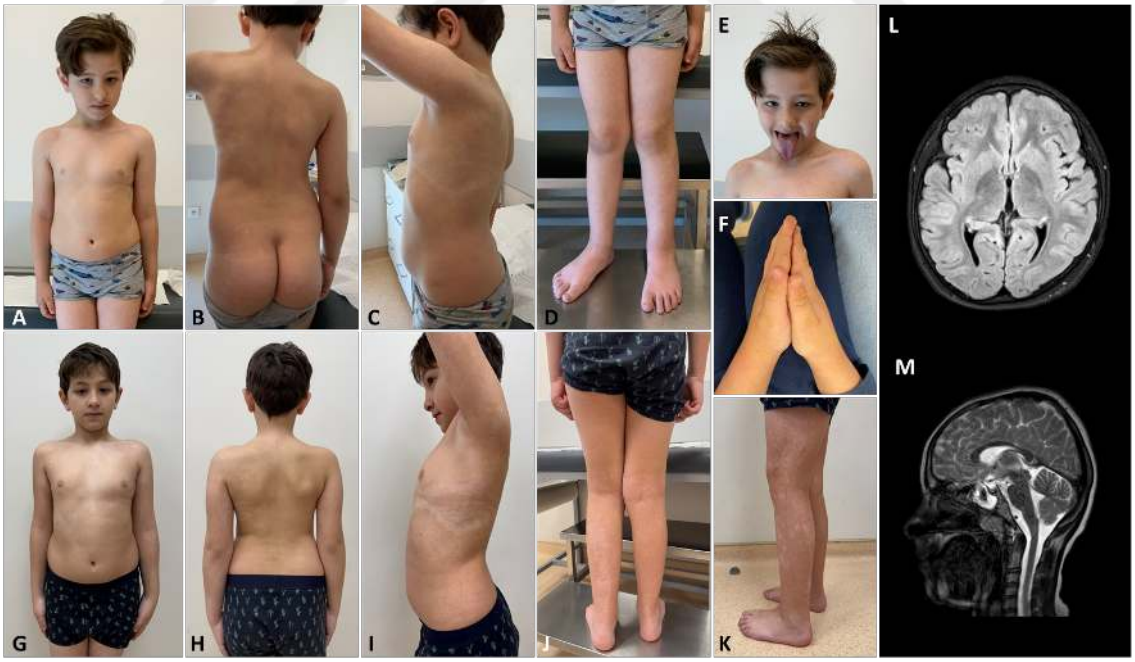

Figure 3-11. **Clinical findings of index 4,** showing **(A-D)** unilateral (left) hemihypertrophy and hypopigmented streaks on the left side of the body following Blaschko lines. **(E)** macroglossia, **(F)** asymmetry of the fingers/hands at 6 years 4 months of age, and **(G-K)** at eight months and eleven months of age. **(L-M)** Cranial MRI revealed no brain overgrowth.

Performed Tests and Results

Peripheral blood samples were collected from the family members and skin biopsy was performed on the index and his father. Skin biopsy was obtained from the hypopigmented area on the left arm of the index and the left forearm of the father.

Cytogenetic Findings

Karyotype analyses on blood lymphocytes and fibroblast cells of both the index and his father revealed no structural or numerical abnormalities. SNP array analysis on the index's DNA samples derived from skin biopsy and peripheral blood revealed no microdeletions/duplications.

Molecular Findings

WES analysis on index DNA from hypopigmented skin revealed a c.5930C > T (p. Thr1977Ile) variant in the *MTOR* gene (NM_004958.3). The variant was detected at a low VAF of 26.7% (16 of 60 NGS reads), suggesting mosaicism. The percent of targeted nucleotides covered at ≥20x depth was 99.06 (CENTOGENE GmbH, Rostock, Germany).

The identified *MTOR* c.5930C>T p.(Thr1977Ile) variant causes an amino acid change from threonine to isoleucine at position 1977. The identified variant was not reported in population databases (gnomAD, ESP, 1000 G, CentoMD); was predicted to be 'deleterious' by SIFT, 'probably damaging' by Polyphen-2, "disease causing" by MutationTaster, and ClinVar interpreted this variant as "Pathogenic" (Variation ID: 584432). According to HGMD Professional 2022.1, this variant has previously been described as disease-causing for Megalencephaly and polymicrogyria (Mirzaa et al., 2016, Carmignac et al., 2021). It is classified as likely pathogenic (class 2) due to partial clinical overlap.

The variant was confirmed on the DNA sample from cultured fibroblast cells of the index with an estimated frequency of 16,6% but was not detected in the DNA sample from peripheral blood and buccal swab by Sanger sequencing. Sanger sequencing in the parental samples (mother: peripheral blood, father: peripheral blood and fibroblast) did

not detect the c.5930C > T variant, indicating a *de novo* state in the index (Figure 3.12). The results were considered **consistent with the diagnosis of *MTOR*-related disorder**.

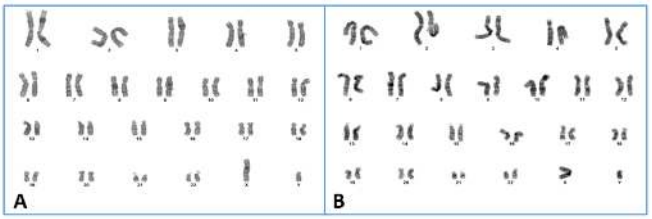

	Index			Mother	Father	
Sample type	**EDTA whole blood gDNA**	**Buccal swab gDNA**	**Fibroblast gDNA**	**EDTA whole blood gDNA**	**EDTA whole blood gDNA**	**Fibroblast gDNA**
Gene (transcript)	***MTOR*** (NM_004958.3)					
Variant Amino acid change	**c.5930C > T** **p. (Thr1977Ile)**					
Genotype Estimated VAF	**WT**	**WT**	**Heterozygous 16,6%**	**WT**	**WT**	**WT**
Sanger sequencing electropherogram	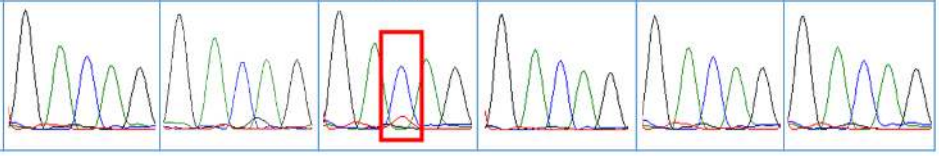					

Figure 3-12. **Genetic analysis results of index 4 and his parents.** Karyotype analyses on fibroblast cells of **(A)** the index and **(B)** his father revealed no structural or numerical abnormalities. Table showing Sanger sequencing results, which revealed heterozygosity for the de novo *mTOR* c.5930C > T variant with an estimated VAF of 16,6% in index fibroblast DNA.

Discussion

Elevated expression of mTOR activation markers on abnormally enlarged or cytomegalic neurons was initially shown by histopathology studies on brain tissue samples from focal cortical dysplasia (Ljungberg et al., 2006). Germline and somatic mutations in *MTOR* have been implicated in a spectrum of brain overgrowth phenotypes (D'Gama et al., 2015; Lee et al., 2012; Mirzaa & Poduri, 2014). However, subsequent studies have reported neurocutaneous features and the emerging pigmentary mosaicism phenotype for various pathogenic *MTOR* variants (Baynam et al., 2015; Mirzaa et al., 2016; Gordo et al., 2018; Handoko et al., 2019; Pelorosso et al., 2019).

Somatic *MTOR* variants have been reported in hemimegalencephaly (Lee et al., 2012) and FCD type II (Lim et al., 2015; Nakashima et al., 2015), in which genetic alterations were limited to the brain. Mosaic *MTOR* variants were recently associated

with hypomelanosis of Ito with/without brain overgrowth (Carmignac et al., 2021). Pathogenic germline variants in the *MTOR* gene on the other hand, are associated with Smith-Kingsmore syndrome (SKS, OMIM: #616638, Inheritance: AD) characterized by intellectual disability, macrocephaly, seizures, umbilical hernia, and facial dysmorphic features. Although pigmentary skin findings, including café-au-lait macules, capillary malformations, hyperpigmentation following Blaschko lines, and hypomelanosis of Ito have been reported in a few cases of SKS, the skin phenotypes are strikingly different from mosaic cases (Baynam et al., 2015; Ghahramani et al., 2015; Gordo et al., 2018).

To date, postzygotic *MTOR*-activating variants associated with hypomelanosis of Ito with neurodevelopmental abnormalities have been reported in 26 cases, and the recurrent p. Thr1977Ile variant identified in our patient was previously reported in seven patients with pigmentary findings and mild-to-severe brain phenotypes. Lee et al. reported the first hemimegalencephaly case with hypomelanosis of Ito, caused by a somatic p. Cys1483Arg variant detected on brain tissue from the affected hemisphere with a VAF of 9,8%, but not on the blood (Lee et al., 2012).

Mirzaa et al. reported three unrelated children who presented with asymmetric megalencephaly and FCD, including polymicrogyria. All had pigmentary mosaicism characterized by hyperpigmented streaks resembling cutis tricolor of the Blaschko-linear type. The p. Thr1977Ile variant was detected with intermediate levels of mosaicism varying from 23%-55% in affected skin and 7%-20% in blood or saliva. Furthermore, in primary rat neuronal cultures, this variant was found to cause constitutive activation of mTORC1 and enlarged neuronal size, establishing a link between the *MTOR* mutations and neuronal hypertrophy found in patients (Mirzaa et al., 2016).

Gordo et al., described a 2-year-old boy with macrocephaly, intellectual disability, facial dysmorphism including hypertelorism, open mouth appearance and smooth philtrum, and linear hyperpigmentation in arms and legs associated with a mosaic p. Cys1483Arg variant in all studied tissues (2% in blood, 11% in saliva, 18% in hyperpigmented skin and 28% in hypopigmented skin) (Gordo et al., 2018).

Handoko et al. reported a 3-year-old girl with megalencephaly, obstructive hydrocephalus due to cerebral aqueductal stenosis, asymmetric polymicrogyria, corpus

callosum dysgenesis, focal grey matter heterotopia, developmental delay, and cutaneous pigmentary mosaicism resembling cutis tricolor of the Blaschko-linear type. The p. Thr1977Ile *MTOR* variant was detected with a VAF of 32% in fibroblast-derived DNA from the hyperpigmented skin, but not in the blood (Handoko et al. 2019).

Pelorosso et al. reported a 9-year-old girl with hemimegalencephaly, severe intellectual disability, intractable seizures, and hypochromic skin patches. Somatic double-hit was detected in the ribosomal protein S6 (*RPS6*) (mosaic p. Arg232His variant: ~15.1% in dysplastic brain tissue and ~11% in blood), and the *MTOR* (somatic p. Ser2215Phe variant: ~8.8% in brain tissue, but not in blood) genes (Pelorosso et al., 2019).

Taylor et al., reported a male newborn with dysgenesis of the corpus callosum, dysplastic megalencephaly, abnormal gyral pattern of the right hemisphere, and whorled hyperpigmented and hypopigmented patches on the trunk, arms, and legs following the lines of Blaschko. The *MTOR* p. Ser2215Phe variant was identified in peripheral blood sample at a VAF of 5% (Taylor et al., 2021).

The largest cohort, including 15 unrelated patients with postzygotic *MTOR* variants exhibiting hypopigmentation and varying neurodevelopmental phenotypes, was reported by Carmignac et al. In total, 11 different mosaic *MTOR* variants were identified by WES, and *MTOR* variants were present in the skin but absent from blood in half of the cases. 14 patients exhibited either well-defined or diffuse linear hypopigmentation along Blaschko's lines, typically in S-shaped, V-shaped, or whorled patterns, most prominent under Wood's light. These patterns were primarily located on the trunk and lower limbs without a clear lateral predominance. One patient did not show linear hypopigmentation but had a hypopigmented patch of scalp hair, a segmental flag-like hypopigmented patch on his shoulder, and iris heterochromia. Moreover, six out of 14 patients had unilateral overgrowth: three had lateralized overgrowth (2 R, 1 L) while the three had segmental overgrowth on the lower limbs. Three patients with the recurrent p. Thr1977Ile variant showed linear hypopigmentation along Blaschko's lines, and two had unilateral overgrowth (one had right hemihypertrophy, the other had overgrowth affecting the lower limbs) (Carmignac et al., 2021).

Carli et al. reported a 7-year-old boy with hemimegalencephaly, generalized seizures, mild developmental delay, HI, and unilateral overgrowth. The p. Cys1483Tyr variant was detected with a frequency of 32% in the DNA extracted from a skin sample, 3% in saliva, and 0.46% in blood (Carli et al., 2021).

Resta et al. reported a boy with macrocephaly, hemimegalencephaly, seizures, mild developmental delay, nevus simplex, and unilateral overgrowth with S/V-shaped and whorled patterned hypopigmentation, along Blaschko's lines. *MTOR* p. Ile1973Phe variant was detected in fibroblast-derived DNA from the hypopigmented skin with a VAF of 20%, but not in blood (Resta et al., 2021).

Adding on to the last three papers, index presented hemihypertrophy/unilateral overgrowth involving the left side of the body. Asymmetric body overgrowth is a feature highly suggestive of somatic mosaicism and has been reported in eight patients to date. This observation adds to the growing evidence that overgrowth should be recognized as an emerging phenotype associated with postzygotic *MTOR* variants. Moreover, index had no history of seizures, macrocephaly and/or brain malformations detected by MRI. In Carmignac et al.'s cohort, only eight patients had macrocephaly (8/15). Concordant with our findings, in their cohort, MRI results of the patients with macrocephaly revealed normal symmetric brains without megalencephaly in nearly half of them (4/7). Among 10 patients with seizures, only five had macrocephaly, whereas the remaining five patients without epilepsy had macrocephaly. Additionally, MRI showed HMEG in six cases with seizures, whereas in four patients without epilepsy, MRI showed either MEG (2/4) or a normal brain (2/4). This observation suggests that brain overgrowth (HMEG or MEG) without apparent brain malformation and/or macrocephaly might indicate pathogenic variants in *MTOR* rather than in other upstream components of the pathway, such as *PIK3CA, PTEN* or *AKT3*.

mTOR is an essential component of mTOR complex 1 and 2 (MTORC1, MTORC2), and is responsible for their catalytic activities. Belonging to the family of the phosphatidylinositol 3-kinase (PI3-K)-related kinases (PIKK), the mTOR protein consists of five domains. The N-terminal includes the HEAT (Huntingtin, Elongation factor 3, protein phosphatase 2A, and TOR1) domain, composed of tandem alpha-helical repeats and is involved in protein-protein interactions of the complex. The C-terminal side consists the remaining four domains: FAT (FRAP, ATM, TRRAP); FRB (FKBP12-

rapamycin binding); catalytic serine-threonine kinase; the small regulatory FIT (Found in TOR) and the FATC (FAT, FRAP, ATM and TRRAP carboxy-terminal). The FAT (FRAP, ATM, TRRAP) domain is found among all the members of the PIKK family and facilitates interactions with other components of the complex. The FKBP12–rapamycin complex binds to the FRB region between the FAT and the kinase domains. FATC domain is located on the last ~30 residues of mTOR, and it interacts with the FAT domain to maintain proper protein mTOR conformation and activity (Bai & Jiang, 2010).

While the majority of the reported somatic *MTOR* variants are located in the FAT and kinase domains (Figure 3.13), hotspot mutations including the Thr1977Ile variant are clustered in the FAT domain. Hyperactivating mutations in the FAT domain result in mTOR hyperactivation and increase mTORC1/2 kinase activities, and thus lead to an increased cell proliferation (Bai & Jiang, 2010; Grabiner et al., 2014).

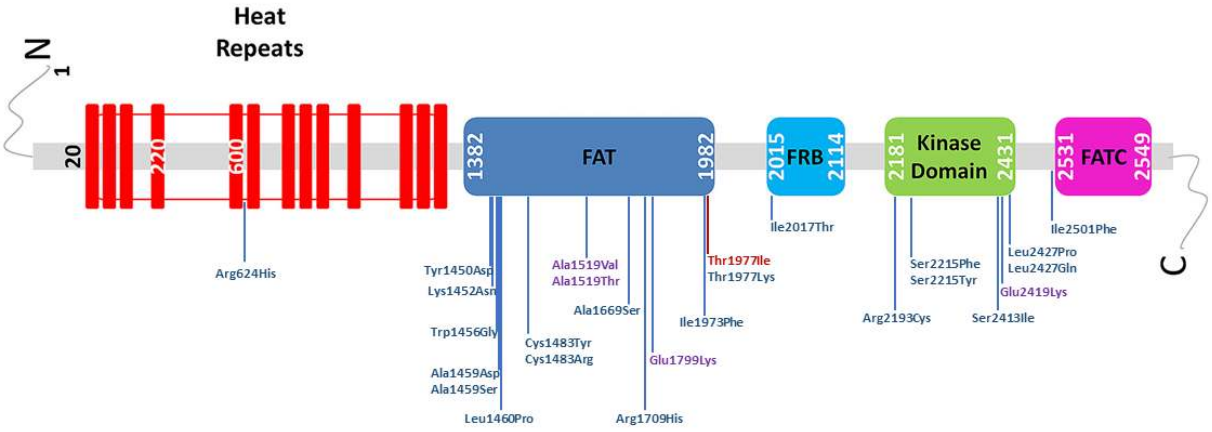

Figure 3-13. **Distribution of the reported postzygotic variants within the mTOR protein**, comprising the Huntingtin, Elongation factor 3, protein phosphatase 2A, and TOR1 (HEAT) repeat; FAT (FRAP, ATM, and TRRAP); FRB (FKBP12-rapamycin binding); kinase (serine-threonine kinase); FATC (FAT, FRAP, ATM and TRRAP carboxy-terminal); and FIT (Found in TOR) domains. Hotspot mutations are indicated in purple. Modified from Gordo et al., 2018.

mTOR is implicated in the regulation of pigmentation and the mechanism underlying cutaneous hypopigmentation observed in patients is hypothesized to result from mTOR complex hyperactivation, similar to the tuberous sclerosis complex (TSC) (Carmignac et al., 2021). TSC is a multisystem disorder caused by LoF mutations in *TSC1* or *TSC2*. Skin lesions observed in TSC include melanotic macules, facial

angiofibromas, and hypochromic patches of connective tissue nevi. The TSC protein complex is an essential regulator of mTORC1. Mutations in *TSC1* and *TSC2* are shown to activate mTOR and suppress melanogenesis by downregulating microphthalmia-associated transcription factor (MITF), leading to the characteristic ash-leaf, hypomelanotic macules (Jeong et al., 2011; Cao et al., 2017). Likewise, in hypopigmented skin samples of patients with *MTOR*-related Hypomelanosis of Ito, a decrease in melanocytes, defective melanosome maturation, and a reduced number of melanosomes in keratinocytes were observed. Additionally, there was an increase in AKT and p70S6K phosphorylation in dermal fibroblasts of the patients (Carmignac et al., 2021). These findings support the hypothesis that upregulated mTORC1 activity inhibits melanogenesis, and thus mTORC1 is a negative regulator of pigmentation.

Rapamycin is a promising mTOR inhibitor, but its therapeutic use for the topical treatment of skin disorders is limited, possibly its insufficient penetration through the dermal barrier due to high molecular weight (914.172 g/mol) and lipophilicity (Rancan et al., 2023). Topical rapamycin application is proven to be effective in the repigmentation of human TSC skin lesions, as inhibiting mTORC1 promotes melanogenesis by increasing the expression of MITF and its downstream targets TRP1 and TRP2 (Wataya-Kaneda et al., 2015; Cao et al., 2017; Yang et al., 2018). A recent study reported the inhibitory effect of rapamycin in inflammation-induced *ex vivo* human skin fibroblasts and keratinocytes, supporting the previous *in vitro* studies (Yang et al., 2018; Rancan et al., 2023). Nonetheless, whether topical application of rapamycin would have a repigmentation effect on *MTOR*-mutated skin remains unknown.

This case adds to the growing evidence on *MTOR*-related pigmentary mosaicism and expands the genotype-phenotype correlation by reporting unilateral overgrowth without accompanying brain malformations. The clinical findings observed in our patient further highlight the differences in phenotypic presentation of germline and mosaic *MTOR* variants, and support that they should not be considered in the same clinical spectrum, despite their common molecular basis and partial clinical overlap.

STUDY 5

RASA1-Related Capillary Malformation-Arteriovenous Malformation Syndrome in a Three-Generation Pedigree Suggesting Constitutional Mosaicism

Clinical Findings

The index was born via spontaneous vaginal delivery at term after an uneventful pregnancy with a birth weight of 4700 g and a height of 55 cm, OFC was not recorded. Overgrowth and skin color changes (dark purple) of the left lower extremity were noticed at birth. Complex lymphovascular malformations were detected in the left lower extremity, and an operation was performed to restore the lymphovascular abnormalities at 6 months of age. Partial benefit was obtained from the operation in such a way that the thickness and the color changes were reduced. A lesion that was determined as compatible with epidermal nevus occurred on her buttock at the age of 6, and cryotherapy was applied. Her neuromotor development and intelligence were normal. Cardiac ECHO was normal except for a patent foramen ovale.

Her body measurements at 11 years 7 months of age were as follows: weight: 50.1 kg (+0.9 SD), height:147.7 cm (-0.34 SD), and OFC: 55 cm (+0.81 SD). She had no facial dysmorphism. Hypertrophic left lower extremity with skin color changes compatible with nevus flammeus was observed. Upper extremities were normal. In addition, a cutaneous capillary malformation (2x3 cm in size) was present at the left lumbar region (Figure 3.15). Complex lymphovascular abnormalities were detected by MRI.

The father also has cutaneous capillary malformations on his left hand and left inferior abdominal region. Pedigree analysis revealed that two children from a different marriage of the father, a nephew and a stepsister of the father, have similar skin lesions, described as compatible with capillary malformations. Paternal grandmother died of internal bleeding at 79 years of age, possibly due to the rupture of internal vascular malformations (Figure 3.14).

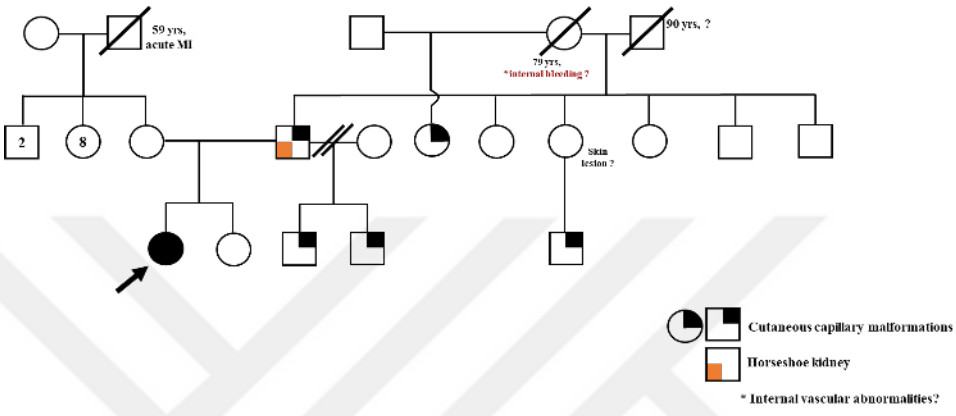

Figure 3-15. **Pedigree analysis of index 5** revealed several similarly affected family members on the paternal side.

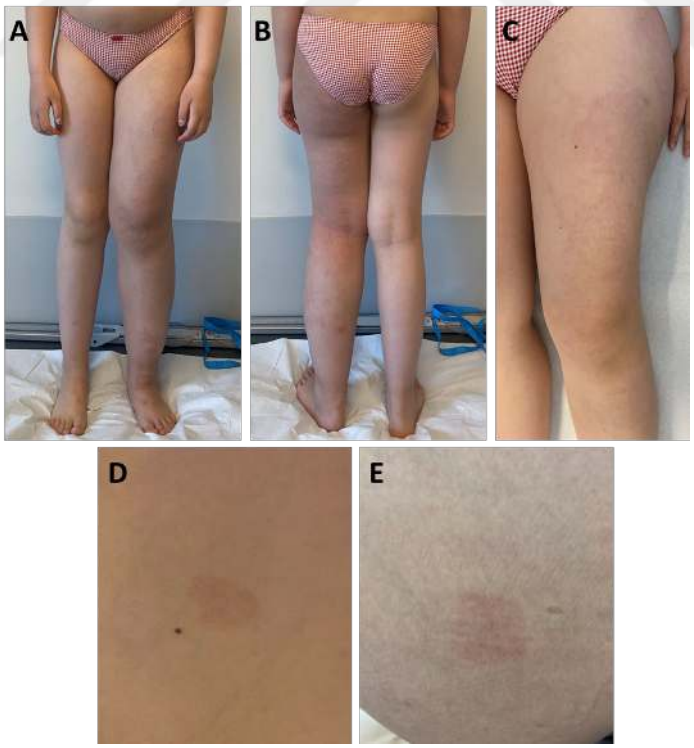

Figure 3-14. **Clinical findings of the index 5 and her father**. At 11 years 7 months of age, she had **(A-B)** hypertrophic left lower extremity, **(C)** skin color changes on left leg compatible with nevus flammeus, **(D)** CM on left lumbar region. **(E)** CM on the father's left inferior abdominal region.
left inferior abdominal region.

Performed Tests and Results

In the index, WES analysis on the DNA derived from peripheral blood revealed a heterozygous splice-site variant of c.1332+2T>C p.(?) in the *RASA1* gene. The variant was detected in 27 out of 81 reads (VAF: 33%), suggestive of potential somatic mosaicism. The percent of targeted nucleotides covered at ≥20x depth was 99.27% (CENTOGENE GmbH, Rostock, Germany).

The identified c.1332+2T>C splice variant is predicted to disrupt the highly conserved donor splice site and has not been previously reported in population databases (gnomAD, ESP, 1000 G, CentoMD). It was predicted to be "disease causing" by MutationTaster. It is classified as likely pathogenic (class 2) according to ACMG recommendations. Although somatic *RASA1* variants are associated with Basal cell carcinoma, the phenotype of the patient was more **consistent with a genetic diagnosis of autosomal dominant Capillary malformation-arteriovenous malformation-1**.

The variant was subsequently confirmed in the index by Sanger sequencing. Sanger sequencing in the father's peripheral blood sample revealed the paternal inheritance of the variant (Figure 3.16). Maternal DNA was not available for analysis. Given the clinical findings, gonadosomatic or constitutional mosaicism in the affected father was suspected; but was not possible to be investigated at the time of diagnosis. Testing a different tissue sample (e.g. buccal swab, skin biopsy), to determine the level of mosaicism and to screen possible second-hit variants, was offered but not opted by the family at that time.

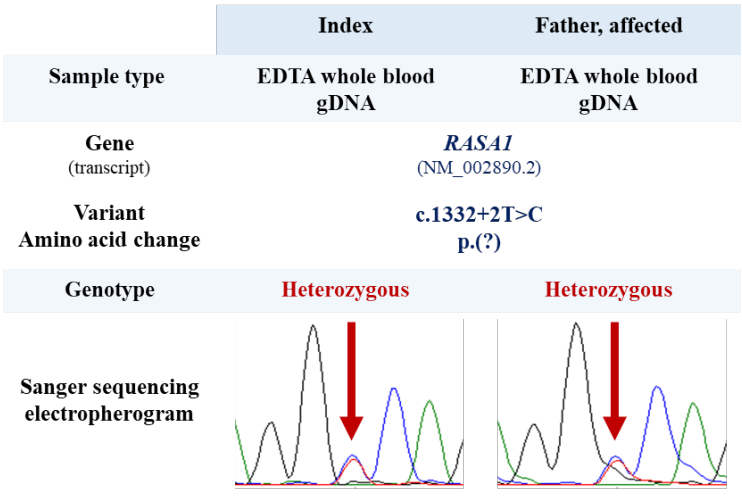

Figure 3-16. **Sequencing electropherograms of the index 5 and her father**, indicating the heterozygous *RASA1* c.1332+2T>C variant.

Discussion

Capillary malformation-arteriovenous malformation (CM-AVM) syndrome represents a spectrum of vascular anomalies with clinical and genetic heterogeneity. It is characterized by the presence of multiple small capillary malformations commonly located on the face and extremities. CMs are typically 1-2 cm in diameter and tend to increase in number with age. Some cases present with fast-flow vascular malformations, including arteriovenous malformations (AVMs) and/or arteriovenous fistulas (AVFs). These lesions may be localized to the skin, muscle, bone, spine, and brain; and can lead to life-threatening complications, such as bleeding, congestive heart failure, and neurological impairment. Symptoms from intracranial AVMs/AVFs often manifest early in life. Lymphatic malformations and limb overgrowth have also been reported in several affected individuals (de Wijn et al., 2012, Burrows et al., 2013, Macmurdo et al., 2016). Overgrowth is typically evident during infancy and varies in severity.

Parkes-Weber syndrome (PKWS) is a specific type of CMAVM that presents with limb overgrowth, more commonly affecting one of the lower extremities (Eerola et al., 2003; Revencu et al., 2013; Johnson and Navarro, 2017). The hallmark of PKWS is a cutaneous blush with underlying multiple micro-AVFs, and soft-tissue and skeletal hypertrophy (Amyere et al., 2017). Clinically, the capillary stains associated with PKWS can be distinguished from regular CMs or port wine stains by surrounding blanched pale halo (Revencu et al. 2013).

To date, pathogenic variants in two genes *RASA1* (CMAVM-1) and *EPHB4* (CMAVM-2) have been associated with CM-AMV syndrome. About 50% of the cases have been attributed to pathogenic variants in *RASA1*, while ~10% have been associated with *EPHB4* variants. In the remaining ~40% of cases, the genetic etiology remains unknown. Even though other genes may be implicated, certain mutations in those two genes could have been overlooked due to the sensitivity limitations of the applied testing methods, or they could be in uncovered regions, such as regulatory or deep intronic regions (Revencu et al., 2020). Large genomic rearrangements may also account for unsolved cases; for instance, *RASA1* genomic rearrangements were identified in ~8% of patients with CVM-AVM1, whereas no genomic rearrangements involving *EPHB4* have been reported to date (Bayrak-Toydemir & Stevenson, 2019).

The *RASA1* encodes for the RAS p21 protein activator 1, which is part of the RAS gene family involved in the regulation of cellular proliferation and differentiation. Parkes-Weber syndrome and CMAVM1 are associated with inactivating autosomal dominant variants in the *RASA1* gene. About 70% of affected individuals are found to have inherited the pathogenic variant from a parent, whereas about 30% harbor a *de novo* variant. Significant intra- and interfamilial variability has been described in terms of lesion number, distribution, and severity. However, studies to date are insufficient to identify genotype-phenotype correlations (Bayrak-Toydemir & Stevenson, 2019).

The presence of an initial germline mutation followed by a somatic second hit mutation is a well-established pathogenic mechanism associated with multifocal lesions, such as in cerebral cavernous malformations or NF1. The presence of somatic mutation, without an initial germline mutation, has also been described in PROS. Constitutional mosaicism, on the other hand, where a pathogenic variant is present in all tissues but at variable levels, appears to be under-recognized and infrequently described (Gordo et al., 2019). All three types of mosaicism have been described in *RASA1*-related cases.

Identifying the second hit variants is challenging due to the limited availability of tissue samples, as surgery is rarely performed for these cases. Several studies have successfully identified second-hit somatic variants in individuals with *RASA1*-related CM-AVM1 or PKWS (Revencu et al., 2013; Macmurdo et al., 2016; Lapinski et al., 2018; Revencu et al., 2020). However, only two studies have confirmed the somatic second hit to be in ***trans*** with the germline variant. In one report, the somatic mutation was detected within a CM lesion shown to be in *trans* with the germline mutation (Lapinski et al., 2018). In another study, two mosaic *RASA1* mutations were identified within an AVM lesion in *trans*: one mutation was present in both blood and the AVM lesion, and the other was confined only to the AVM lesion. Notably like many mosaic syndromes, the mosaicism level of the first hit mutation was higher in the AVM tissue compared to blood (Revencu et al., 2020).

Constitutional mosaicism in CM-AVM1 was also reported in both blood and affected tissue, with no second hit detected despite high-throughput sequencing in the affected tissue (Gordo et al. 2019). Moreover, two somatic pathogenic variants in the *RASA1* gene were reported in a CM lesion without an initial germline variant in blood (Flores Daboub et al., 2020). However, it is impossible to comment on true somatic

mosaicism as the germline testing on blood was only performed by Sanger sequencing and not with NGS to completely rule out low-level mosaicism. In our study, unfortunately, the evaluation of potential constitutional mosaicism or second-hit mutations could not be conducted in either the index case or her affected father, due to the unavailability of tissue samples.

In conclusion, it is not possible to generalize the type of mosaicism in *RASA1*-related cases. While germline mutations in *RASA1* account for approximately half of diagnosed cases, the underlying mechanisms in many patients remain unresolved, partly due to technical limitations and the inherent complexity of mosaicism. Evidence supports a two-hit model involving both germline and somatic variants in some individuals; however, detecting somatic events is challenging because of limited access to affected tissues. The range of mosaicism, including somatic, gonadal, and constitutional, further complicates diagnosis and genetic counseling. Given the wide phenotypic variability and the possibility of mosaicism even without detectable germline mutations, each patient and family must be evaluated individually; and somatic testing of affected tissue, where available, should be incorporated into diagnostic workflows.

STUDY 6

Superimposed Mosaicism: Segmental Neurofibromatosis Type 1 with Pigmented Cutaneous Neurofibromas

Clinical Findings

Index was born at term via normal spontaneous vaginal delivery, and no issues were reported in the antenatal and perinatal periods. Neuromotor development was reported to be normal. The family recalls no noticeable findings at birth, but a brown spot on the left side of the forehead by the age of one, and a darkening on the left eyebrow was noticed at age two. By the age of five, the left eyebrow showed further darkening and increased hair growth. At age 8, the nasal bridge had widened, and the eyebrow hair growth intensified. When the lesion became darker and more pronounced at age 10, the family consulted plastic surgery. The patient underwent surgery at age 11 with a diagnosis of a giant hairy nevus on the face, and a portion of the tumorous tissue in the left eyebrow was excised. The report of the preoperative MRI evaluation was not available. At age 12, the darkening and hair growth on the left cheek became more noticeable. He further reports that the lesion and hypopigmented spots became increasingly pronounced over time.

Before military service, he was evaluated by a plastic surgeon and was diagnosed with neurofibromatosis and recommended MRI evaluation. For treatment, partial excision and partial facial surgery with prior autograft preparation in the facial tissue were suggested. The patient declined this treatment option, and then six sessions of laser treatment were administered.

An incisional biopsy from the lesion revealed diffuse-type cutaneous neurofibroma with increased pigmentation in the basal layer of the overlying epidermis.

Dermatology consultation concluded that the findings were consistent with segmental neurofibroma and hypopigmented lesions. He also had a history of shingles in the left lower quadrant [at 23 years of age] and alopecia areata [at 27 years of age]. Genetic testing at an outer center reported no mutation(s) on all exons and introns of the *NF1, NF2, ATM, BRAF, PTEN, SDHAF2, SDHB, SDHC, SDHD, SH3BP2, and SPRED1* genes on the DNA obtained from a punch biopsy of the facial neurofibroma.

The first consultation at the medical genetics' outpatient clinics was at 27 years of age. He had a height of 174 cm, weight of 72 kg, and OFC of 58-60 cm (Head circumference measurement could not be accurately performed due to the facial neurofibroma on the upper left side of the face).

He had facial neurofibroma extending from the midline of the forehead with a width of approximately 5 cm, stretching about 10 cm to the midline of the nose, partially covering the left upper eyelid, expanding 5 cm to the left cheek, and extending 6 cm below the left lower eyelid. There was an increased hair growth in the affected area of the left cheek and noticeable dark hair growth in the left eyebrow. Additionally, the nasal root and bridge were widened due to the lesion. Oral examination was normal.

He had a supernumerary nipple on the right side of the left breast. In the midline of the abdomen, above the umbilicus, a 1x1 cm lesion consistent with seborrheic keratosis was noted. On the abdomen, multiple hypopigmented patches including a 5x5 cm patch in the right medial breast region, a 4x3 cm patch in the left medial breast region, a 5x7 cm patch in the left upper quadrant, a 1x1 cm patch in the right upper quadrant, and two small patches under 1 cm in the epigastrium were observed. Leukotrichia was observed on the hypopigmented area. Depigmentation was noted around the umbilicus and in the surrounding umbilical area. No hair growth was observed in the inguinal and axillary regions. A small café-au-lait (CAL) spot (<5 mm in diameter) was noted on the right lumbar side. Striae were observed on the back.

Cardiovascular examination revealed normal S1 and S2 sounds, with no additional sounds or murmurs detected. Gastrointestinal examination showed a relaxed abdomen with no organomegaly. Genital examination revealed male external genitalia, with a dark-colored pubertal penis. Hyperpigmented spots were more prominent on the glans penis and present on the scrotum.

Performed Tests and Results

A peripheral blood sample was drawn, buccal swab sample was collected, and four different biopsies were obtained: two surgically removed from the pigmented cutaneous neurofibroma on the face, one from the hypopigmented area on the left trunk, and the other from the hyperpigmented area/CaL lesion located on the right abdomen (Figure 3.17). At 27 years of age, the index underwent comprehensive NF1 mutation analysis [performed by The University of Alabama at Birmingham, Department of Genetics].

Molecular testing on neural crest-derived cell types, such as Schwann cells in neurofibromas or melanocytes in pigmented skin, is the recommended diagnostic approach for NF1. For this, melanocytes were cultured as described from all biopsies (Maertens et al., 2007; De Schepper et al., 2008). Schwann cell culture from the facial neurofibromas was attempted as described (Maertens et al., 2006), but was not successful. DNA was extracted from EDTA blood, cultured melanocytes and uncultured skin biopsies of the patient. Total RNA was extracted from cultured melanocytes and cultured lymphocytes.

Six microsatellite polymorphism markers (two intragenic microsatellite polymorphisms, IVS27b, IVS38 and 4 extragenic markers D17S841, D17S1294, D17S1800, D17S933) were analyzed as a first approach to determine whether 2 copies of the *NF1* gene were present (Garcia-Linares et al., 2010). If no heterozygous signal is observed for any of these markers, FISH analysis was performed using PAC clones 22 (926B9; 5' NF1) and 13 (1002G3; 3' NF1) to confirm or rule out the a total gene deletion. Next, the coding regions of the *NF1* gene is analyzed by long-range RT-PCR and direct cycle sequencing, starting from 5 overlapping RT-PCR fragments, spanning exons 1-17 (1-12b), 16-26 (12a-20), 25-37 (19b-28), 37-48 (28-39) and exons 47-58 (38-49) (NCBI (Legacy) numbering). Sequencing is performed using dye-terminator chemistry on an ABI PRISM 3730 capillary sequencer, *NF1* exon 1 is then sequenced at the gDNA level. If no mutation is identified by direct cycle sequencing, MLPA is performed to rule out *NF1* deletions/duplications (MRC Holland P081C1- P082C1, P122C2, P225D1 probe mixes).

Molecular Findings

Independent melanocyte cultures established from the two biopsies of a facial neurofibroma revealed two different pathogenic variants: an atypical total *NF1* gene deletion (~1.4 Mb) and deletion of *NF1* exons 2 to 36 (c.(60+599_92)_(4662-12_4772+30132)del). These *NF1* deletions were confirmed in the uncultured skin biopsy samples from the same facial neurofibroma lesions. No deletions, nor any other *NF1/2* variants, were detected in tissues taken from the hypo-/hyperpigmented areas on the trunk and abdomen or in blood lymphocytes (Figure 3.17)

Altogether, restricted tissue distribution supports **the diagnosis of segmental neurofibromatosis (SNF).**

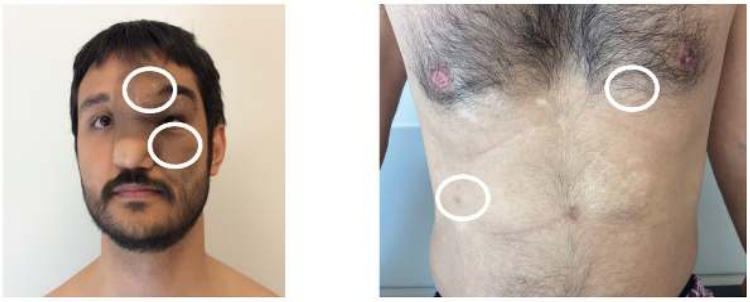

Sample type	gDNA derived from facial cutaneous neurofibroma #1	gDNA derived from facial cutaneous neurofibroma #2	gDNA derived from Café-au-lait spot (R abdomen)	gDNA derived from hypopigmented patch (L trunk)	gDNA derived from EDTA whole blood
NF1 Variant(s) (NM_000267.3)	Whole gene deletion (~1,4MB)		Not detected	Not detected	Not detected
	Deletion spanning exon 2 to exon 36 c.(60+599_92)_(4662-12_4772+30132)del				

Figure 3-17. **Detection of tissue-specific *NF1* deletions in index 6.** Locations of the biopsies are shown in the upper panel (white-circled). gDNA was isolated from five different tissue sources as indicated.

Discussion

Neurofibromatosis type 1 (NF1) is a multisystem disorder characterized by multiple café-au-lait spots, freckles in skin folds (known as intertriginous freckling), and various types of neurofibromas. Distinctive ophthalmologic signs include Lisch nodules and/or choroidal abnormalities. Low-grade optic and non-optic gliomas occur in less than 20% of NF1 patients. The majority of the patients develop benign cutaneous neurofibromas. However, those with numerous or large plexiform or deep nodular

neurofibromas have an increased risk of developing malignant peripheral nerve sheath tumors, which tend to occur at a younger age and have a poor prognosis compared to the general population. Additionally, women with NF1 have a higher risk for breast cancer risk and pregnancy-related complications. Hypertension is prevalent among NF1 patients, and NF1 vasculopathy can lead to serious cardiovascular issues, including stroke, in children and young adults. Some individuals may suffer significant disabilities from vertebral or tibial dysplasia. While less common, NF1 can also be associated with severe gastrointestinal, endocrine, or pulmonary diseases. Furthermore, intellectual disabilities, learning difficulties, and behavioral issues are often reported in some individuals (Friedman, 2022).

NF1 is inherited in an autosomal dominant pattern and is caused by mutations in the neurofibromin 1 (*NF1*) gene, which spans a large locus of 350 kilobase pairs on chromosome 17q11.2 and consists of 61 exons. Approximately half of the cases are familial, but the remaining half arise from *de novo NF1* mutations. Diagnostic criteria for NF1 include the presence of any of the following clinical features: (1) six or more CAL macules with round or oval shape, a uniform light to dark brown color, and well-demarcated margins (5 mm in diameter in prepubertal individuals, 15 mm in diameter in postpubertal individuals), (2) freckling in the axillary or inguinal regions, (3) two or more neurofibromas of any type or one plexiform neurofibroma, (4) optic pathway glioma, (5) two or more Lisch nodules identified via slit-lamp examination or two or more choroidal abnormalities (bright, patchy nodules detected by optical coherence tomography/near-infrared reflectance imaging), (6) a distinctive osseous lesion such as sphenoid dysplasia, anterolateral bowing of the tibia, or pseudarthrosis of a long bone, (7) a parent who meets the diagnostic criteria for NF1, (8) identification of a germline *NF1* pathogenic variant (Friedman, 2022).

A pathogenic germline variant of *NF1* must be identified for a genetic test to serve as a criterion for diagnosis. However, a negative NF1 molecular test does not definitively rule out NF1 (Accetturo et al., 2020; Legius et al., 2021). Some individuals who meet the clinical criteria for NF1 may not have a detectable pathogenic variant with current diagnostic technologies. In addition, many clinical manifestations of NF1 increase with age, meaning that some individuals with definite NF1 in adulthood may not meet the diagnostic criteria in early childhood, as certain features only appear over time. In

addition, postzygotic *NF1* mutations during fetal development also cause phenotypic diversity, known as mosaic NF1.

Mosaic NF1, resulting from somatic mosaicism of an *NF1* pathogenic variant, can present with clinical features localized to one or more body segments or as generalized NF1 (Ejerskov et al. 2021). Early somatic mutations, occurring before tissue differentiation, typically result in a generalized NF1 phenotype. This generalized mosaic pattern often appears clinically similar to classical nonmosaic NF1, but the symptoms are generally milder. In these cases, blood leukocytes typically do not carry the specific *NF1* mutation. On the other hand, late somatic mutations lead to a more limited phenotype. Localized mosaic neurofibromatosis, also referred as type V neurofibromatosis or segmental neurofibromatosis (SNF), is a rare form of the condition where skin lesions are confined to a specific body segment. SNF generally does not progress to the generalized form, and severe manifestations are less common. Lisch nodules, which are typically seen in generalized NF, are rarely found in SNF. Systemic involvement is rare while learning difficulties, plexiform neurofibromas, optic pathway gliomas, and pseudarthrosis are observed in less than 10% of cases. Individuals with the mosaic form, even with a generalized phenotype, are less likely to have severe disease.

The most common cutaneous finding of SNF is neurofibromas, while café-au-lait spots and axillary freckling occur less frequently. Clinically, patients with SNF can be categorized into four groups: (1) patients with only pigmentary lesions, (2) patients with only neurofibromas, (3) patients with both pigmentary lesions and neurofibromas, and (4) patients with isolated plexiform neurofibromas. Skin manifestation is usually limited to the affected area, with cervical and thoracic regions being the most commonly affected. The lesions are usually unilateral, although bilateral cases, both symmetric and asymmetric, have been reported. The CAL spots may follow Blaschko's lines whereas neurofibromas are confined to a single dermatome. The extent varies from a narrow strip to one quadrant and/or to a half-body, and a darker background may cover the affected region (Ruggieri & Huson, 2001; Ozarslan et al., 2021).

SNF is commonly underdiagnosed due to its milder clinical presentation, with skin lesions often going unnoticed or being mistaken for birthmarks or harmless nodules. Most patients remain asymptomatic, seeking medical attention primarily for cosmetic reasons or receiving an incidental diagnosis. However, individuals with spinal

neurofibromas or lesions on major peripheral nerves may experience pain or neurological symptoms. Increased risk for certain malignancies is rare but has been reported, particularly those arising from neural crest cells including peripheral nerve sheath tumors, adrenal ganglioneuroma, and malignant melanoma. Other reported cancers include breast cancer, colon cancer, gastric cancer, lung cancer, and Hodgkin lymphoma (Dang & Cohen, 2010).

Although clear-cut genotype–phenotype correlations are not established, various phenotypic differences between *NF1*-deleted and *NF1*-mutated cases have been identified. Intragenic *NF1* variants constitute the majority of germline mutations linked to NF1, while NF1 microdeletions in 5%-11% of all patients with NF1 (Kehrer-Sawatzki et al 2020). Patients with large deletions encompassing the entire *NF1* gene and neighboring genomic regions are associated with more severe and atypical disease presentation compared to patients with intragenic variants (Kang et al., 2020).

Four types of large NF1 deletion (type-1, 2, 3, and atypical) have been described, they are distinguishable in terms of their size and breakpoint location, by the number of genes located within the deletion region and by the frequency of somatic mosaicism with normal cells lacking the deletion (Kehrer-Sawatzki & Cooper, 2021). Of them, 70-80% are accounted for type-1 *NF1* deletions, which encompass 1.4-Mb and include 14 protein-coding genes and five microRNA genes (Dorschner et al., 2000; Jenne et al., 2001). Most type-1 *NF1* deletions are caused by interchromosomal non-allelic homologous recombination (NAHR) during maternal meiosis mediated by the low-copy repeats, NF1-REPa and NF1-REPc (López Correa et al., 2000). Within these low copy repeats, recurrent breakpoints have been detected within two NAHR hotspots, termed paralogous recombination sites 1 (PRS1) and 2 (PRS2) (Forbes et al., 2004; De Raedt et al., 2006). Type-1 deletions typically occur in the germline and are associated with NF1 microdeletion syndrome (MIM #613675), which is often linked to a more severe clinical phenotype characterized by an increased number of cutaneous and plexiform neurofibromas, earlier tumor onset with an increased risk of malignant peripheral nerve sheath tumors, delayed cognitive development/learning disabilities, generalized overgrowth and dysmorphic features of coarse facies, flat forehead, ocular hypertelorism, broad nasal tip, low-set ears, and broad neck (Mautner et al., 2010; Pasmant et al., 2010; Pacot et al., 2021; Kehrer-Sawatzki & Cooper, 2021).

Type-2 deletions, account for approximately 10% of all patients with *NF1* microdeletions. Often occurring postzygotically from mitotic NAHR between the *SUZ12* gene and its pseudogene *SUZ12P*, type-2 deletions span 13 protein-coding genes and are 1.2 Mb in size (Vogt et al., 2012). About 70% of the cases are mosaic, with a higher VAF in blood (94–99%) compared to skin fibroblasts (39–91%) and urine cells (24–82%) (Roehl et al., 2012). Type-3 *NF1* deletions, occurring in only 1–4%, encompass 1-Mb and are mediated by NAHR between NF1-REPb and NF1-REPc and include 9 protein-coding genes. Approximately 8–10% of all ***NF1*** microdeletions are considered to be atypical, as identified in index (Pasmant et al., 2010; Messiaen et al., 2011). Unlike type-1, type-2, and type-3 deletions, atypical NF1 deletions do not have recurrent breakpoints and they vary in size and the number of genes encompassed. They may occur in germline, but the majority represent mosaic deletions arise postzygotically due to errors in replication, DNA double-strand break repair, or retrotransposon-mediated mechanisms (Kehrer-Sawatzki & Cooper, 2021).

Identification of two distinct deletions in our patient's facial cutaneous neurofibromas, but not in the blood, CAL spot, or hypopigmented patch, underscores the role of somatic mosaicism in disease pathogenesis. However, the presence of a total *NF1* gene deletion in one allele, and another large deletion spanning exons 2-36 in the second allele suggests a higher genetic complexity and mutation burden.

NF1 is a tumor suppressor gene that follows the Knudson two-hit hypothesis of tumor formation. The two-hit hypothesis provides a plausible explanation for our molecular observations in this case, wherein a first somatic mutation is followed by a second mutation during development, leading to biallelic loss of NF1 function and promoting tumor formation (Figure 3.18). This mechanism has been observed in various *NF1*-related benign and malignant tumors, including CAL macules, and is well-documented in Schwann cells within cutaneous neurofibromas. Second-hit variants are expected to be present in higher VAFs in neural-crest derived cells. Adding further complexity, the mutational spectrum of *NF1* varies between first-hit and second-hit mutations. Somatic frameshift mutations, with deletions of at least 4 nucleotides, are reported frequently as second-hit mutations, whereas somatic missense mutations are less common.

All neurofibromas originate from the Schwann cell lineage, and cutaneous neurofibromas consist of neoplastic Schwann cells along with non-neoplastic components such as mast cells and fibroblasts. Other common cell types include perineurial cells, nerve sheath elements, and adnexal structures such as hair follicles, eccrine sweat glands, and sebaceous glands. Additionally, pigmented cutaneous neurofibromas may be linked to melanocytic cells or melanotic Schwann cells (Ortonne et al., 2018). In the index, pigmented cutaneous facial neurofibromas shared an atypical total gene deletion of ~1.4 Mb, and another second-hit deletion encompassing exons 2 to 36 in the non-deleted NF1 gene copy. Identification of these variants in cultured melanocytes and uncultured biopsy samples containing all skin layers (epidermis, dermis, and subcutaneous tissue) correlates with previous findings. The segmental localization of these neurofibromas can be explained by superimposed mosaicism, that potentially resulting from the the total *NF1* deletion later during embryonic development, thus affected only a subset of cells. The subsequent second-hit deletion during postnatal development and clonal expansion within the same specific region may contributed to the development of neurofibromas in the index.

Overall, this case adds to the growing body of evidence that the clinical variability in segmental NF1 is closely tied to the extent of mosaicism. Further genetic analysis could shed light on the mechanisms responsible for this divergence, particularly concerning the atypical *NF1* microdeletions.

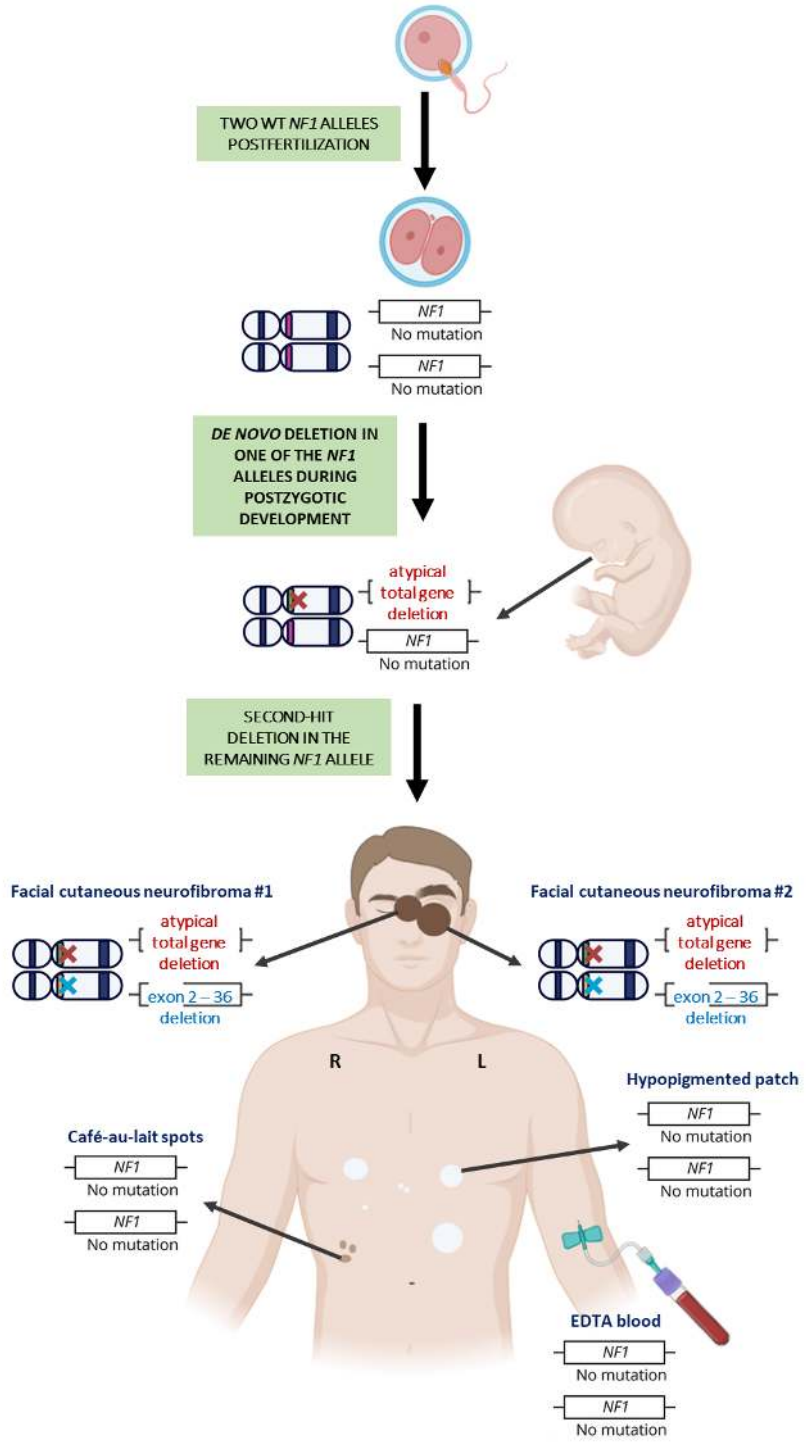

Figure 3-18. **Schematic illustration of the proposed superimposed mosaicism model in index 6**. A postzygotic *de novo* atypical whole-gene deletion arose during early embryonic development, led to somatic mosaicism in affected tissues. Subsequent second-hit deletion involving exons 2 to 36 of the *NF1* gene occurred in the remaining allele within facial cutaneous neurofibromas. In contrast, no *NF1* mutations were detected in DNA from CaL spots, hypopigmented patches, or peripheral blood.

STUDY 7

A Recurrent Homozygous Variant in *MFN2* Causes Multiple Symmetric Lipomatosis

Clinical Findings

A 20-year-old female patient was referred by the endocrinology department for genetic consultation with a preliminary diagnosis of lipodystrophy. Her parents are first cousins. She developed excess fat on her upper body at age 11-12 years, while fat on her lower extremities decreased. At age 18, by biochemical and hormonal assays, Cushing's syndrome was ruled out and she was administered metformin for six months.

At 20 years and 7 months of age, she had a weight of 73.5 kg, height of 159 cm and OFC of 53.5 cm (BMI: 29.07). She exhibited excess lipomatous tissue of the neck, upper arms, trunk, back, and mons pubis. The adipose tissue was soft, unencapsulated, and poorly defined. Additionally, she had multiple acneiform lesions on her upper arms and back, which were diagnosed as Hidradenitis suppurativa by dermatologists (Figure 3.19 A-D). As of age 22, she had not shown any signs of neuropathy or other finding.

Her clinical findings suggested multiple lipomatosis type 3 according to Schiltz's classification, which primarily affects the upper body while sparing the lower extremities, face, and forearms. MRI confirmed the accumulation of subcutaneous unencapsulated lipomas with no clear margins (Figure 3.19 E-G).

Performed Tests and Results

Peripheral blood, buccal swab and skin biopsy samples were obtained from the index. The literature was reviewed for rare adipose disorders. Firstly, *PIK3CA* hotspot

mutations were ruled out by qPCR on the DNA sample obtained from blood plasma, buccal swab, and skin biopsy samples. Then, WES was planned to rule out all possible adipose disorders.

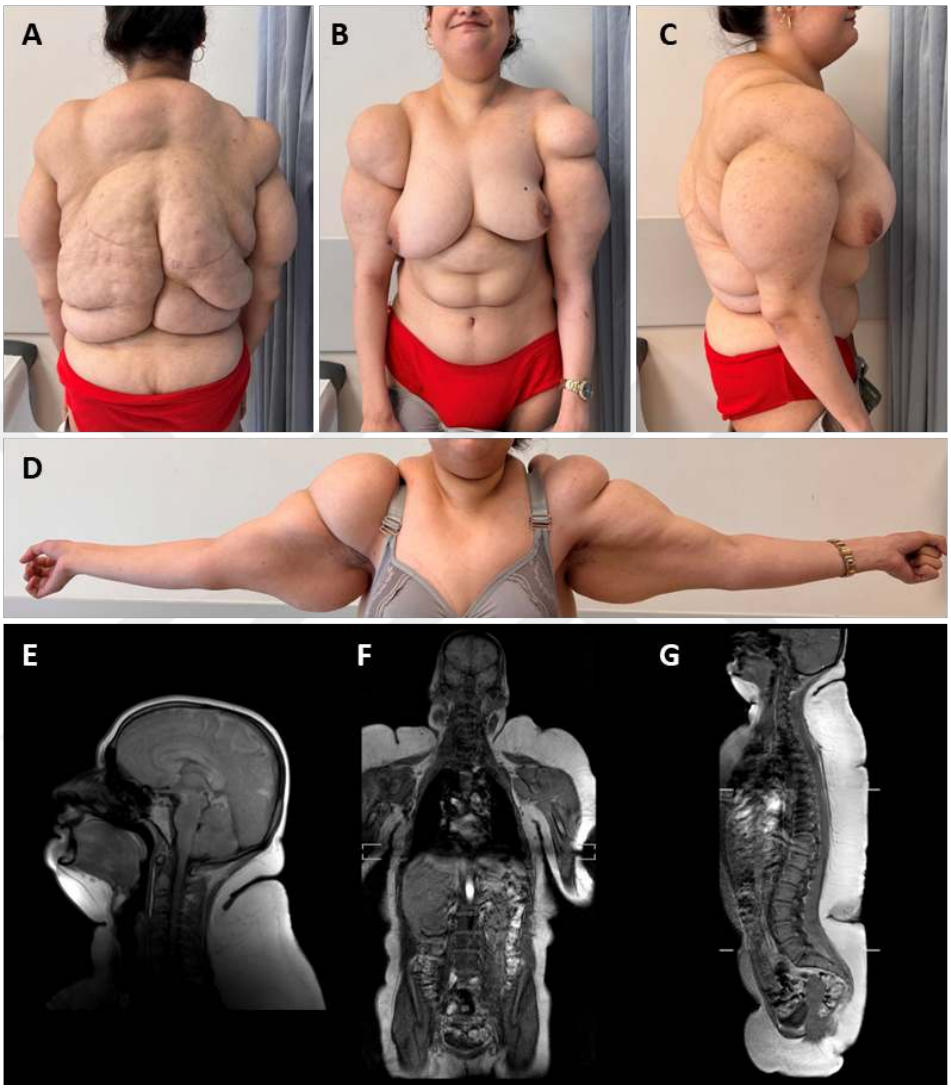

Figure 3-19. **Clinical images of index 7** showing **(A-D)** symmetric excess lipomatous tissue extending from the neck, upper arms, trunk, back, and mons pubis. **(E)** MRI images confirming the subcutaneous unencapsulated lipomas with no clear margins.

Molecular Findings

WES analysis on DNA from skin biopsy revealed a homozygous pathogenic c.2119C>T p.(Arg707Trp) variant in the *MFN2* gene, and potentially relevant homozygous c.1337T>C p.(Leu446Pro) variant in the *GCKR* gene. The percent of

targeted nucleotides covered at ≥20x depth was 98.83% (CENTOGENE GmbH, Rostock, Germany).

The identified missense variant Leu446Pro in the glucokinase regulatory protein (*GCKR*) gene is reported as "benign" with a high MAF in the databases (gnomAD: 0.65, PolyPhen: Benign, SIFT: Tolerated, MutationTaster: Polymorphism); and is classified as a risk factor for "fasting plasma glucose level quantitative trait locus-5 (FGQTL5, MIM #613463). This common variant is associated with increased plasma triglyceride and C-reactive protein but lower fasting glucose concentrations. In the index, all three levels were within their normal ranges, so this variant was considered non-relevant.

The identified *MFN2* variant causes an amino acid change from Arginine to Tryptophan at position 707 in the 17th exon of the gene. According to HGMD Professional 2024.2, this variant has previously been described as disease-causing for "Axonal neuropathy, severe, early-onset" (Nicholson et al., 2008). ClinVar lists this variant as "Pathogenic/Likely pathogenic" (Variation ID: 2280). It was reported in gnomAD with MAF of 0.00025; and predicted to be "Disease causing" by MutationTaster, "Probably Damaging" by PolyPhen, and "Deleterious" by SIFT. It is classified as pathogenic (class 1) based on ACMG/AMP/ClinGen SVI guidelines.

The variant was confirmed in the DNA samples obtained from EDTA blood (whole blood, blood plasma, RBC), skin biopsy, and buccal swab of the index by Sanger sequencing (Figure 3.20).

Sample type	EDTA whole blood gDNA	Skin biopsy gDNA	Buccal swab gDNA	Blood Plasma ccfDNA	RBC ccfDNA
Gene (transcript) Variant Amino acid change	*MFN2* (NM_001127660.1) c.2119 C>T p.(Arg707Trp)				
Genotype	Homozygous	Homozygous	Homozygous	Homozygous	Homozygous
Sanger sequencing electropherogram	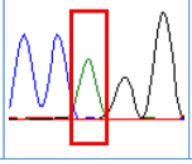	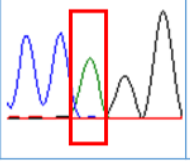	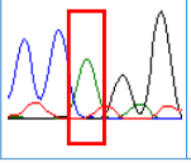	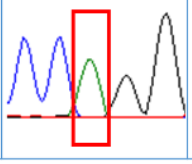	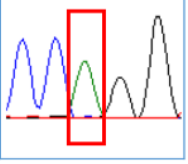

Figure 3-20. **Sanger sequencing electropherogram images of index 7**, indicating homozygosity for *MFN2* c.2119 C>T change in all five sample types tested.

Discussion

Lipomas are the most common type of soft tissue tumors, typically presenting as benign, slow-growing masses composed of mature adipocytes. When multiple lipomas develop without associated lipoatrophy, the condition is called lipomatosis. Lipomatosis can either be an isolated condition or part of a syndromic disorder, such as in PROS and Cowden syndrome, which makes classification and management more complex. Different forms of isolated lipomatosis include familial multiple lipomatosis (FML) with hereditary subcutaneous lipomas, multiple symmetric lipomatosis (MSL), Dercum disease (Adiposis Dolorosa/Ander syndrome), characterized by painful lipomas, mesosomatic lipomatosis (Roch-Leri lipomatosis) with distinctive fat distribution, and rarer types such as hibernomas (benign tumors of brown fat), epidural lipomatosis (fat buildup in the spinal canal), and familial angiolipomatosis (multiple angiolipomas with a genetic predisposition).

Multiple symmetric lipomatosis (MSL), also known as Madelung's disease or Launois-Bensaude syndrome, is an ultrarare disorder characterized by an abnormal buildup of unencapsulated, symmetric lipomatous masses, metabolic disturbances, and, in some cases peripheral neuropathy. MSL is clinically characterized by symmetrical fat deposition of adipose tissue, mainly in the neck, shoulders, and upper trunk, occasionally also on the upper arms, thighs, and abdomen. Usually, there is a significant increase in upper body fat coupled with a decrease in fat in the lower limbs of affected individuals. The lipomatous masses are painless and lack a defined capsule, which distinguishes them from typical lipomas (Enzi et al., 2002). Often mistaken for obesity due to excessive fat accumulation, the cosmetic and functional burden of MSL is usually the main reason that prompts patients to undergo medical intervention. The primary treatment options include surgical excision or liposuction, depending on the size, number, and location of the fatty masses.

In some cases, lipomas can cause functional impairment, such as respiratory difficulties or dysphagia due to compression of nearby structures like the airway or esophagus. In addition to lipomatous deposits, MSL is frequently associated with metabolic conditions such as hyperlipidemia, hyperuricemia, hypertension, hypothyroidism, insulin resistance, and hepatic steatosis (Enzi et al., 2002). Although

most patients with MSL do not experience neurological symptoms, some may develop peripheral neuropathy.

Diagnosis relies on physical examination and medical history, with onset ranging from childhood to young adulthood. One of the most notable features of the MSL phenotype is the low or undetectable serum leptin levels despite normal or increased overall adipose tissue and relatively normal histology of the upper-body lipomatous fat (Sawyer et al., 2015; Rocha et al., 2017; Capel et al., 2018). Elevated serum lactate and serum FGF21 levels have also been reported. Since circulating leptin levels usually correlate with fat mass and are affected by fat distribution, this discrepancy is notable. Additionally, patients often have low serum adiponectin levels, which aligns with the "adiponectin paradox" seen in obesity-related insulin resistance (Arita et al., 1999).

Several classifications have been proposed based on the distribution of fat deposits, and three different classifications are used in the literature. Enzi classified MSL into two phenotypes in 1984: Type I, which is characterized by lipomas concentrated in the neck, shoulders, supraclavicular triangles and proximal upper limbs, and Type II, which is characterized by lipomas in the abdomen and thighs (upper legs), while the neck and upper trunk are not affected (Enzi et al., 1984). In 1991, Donhauser further subdivided them into four phenotypes: Type I, characterized by collar-like masses on the neck, upper back, shoulder girdle, and upper arm; Type II by masses on the shoulder girdle, deltoid region, upper arms, and chest, giving a pseudoathletic appearance; Type III by gynecoid masses involving the lower body, especially the thighs and medial aspect of the knees (inner knees); and Type IV by masses confined to the abdomen (Donhauser et al., 1991). The latest classification by Schiltz from 2018 divides the MSL into five types: Type Ia, in which fat accumulation is limited to the neck; Type Ib, which affects the neck, shoulder girdle and upper arms; Type Ic, which extends to the neck, shoulder girdle, upper arms and chest, abdomen, upper and lower back; Type II is characterized by fat deposits on the hips, buttocks and thighs (upper legs). Type III shows a generalized distribution of adipose tissue that omits the head, forearms and lower legs (calves) (Schiltz et al., 2018).

The pathophysiology of MSL is multifactorial, and various hypotheses regarding potential triggers of MSL have been proposed, including psychological trauma, hypothalamic or pituitary lesions, and parathyroid gland tumors (Lemaitre et al., 2021).

Excessive alcohol consumption has been linked to accelerated progression of lipomatosis in some MSL patients, which is hypothesized to induce acquired immuno-inflammatory and mitochondrial dysfunction through the toxic effects of the alcohol metabolite acetaldehyde (Hirose et al., 2006; Pinto et al., 2017; Lemaitre et al., 2021). While neurological multisystem involvement is common in patients, it cannot be solely attributed to alcohol abuse, making the association between MSL and alcohol consumption subject to debate.

The first genetically determined form of MSL identified was associated with MERRF syndrome (myoclonic epilepsy with ragged red fibers), which is caused by pathogenic variants in the mtDNA lysine tRNA (*MT-TK*) gene (Klopstock et al., 1997; Perera et al., 2018). Mutations in lipase E, hormone-sensitive type (*LIPE*), calcyphosin-like (*CAPSL*), Cbl proto-oncogene B (*CBLB*) have also been reported in patients with MSL (Farhan et al, 2014, Zolotov et al., 2017; Lindner et al, 2019; Chen et al, 2020). To date, *MFN2* is the only gene associated with Mendelian MSL in OMIM, with its null variants associated with autosomal recessive MSL with or without peripheral neuropathy (MIM #151800). The disease is solely associated with the MFN2 R707W variant, identified in the index (Sawyer et al., 2015). Majority of the reported cases were homozygous for the R707W variant, while compound heterozygosity for R707W and a second null variant was also rarely reported (Rocha et al., 2017; Capel et al., 2018).

The *MFN2* gene encodes the mitofusin-2 protein (MFN2), a key component of the outer mitochondrial membrane responsible for regulating mitochondrial fusion, an essential process for maintaining mitochondrial function and integrity (Chen et al., 2003). In addition, MFN2 has also been identified as an important regulator of interactions between mitochondria and organelles, particularly with the endoplasmic reticulum (ER) (de Brito and Scorrano, 2008). Controlled by *MFN2*, several studies have emphasized the crucial role of mitochondrial dynamics as a “nutrient sensor” that enables neuronal cells to adapt to fluctuations in nutrient availability (Mandl et al, 2009; Baltzer et al, 2010; Dietrich et al, 2013; Schneeberger et al, 2013).

Mitochondrial fusion relies on the trans-dimerization of mitofusins located on opposing membranes. This process necessitates a GTPase-independent extended conformation, characterized by an anti-parallel dimer formed between second heptad repeat (HR2) domains of MFN1 and/or MFN2 (Koshiba et al., 2004; Franco et al.,

2016). The HR2 domain is involved in different interfaces in GDP-bound monomers, GTP-bound cis-oligomers, GTPase-independent trans-dimers, and MFN2/MFN1 trans heterodimers. The Arg707 residue is located within the highly conserved HR2 coiled-coil domain at the C-terminal of MFN2. In silico protein models revealed that Arg707 plays a distinct role in stabilizing different MFN2 conformations: it forms an ion pair with Asp742 in the trans-antiparallel homodimer, while in the MFN1 heterodimer, it interacts with Glu728. In all other conformations, Arg707 is exposed on the surface and does not directly participate in intra- or intermolecular helix packing. Consequently, Arg707 mutations are hypothesized to destabilize trans-dimerization by disrupting the ion pair, while having a lesser impact on other conformations (Rocha et al., 2017). The *MFN2* R707W variant may disrupt this binding and subsequent MFN oligomerization and thus mitochondrial fusion and tethering to other organelles.

In vitro studies on MFN2-null cells revealed that the R707W mutant exhibited a reduced ability to tubulate mitochondria. This led to mitochondrial aggregation, defective homo-oligomer formation, and the development of smaller oligomeric complexes compared to wild-type MFN2 (Rocha et al., 2017). Additionally, primary overgrown adipose tissue from patients showed hyperplasia of unilocular adipocytes that were negative for UCP1, along with the proliferation of enlarged mitochondria featuring fragmented cristae. Transcriptome analyses further indicated a dysregulation of mitochondrial function and oxidative phosphorylation. Changes were observed in the expression of genes involved in cellular stress response pathways, particularly those related to oxidative stress and the unfolded protein response, as well as an upregulation of signatures associated with tissue proliferation and survival. Notably, the expression of leptin and adiponectin [two important hormones regulating metabolic function and adipose tissue homeostasis] was also found to be reduced. Despite these metabolic disturbances in adipose tissue, patients' fibroblasts exhibited normal MFN2 expression, appropriate mitochondrial localization, and structurally intact mitochondria. These findings suggest that the pathological effects of the MFN2 R707W variant are tissue-specific (Rocha et al., 2017).

In *in vivo* studies, the global knockout of Mfn2 in mice resulted in embryonic lethality (Chen et al., 2003). Several tissue-specific Mfn2 knockout mouse models have been investigated, including those targeting cardiac or skeletal muscle (Chen and Dorn,

2013; Sebastián et al., 2016), dopaminergic neurons (Pham et al., 2012), hypothalamic POMC neurons (Schneeberger et al., 2013), proximal renal tubules (Gall et al., 2015), and three models targeting adipose tissue (Boutant et al., 2017; Mahdaviani et al., 2017; Mancini et al., 2019). In adipocyte-specific Mfn2 knockout mice, the absence of mitofusin 2 in fat cells caused significant metabolic disturbances, regardless whether the Mfn2 deletion was induced during embryonic development (Boutant et al., 2017; Mahdaviani et al., 2017) or in adulthood using tamoxifen (Mancini et al., 2019).

Embryonically induced adipocyte-specific knockout mice showed increased fat accumulation in the brown adipose tissue, even on a low-fat diet (Boutant et al., 2017). In contrast, brown adipocyte-specific knock-out mice fed with a standard diet had body weight and composition similar to the control mice. However, they had increased mass of brown adipose tissue with larger lipid droplets, suggesting lipohypertrophy (Mahdaviani et al., 2017). Both adipocyte-specific and brown adipocyte-specific knock-out mice had improved insulin sensitivity and resistance to obesity even with a high-fat diet, but showed cold intolerance. When Mfn2 deletion was induced in all adipocytes during adulthood (Ati-mfn2-ko), the mice exhibited increased food intake, excessive fat accumulation, and impaired glucose homeostasis, regardless of their diet. Their body weight and adiposity under a standard diet resembled control mice on a high-fat diet. They had increased plasma leptin and decreased adiponectin levels. The transcriptional profile of their adipose tissues revealed enhanced adipocyte proliferation, increased tissue lipogenesis, and reduced systemic glucose utilization (Mancini et al., 2019). While not fully aligning with the human phenotype, these observations highlighted that the disrupted mitochondrial dynamics due to *MFN2* deficiency in adipocytes, especially in brown adipocytes, affect energy expenditure and contribute to obesity-related metabolic dysfunction by influencing insulin sensitivity and glucose homeostasis.

Later, the model of homozygous Mfn2 R707W knock-in mice demonstarated that the R707W mutation retains important aspects of Mfn2 function in adipose tissue and preserves significant functional capacity. These mice retained normal fat mass, insulin sensitivity and thermogenic capacity, but had selectively disrupted mitochondrial morphology in adipose tissue. Consistent with the human phenotype and *in vitro* observations, both standard and high-fat diets resulted in decreased serum leptin and adiponectin levels in R707W knock-in mice (Mann et al., 2023). In addition,

transcriptomic analysis revealed increased mTORC1 activation in adipose tissue, suggesting the role of integrated mitochondrial stress response in metabolic dysfunction. Given the promising results of mTORC1 inhibition in mitochondrial diseases, the potential efficacy of the mTOR inhibitors everolimus and rapamycin (sirolimus) in *MFN2*-related MSL remain to be further investigated (Johnson et al., 2013; Sage-Schwaede et al., 2019).

A deeper understanding of the pathophysiological mechanisms underlying MSL could provide valuable insights into other metabolic and neurodegenerative diseases associated with mitochondrial dysfunction. As current treatments are largely symptomatic and rely on surgical interventions and treatment of metabolic complications, further exploration of the molecular pathways linking mitochondrial dysfunction and lipomatosis is critical for the development of targeted therapeutic strategies. The development of targeted therapeutic strategies aimed at restoring mitochondrial function, optimizing lipid metabolism, and attenuating the effects of *MFN2* variants hold the potential to alleviate clinical manifestations and improve patient outcomes.

STUDY 8

Novel Mosaic Mutation in Fibroblast Growth Factor Receptor 2 Leads to Blended Phenotype of Systematized Keratinocytic Epidermal Nevi and Beare-Stevenson Cutis Gyrata Syndrome

Clinical Findings

The patient, a 2-month-old baby girl, presented with craniofacial and trunk/distal extremity skin abnormalities. The patient was not followed up during the antenatal term but noted to be large for gestational age.

Physical examination was notable for abnormal epidermal morphology, with keratinocytic and hyperpigmented lesions following Blaschko's lines on the trunk and extremities. Additional findings included epidermal acanthosis and a generalized skin rash (Figure 3.21). She had a congenital abnormal hair pattern, with tufted hair and irregularities in the scalp hair structure. She had furrowed skin with a corrugated appearance consistent with cutis gyrata affecting almost all the craniofacial area (Figure 3.21 A-B).

Macrocephaly was noted upon physical examination, accompanied by a prominent forehead and large anterior fontanelle. She had an overall abnormal facial morphology, dysmorphic findings included epicanthus, hypertelorism, midface hypoplasia, strabismus and gingival overgrowth. She had absent lower eyelashes and sparse and almost absent upper eyelashes. She further had abnormal eyebrow morphology, with left eyebrow aplasia and hypoplastic right eyebrow (Figure 3.21 A-B). She had urogenital anomalies including closed vaginal orifice and anteriorly placed anus with an anal polyp.

Neuroimaging revealed central nervous system abnormalities, including bilateral ventriculomegaly with intra and extra-cerebral abundant cerebrospinal fluid, and unilateral cerebellar hypoplasia. Additionally, there were signs suggestive of possible neuronal migration defects, which may contribute to the neurodevelopmental profile (Figure 3.22).

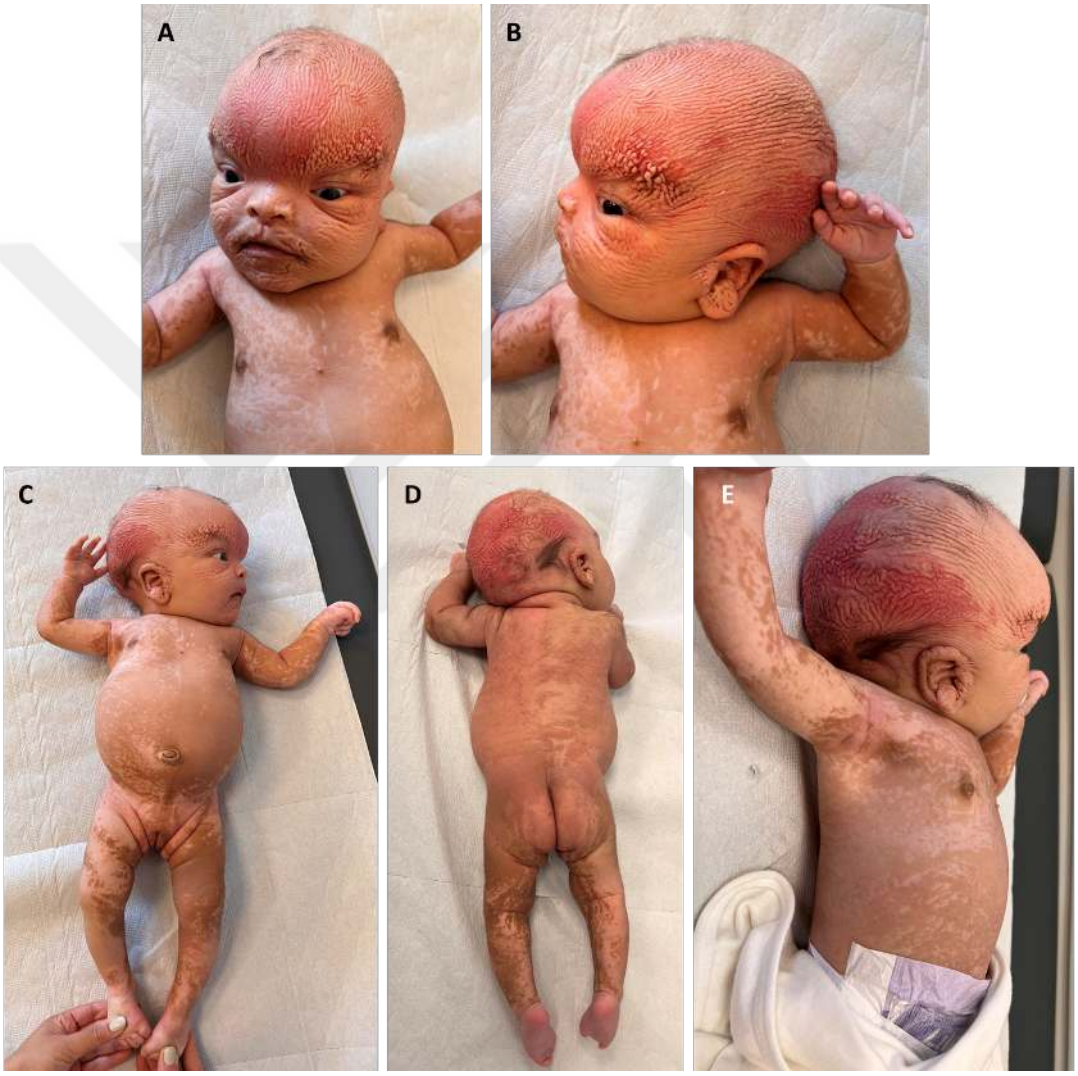

Figure 3-21. **Clinical findings of the index** 8 at 40 days of age included**(A-B)** furrowed skin with a corrugated appearance consistent with cutis gyrata affecting almost all the craniofacial area and dysmorphic findings of macrocephaly, large anterior fontanelle, prominent forehead, hypertelorism and midface hypoplasia, **(C-E)** keratinocytic and hyperpigmented skin lesions following Blaschko's lines on the trunk and extremities.

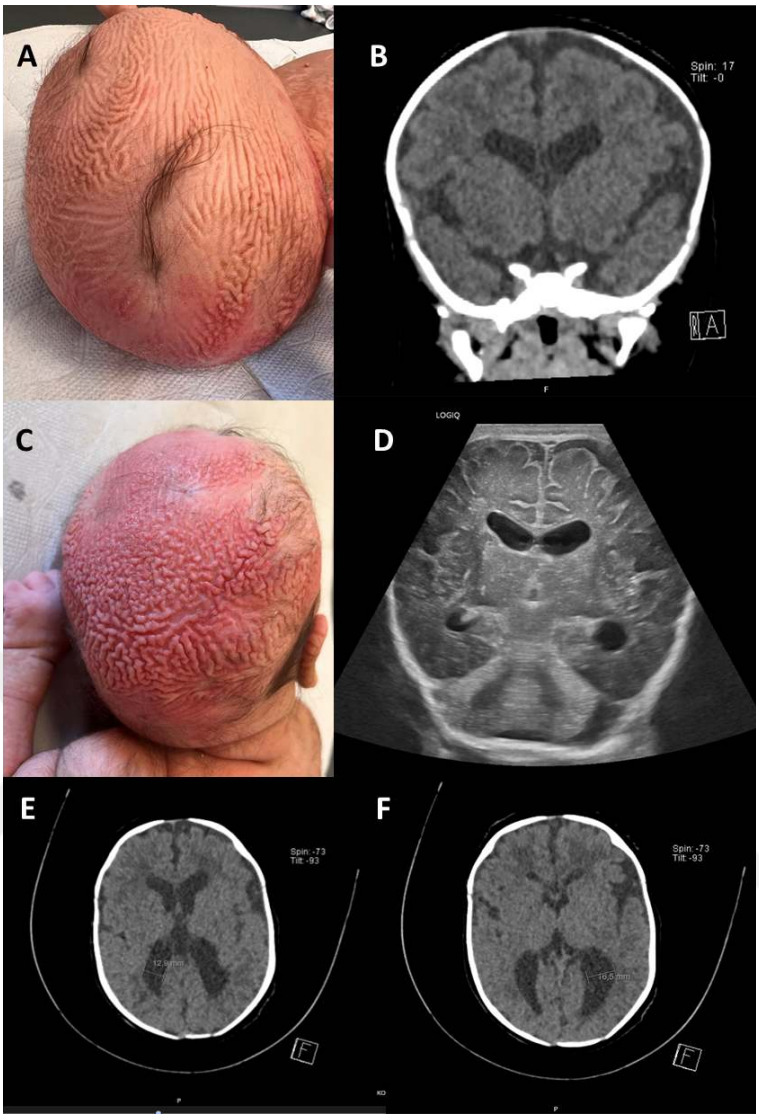

Figure 3-22. **Cranial imaging of index 8** at 40 days of age revealed **(A-D)** unilateral cerebellar hypoplasia and possibly neuronal migration defects, **(E-F)** bilateral ventriculomegaly.

Performed Tests and Results

The literature was thoroughly reviewed to analyze similar cases and identify the genes to be targeted. Only features explicitly stated by the authors or those that could be reliably inferred from descriptions or patient images were considered. Beare-Stevenson cutis gyrata syndrome and keratinocytic epidermal nevus (KEN) syndrome with possible underlying mosaicism were considered for the differential diagnosis.

Sampling

Three independent skin biopsies and EDTA blood sample were obtained for diagnostic evaluation. Skin sample #1 was collected from the right eyebrow (hairy region); skin sample #2 from the margin of a hypo-hyperpigmented lesion on the right upper arm, and skin sample #3 from a papilloma located in the thoracic region.

Histopathological Evaluation

Each of the three specimens was examined through multiple sections.

In skin sample #1, the sampling included the apex of one of the scalp's gyrations, with no notable features observed in the epidermis. The dermis contained numerous vellus hair follicles, some associated with sebaceous glands and arrector pili muscle bundles. However, eccrine sweat glands were not observed, possibly due to the biopsy being of superficial character and not including the deep dermis. The eccrine excretory duct, which opens to the surface, was also not observed. Given the marked wrinkling of the skin, an evaluation of the elastic tissue in the dermis was performed using Elastica-von Gieson staining, but no elastic fibers were found in the dermis. This case can be summarized with two cardinal findings: the absence of eccrine sweat glands or ducts, and the lack of elastic fibers.

In skin sample #2, two distinct areas were identified. The first area, which is smaller, showed no specific features in the epidermis. In the area with continuity, there was mild acanthosis and more pronounced papillomatosis in the epidermis. Clinically, there was no evident difference in pigmentation between these two areas, making it difficult to determine if this was related to epidermal thickness or melanin pigment distribution. The Masson-Fontana staining to assess melanin distribution revealed no significant difference between the two areas. Hair follicles and eccrine sweat glands were present in the dermis.

Skin sample #3 excised from the thoracic region included all skin appendages in their structure and were observed to be pedunculated polypoid formations. Only in the superficial epidermis, a slight accentuation of acanthosis and papillomatosis was noted at the apex of the formation.

It was challenging to draw a comprehensive clinical interpretation covering all the findings from these three specimens. However, the main findings in skin sample #1 and #3 specimens were concluded as epidermal nevus. Absence of eccrine sweat glands or ducts and the absence of elastic tissue findings in skin sample #2, was noted as a possible indication of ectodermal dysplasia.

Molecular Findings

Specific primers were designed to amplify the mutation of interest in the genes on the differential diagnosis list. Firstly, Barber-Say syndrome was ruled out by *TWIST2* whole gene sequencing on the DNA sample obtained from EDTA blood and skin sample #2. Then, hotspot regions of the previously reported cases (Hafner et al., 2012) with KEN were tested on the DNA sample obtained from the uncultured skin sample of the margin of a hypo-hyperpigmented lesion on the right upper arm (skin sample #2). No mutation was identified in the listed points by Sanger sequencing (Table 3.3).

Table 3-3. **List of the targeted mutational analysis of selected genes for the differential diagnosis.**

				Sample type	
Gene	**NCBI Accession Number**	**Method**	**Variant of interest Amino acid change**	**EDTA whole blood gDNA**	**Skin sample #2 gDNA**
TWIST2	NM_057179	Sanger sequencing of exons 1-2	whole gene	**not detected**	**not detected**
FGFR2	NM_000141	Sanger sequencing of exon 9	c.1115C>G p.(S372C) c.1124A>G p.(Y375C) c.1145G>A p.(C382R)	n/a	**not detected**
FGFR3	NM_000142	Sanger sequencing of exon 5-7	c.742C>T p.(R248C) c.746C>G p.(S249C)	**not detected**	**not detected**
HRAS	NM_005343	Sanger sequencing of exon 2	c.37G>C p.(G13R)	n/a	**not detected**
KRAS	NM_004985	Sanger sequencing of exon 2	c.35G>A p.(G12D)	n/a	**not detected**
AKT1	NM_005163	Sanger sequencing of exon 2	c.49G>A p.(E17K)	n/a	**not detected**
PIK3CA	NM_006218	Hotspot mutation screening by qPCR	c.1624G>A p.(E542K) c.1633G>A p.(E545K) c.3140A>G p.(H1047R)	n/a	**not detected**

Lastly, WES analysis was performed on DNA sample obtained from the skin sample #2. A likely pathogenic variant in the *FGFR2* gene was identified at a variant allele fraction (VAF) of 20.7% (30 of the 145 NGS reads) in the analyzed sample, indicating a mosaic state. The percent of targeted nucleotides covered at ≥20x depth was 99.47% (CENTOGENE GmbH, Rostock, Germany).

The *FGFR2* variant c.1979A>T p.(Lys660Met) causes an amino acid change from lysine to methionine at position 660 in the 14th exon. To the best of our knowledge, this is a novel variant not previously reported in the literature. It is classified as likely pathogenic based on the ACMG/AMP/ClinGen SVI guidelines.

FFPE tissue sections were obtained from skin biopsy #1 and #3. This variant was confirmed in all three skin samples and the EDTA blood sample of the index (Figure 3.23). Estimated VAFs were 8.6% for EDTA blood, 37,5% for skin biopsy #1, 18,6% for skin biopsy #2 and 27% for skin biopsy #3.

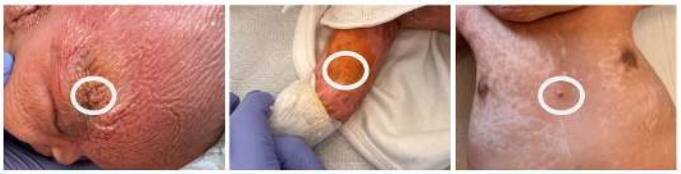

Sample type	gDNA derived from EDTA blood	gDNA derived from skin biopsy #1	gDNA derived from skin biopsy #2	gDNA derived from skin biopsy #3
Gene (transcript)	***FGFR2*** (NM_022970.3)			
Variant Amino acid change	**c.1979A>T p.(Lys660Met)**			
Genotype Estimated VAF	**Heterozygous 8,6%**	**Heterozygous 37,5%**	**Heterozygous 18,6%**	**Heterozygous 27%**
Sanger sequencing electropherogram	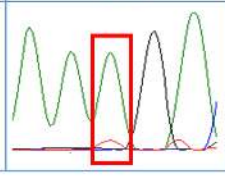	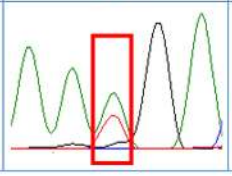	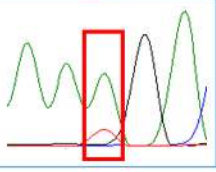	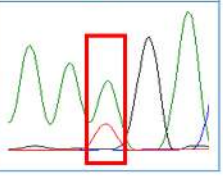

Figure 3-23. **Sanger sequencing electropherogram images of index 8**, indicating heterozygosity for *FGFR2* c.1979A>T change in all four sample types tested. Locations of the biopsies obtained are circled with on the images in the top panel.

Discussion

Craniosynostosis is the premature fusion of one or multiple cranial sutures, leading to craniofacial deformities in approximately 1 in 2,500 births globally. In most instances (85%), craniosynostosis manifests as an isolated, sporadic condition (non-syndromic craniosynostosis), while in the remaining cases (15%), it is associated with specific syndromes (syndromic craniosynostosis). Patients with syndromic craniosynostosis often experience more severe symptoms than those with isolated single-suture fusion (Yapijakis et al., 2023). Most cases of craniosynostosis are compatible with survival, although a high mortality rate is observed during the neonatal period in some conditions.

OMIM has stored more than 250 syndromes associated with craniosynostosis to date (OMIM, 12.11.2024). The fibroblast growth factor/FGF receptor (FGF/FGFR) signaling is crucial for various biological processes, particularly in bone development and homeostasis, as it regulates the differentiation of mesenchymal and neuroectodermal cells (Moosa & Wollnik, 2016). The FGFR family is one of the most diverse growth factor groups in vertebrates with 22 factors and five transmembrane receptors. Among these five receptors, FGFR1–FGFR4 are high-affinity tyrosine kinase receptors while FGFRL1 (Fibroblast Growth Factor Receptor-Like 1) contains a truncated intracellular domain with no tyrosine kinase activity and serves as a decoy receptor. FGFRs are activated through the formation of a trimolecular complex with FGF and heparin sulfate proteoglycans (HSPGs). This interaction triggers receptor dimerization, autophosphorylation, and subsequent downstream signaling (Azoury et al., 2017; Xie et al., 2020). Mutations in the encoding genes of the three members (*FGFR1*, *FGFR2*, *FGFR3*) lead to unregulated FGF signaling, which results in premature closure of sutures, the characteristic feature of craniosynostosis syndromes.

Heterozygous activating mutations of Fibroblast Growth Factor Receptor 2 (*FGFR2*) are predominantly associated with craniosynostosis syndromes, including Apert syndrome (OMIM: #101200, Inheritance: AD); Crouzon syndrome (OMIM: #123500, Inheritance: AD); Pfeiffer syndrome (OMIM: #101600, Inheritance: AD); Saethre-Chotzen syndrome (OMIM: #101400, Inheritance: AD); Beare-Stevenson cutis gyrata syndrome (OMIM: #123790, Inheritance: AD); Antley-Bixler syndrome without genital anomalies or disordered steroidogenesis (OMIM: #207410, Inheritance: AD);

Craniofacial-skeletal-dermatologic dysplasia (OMIM: #101600, Inheritance: AD); Bent bone dysplasia syndrome (OMIM: #614592, Inheritance: AD), Jackson-Weiss syndrome (OMIM: #123150, Inheritance: AD); Scaphocephaly, maxillary retrusion, and impaired intellectual development (OMIM: #609579, Inheritance: NS); Scaphocephaly with Axenfeld-Rieger anomaly (OMIM: NS, Inheritance: NS) and Craniosynostosis, nonspecific (OMIM: NS, Inheritance: NS). Additional associations include LADD syndrome 1 (Lacrimo-Auriculo-Dento-Digital syndrome) (OMIM: #149730, Inheritance: AD) and various cancer types including gastric, breast, colon, endometrial, esophageal cancer and cholangiocarcinoma (Zhang et al., 2009; Reintjes et al., 2013; Helsten et al., 2016; Smyth et al., 2017). Furthermore, isolated skin phenotypes including keratinocytic epidermal nevi (KEN) (Hafner et al., 2012; Toll et al., 2016; Garcias-Ladaria et al, 2018; Tanaka et al., 2018) and nevi derived from adnexal structures including nevus comedonicus, Hidradenitis Suppurativa (Higgins et al., 2017), segmental hypopigmented acneiform nevus/Munro acne nevus (Munro & Wilkie, 1998; Kiritsi et al., 2015), cerebriform (Theiler et al., 2021) and papillomatous pedunculated sebaceous nevus (Kuentz et al., 2017) has also been related to postzygotic somatic mutations in the *FGFR2*.

Beare-Stevenson cutis gyrata syndrome (BSS) was first described by Beare in 1969, in patients with facial features resembling Crouzon syndrome but distinguished by the presence of cutis gyrata (Beare et al., 1969). BSS is characterized by distinct craniofacial, respiratory, neurologic, integumentary, and anogenital anomalies. Craniofacial features often include a cloverleaf skull due to multisuture craniosynostosis, along with midface retrusion, proptosis, abnormal ear shape, cleft palate, conductive hearing loss, natal teeth, and a relatively prominent lower jaw. Neonatal death is common. Respiratory complications arise from multiple airway obstructions, such as choanal stenosis and tracheal abnormalities, often necessitating endotracheal intubation or tracheostomy. Intellectual disability is universal among surviving individuals, with frequently reported hydrocephalus and Chiari I malformations. Most surviving cases also had significant developmental delay. Characterizing skin manifestations, cutis gyrate and generalized acanthosis nigricans are often evident at birth. Cutis gyrata, the hallmark feature of BSS, is characterized by redundant scalp skin with deep furrows and convolution. Acanthosis nigricans is marked

by pigmented, velvety patches commonly observed on the hands, feet, or genital area. Hirsutism, skin tags, papillomatosis on face, axillae or perianal/genital areas, prominent umbilicus, and accessory nipples are also reported. Additional findings may involve genitourinary anomalies such as bifid scrotum or exaggerated rugosity of the labia majora, anteriorly placed anus and pyloric stenosis.

Fibroblast growth factor receptors (FGFRs) share similar organization, with three extracellular immunoglobulin-like domains (IgI, IgII, IgIII), a transmembrane (TM) domain and a cytoplasmic tyrosine kinase (TK) and additional regulatory sequences. The Ig-like domains bind fibroblast growth factors (FGFs) resulting in the dimerization of extracellular FGFRs and trans-phosphorylation of the TK domain. Specificity of FGF binding is determined by the IgIII domain, which is coded by exons 7-9. The N-terminal region of the IgIII comprises the IIIa sequence (exon 7), while the C-terminal region consists of mutually exclusive IIIb or IIIC sequences. FGFR2 generates two functionally distinct isoforms, isoform b (FGFR2-IIIb) or c (FGFR2-IIIc), through alternative splicing of IgIII C-terminal region. This isoform differentiation is mediated by the selective inclusion of exon 8 to form FGFR2-IIIb or exon 9 to create FGFR2-IIIc (Miki et al. 1992; Ornitz et al. 1996). The resulting structural variations influence FGF-binding specificity, thereby dictating the differential roles of these isoforms in various cellular and developmental contexts. IIIb/IIIc choice is strictly tissue specific, FGFR2-IIIb is expressed in epithelial cells while FGFR2-IIIc is restricted to mesenchymal cells (Bochukova et al., 2009).

Missense *FGFR2* mutations linked with syndromic craniosynostosis are clustered in IgIII or TK domains (Jezela-Stanek and Krajewska-Walasek, 2013). Within IgIII, the mutational spectrum tends to be narrow in either exon IIIa or IIIc (typically associated with a Crouzon or Pfeiffer syndrome) or in the intronic sequence preceding exon IIIc (usually causing Apert syndrome). However, the phenotypic expression was variable to define clear genotype–phenotype correlations. Among them, only BSS is associated with two recurrent missense variants of *FGFR2*, Ser372Tyr and Tyr375Cys, located in the carboxyl-terminal end of the linker region between the IgIII and transmembrane domains (Kan et al., 2002).

Disease-causing *FGFR* variants are predominantly missense variants, with all identified mutations contributing to a GoF effect in the protein level. Several

mechanisms have been proposed to explain the GoF effect of *FGFR2* variants, including (a) an increased binding affinity for FGF ligands (Anderson et al., 1998), (b) an alteration in ligand-binding specificity that enables interactions with inappropriate FGFs (Yu et al., 2000), (c) ligand-independent covalent dimerization (Neilson & Friesel, 1995; Robertson et al., 1998), and (d) the aberrant expression of alternative splice variants (Oldridge et al., 1999). These molecular mechanisms underlie the dominant inheritance pattern in associated syndromes. Furthermore, strong correlation between *de novo* mutations and advanced paternal age was reported in Apert, Crouzon and Pfeiffer syndromes' (Moloney et al., 1996; Glaser et al., 2000). However, there was no correlation suggested in BSS.

With the index, there are only 20 molecularly solved BSS/BSS-like cases reported till now (Table 3.4). Recurrent Ser372Tyr and Tyr375Cys variants were identified in 85% (17/20) of the cases. In the remaining three cases with overlapping cutaneous findings, who initially diagnosed as BSS-like, CS and SFM syndromes, different variants two lying within the IgIII domain were reported, which are a 63 bp deletion in *FGFR2* exon 7 (c.859del63, that results in the loss of 21 aminoacids from 287 to 308) and a missense variants in exon 7 (c.799T>C, p.Ser267Pro); and a mosaic missense variant in exon 12 (c.1647C>A, p.Asn549Lys) (Fig.43) on tyrosine kinase domain 1 (TK1).

The Lys660Met variant identified in the index is located within the tyrosine kinase 2 (TK2) domain that regulates the activity of the receptor. Lysine 660 residue in *FGFR2* is paralogous to lysine 650 residue in *FGFR3*. Both lysine residues are highly conserved among species and all four human FGFRs; and are located close to the activation loop of the TK domain (Figure 3.24 A, C). Under normal physiological conditions, the activation loop stabilizes the receptor in an inactive conformation, preventing premature substrate binding. Upon FGF-binding, receptor dimerization induces a conformational rearrangement, allowing for autophosphorylation of key tyrosine residues within the TK domain and subsequent activation of downstream signaling pathways. Moreover, they are involved in cell proliferation, migration, survival, and differentiation by activation of downstream signaling pathways, such as the PI3K-AKT-mTOR, PLCγ-PKC, or the RAS-MAPK signaling cascades (Figure 3.24 B).

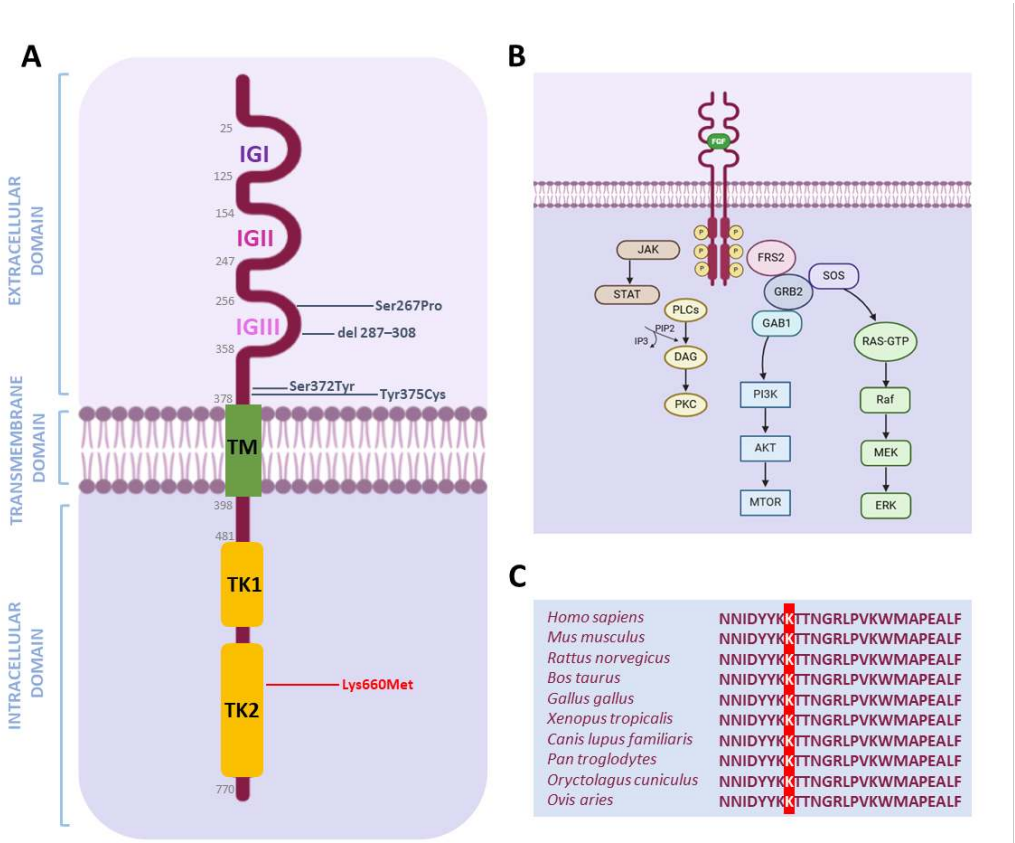

Figure 3-24. **The structure and function of FGFR2. (A)** Reported variants in BSS/BSS-like cases and their location within the FGFR2 receptor. Red arrow points to the location of the variant identified in the index. **(B)** Overview of the FGF/FGFR signaling. FGFRs activate downstream PI3K-AKT-mTOR, PLCγ-PKC, or the RAS-MAPK signaling cascades. **(C)** Sequence alignment of codon 660 (highlighted in red) is highly conserved across species.

Germline variants affecting the lysine 650 in *FGFR3* have been implicated in several skeletal dysplasias, including thanatophoric dysplasia type I (TDI) and thanatophoric dysplasia type II (TDII), and severe achondroplasia with developmental delay and acanthosis nigricans (SADDAN) syndrome. The underlying pathogenic *FGFR3* lysine 650 variants are shown to destabilize the inactive conformation of the activation loop and result in ligand-independent TK activation. Supported by several studies, variants at this residue lead to enhanced kinase activity, whereas mutations in adjacent residues generally have a smaller effect. The *FGFR3* Lys650Met variant, paralogous to the *FGFR2* Lys660Met variant identified in index, is the recurrent missense variant associated with SADDAN syndrome. The variant is shown to lead to a dramatic increase in constitutive receptor kinase activity, approximately 60 times

greater than the common achondroplasia variant (p.Gly380Arg) and three times greater than the common TD2 variant (p.Lys650Glu) (Tavormina et al., 1999; Webster et al., 1996).

Protein structure simulation showed minor structural differences between the WT-FGFR2 and Met660-mutant-FGFR2 proteins (Figure 3.25). The Met660 mutation may mimic a mechanism observed in paralogous mutations, leading to constitutive receptor activation. By replacing the positively charged Lys660 with hydrophobic Met660, the mutation might disrupt key electrostatic interactions or hydrogen bonds, destabilizing the inactive kinase form and encouraging a shift to a more active conformation.

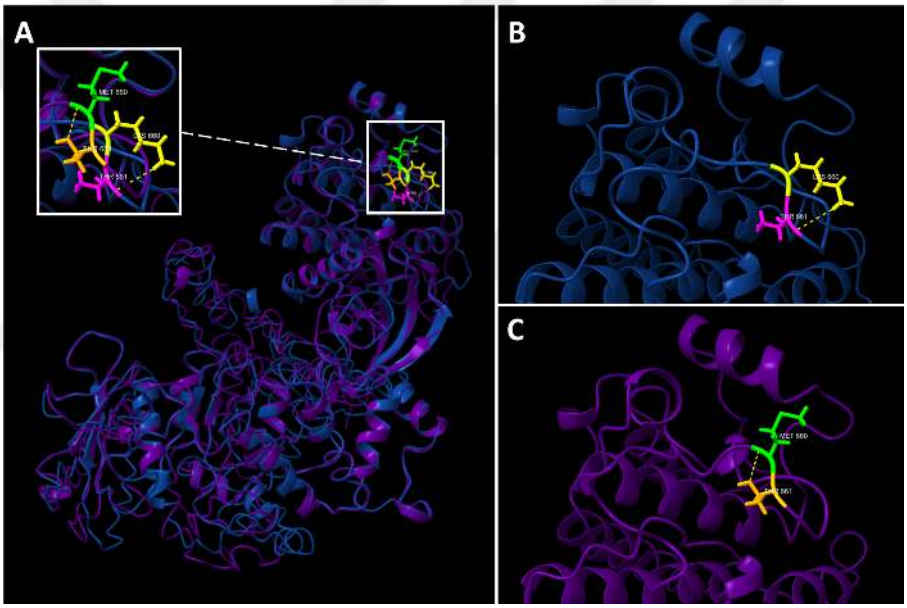

Figure 3-25. **Protein structure simulation results (A)** 3D structures of the wild-type (blue) and mutated (purple) FGFR2 protein. Compared to the wild-type Lys660 **(B)**, the mutant Met660 exhibits minor structural deviations, including a weaker hydrogen bond with Thr661 (2.550 Å vs. 1.959 Å in the WT) and a slightly distorted bond angle (151.221°).

Characteristic skin findings of BSS are not shared with any of the *FGFR2*-related craniosynostosis syndromes. Acne is associated with S252W or P253R variants in Apert syndrome. In Saethre-Chotzen syndrome, a lower frontal hairline has been noted, but no other consistent skin-related findings have been reported (Wenger et al., 1998). While cutaneous features are described rarely in Muenke syndrome, Pfeiffer syndrome, Jackson-Weiss syndrome, and Antley-Bixler syndrome lack specific cutaneous

manifestations (Roscioli et al., 2001; Wenger et al., 1998). On the other hand, SADDAN syndrome has overlapping cutaneous findings with BSS. Acanthosis nigricans is reported in all surviving infants or toddlers with the paralogous *FGFR3* Lys650Met variant, while skin tags, multiple nevi, and deeply furrowed palms and soles have been reported in few. SADDAN dysplasia is generally compatible with survival into adulthood and is associated with atypical bone deformities, neurodevelopmental abnormalities, but no cloverleaf skull or craniosynostosis has been reported.

Recently, Schmidt et al. (2024) identified a mosaic *FGFR2* variant c.1647C>A, p.(Asn549Lys) confined to affected skin tissue in a patient clinically diagnosed with Schimmelpenning-Feuerstein-Mims (SFM) syndrome. Her clinical findings included hallmark BSS features of cutis gyrata and acanthosis nigricans, alongside extensive sebaceous nevi, irregular epidermal hyperplasia, and focal hypopigmented streaks. Adding to these cases, our observation highlights that mosaic *FGFR2* variants in the intracellular domain (TK1 and TK2) can produce the full dermatological phenotype of BSS, even in the absence of severe craniosynostosis. Yet, the mechanism by which FGFR variants cause cutaneous findings is not well understood, but FGFs and FGFRs are involved in many early developmental processes and can have effects on many tissue types. The “b” isoform (FGFR2-IIIb) is expressed exclusively on epithelial cells and activated by the specific high-affinity binding of FGF7 and FGF10. FGFR2-IIIb promotes not only the early, but also the late steps of keratinocyte differentiation (Rosato et al., 2018).

One possible explanation for the generalized hyperpigmentation in index is that the mosaic mutation in exon 14 has led to constitutive activation of the FGFR2 signaling and stimulation of p38 MAPK, which in turn enhances MITF-M expression in the epidermis, leading to enhanced keratinocyte proliferation and melanocyte differentiation. A knock-in mouse model of BSS has identified p38 MAPK as a key regulator in melanogenesis and an important signaling pathway mediating the skin abnormalities in BSS (Wang et al., 2012). In the study by Wang et al, Fgfr2±/Y394C mice exhibited ligand-independent phosphorylation of FGFR2 and activation of p38 signaling in mutant skin and calvarial tissues. These changes resulted in craniosynostosis, epidermal hyperplasia, and furrowed skin, which are similar to the human BSS phenotype. Pharmacological inhibition of p38 effectively mitigated these

abnormalities in Fgfr2+/Y394C mice, suggesting that targeting $p38^{MAPK}$-MSK1-CREB-MITF-M pathway may be a promising therapeutic approach for addressing both the dermatological and craniofacial manifestations of BSS (Wang et al., 2012).

In conclusion, this study identifies a novel FGFR2 mutation as the cause of an ultra-rare clinical phenotype, thereby expanding the genotypic and phenotypic spectrum of *FGFR2*-related syndromes. This index case holds particular significance as the first documented mosaic BSS case and the second report of a mosaic *FGFR2*-associated neurocutaneous syndrome in the literature.

Table 3-4. **Clinical and molecular findings of the 20 molecularly solved BSS/BSS-like cases,** including this study.

Reported cases	*Hall et al. 1992, Przylepa et al. 1996**			*Krepelova et al. 1998*	*Wang et al. 2002*	*Akal et al. 2002*	*Vargas et al. 2003*		*McGaughran et al. 2006*	*Eun et al. 2007*	*Fonseca et al. 2008*	*Slavotinek et al.2009 & Tao et al. 2010*	*Barge-Schaapveld et al. 2011*		*Wenger et al. 2015*		*Ron et al. 2016*	*LeBlanc et al. 2018*	*Ferreira et al. 2020*	*Schmidt et al., 2024*	*This report*
Patient	1	4	FBSKM	1	1	1	1	2	1	1	1	1	1	2	1	2	1	1	1	1	1
Age of deceased	5m, respiratory failure	17m, alive	nr	6 w, alive	3y, alive	8m, alive	46d, cardio respiratory arrest	21d, cardio respiratory arrest	18m alive	21d, respiratory failure	1d	6y alive	25d, respiratory failure	3d, respiratory failure	8d, respiratory failure	5w, respiratory failure	3d, respiratory failure	6m, alive	60d, cardio respiratory arrest	2y 9m alive	Alive
Sex	M	F	F	F	M	F	F	F	M	M	nr	M	M	F	F	F	M	M	M	F	F
***FGFR2* variant**	Ser372Cys	Tyr375Cys	Tyr375Cys	Tyr375Cys	Tyr375Cys	Tyr375Cys	Tyr375Cys	Tyr375Cys	Tyr375Cys	Tyr375Cys	Tyr375Cys	c.1506del63	Tyr375Cys	Tyr375Cys	Tyr375Cys	Ser372Cys	Tyr375Cys	Ser267Pro	Tyr375Cys	Asn549Lys	Lys660Met
Clinical diagnosis	BSS	BSS	BSS	BSS	BSS	BSS	BSS	BSS	BSS	BSS	BSS	BSS	BSS	BSS	BSS	BSS	BSS	CS	BSS	SFM	BSS
Clinical features																					
Craniofacial anomalies	+	+	+	+	+	+	+	+	+	+	+	+	+	+	+	+	+	+	+	+	+
Craniosynostosis	+	+	+	+	+	+	+	+	+	+	+	+	+	+	+	+	.	+	+	+	+
Cranial shape	Acrocephalic	Turricephalic	Turricephalic	Turricephalic	Turricephalic	Turricephalic	Turricephalic	Turricephalic	Turricephalic	Turricephalic	Turricephalic	Turricephalic	Turricephalic	Turricephalic	Turricephalic	Turricephalic	.	Turribrachycephalic	Turricephalic	Macrocephalic	Turricephalic
Hydrocephalus	.	+	+	.	+	+	+	+	+	+	+	+	.	+	+	+	+	.	+	.	.
Palatal anomalies (narrow/high/cleft palate/bifid uvula)	+	+	+	nr	+	nr	+	+	+	+	+	+	+	+	nr	+	.	nr	.	nr	+
Choanal atresia/stenosis	+	+	+	+	+	nr	.	+	+	+	+	+	+	+	+	+	+	.	+	+	.
Hypertelorism	+	+	+	+	+	nr	+	+	+	nr	+	+	+	+	+	+	+	+	+	+	+
Midface hypoplasia	+	+	+	+	+	nr	+	+	+	+	+	+	+	+	nr	nr	+	.	+	+	+
Proptosis/exophthalmos	+	+	+	+	+	+	+	+	+	+	+	+	+	+	+	+	+	+	+	.	+
Downslanting palpebral fissures	+	+	+	nr	+	nr	+	n/a	+	n/a	n/a	nr	+	+	nr	nr	nr	nr	nr	.	+
Posteriorly rotated low set ears	+	+	+	+	+	nr	+	.	nr	+	+	+	+	+	+	+	nr	+	nr	+	+
Cutaneous findings	+	+	+	+	+	+	+	+	+	+	+	+	+	+	+	+	+	+	+	+	+
Cutis gyrata	+	+	+	+	+	+	+	+	+	+	+	+	+	+	+	+	+	+	+	+	+
Acanthosis nigricans	+	+	+	.	+	nr	.	.	.	+	nr	+	nr	.	nr	nr	+	nr	.	+	.
Skin tag(s)	+	+	+	nr	nr	+	+	+	+	+	nr	+	nr	nr	+	+	+	nr	.	nr	+
Rugated/furrowed skin	+	+	+	+	+	+	+	+	+	+	+	+	nr	nr	+	nr	+	+	nr	+	+
Preauricular creases	+	+	+	+	+	nr	+	+	nr	+	+	+	nr	nr	+	+	+	+	nr	.	+
Hypoplastic nails	+	nr	nr	nr	nr	nr	+	.	nr	nr	n/a	+	nr	nr	nr	nr	nr	nr	nr	nr	.
Prominent umbilicus	+	+	+	+	+	+	+	+	+	+	+	+	nr	+	+	+	+	+	+	nr	+
Anogenital anomalies	+	+	+	+	nr	nr	+	+	+	+	+	+	+	+	+	+	+	nr	+	.	+
Anteriorly placed anus	n/a	+	nr	+	n/a	nr	+	+	+	n/a	nr	+	nr	+	nr	+	nr	nr	n/a	nr	+
Hypospadias	nr	n/a	n/a	n/a	nr	n/a	n/a	n/a	+	+	nr	+	+	n/a	n/a	n/a	+	n/a	+	n/a	n/a
Cryptorchidism	nr	n/a	n/a	n/a	nr	n/a	n/a	n/a	.	.	nr	+	nr	n/a	n/a	n/a	nr	n/a	nr	n/a	n/a
Hypoplastic genitalia	n/a	.	nr	.	n/a	nr	+	.	+	n/a	nr	n/a	nr	nr	nr	nr	nr	nr	n/a	nr	+
Bifid scrotum	+	n/a	n/a	n/a	.	nr	nr	nr	+	.	nr	.	+	nr	nr	nr	+	nr	.	n/a	nr
Other	extended scrotal raphé	umbilical hernia, coarse rugated labia majora	sacrococcygeal polyp	hypertrophy of the clitoris					sacral appendage		rugated labia majora, perineal fissure from genital toanal mucosa, lumbosacral dimple	sacral appendage	sacral dimple		sacral dimple, rugated labia majora, prominent clitoris	sacral dimple, rugated labia, prominent clitoris					closed vaginal orifice and anteriorly placed anus with an anal polyp
Additional findings	retroverted tip of coccyx, extension and supination limitation at the elbows, Advanced paternal age (43y), dizygotic twin pregnancy	right intermittent exotropia, beaked nose, prominent antitragus, hypoplastic ear lobules, cardio respiratory distress		retroverted tip of coccyx, radial deviation of thumbs, broad distal phalanges of the thumbs		red nevus with skin tags on her forehead			bilateral conductive hearing loss, advanced paternal age		neonatal teeth	neonatal teeth, gingival hyperplasia, external ear canal atresia, mild moderate mixed hearing loss, mild optic nerve hypoplasia, high myopia with astigmatism, obstructive sleep apnea, slightly broad thumbs and halluces and mild syndactyly of the 2/3 toes with overlapping fourth toe, Advanced paternal age (48y),dizygotic twin pregnancy					monozygotic twin pregnancy	slightly broad thumbs with radial deviation at the distal interphalangeal joint, slightly broad halluces, prominent deep transverse natal cleft adjacent to the central natal cleft	discrete dilation of the kidneys at 27th GWs, natal tooth, subsequent seizures, small femurs, short toes, Advanced maternal & paternal age 37y, ART pregnancy, father with Vas deferens	nevus sebaceous, corneal clouding, defects of the retina and choroid as well as broad great toes on both sides	keratinocytic and hyperpigmented skin lesions following Blaschko's lines on the trunk and extremities, absent lower eyelashes and sparse and almost absent upper eyelashes, left eyebrow aplasia and hypoplastic right eyebrow

UNRESOLVED CASES

STUDY 9

Unresolved Complex Neurocutaneous-Vascular Presentation of NF2 Features and Blue Rubber Nevus–Like Lesions

Clinical Findings

Index was referred from the department of general surgery for genetic consultation at 35 years of age due to clinical diagnosis of NF2. She had multiple neurofibromas on the neck, brain, orbita, and abdomen; along with slightly raised, purple varicose/hemangiomatous lesions (mainly small blue dots) limited to the right upper arm and right half of the trunk (Figure 3.26 A-D). She had severe proptosis and mild facial asymmetry. She reported loss of sensation in the right half of the upper lip. Her neurological examination was normal. Intracranial neurofibromas were expanding into the right internal acoustic canal, and she had reported unilateral (right) hearing loss, possibly secondary to vestibular schwannoma. Her last follow-up visit was at 42 years of age, and her clinical findings were stable.

At 7 years of age, she was consulted by the Dermatology department after lesions similar to hemangioma/varicose veins appeared on her arms; however, no histological diagnosis could be made at that time. An abdominal mass was detected at the age of 22; cyst aspiration and alcohol ablation were performed percutaneously on the liver and adrenal glands. Histopathology was reported as benign, and follow-ups were uneventful.

She reports swelling in the eyes and mass on the right parotid gland and cheek since 24 years of age. Cranial MRI at the age of 35, revealed a 4.5 mm long schwannoma

in the right internal acoustic canal. In both orbits, lesions with hyperintense signal characteristics were consistent with plexiform neurofibroma filling the intraconal area in the retrobulbar area. Compression on the optic nerves was more pronounced on the right. The lesion on the left showed minimal extension to the fissure inferiorly, while the lesion on the right extended posteriorly to the cavernous sinus and inferiorly to the infraorbital fissure level. It extends posteriorly to the pterygoid plates through the foramen ovale along the mandibular nerve on the right, and laterally toward the mandible via the mandibular nerve along the pterygoid muscles and widens the mandibular nerve canal. The right ICA was surrounded by schwannomas along the canal. She also had multiple meningiomas. There was a 9 mm meningioma located on the dura of the left occipital lobe, as well as symmetrical meningiomas measuring 2-3 mm on the right occipital lobe. Additionally, a 3 mm meningioma was found in the posterior area, and an 8.5 mm meningioma was detected in the anterior area of the right cerebellar hemisphere. Neurofibromas are reported to be non-progressive in the follow-up MRIs. (Figure 3.26 E-G).

At the age of 32, the neurofibromas in the brain were excised with craniotomy and intracranial debulking. The right seventh and eighth cranial nerves were affected. Also, the space-occupying effects of the abdominal masses due to compression have begun to significantly impact her quality of life.

At the age of 35, splenomegaly and hemangiomas of varying sizes in all segments of the liver were detected during a routine follow-up, and she underwent subtotal hepatectomy and cholecystectomy. A giant sinusoidal (cavernous) hemangioma of 18 cm in diameter covering segments 6-7 and part of 8. In the area corresponding to the bilateral surrenal lobe, there were multiple cystic formations in the retroperitoneum, the largest of which was ~5 cm in diameter. A dermoid cyst of ~4 cm in diameter in the left ovary was also removed. She had hysteroscopic myomectomy and polypectomy operation at 40 years of age. She received 78 regimens of off-label Bevacizumab treatment and is reported to be benefiting, as her routine imaging findings reported to be stable.

Performed Tests and Results

At the first visit, peripheral blood sample was collected and *NF2* whole gene sequencing by Sanger sequencing was planned. No variants were detected in *NF2* gene on DNA sample derived from peripheral blood.

At the last visit, skin biopsy was obtained from the affected skin, on a hemangiomatous/cavernous malformation on the right inner arm. *NF2* variants were ruled out on uncultured skin DNA by targeted NGS analysis (Oncopanel). Then, WES was planned. WES analysis on uncultured skin DNA revealed no change compatible with the phenotype. However, two heterozygous changes, c.2080A>T p.(Ser694Cys) and c.2729A>G p.(Tyr910Cys), in the *PPIP5K2* gene were reported as a potentially relevant finding. Ser694Cys change was not reported in population databases (gnomAD, 1000 G, CentoMD); predicted to be 'possibly damaging' by Polyphen-2 and 'disease causing by MutationTaster. Tyr910Cys change was reported in gnomAD with an allele frequency of 0.000012 (absent in 1000 G, CentoMD); predicted to be 'benign" by Polyphen-2 and 'disease causing by MutationTaster. Both variants were classified as a VUS based on ACMG criteria. Segregation analysis on the parent was suggest but could not be performed. Blue rubber nevus syndrome was considered in the differential diagnosis; however, histopathologic examinations have yet to be performed.

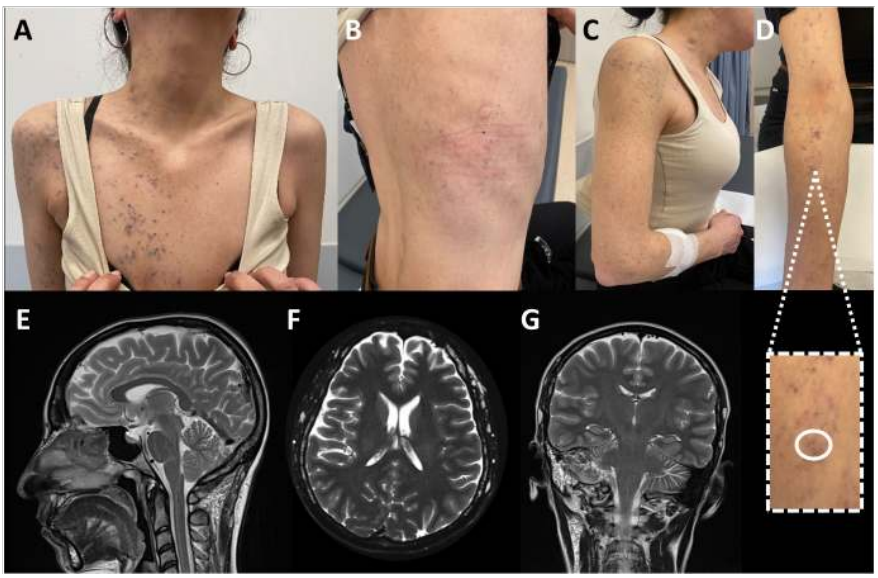

Figure 3-26. **Clinical images of the index 9** showing **(A-C)** varicose/hemangiomatous lesions limited to the right upper arm and right half of the trunk. **(D)** Close-up to the right inner arm shows the location of the skin biopsy. **(E-G)** Cranial MRI showing plexiform neurofibroma on the right internal acoustic canal and multiple meningiomas.

STUDY 10

Unresolved Segmental Cutaneous Disorder Mimicking NF1

Clinical Findings

The index was born 41st GW due to prolonged labor via spontaneous vaginal delivery at term after an uneventful pregnancy with a birth weight of 3665 g and a height of 55 cm; OFC was not recorded. His neuromotor development and intelligence were reported as normal.

First consultation was at 36 months of age, he had a weight of 20 kg (2,96 SD); height of 104 cm (2,15 SD) and OFC of 51,5 cm (1,85 SD). He presented with multiple CaL spots on the right gluteal, femoral, and crural regions (more than five, each larger than 0.5 cm), freckling in the right inguinal region, and fetal finger pads on both hands and feet. He did not have any facial dysmorphism. Lisch nodules were identified on the ophthalmologic examination. NF1 was considered in the differential diagnosis.

At 7 years 2 months of age, he had a weight of 37,1 kg (2,62 SDS); height of 137 cm (2,8 SDS) and OFC of 53,5 cm (0,95 SDS). In addition to the previous skin findings on the right side of the body, a 20x20 cm hyperpigmented macular lesion covering the left chest wall and extending over to the axillary region, along with hypopigmented patches on the left upper arm, were present (Figure 3.27).

Performed Tests and Results

At the first visit at three months of age, peripheral blood sample was collected. Chromosome analysis by SNP array and karyotype analysis revealed a normal male

constitution. *NF1* whole gene analysis by MLPA revealed no molecular pathology on the DNA sample derived from peripheral blood.

At five years of age, *NF1* and *SPRED1* whole-gene analysis by NGS and CNV analysis on DNA sample derived from peripheral blood did not reveal any variants (Alabama).

At seven years of age, skin biopsy was performed on affected skin, both on the hyperpigmented (right) and hypopigmented (left) areas. Skin findings on the right side were considered to be related to NF1, while those on the left side considered non-NF1-related. Karyotype analysis on both fibroblast cells revealed a normal male karyotype. Targeted NGS (Oncopanel) and MLPA analysis was performed, and NF1 was ruled out on the DNA sample from uncultured skin biopsy from the right hyperpigmented lesion.

WES analysis on DNA sample derived from uncultured skin biopsy from left hypopigmented spot revealed no change compatible with the phenotype.

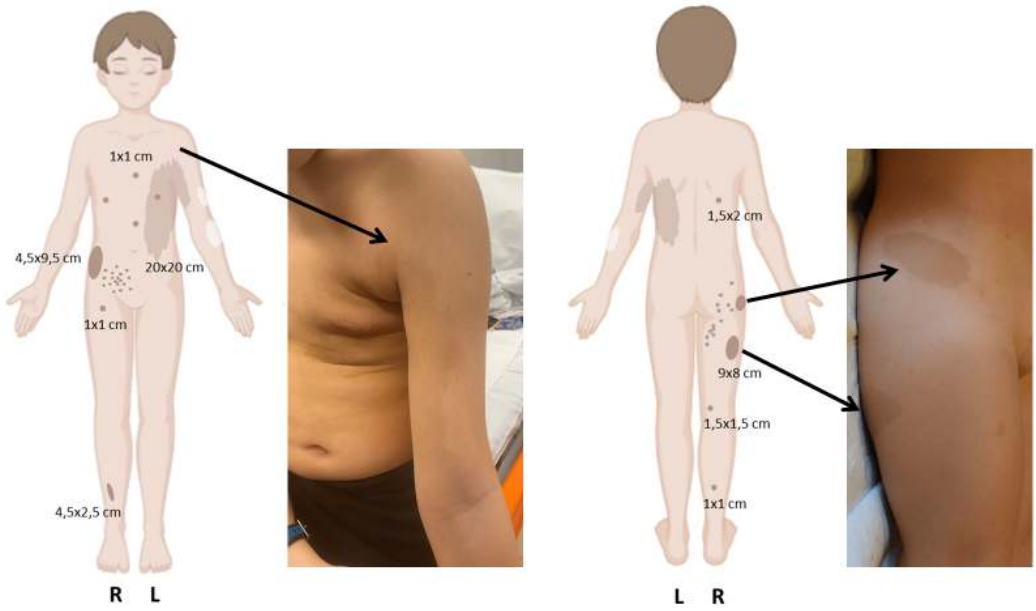

Figure 3-27. **Illustration of the skin findings of index 10** showing multiple CaL spots with their corresponding sizes on the right gluteal, femoral and crural regions, along with inguinal freckling; hyperpigmented macular lesion on left chest wall and back, hypopigmented patches on left upper arm.

STUDY 11

Unresolved Neurocutaneous Syndrome with Hypomelanosis of Ito, Intellectual Disability, Epilepsy and Dysmorphic Features

Clinical Findings

A 22-year-old patient who was followed up with the diagnosis of autism spectrum disorder and epilepsy was referred for genetic consultation.

The index was born via cesarean section at term due to breech presentation. Slight bruising was noticed and he had stayed in an incubator for 3 days for heart rhythm monitoring. His mother reports a weak sucking reflex in the neonatal term. He had febrile seizures as a baby (2-3 times) and a non-febrile seizure at age 7, reported to be due to an infection. He had been followed up by pediatric neurology and psychiatry departments due to global developmental delay and severe intellectual disability (autism spectrum disorder + language delay + cognitive impairment). He graduated from high school with special education.

He was consulted by the dermatology department at 3 years of age and diagnosed with Hypomelanosis of Ito. Skin biopsy was performed to rule out tissue mosaicism, and karyotype analysis was reported to be normal. No genetic consultation or further diagnostic tests were performed.

At 17 years of age, he had a generalized tonic-clonic seizure lasting 2-3 minutes, and postictal confusion lasted about 1 hour. Urinary incontinence and tongue biting were described with no Todd's paresis. He could not express a headache. Seizures continued every 15 days despite using Levetiracetam regularly. Depakine was added to the treatment 4-5 months later, and seizures began occuring once every 3 months with shortened severity and duration. In the pre-seizure period, his gaze becomes dull, then

his pupils dilate. All seizures are generalized tonic-clonic, with a more prominent tonic phase, and urinary incontinence continues to be 80%.

At 22 years of age, he was referred for medical genetics consultation. He had a weight of 60 kg (SD); height of 180 cm (2,15 SD) and OFC of 55,5 cm (1,85 SD). He was cooperative, and he responded meaningfully to verbal commands. His facial appearance was dysmorphic. Dental anomalies included palatal supernumerary teeth, missing upper front incisors (dentures), molar-shaped incisors and impacted lower jaw molars. He had striking hypopigmented lesions on the arms, trunk, back and legs that follow the lines of Blaschko (Figure 3.28 A-E). Cranial MRI findings included global cerebral atrophy, bilateral atrophy of putamen and globus pallidus, bilateral grade 2 hippocampal atrophy and mild signal increase in the right hippocampus consistent with possible accompanying hippocampal sclerosis (Figure 3.28 F-G)

Performed Tests and Results

Peripheral blood, buccal swab and skin biopsy sample from the margin of the hypo/hyperpigmented lesion on upper arm, were obtained. On peripheral blood sample, chromosome analysis by SNP array and karyotype analysis revealed normal male constitution. WES analysis on DNA samples derived from peripheral blood and uncultured skin biopsy revealed no change compatible with the phenotype.

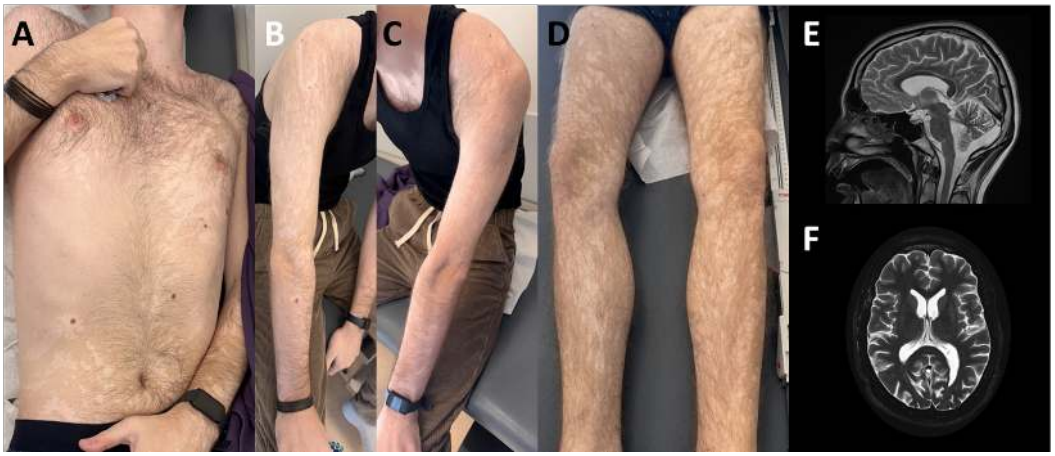

Figure 3-28. **Clinical images of index 11** showing hypopigmented lesions on the **(A)** trunk **(B-C)** arms, **(D)** legs and **(E)** back that follow the lines of Blaschko. **(F-G)** Cranial MRI showing global cerebral atrophy and possibly hippocampal sclerosis.

CONCLUSION

Mosaicism represents a fundamental biological phenomenon with broad implications for human health and disease. By consolidating historical insights, clinical observations, and molecular evidence, this thesis firmly establishes that postzygotic genetic variation arising at distinct developmental stages can lead to a diverse array of phenotypes, ranging from subtle pigmentary changes to severe multisystem disorders. From a clinical perspective, recognizing mosaicism has redefined diagnostic paradigms for many rare disorders. Beyond rare developmental syndromes, the principles of mosaicism extend into cancer biology, aging, and multifactorial diseases, highlighting its relevance as a unifying concept in medical genetics.

Mosaic syndromes constitute an expanding group of identifiable clinical manifestations, although each clinical picture is in itself rare. The difficulties and limitations in detecting somatic mosaicism often hinder definite diagnosis of the affected individuals. Yet, the knowledge and data on the genetic basis of somatic mosaicism remain limited. Methodological advances, particularly high-depth next-generation sequencing and optimized tissue sampling strategies, have enhanced diagnostic yield by transforming our capacity to detect low-level mosaic variants that evade standard diagnostic approaches. Nevertheless, limitations remain, especially in tissues inaccessible to routine biopsy, emphasizing the need for refined, minimally invasive, and highly sensitive molecular diagnostic tools. The need for further methodological refinement, integration of emerging genomic and multi-omic technologies, and deeper exploration of tissue-specific mutational landscapes remains.

This PhD thesis sought to address these challenges by confirming clinical diagnoses of individuals in this patient group at the genomic level using advanced molecular and cytogenetic diagnostic techniques. By integrating thorough clinical phenotyping with genomic analyses, we were able to identify, characterize, and redefine the molecular basis of various rare mosaic disorders. These results not only confirmed the suspected diagnoses but also offered new insights into genotype-phenotype correlations,

further refining the understanding of the variability and complexity in mosaic syndromes. Moreover, by systematically analyzing each case, this thesis demonstrated both the diagnostic potential and current limitations of genomic investigation in mosaic disorders.

The research is structured around two main components: a well-defined cohort of 15 patients suspected of PROS, and ten additional patients, each representing a unique single-case study.

In the PROS cohort (1), a molecular diagnosis was achieved for 6 out of 15 patients. Initial screening using hotspot qPCR detected pathogenic PIK3CA variants in three patients. Further testing with targeted next-generation sequencing (NGS) and whole exome sequencing (WES) identified three additional cases involving *PIK3CA*, *MFN2*, and *FGFR2*, while one case remained inconclusive. Six patients are still undergoing investigation. Altogether, a molecular diagnosis was established in 6 out of 15 patients, highlighting both the importance of lesional sampling and the limitations of the current technologies.

Seven single-case studies with genomic diagnosis illustrated the wide etiological spectrum of mosaicism, which were (2) skin-limited mosaic trisomy 22, (3) mosaic variegated aneuploidy type 1 due to compound heterozygous *BUB1B* variants, (4) *MTOR*-related pigmentary mosaicism with unilateral body overgrowth, (5) Capillary malformation–arteriovenous malformation syndrome 1 due to a *RASA1* variant (6) Segmental NF1 with pigmented cutaneous neurofibromas due to superimposed mosaicism, (7) Multiple Symmetric Lipomatosis caused by homozygous MFN2 p.R707W variant, and (8) a unique, mosaic *FGFR2*-related blended phenotype of systematized keratinocytic epidermal nevi and Beare-Stevenson cutis gyrata syndrome. The identified variants/changes are involved in key biological pathways, including PI3K-AKT-mTOR and RAS-RAF-MAPK, along with the components of cell-cycle regulation, mitochondrial dynamics, and chromosomal architecture. Mosaic alterations in these pathways lead to phenotypic variability that complicates and challenges existing genotype-phenotype correlations. Additionally, timing of the mutational event emerges as a critical determinant of tissue involvement, variant allele frequency, and clinical severity, ranging from early embryonic mutations, which produce widespread, high-level mosaicism, to later mutations that result in organ- or tissue-specific manifestations.

Unresolved cases included (9) complex neurocutaneous-vascular presentation of NF2 features and blue rubber nevus–like lesions, (10) segmental cutaneous disorder mimicking NF1, and (11) Hypomelanosis of Ito with intellectual disability, epilepsy, and dysmorphic features, despite comprehensive genetic evaluations. These cases highlighted the persistent challenges in detecting low-level mosaic variants, particularly in conditions with high allelic heterogeneity or segmental tissue involvement. In such cases, the pathogenic variant may be confined to affected tissues that are either inaccessible or underrepresented in the tested samples. Furthermore, these findings highlight the limitations of current sequencing depth, bioinformatic pipelines, and variant interpretation frameworks in such contexts. The unresolved status of these cases may suggest the possibility of novel disease genes, cryptic structural variants, or previously unrecognized genotype-phenotype correlations. Thus, routine reanalysis of genomic data and integration of emerging technologies such as deep sequencing, long-read sequencing, and single-cell genomics is warranted to improve future diagnostic yield.

The accurate and comprehensive classification and subtyping of mosaicism is important and hold a significant clinical utility. It can help to define the natural history of these disorders, tailor follow-up protocols, guide interventions and treatment decisions, and refine genetic counseling, especially regarding potential germline involvement. The data obtained from each study led to personalized management and surveillance plans to facilitate the well-being of the patients and informed counseling for their families. These contributions were particularly important for disorders with progressive or multisystem involvement, where early detection and intervention can alter the long-term outcomes.

Beyond its clinical impact, this work advances the methodological framework for diagnosing mosaicism. By demonstrating how advanced genomic tools can be integrated into routine diagnostic processes, the study paves the way for broader application of these methods in both research and clinical settings. Moreover, the clinically and genetically well-documented cases presented in this thesis can serve as a resource for longitudinal studies. Such studies could aim to define the natural history of specific mosaic disorders and investigate potential therapeutic targets. In parallel, the data generated will contribute to international databases, thereby strengthening collaborative efforts to map the full spectrum of the associated phenotypes.

Taken together, this work reinforces our understanding of mosaicism as a fundamental, yet poorly understood and poorly explored concept in medical genetics, demonstrating the importance of personalized diagnosis for improved genetic counseling and care for patients and their families. Studies conducted in this thesis have improved/will improve the understanding of diagnostic approaches employed in somatic mosaicism, and contribute further delineation of the associated phenotypic and/or genotypic variables. The unsolved cases provide resources for future research and fuels our continued desire to explore the unknown in cell and human biology.

BIBLIOGRAPHY

Abdelgadir, D., Nowaczyk, M. J., & Li, C. (2013). Trisomy 22 mosaicism and normal developmental outcome: report of two patients and review of the literature. *American journal of medical genetics. Part A*, *161A*(5), 1126–1131. https://doi.org/10.1002/ajmg.a.35812

Accetturo, M., Bartolomeo, N., & Stella, A. (2020). In-silico Analysis of *NF1* Missense Variants in ClinVar: Translating Variant Predictions into Variant Interpretation and Classification. *International journal of molecular sciences*, *21*(3), 721. https://doi.org/10.3390/ijms21030721

Adams, D. M., Trenor, C. C., 3rd, Hammill, A. M., Vinks, A. A., Patel, M. N., Chaudry, G., Wentzel, M. S., Mobberley-Schuman, P. S., Campbell, L. M., Brookbank, C., Gupta, A., Chute, C., Eile, J., McKenna, J., Merrow, A. C., Fei, L., Hornung, L., Seid, M., Dasgupta, A. R., Dickie, B. H., … Azizkhan, R. G. (2016). Efficacy and Safety of Sirolimus in the Treatment of Complicated Vascular Anomalies. *Pediatrics*, *137*(2), e20153257. https://doi.org/10.1542/peds.2015-3257

Alexander, A., & Blaschko, A. (1895). Ein Fall von Naevus linearis (Ichthyosis linearis) unius lateris. *Dermatologische Zeitschrift*, *2*, 343–361.

Alomari A. I. (2009). Characterization of a distinct syndrome that associates complex truncal overgrowth, vascular, and acral anomalies: a descriptive study of 18 cases of CLOVES syndrome. *Clinical dysmorphology*, *18*(1), 1–7. https://doi.org/10.1097/MCD.0b013e328317a716

Alqahtani, A., Ayesh, H. S. K., & Halawani, H. (2019). PIK3CA Gene Mutations in Solid Malignancies: Association with Clinicopathological Parameters and Prognosis. *Cancers*, *12*(1), 93. https://doi.org/10.3390/cancers12010093

Altschul, S. F., Gish, W., Miller, W., Myers, E. W., & Lipman, D. J. (1990). Basic local alignment search tool. *Journal of molecular biology*, *215*(3), 403–410. https://doi.org/10.1016/S0022-2836(05)80360-2

Amyere, M., Revencu, N., Helaers, R., Pairet, E., Baselga, E., Cordisco, M., Chung, W., Dubois, J., Lacour, J. P., Martorell, L., Mazereeuw-Hautier, J., Pyeritz, R. E., Amor, D. J., Bisdorff, A., Blei, F., Bombei, H., Dompmartin, A., Brooks, D., Dupont, J., González-Enseñat, M. A., … Vikkula, M. (2017). Germline Loss-of-Function Mutations in EPHB4 Cause a Second Form of Capillary Malformation-Arteriovenous Malformation (CM-AVM2) Deregulating RAS-MAPK Signaling. *Circulation*, *136*(11), 1037–1048. https://doi.org/10.1161/CIRCULATIONAHA.116.026886

Anderson, J., Burns, H. D., Enriquez-Harris, P., Wilkie, A. O., & Heath, J. K. (1998). Apert syndrome mutations in fibroblast growth factor receptor 2 exhibit increased affinity for FGF ligand. *Human molecular genetics*, *7*(9), 1475–1483. https://doi.org/10.1093/hmg/7.9.1475

Arita, Y., Kihara, S., Ouchi, N., Takahashi, M., Maeda, K., Miyagawa, J., Hotta, K., Shimomura, I., Nakamura, T., Miyaoka, K., Kuriyama, H., Nishida, M., Yamashita, S., Okubo, K., Matsubara, K., Muraguchi, M., Ohmoto, Y., Funahashi, T., & Matsuzawa, Y. (1999). Paradoxical decrease of an adipose-specific protein, adiponectin, in obesity. *Biochemical and biophysical research communications*, *257*(1), 79–83. https://doi.org/10.1006/bbrc.1999.0255

Azoury, S. C., Reddy, S., Shukla, V., & Deng, C. X. (2017). Fibroblast Growth Factor Receptor 2 (*FGFR2*) Mutation Related Syndromic Craniosynostosis. *International journal of biological sciences*, *13*(12), 1479–1488. https://doi.org/10.7150/ijbs.22373

Bai, X., & Jiang, Y. (2010). Key factors in mTOR regulation. *Cellular and molecular life sciences : CMLS*, *67*(2), 239–253. https://doi.org/10.1007/s00018-009-0163-7

Baikie, A. G., Garson, O. M., & Birrell, R. G. (1965). Mosaicism for trisomy 17-18 and trisomy 13-15 in man. *Nature*, *207*(5004), 1419–1420. https://doi.org/10.1038/2071419a0

Bain, A. D., Insley, J., Douglas, D. M., Gauld, I. K., & Scott, H. A. (1965). Normal-trisomy 13-15 mosaicism in two infants. *Archives of disease in childhood*, *40*(212), 442–445. https://doi.org/10.1136/adc.40.212.442

Baltzer, C., Tiefenböck, S. K., & Frei, C. (2010). Mitochondria in response to nutrients and nutrient-sensitive pathways. *Mitochondrion*, *10*(6), 589–597. https://doi.org/10.1016/j.mito.2010.07.009

Baynam, G., Overkov, A., Davis, M., Mina, K., Schofield, L., Allcock, R., Laing, N., Cook, M., Dawkins, H., & Goldblatt, J. (2015). A germline MTOR mutation in Aboriginal Australian siblings with intellectual disability, dysmorphism, macrocephaly, and small thoraces. *American journal of medical genetics. Part A*, *167*(7), 1659–1667. https://doi.org/10.1002/ajmg.a.37070fgf

Bayrak-Toydemir, P., & Stevenson, D. A. (2019, September 12). *Capillary Malformation-Arteriovenous Malformation Syndrome*. GeneReviews® - NCBI Bookshelf. https://www.ncbi.nlm.nih.gov/books/NBK52764/

Beare, J. M., Dodge, J. A., & Nevin, N. C. (1969). Cutis gyratum, acanthosis nigricans and other congenital anomalies. A new syndrome. *The British journal of dermatology*, *81*(4), 241–247.

Bennett, J. T., Tan, T. Y., Alcantara, D., Tétrault, M., Timms, A. E., Jensen, D., Collins, S., Nowaczyk, M. J. M., Lindhurst, M. J., Christensen, K. M., Braddock, S. R., Brandling-Bennett, H., Hennekam, R. C. M., Chung, B., Lehman, A., Su, J., Ng, S.,

Amor, D. J., University of Washington Center for Mendelian Genomics, Care4Rare Canada Consortium, … McDonell, L. M. (2016). Mosaic Activating Mutations in FGFR1 Cause Encephalocraniocutaneous Lipomatosis. *American journal of human genetics*, *98*(3), 579–587. https://doi.org/10.1016/j.ajhg.2016.02.006

Biesecker, L. G., Peters, K. F., Darling, T. N., Choyke, P., Hill, S., Schimke, N., Cunningham, M., Meltzer, P., & Cohen, M. M., Jr (1998). Clinical differentiation between Proteus syndrome and hemihyperplasia: description of a distinct form of hemihyperplasia. *American journal of medical genetics*, *79*(4), 311–318. https://doi.org/10.1002/(sici)1096-8628(19981002)79:4<311::aid-ajmg14>3.0.co;2-u

Blaschko, A. (1901). Die Nervenverteilung in der Haut in ihrer Beziehung zu den Erkrankungen der Haut: Bericht, erstattet dem VII. Congress der deutschen dermatologischen Gesellschaft, abgehalten zu Breslau 28-30. Mai 1901.

Boccuto, L., & Neri, G. (2021). Overgrowth in myth and art. *American journal of medical genetics. Part C, Seminars in medical genetics*, *187*(2), 176–181. https://doi.org/10.1002/ajmg.c.31910

Bochukova, E. G., Roscioli, T., Hedges, D. J., Taylor, I. B., Johnson, D., David, D. J., Deininger, P. L., & Wilkie, A. O. (2009). Rare mutations of FGFR2 causing apert syndrome: identification of the first partial gene deletion, and an Alu element insertion from a new subfamily. *Human mutation*, *30*(2), 204–211. https://doi.org/10.1002/humu.20825

Bolanos-Garcia, V. M., & Blundell, T. L. (2011). BUB1 and BUBR1: multifaceted kinases of the cell cycle. *Trends in biochemical sciences*, *36*(3), 141–150. https://doi.org/10.1016/j.tibs.2010.08.004

Boutant, M., Kulkarni, S. S., Joffraud, M., Ratajczak, J., Valera-Alberni, M., Combe, R., Zorzano, A., & Cantó, C. (2017). Mfn2 is critical for brown adipose tissue thermogenic function. *The EMBO journal*, *36*(11), 1543–1558. https://doi.org/10.15252/embj.201694914

Boveri, T. (1914). *Zur frage der entstehung maligner tumoren*. Gustav Fischer.

British Museum. (n.d.). *The Hottentot Venus [Etching]*. Museum Number: 1851,0308.638. Retrieved from https://www.britishmuseum.org/collection/object/P_1851-0308-638

Buedts, L., & Vandenberghe, P. (2016). Circulating cell-free DNA in hematological malignancies. *Haematologica*, *101*(9), 997–999. https://doi.org/10.3324/haematol.2015.131128

Burnet, F. M. (1959). *The clonal selection theory of acquired immunity.* Vanderbilt University Press. https://doi.org/10.5962/bhl.title.8281

Burrows, P. E., Gonzalez-Garay, M. L., Rasmussen, J. C., Aldrich, M. B., Guilliod, R., Maus, E. A., Fife, C. E., Kwon, S., Lapinski, P. E., King, P. D., & Sevick-Muraca, E.

M. (2013). Lymphatic abnormalities are associated with RASA1 gene mutations in mouse and man. *Proceedings of the National Academy of Sciences of the United States of America*, *110*(21), 8621–8626. https://doi.org/10.1073/pnas.1222722110

Canaud, G., Lopez Gutierrez, J. C., Irvine, A. D., Vabres, P., Hansford, J. R., Ankrah, N., Branle, F., Papadimitriou, A., Ridolfi, A., O'Connell, P., Turner, S., & Adams, D. M. (2023). Alpelisib for treatment of patients with PIK3CA-related overgrowth spectrum (PROS). *Genetics in medicine : official journal of the American College of Medical Genetics*, *25*(12), 100969. https://doi.org/10.1016/j.gim.2023.100969

Cancer Genome Atlas Network (2012). Comprehensive molecular portraits of human breast tumours. *Nature*, *490*(7418), 61–70. https://doi.org/10.1038/nature11412

Cantley, L. C. (2002). The Phosphoinositide 3-Kinase pathway. *Science, 296*(5573), 1655–1657. https://doi.org/10.1126/science.296.5573.1655

Cao, J., Tyburczy, M. E., Moss, J., Darling, T. N., Widlund, H. R., & Kwiatkowski, D. J. (2017). Tuberous sclerosis complex inactivation disrupts melanogenesis via mTORC1 activation. *The Journal of clinical investigation*, *127*(1), 349–364. https://doi.org/10.1172/JCI84262

Capel, E., Vatier, C., Cervera, P., Stojkovic, T., Disse, E., Cottereau, A. S., Auclair, M., Verpont, M. C., Mosbah, H., Gourdy, P., Barraud, S., Miquel, A., Züchner, S., Bonnefond, A., Froguel, P., Christin-Maitre, S., Delemer, B., Fève, B., Laville, M., Robert, J., … Jéru, I. (2018). MFN2-associated lipomatosis: Clinical spectrum and impact on adipose tissue. *Journal of clinical lipidology*, *12*(6), 1420–1435. https://doi.org/10.1016/j.jacl.2018.07.009

Carli, D., Ferrero, G. B., Fusillo, A., Coppo, P., La Selva, R., Zinali, F., Cardaropoli, S., Ranieri, C., Iacoviello, M., Resta, N., & Mussa, A. (2021). A new case of Smith-Kingsmore syndrome with somatic MTOR pathogenic variant expands the phenotypic spectrum to lateralized overgrowth. *Clinical genetics*, *99*(5), 719–723. https://doi.org/10.1111/cge.13931

Carmignac, V., Mignot, C., Blanchard, E., Kuentz, P., Aubriot-Lorton, M. H., Parker, V. E. R., Sorlin, A., Fraitag, S., Courcet, J. B., Duffourd, Y., Rodriguez, D., Knox, R. G., Polubothu, S., Boland, A., Olaso, R., Delepine, M., Darmency, V., Riachi, M., Quelin, C., Rollier, P., … Vabres, P. (2021). Clinical spectrum of MTOR-related hypomelanosis of Ito with neurodevelopmental abnormalities. *Genetics in medicine : official journal of the American College of Medical Genetics*, *23*(8), 1484–1491. https://doi.org/10.1038/s41436-021-01161-6

Carol, W. L. L. (1944). *Leerboek der huidziekten*. Scheltema & Holkema.

Chemke, J., Rappaport, S., & Etrog, R. (1983). Aberrant melanoblast migration associated with trisomy 18 mosaicism. *Journal of medical genetics*, *20*(2), 135–137. https://doi.org/10.1136/jmg.20.2.135

Chen, H., Detmer, S. A., Ewald, A. J., Griffin, E. E., Fraser, S. E., & Chan, D. C. (2003). Mitofusins Mfn1 and Mfn2 coordinately regulate mitochondrial fusion and are essential for embryonic development. *The Journal of cell biology*, *160*(2), 189–200. https://doi.org/10.1083/jcb.200211046

Chen, K., Wan, X., Zhao, L., Zhao, S., Peng, L., Yang, W., Yuan, J., Zhu, L., & Mo, Z. (2020). Cbl Proto-Oncogene B (CBLB) c.197A>T Mutation Induces Mild Metabolic Dysfunction in Partial Type I Multiple Symmetric Lipomatosis (MSL). *Diabetes, metabolic syndrome and obesity: targets and therapy*, 13, 3535–3549. https://doi.org/10.2147/DMSO.S273780

Chen, Y., & Dorn, G. W., 2nd (2013). PINK1-phosphorylated mitofusin 2 is a Parkin receptor for culling damaged mitochondria. *Science (New York, N.Y.)*, *340*(6131), 471–475. https://doi.org/10.1126/science.1231031

Clarke, C. M., Edwards, J. H., & Smallpeice, V. (1961). 21-trisomy/normal mosaicism in an intelligent child with some mongoloid characters. *Lancet (London, England)*, *1*(7185), 1028–1030. https://doi.org/10.1016/s0140-6736(61)91833-5

ClinicalTrials.gov (2017). *Trial of Taselisib (GDC-0032) in PIK3CA-related overgrowth (NCT03290092)*. Retrieved May 5, 2025, from https://clinicaltrials.gov/study/NCT0329009

ClinicalTrials.gov. (2020). *Retrospective chart review study of patients with PIK3CA-related overgrowth spectrum who have received alpelisib (EPIK-P1) (NCT04285723).* Retrieved May 5, 2025, from https://clinicaltrials.gov/study/NCT04285723

ClinicalTrials.gov. (2021). *Study Assessing the Efficacy, Safety and PK of Alpelisib (BYL719) in Pediatric and Adult Patients With PIK3CA-related Overgrowth Spectrum (EPIK-P2)(NCT04589650).* Retrieved May 5, 2025, from https://www.clinicaltrials.gov/study/NCT04589650

Cohen, M. M., Jr, & Hayden, P. W. (1979). A newly recognized hamartomatous syndrome. *Birth defects original article series*, *15*(5B), 291–296.

Collins, G. N. (1913). Mosaic coherence of characters in seeds of maize. *Plant Industry Circular No. 132*, pp. 19–21. U.S. Department of Agriculture.

Cooley Coleman, J. A., Gass, J. M., Srikanth, S., Pauly, R., Ziats, C. A., Everman, D. B., Skinner, S. A., Bell, S., Louie, R. J., Cascio, L., Patterson, W. G., Jones, J. R., Di Donato, N., Stevenson, R. E., & Boccuto, L. (2023). Clinical and functional characterization of germline PIK3CA variants in patients with PIK3CA-related overgrowth spectrum disorders. *Human molecular genetics*, *32*(9), 1457–1465. https://doi.org/10.1093/hmg/ddac296

Cotterman C. W. (1956). Somatic mosaicism for antigen A2. *Acta genetica et statistica medica*, *6*(4), 520–521. https://doi.org/10.1159/000150891

Curth, H. O., & Warburton, D. (1965). The Genetics of Incontinentia Pigmenti. *Archives of dermatology*, *92*, 229–235. https://doi.org/10.1001/archderm.92.3.229

D'Alfonso, T. M., Pareja, F., Da Cruz Paula, A., Vahdatinia, M., Gazzo, A., Ferrando, L., da Silva, E. M., Cheng, E., Sclafani, L., Chandarlapaty, S., Zhang, H., Hoda, S. A., Wen, H. Y., Brogi, E., Weigelt, B., & Reis-Filho, J. S. (2021). Whole-exome sequencing analysis of juvenile papillomatosis and coexisting breast carcinoma. *The journal of pathology. Clinical research*, *7*(2), 113–120. https://doi.org/10.1002/cjp2.190

Dang, J. D., & Cohen, P. R. (2010). Segmental neurofibromatosis and malignancy. *Skinmed*, *8*(3), 156–159.

Danon, M., & Sachs, L. (1957). Sex chromosomes and human sexual development. *Lancet (London, England)*, *273*(6984), 20–25. https://doi.org/10.1016/s0140-6736(57)90575-5

de Brito, O. M., & Scorrano, L. (2008). Mitofusin 2 tethers endoplasmic reticulum to mitochondria. *Nature*, *456*(7222), 605–610. https://doi.org/10.1038/nature07534

De Schepper, S., Maertens, O., Callens, T., Naeyaert, J. M., Lambert, J., & Messiaen, L. (2008). Somatic mutation analysis in NF1 café au lait spots reveals two NF1 hits in the melanocytes. *The Journal of investigative dermatology*, *128*(4), 1050–1053. https://doi.org/10.1038/sj.jid.5701095

de Wijn, R. S., Oduber, C. E., Breugem, C. C., Alders, M., Hennekam, R. C., & van der Horst, C. M. (2012). Phenotypic variability in a family with capillary malformations caused by a mutation in the RASA1 gene. *European journal of medical genetics*, *55*(3), 191–195. https://doi.org/10.1016/j.ejmg.2012.01.009

Death Of The “Elephant Man.” (1890). *The British Medical Journal*, *1*(1529), 916–917. http://www.jstor.org/stable/20238863

D'Gama, A. M., Geng, Y., Couto, J. A., Martin, B., Boyle, E. A., LaCoursiere, C. M., Hossain, A., Hatem, N. E., Barry, B. J., Kwiatkowski, D. J., Vinters, H. V., Barkovich, A. J., Shendure, J., Mathern, G. W., Walsh, C. A., & Poduri, A. (2015). Mammalian target of rapamycin pathway mutations cause hemimegalencephaly and focal cortical dysplasia. *Annals of neurology*, *77*(4), 720–725. https://doi.org/10.1002/ana.24357

Di Donato, N., Rump, A., Mirzaa, G. M., Alcantara, D., Oliver, A., Schrock, E., Dobyns, W. B., & O'Driscoll, M. (2016). Identification and Characterization of a Novel Constitutional PIK3CA Mutation in a Child Lacking the Typical Segmental Overgrowth of "PIK3CA-Related Overgrowth Spectrum". *Human mutation*, *37*(3), 242–245. https://doi.org/10.1002/humu.22933

Diehl, F., Schmidt, K., Choti, M. A., Romans, K., Goodman, S., Li, M., Thornton, K., Agrawal, N., Sokoll, L., Szabo, S. A., Kinzler, K. W., Vogelstein, B., & Diaz, L. A., Jr (2008). Circulating mutant DNA to assess tumor dynamics. *Nature medicine*, *14*(9), 985–990. https://doi.org/10.1038/nm.1789

Dietrich, M. O., Liu, Z. W., & Horvath, T. L. (2013). Mitochondrial dynamics controlled by mitofusins regulate Agrp neuronal activity and diet-induced obesity. *Cell*, *155*(1), 188–199. https://doi.org/10.1016/j.cell.2013.09.004

Donhauser, G., Vieluf, D., Ruzicka, T., & Braun-Falco, O. (1991). Benigne symmetrische Lipomatose Launois-Bensaude Typ III und Bureau-Barrière-Syndrom [Benign symmetric Launois-Bensaude type III lipomatosis and Bureau-Barrière syndrome]. *Der Hautarzt; Zeitschrift fur Dermatologie, Venerologie, und verwandte Gebiete*, *42*(5), 311–314.

Dorschner, M. O., Sybert, V. P., Weaver, M., Pletcher, B. A., & Stephens, K. (2000). NF1 microdeletion breakpoints are clustered at flanking repetitive sequences. *Human molecular genetics*, *9*(1), 35–46. https://doi.org/10.1093/hmg/9.1.35

Dou, Y., Yang, X., Li, Z., Wang, S., Zhang, Z., Ye, A. Y., Yan, L., Yang, C., Wu, Q., Li, J., Zhao, B., Huang, A. Y., & Wei, L. (2017). Postzygotic single-nucleotide mosaicisms contribute to the etiology of autism spectrum disorder and autistic traits and the origin of mutations. *Human mutation*, *38*(8), 1002–1013. https://doi.org/10.1002/humu.23255

Douzgou, S., Rawson, M., Baselga, E., Danielpour, M., Faivre, L., Kashanian, A., Keppler-Noreuil, K. M., Kuentz, P., Mancini, G. M. S., Maniere, M. C., Martinez-Glez, V., Parker, V. E., Semple, R. K., Srivastava, S., Vabres, P., De Wit, M. Y., Graham, J. M., Jr, Clayton-Smith, J., Mirzaa, G. M., & Biesecker, L. G. (2022). A standard of care for individuals with PIK3CA-related disorders: An international expert consensus statement. *Clinical genetics*, *101*(1), 32–47. https://doi.org/10.1111/cge.14027

Dyer, S. C., Austine-Orimoloye, O., Azov, A. G., Barba, M., Barnes, I., Barrera-Enriquez, V. P., Becker, A., Bennett, R., Beracochea, M., Berry, A., Bhai, J., Bhurji, S. K., Boddu, S., Branco Lins, P. R., Brooks, L., Ramaraju, S. B., Campbell, L. I., Martinez, M. C., Charkhchi, M., Cortes, L. A., … Yates, A. D. (2025). Ensembl 2025. *Nucleic acids research*, *53*(D1), D948–D957. https://doi.org/10.1093/nar/gkae1071

Eerola, I., Boon, L. M., Mulliken, J. B., Burrows, P. E., Dompmartin, A., Watanabe, S., Vanwijck, R., & Vikkula, M. (2003). Capillary malformation-arteriovenous malformation, a new clinical and genetic disorder caused by RASA1 mutations. *American journal of human genetics*, *73*(6), 1240–1249. https://doi.org/10.1086/379793

Ejerskov, C., Raundahl, M., Gregersen, P. A., & Handrup, M. M. (2021). Clinical features and disease severity in patients with mosaic neurofibromatosis type 1: a single-center study and literature review. *Orphanet journal of rare diseases*, *16*(1), 180. https://doi.org/10.1186/s13023-021-01796-3

Elazezy, M., & Joosse, S. A. (2018). Techniques of using circulating tumor DNA as a liquid biopsy component in cancer management. *Computational and structural biotechnology journal*, *16*, 370–378. https://doi.org/10.1016/j.csbj.2018.10.002

Elowe, S., & Bolanos-Garcia, V. M. (2022). The spindle checkpoint proteins BUB1 and BUBR1: (SLiM)ming down to the basics. *Trends in Biochemical Sciences, 47*(4), 352–366. https://doi.org/10.1016/j.tibs.2022.01.004

Engelman J. A. (2009). Targeting PI3K signalling in cancer: opportunities, challenges and limitations. *Nature reviews. Cancer*, *9*(8), 550–562. https://doi.org/10.1038/nrc2664

Enzi G. (1984). Multiple symmetric lipomatosis: an updated clinical report. *Medicine*, *63*(1), 56–64. https://doi.org/10.1097/00005792-198401000-00004

Enzi, G., Busetto, L., Ceschin, E., Coin, A., Digito, M., & Pigozzo, S. (2002). Multiple symmetric lipomatosis: clinical aspects and outcome in a long-term longitudinal study. *International journal of obesity and related metabolic disorders : journal of the International Association for the Study of Obesity*, *26*(2), 253–261. https://doi.org/10.1038/sj.ijo.0801867

Farhan, S. M., Robinson, J. F., McIntyre, A. D., Marrosu, M. G., Ticca, A. F., Loddo, S., Carboni, N., Brancati, F., & Hegele, R. A. (2014). A novel LIPE nonsense mutation found using exome sequencing in siblings with late-onset familial partial lipodystrophy. *The Canadian journal of cardiology*, *30*(12), 1649–1654. https://doi.org/10.1016/j.cjca.2014.09.007

Flores Daboub, J. A., Grimmer, J. F., Frigerio, A., Wooderchak-Donahue, W., Arnold, R., Szymanski, J., Longo, N., & Bayrak-Toydemir, P. (2020). Parkes Weber syndrome associated with two somatic pathogenic variants in *RASA1*. *Cold Spring Harbor molecular case studies*, *6*(4), a005256. https://doi.org/10.1101/mcs.a005256

Florez, L., & Lacassie, Y. (2005). Mosaic trisomy 22: report of a patient with normal intelligence. *American journal of medical genetics. Part A*, *132A*(2), 223–225. https://doi.org/10.1002/ajmg.a.30401

Forbes, S. H., Dorschner, M. O., Le, R., & Stephens, K. (2004). Genomic context of paralogous recombination hotspots mediating recurrent NF1 region microdeletion. *Genes, chromosomes & cancer*, *41*(1), 12–25. https://doi.org/10.1002/gcc.20065

Ford, C. E., Polanı, P. E., Brıggs, J. H., & Bıshop, P. M. (1959). A presumptive human XXY/XX mosaic. Nature, 183(4667), 1030–1032. https://doi.org/10.1038/1831030a0

Forteza, G., Baguena, R., Amat, E., Barcia, D., & Juan, A. (1964). Mos'aico trisom'ia d1/ normal en una ni na de seis a nos con un sindrome de trisomia d1 incompleto [Mosaic trisomy d1/ normal in a 6-year-old girl with an incomplete syndrome of trisomy d1]. *Medicina espanola*, *51*, 83–93.

Fraccaro, M., Kaıjser, K., & Lındsten, J. (1960). Somatic chromosome complement in continuously cultured cells of two individuals with gonadal dysgenesis. *Annals of human genetics*, *24*, 45–61. https://doi.org/10.1111/j.1469-1809.1959.tb01714.x

Franco, A., Kitsis, R. N., Fleischer, J. A., Gavathiotis, E., Kornfeld, O. S., Gong, G., Biris, N., Benz, A., Qvit, N., Donnelly, S. K., Chen, Y., Mennerick, S., Hodgson, L., Mochly-Rosen, D., & Dorn, G. W. I. I. (2016). Correcting mitochondrial fusion by manipulating mitofusin conformations. *Nature*, *540*(7631), 74–79. https://doi.org/10.1038/nature20156

Friedman, J. M. (2022, April 21). *Neurofibromatosis 1*. GeneReviews® - NCBI Bookshelf. https://www.ncbi.nlm.nih.gov/books/NBK1109/

Fritsch, C., Huang, A., Chatenay-Rivauday, C., Schnell, C., Reddy, A., Liu, M., Kauffmann, A., Guthy, D., Erdmann, D., De Pover, A., Furet, P., Gao, H., Ferretti, S., Wang, Y., Trappe, J., Brachmann, S. M., Maira, S. M., Wilson, C., Boehm, M., Garcia-Echeverria, C., … Sellers, W. R. (2014). Characterization of the novel and specific PI3Kα inhibitor NVP-BYL719 and development of the patient stratification strategy for clinical trials. *Molecular cancer therapeutics*, *13*(5), 1117–1129. https://doi.org/10.1158/1535-7163.MCT-13-0865

Gall, J. M., Wang, Z., Bonegio, R. G., Havasi, A., Liesa, M., Vemula, P., & Borkan, S. C. (2015). Conditional knockout of proximal tubule mitofusin 2 accelerates recovery and improves survival after renal ischemia. *Journal of the American Society of Nephrology : JASN*, *26*(5), 1092–1102. https://doi.org/10.1681/ASN.2014010126

García-Castillo, H., Vásquez-Velásquez, A. I., Rivera, H., & Barros-Núñez, P. (2008). Clinical and genetic heterogeneity in patients with mosaic variegated aneuploidy: delineation of clinical subtypes. *American journal of medical genetics. Part A*, *146A*(13), 1687–1695. https://doi.org/10.1002/ajmg.a.32315

Garcia-Linares, C., Fernández-Rodríguez, J., Terribas, E., Mercadé, J., Pros, E., Benito, L., Benavente, Y., Capellà, G., Ravella, A., Blanco, I., Kehrer-Sawatzki, H., Lázaro, C., & Serra, E. (2011). Dissecting loss of heterozygosity (LOH) in neurofibromatosis type 1-associated neurofibromas: Importance of copy neutral LOH. *Human mutation*, *32*(1), 78–90. https://doi.org/10.1002/humu.21387

Garcias-Ladaria, J., Cuadrado Rosón, M., & Pascual-López, M. (2018). Epidermal Nevi and Related Syndromes -- Part 1: Keratinocytic Nevi. Nevus epidérmicos y síndromes relacionados. Parte 1: nevus queratinocíticos. *Actas dermo-sifiliograficas*, *109*(8), 677–686. https://doi.org/10.1016/j.ad.2018.05.005

Garcias-Ladaria, J., Cuadrado Rosón, M., & Pascual-López, M. (2018). Epidermal Nevi and Related Syndromes - Part 2: Nevi Derived from Adnexal Structures. Nevus epidérmicos y síndromes relacionados. Parte 2: Nevus derivados de estructuras anexiales. *Actas dermo-sifiliograficas*, *109*(8), 687–698. https://doi.org/10.1016/j.ad.2018.05.004

García-Vargas, A., Hafner, C., Pérez-Rodríguez, A. G., Rodríguez-Rojas, L. X., González-Esqueda, P., Stoehr, R., Hernández-Torres, M., & Happle, R. (2008). An epidermal nevus syndrome with cerebral involvement caused by a mosaic FGFR3 mutation. *American journal of medical genetics. Part A*, *146A*(17), 2275–2279. https://doi.org/10.1002/ajmg.a.32429

Garson, O. M., Baikie, A. G., Ferguson, J., & Greer, C. H. (1969). Double autosomal trisomy and mosaicism for three cell lines in man: coexisting trisomy 13-15, trisomy 17-18, and a minority cell line trisomic for a chromosome of both groups. *Journal of medical genetics*, *6*(2), 209–215. https://doi.org/10.1136/jmg.6.2.209

Ghahramani, N., Klein, S., Ghahremani, S., Lee, H., Strom, S., Deignan, J., ... & Martinez-Agosto, J. A. (2015). Activating mutations in mTOR cause human overgrowth associated with macrocephaly, Intellectual Disability, and distinct dysmorphic features. In *ACMG Annual Clinical Genetics Meeting. Salt Lake City, Utah*.

Glaser, R. L., Jiang, W., Boyadjiev, S. A., Tran, A. K., Zachary, A. A., Van Maldergem, L., Johnson, D., Walsh, S., Oldridge, M., Wall, S. A., Wilkie, A. O., & Jabs, E. W. (2000). Paternal origin of FGFR2 mutations in sporadic cases of Crouzon syndrome and Pfeiffer syndrome. *American journal of human genetics*, *66*(3), 768–777. https://doi.org/10.1086/302831

Gordo, G., Rodriguez-Laguna, L., Agra, N., Mendez, P., Feito, M., Lapunzina, P., Lopez-Gutierrez, J. C., & Martinez-Glez, V. (2019). Constitutional mosaicism in RASA1-related capillary malformation-arteriovenous malformation. *Clinical genetics*, *95*(4), 516–519. https://doi.org/10.1111/cge.13499

Gordo, G., Tenorio, J., Arias, P., Santos-Simarro, F., García-Miñaur, S., Moreno, J. C., Nevado, J., Vallespin, E., Rodriguez-Laguna, L., de Mena, R., Dapia, I., Palomares-Bralo, M., Del Pozo, Á., Ibañez, K., Silla, J. C., Barroso, E., Ruiz-Pérez, V. L., Martinez-Glez, V., & Lapunzina, P. (2018). mTOR mutations in Smith-Kingsmore syndrome: Four additional patients and a review. *Clinical genetics*, *93*(4), 762–775. https://doi.org/10.1111/cge.13135

Grabiner, B. C., Nardi, V., Birsoy, K., Possemato, R., Shen, K., Sinha, S., Jordan, A., Beck, A. H., & Sabatini, D. M. (2014). A diverse array of cancer-associated MTOR mutations are hyperactivating and can predict rapamycin sensitivity. *Cancer discovery*, *4*(5), 554–563. https://doi.org/10.1158/2159-8290.CD-13-0929

Groesser, L., Herschberger, E., Ruetten, A., Ruivenkamp, C., Lopriore, E., Zutt, M., Langmann, T., Singer, S., Klingseisen, L., Schneider-Brachert, W., Toll, A., Real, F. X., Landthaler, M., & Hafner, C. (2012). Postzygotic HRAS and KRAS mutations cause nevus sebaceous and Schimmelpenning syndrome. *Nature genetics*, *44*(7), 783–787. https://doi.org/10.1038/ng.2316

Groesser, L., Herschberger, E., Sagrera, A., Shwayder, T., Flux, K., Ehmann, L., Wollenberg, A., Torrelo, A., Bagazgoitia, L., Diaz-Ley, B., Tinschert, S., Oschlies, I.,

Singer, S., Mickler, M., Toll, A., Landthaler, M., Real, F. X., & Hafner, C. (2013). Phacomatosis pigmentokeratotica is caused by a postzygotic HRAS mutation in a multipotent progenitor cell. *The Journal of investigative dermatology*, *133*(8), 1998–2003. https://doi.org/10.1038/jid.2013.24

Haber, D. A., & Velculescu, V. E. (2014). Blood-based analyses of cancer: circulating tumor cells and circulating tumor DNA. *Cancer discovery*, *4*(6), 650–661. https://doi.org/10.1158/2159-8290.CD-13-1014

Häcker, V. (1904). Über die Ergebnisse der Bastardlehre, ihre zellengeschichtliche Begründung und ihre Bedeutung für die praktische Tierzucht. *Arch Rassen Gesellschaftsbiol*, *1*, 321-338.

Haensch, R. (1961). Ekzem und nervale Faktoren. *Archiv für klinische und experimentelle Dermatologie*, *214*, 35–40. https://doi.org/10.1007/BF00492997

Hafner, C., López-Knowles, E., Luis, N. M., Toll, A., Baselga, E., Fernández-Casado, A., Hernández, S., Ribé, A., Mentzel, T., Stoehr, R., Hofstaedter, F., Landthaler, M., Vogt, T., Pujol, R. M., Hartmann, A., & Real, F. X. (2007). Oncogenic PIK3CA mutations occur in epidermal nevi and seborrheic keratoses with a characteristic mutation pattern. *Proceedings of the National Academy of Sciences of the United States of America*, *104*(33), 13450–13454. https://doi.org/10.1073/pnas.0705218104

Hafner, C., Toll, A., Gantner, S., Mauerer, A., Lurkin, I., Acquadro, F., Fernández-Casado, A., Zwarthoff, E. C., Dietmaier, W., Baselga, E., Parera, E., Vicente, A., Casanova, A., Cigudosa, J., Mentzel, T., Pujol, R. M., Landthaler, M., & Real, F. X. (2012). Keratinocytic epidermal nevi are associated with mosaic RAS mutations. *Journal of medical genetics*, *49*(4), 249–253. https://doi.org/10.1136/jmedgenet-2011-100637

Hall J. G. (1988). Review and hypotheses: somatic mosaicism: observations related to clinical genetics. *American journal of human genetics*, *43*(4), 355–363.

Handoko, M., Emrick, L. T., Rosenfeld, J. A., Wang, X., Tran, A. A., Turner, A., Belmont, J. W., Undiagnosed Diseases Network, Lee, B. H., Bacino, C. A., & Chao, H. T. (2019). Recurrent mosaic MTOR c.5930C > T (p.Thr1977Ile) variant causing megalencephaly, asymmetric polymicrogyria, and cutaneous pigmentary mosaicism: Case report and review of the literature. *American journal of medical genetics. Part A*, *179*(3), 475–479. https://doi.org/10.1002/ajmg.a.61007

Hanks, S., Coleman, K., Reid, S., Plaja, A., Firth, H., Fitzpatrick, D., Kidd, A., Méhes, K., Nash, R., Robin, N., Shannon, N., Tolmie, J., Swansbury, J., Irrthum, A., Douglas, J., & Rahman, N. (2004). Constitutional aneuploidy and cancer predisposition caused by biallelic mutations in BUB1B. *Nature Genetics, 36*(11), 1159–1161. https://doi.org/10.1038/ng1449

Hanks, S., Coleman, K., Summersgill, B., Messahel, B., Williamson, D., Pritchard-Jones, K., Strefford, J., Swansbury, J., Plaja, A., Shipley, J., & Rahman, N. (2006).

Comparative genomic hybridization and BUB1B mutation analyses in childhood cancers associated with mosaic variegated aneuploidy syndrome. *Cancer letters*, *239*(2), 234–238. https://doi.org/10.1016/j.canlet.2005.08.006

Happle R. (1985). Lyonization and the lines of Blaschko. *Human genetics*, *70*(3), 200–206. https://doi.org/10.1007/BF00273442

Happle R. (2006). X-chromosome inactivation: role in skin disease expression. *Acta paediatrica (Oslo, Norway: 1992). Supplement*, *95*(451), 16–23. https://doi.org/10.1111/j.1651-2227.2006.tb02384.x

Happle, R. (1976, October). Genetic mechanisms giving rise to linear skin lesions. In *Joint meeting of the Vereinigung Südwestdeutscher Dermatologen and the Vereinigung Rheinisch-Westfälischer Dermatologen, Heidelberg* (pp. 8-10).

Happle, R. (2017). The Molecular Revolution in Cutaneous Biology: Era of Mosaicism. *The Journal of investigative dermatology*, *137*(5), e73–e77. https://doi.org/10.1016/j.jid.2016.03.045

Happle, R. (2020). An Early Description of a "Human Mosaic" Involving the Skin: A Story from 1945. *Acta dermato-venereologica*, *100*(7), adv00090. https://doi.org/10.2340/00015555-3426

Happle, R., & Assim, A. (2001). The lines of Blaschko on the head and neck. *Journal of the American Academy of Dermatology*, *44*(4), 612–615. https://doi.org/10.1067/mjd.2001.112386

Happle, R., & Torrelo, A. (2022a). Didymotic skin disorders. In *Springer eBooks* (pp. 113–117). https://doi.org/10.1007/978-3-030-89937-0_8

Heitzer, E., Haque, I. S., Roberts, C. E. S., & Speicher, M. R. (2019). Current and future perspectives of liquid biopsies in genomics-driven oncology. *Nature reviews. Genetics*, *20*(2), 71–88. https://doi.org/10.1038/s41576-018-0071-5

Helsten, T., Elkin, S., Arthur, E., Tomson, B. N., Carter, J., & Kurzrock, R. (2016). The FGFR Landscape in Cancer: Analysis of 4,853 Tumors by Next-Generation Sequencing. *Clinical cancer research : an official journal of the American Association for Cancer Research*, *22*(1), 259–267. https://doi.org/10.1158/1078-0432.CCR-14-3212

Higgins, R., Pink, A., Hunger, R., Yawalkar, N., & Navarini, A. A. (2017). Generalized Comedones, Acne, and Hidradenitis Suppurativa in a Patient with an *FGFR2* Missense Mutation. *Frontiers in medicine*, *4*, 16. https://doi.org/10.3389/fmed.2017.00016

Hirose, A., Okada, Y., Morita, E., & Tanaka, Y. (2006). Benign symmetric lipomatosis associated with alcoholism. *Internal medicine (Tokyo, Japan)*, *45*(17), 1001–1005. https://doi.org/10.2169/internalmedicine.45.1791

Hirschhorn, K., Decker, W. H., & Cooper, H. L. (1960). Human intersex with chromosome mosaicism of type XY/XO. Report of a case. *The New England journal of medicine*, *263*, 1044–1048. https://doi.org/10.1056/NEJM196011242632102

Hoadley, K. A., Yau, C., Wolf, D. M., Cherniack, A. D., Tamborero, D., Ng, S., Leiserson, M. D. M., Niu, B., McLellan, M. D., Uzunangelov, V., Zhang, J., Kandoth, C., Akbani, R., Shen, H., Omberg, L., Chu, A., Margolin, A. A., Van't Veer, L. J., Lopez-Bigas, N., Laird, P. W., … Stuart, J. M. (2014). Multiplatform analysis of 12 cancer types reveals molecular classification within and across tissues of origin. *Cell*, *158*(4), 929–944. https://doi.org/10.1016/j.cell.2014.06.049

Hoste, G., Slembrouck, L., Jongen, L., Punie, K., Matton, T., Vander Borght, S., Vanden Bempt, I., Menten, J., Wildiers, H., Floris, G., Arteaga, C., & Neven, P. (2018). Unexpected Benefit from Alpelisib and Fulvestrant in a Woman with Highly Pre-treated ER-Positive, HER2-Negative PIK3CA Mutant Metastatic Breast Cancer. *Clinical drug investigation*, *38*(11), 1071–1075. https://doi.org/10.1007/s40261-018-0696-3

Howell, M., & Ford, P. (1980). *The true history of the Elephant Man*. Allison & Busby.

Huntley, C., Hodder, A., & Ramachandran, M. (2015). Clinical and historical aspects of the Elephant Man: Exploring the facts and the myths. *Gene, 555*(1), 63–65. https://doi.org/10.1016/j.gene.2014.09.056

Ilumina. (n.d.). *TruSight Hereditary Cancer Panel gene list*. Retrieved from https://emea.illumina.com/content/dam/illumina-marketing/documents/products/gene_lists/gene_list_trusight_cancer.xlsx

Jackson R. (1976). The lines of Blaschko: a review and reconsideration: Observations of the cause of certain unusual linear conditions of the skin. *The British journal of dermatology*, *95*(4), 349–360. https://doi.org/10.1111/j.1365-2133.1976.tb00835.x

Jacobs, P. A., Harnden, D. G., Buckton, K. E., Brown, W. M., King, M. J., Mcbride, J. A., Macgregor, T. N., & Maclean, N. (1961). Cytogenetic studies in primary amenorrhoea. *Lancet (London, England)*, *1*(7188), 1183–1189. https://doi.org/10.1016/s0140-6736(61)91939-0

Jacquemont, S., Bocéno, M., Rival, J. M., Méchinaud, F., & David, A. (2002). High risk of malignancy in mosaic variegated aneuploidy syndrome. *American journal of medical genetics*, *109*(1), 17–16. https://doi.org/10.1002/ajmg.10281

Jamuar, S. S., Lam, A. T., Kircher, M., D'Gama, A. M., Wang, J., Barry, B. J., Zhang, X., Hill, R. S., Partlow, J. N., Rozzo, A., Servattalab, S., Mehta, B. K., Topcu, M., Amrom, D., Andermann, E., Dan, B., Parrini, E., Guerrini, R., Scheffer, I. E., Berkovic, S. F., … Walsh, C. A. (2014). Somatic mutations in cerebral cortical malformations. *The New England journal of medicine*, *371*(8), 733–743. https://doi.org/10.1056/NEJMoa1314432

Jansen, L. A., Mirzaa, G. M., Ishak, G. E., O'Roak, B. J., Hiatt, J. B., Roden, W. H., Gunter, S. A., Christian, S. L., Collins, S., Adams, C., Rivière, J. B., St-Onge, J., Ojemann, J. G., Shendure, J., Hevner, R. F., & Dobyns, W. B. (2015). PI3K/AKT pathway mutations cause a spectrum of brain malformations from megalencephaly to focal cortical dysplasia. *Brain : a journal of neurology*, *138*(Pt 6), 1613–1628. https://doi.org/10.1093/brain/awv045

Jenne, D. E., Tinschert, S., Reimann, H., Lasinger, W., Thiel, G., Hameister, H., & Kehrer-Sawatzki, H. (2001). Molecular characterization and gene content of breakpoint boundaries in patients with neurofibromatosis type 1 with 17q11.2 microdeletions. *American journal of human genetics*, *69*(3), 516–527. https://doi.org/10.1086/323043

Jeong, H. S., Lee, S. H., Yun, H. Y., Baek, K. J., Kwon, N. S., Park, K. C., & Kim, D. S. (2011). Involvement of mTOR signaling in sphingosylphosphorylcholine-induced hypopigmentation effects. *Journal of biomedical science, 18*(1), 55. https://doi.org/10.1186/1423-0127-18-55

Jezela-Stanek, A., & Krajewska-Walasek, M. (2013). Genetic causes of syndromic craniosynostoses. *European journal of paediatric neurology : EJPN : official journal of the European Paediatric Neurology Society*, *17*(3), 221–224. https://doi.org/10.1016/j.ejpn.2012.09.009

Johnson, C. M., & Navarro, O. M. (2017). Clinical and sonographic features of pediatric soft-tissue vascular anomalies part 2: vascular malformations. *Pediatric radiology*, *47*(9), 1196–1208. https://doi.org/10.1007/s00247-017-3906-x

Johnson, S. C., Yanos, M. E., Kayser, E. B., Quintana, A., Sangesland, M., Castanza, A., Uhde, L., Hui, J., Wall, V. Z., Gagnidze, A., Oh, K., Wasko, B. M., Ramos, F. J., Palmiter, R. D., Rabinovitch, P. S., Morgan, P. G., Sedensky, M. M., & Kaeberlein, M. (2013). mTOR inhibition alleviates mitochondrial disease in a mouse model of Leigh syndrome. *Science (New York, N.Y.)*, *342*(6165), 1524–1528. https://doi.org/10.1126/science.1244360

Juric, D., Rodon, J., Tabernero, J., Janku, F., Burris, H. A., Schellens, J. H. M., Middleton, M. R., Berlin, J., Schuler, M., Gil-Martin, M., Rugo, H. S., Seggewiss-Bernhardt, R., Huang, A., Bootle, D., Demanse, D., Blumenstein, L., Coughlin, C., Quadt, C., & Baselga, J. (2018). Phosphatidylinositol 3-Kinase α-Selective Inhibition With Alpelisib (BYL719) in PIK3CA-Altered Solid Tumors: Results From the First-in-Human Study. *Journal of clinical oncology : official journal of the American Society of Clinical Oncology*, *36*(13), 1291–1299. https://doi.org/10.1200/JCO.2017.72.7107

Kajii, T., Kawai, T., Takumi, T., Misu, H., Mabuchi, O., Takahashi, Y., Tachino, M., Nihei, F., & Ikeuchi, T. (1998). Mosaic variegated aneuploidy with multiple congenital abnormalities: homozygosity for total premature chromatid separation trait. *American journal of medical genetics*, *78*(3), 245–249. https://doi.org/10.1002/(sici)1096-8628(19980707)78:3<245::aid-ajmg7>3.0.co;2-o

Kan, S. H., Elanko, N., Johnson, D., Cornejo-Roldan, L., Cook, J., Reich, E. W., Tomkins, S., Verloes, A., Twigg, S. R., Rannan-Eliya, S., McDonald-McGinn, D. M., Zackai, E. H., Wall, S. A., Muenke, M., & Wilkie, A. O. (2002). Genomic screening of fibroblast growth-factor receptor 2 reveals a wide spectrum of mutations in patients with syndromic craniosynostosis. *American journal of human genetics*, *70*(2), 472–486. https://doi.org/10.1086/338758

Kandoth, C., McLellan, M. D., Vandin, F., Ye, K., Niu, B., Lu, C., Xie, M., Zhang, Q., McMichael, J. F., Wyczalkowski, M. A., Leiserson, M. D. M., Miller, C. A., Welch, J. S., Walter, M. J., Wendl, M. C., Ley, T. J., Wilson, R. K., Raphael, B. J., & Ding, L. (2013). Mutational landscape and significance across 12 major cancer types. *Nature*, *502*(7471), 333–339. https://doi.org/10.1038/nature12634

Kang, E., Kim, Y. M., Seo, G. H., Oh, A., Yoon, H. M., Ra, Y. S., Kim, E. K., Kim, H., Heo, S. H., Kim, G. H., Osborn, M. J., Tolar, J., Yoo, H. W., & Lee, B. H. (2020). Phenotype categorization of neurofibromatosis type I and correlation to NF1 mutation types. *Journal of human genetics*, *65*(2), 79–89. https://doi.org/10.1038/s10038-019-0695-0

Keegan, N. M., Gleeson, J. P., Hennessy, B. T., & Morris, P. G. (2018). PI3K inhibition to overcome endocrine resistance in breast cancer. *Expert opinion on investigational drugs*, *27*(1), 1–15. https://doi.org/10.1080/13543784.2018.1417384

Kehinde, F. I., Anderson, C. E., McGowan, J. E., Jethva, R. N., Wahab, M. A., Glick, A. R., Sterner, M. R., Jr, Pascasio, J. M., Punnett, H. H., & Liu, J. (2014). Co-occurrence of non-mosaic trisomy 22 and inherited balanced t(4;6)(q33;q23.3) in a liveborn female: case report and review of the literature. *American journal of medical genetics. Part A*, *164A*(12), 3187–3193. https://doi.org/10.1002/ajmg.a.36778

Kehrer-Sawatzki, H., & Cooper, D. N. (2021). Classification of NF1 microdeletions and its importance for establishing genotype/phenotype correlations in patients with NF1 microdeletions. *Human genetics*, *140*(12), 1635–1649. https://doi.org/10.1007/s00439-021-02363-3

Keppler-Noreuil, K. M., Rios, J. J., Parker, V. E., Semple, R. K., Lindhurst, M. J., Sapp, J. C., Alomari, A., Ezaki, M., Dobyns, W., & Biesecker, L. G. (2015). PIK3CA-related overgrowth spectrum (PROS): diagnostic and testing eligibility criteria, differential diagnosis, and evaluation. *American journal of medical genetics. Part A*, *167A*(2), 287–295. https://doi.org/10.1002/ajmg.a.36836

Keppler-Noreuil, K. M., Sapp, J. C., Lindhurst, M. J., Parker, V. E., Blumhorst, C., Darling, T., Tosi, L. L., Huson, S. M., Whitehouse, R. W., Jakkula, E., Grant, I., Balasubramanian, M., Chandler, K. E., Fraser, J. L., Gucev, Z., Crow, Y. J., Brennan, L. M., Clark, R., Sellars, E. A., Pena, L. D., … Biesecker, L. G. (2014). Clinical delineation and natural history of the PIK3CA-related overgrowth spectrum. *American journal of medical genetics. Part A*, *164A*(7), 1713–1733. https://doi.org/10.1002/ajmg.a.36552

Khalid, R., & Fadl-Elmula, I. (2024). A rare mosaic trisomy 22 syndrome in a 7-year-old boy: rare case report. *Sudanese journal of paediatrics*, *24*(2), 175–179. https://doi.org/10.24911/SJP.106-1713472421

Kinsler, V. A., Thomas, A. C., Ishida, M., Bulstrode, N. W., Loughlin, S., Hing, S., Chalker, J., McKenzie, K., Abu-Amero, S., Slater, O., Chanudet, E., Palmer, R., Morrogh, D., Stanier, P., Healy, E., Sebire, N. J., & Moore, G. E. (2013). Multiple congenital melanocytic nevi and neurocutaneous melanosis are caused by postzygotic mutations in codon 61 of NRAS. *The Journal of investigative dermatology*, *133*(9), 2229–2236. https://doi.org/10.1038/jid.2013.70

Kiritsi, D., Lorente, A. I., Happle, R., Bernabeu Wittel, J., & Has, C. (2015). Blaschko line acne on pre-existent hypomelanosis reflecting a mosaic FGFR2 mutation. *The British journal of dermatology*, *172*(4), 1125–1127. https://doi.org/10.1111/bjd.13491

Klopstock, T., Naumann, M., Seibel, P., Shalke, B., Reiners, K., & Reichmann, H. (1997). Mitochondrial DNA mutations in multiple symmetric lipomatosis. *Molecular and cellular biochemistry, 174*(1-2), 271–275.

Koshiba, T., Detmer, S. A., Kaiser, J. T., Chen, H., McCaffery, J. M., & Chan, D. C. (2004). Structural basis of mitochondrial tethering by mitofusin complexes. *Science (New York, N.Y.)*, *305*(5685), 858–862. https://doi.org/10.1126/science.1099793

Koulischer, L., Pelc, S., & Perier, O. (1963). A case of trisomy-18 mosaicism. *Lancet (London, England)*, *2*(7314), 945–946. https://doi.org/10.1016/s0140-6736(63)90658-5

Kraus, E. J. (1916). Somatic Segregation: Variations in Plants May Be Divided in Two Classes, One of Which Breeds True While the Other Does Not--Modern Work Shows Importance of Former Class in Practical Breeding--Further Study May Aid in Understanding Causes of Variation in General. *Journal of Heredity, 7*(1), 3–8. https://doi.org/10.1093/jhered/7.1.3

Krupp, D. R., Barnard, R. A., Duffourd, Y., Evans, S. A., Mulqueen, R. M., Bernier, R., Rivière, J. B., Fombonne, E., & O'Roak, B. J. (2017). Exonic Mosaic Mutations Contribute Risk for Autism Spectrum Disorder. *American journal of human genetics*, *101*(3), 369–390. https://doi.org/10.1016/j.ajhg.2017.07.016

Kuentz, P., Fraitag, S., Gonzales, M., Dhombres, F., St-Onge, J., Duffourd, Y., Joyé, N., Jouannic, J. M., Picard, A., Marle, N., Thevenon, J., Thauvin-Robinet, C., Faivre, L., Rivière, J. B., & Vabres, P. (2017). Mosaic-activating FGFR2 mutation in two fetuses with papillomatous pedunculated sebaceous naevus. *The British journal of dermatology*, *176*(1), 204–208. https://doi.org/10.1111/bjd.14681

Kuentz, P., St-Onge, J., Duffourd, Y., Courcet, J. B., Carmignac, V., Jouan, T., Sorlin, A., Abasq-Thomas, C., Albuisson, J., Amiel, J., Amram, D., Arpin, S., Attie-Bitach, T., Bahi-Buisson, N., Barbarot, S., Baujat, G., Bessis, D., Boccara, O., Bonnière, M., Boute, O., … Rivière, J. B. (2017). Molecular diagnosis of PIK3CA-related overgrowth spectrum (PROS) in 162 patients and recommendations for genetic testing. *Genetics in*

medicine : official journal of the American College of Medical Genetics, *19*(9), 989–997. https://doi.org/10.1038/gim.2016.220

Kurek, K. C., Luks, V. L., Ayturk, U. M., Alomari, A. I., Fishman, S. J., Spencer, S. A., Mulliken, J. B., Bowen, M. E., Yamamoto, G. L., Kozakewich, H. P., & Warman, M. L. (2012). Somatic mosaic activating mutations in PIK3CA cause CLOVES syndrome. *American journal of human genetics*, *90*(6), 1108–1115. https://doi.org/10.1016/j.ajhg.2012.05.006

Lapinski, P. E., Doosti, A., Salato, V., North, P., Burrows, P. E., & King, P. D. (2018). Somatic second hit mutation of RASA1 in vascular endothelial cells in capillary malformation-arteriovenous malformation. *European journal of medical genetics*, *61*(1), 11–16. https://doi.org/10.1016/j.ejmg.2017.10.004

Lee, J. H., Huynh, M., Silhavy, J. L., Kim, S., Dixon-Salazar, T., Heiberg, A., Scott, E., Bafna, V., Hill, K. J., Collazo, A., Funari, V., Russ, C., Gabriel, S. B., Mathern, G. W., & Gleeson, J. G. (2012). De novo somatic mutations in components of the PI3K-AKT3-mTOR pathway cause hemimegalencephaly. *Nature genetics*, *44*(8), 941–945. https://doi.org/10.1038/ng.2329

Leest, P. V., Boonstra, P. A., Elst, A. T., Kempen, L. C. V., Tibbesma, M., Koopmans, J., Miedema, A., Tamminga, M., Groen, H. J. M., Reyners, A. K. L., & Schuuring, E. (2020). Comparison of Circulating Cell-Free DNA Extraction Methods for Downstream Analysis in Cancer Patients. *Cancers*, *12*(5), 1222. https://doi.org/10.3390/cancers12051222

Legius, E., Messiaen, L., Wolkenstein, P., Pancza, P., Avery, R. A., Berman, Y., Blakeley, J., Babovic-Vuksanovic, D., Cunha, K. S., Ferner, R., Fisher, M. J., Friedman, J. M., Gutmann, D. H., Kehrer-Sawatzki, H., Korf, B. R., Mautner, V. F., Peltonen, S., Rauen, K. A., Riccardi, V., Schorry, E., … Plotkin, S. R. (2021). Revised diagnostic criteria for neurofibromatosis type 1 and Legius syndrome: an international consensus recommendation. *Genetics in medicine : official journal of the American College of Medical Genetics*, *23*(8), 1506–1513. https://doi.org/10.1038/s41436-021-01170-5

Lemaitre, M., Chevalier, B., Jannin, A., Bourry, J., Espiard, S., & Vantyghem, M. C. (2021). Multiple symmetric and multiple familial lipomatosis. *Presse medicale (Paris, France : 1983)*, *50*(3), 104077. https://doi.org/10.1016/j.lpm.2021.104077

Leoni, C., Gullo, G., Resta, N., Fagotti, A., Onesimo, R., Schwartz, B., Kazakin, J., Abbadessa, G., Crown, J., Collins, C. D., Ranieri, C., Scambia, G., & Zampino, G. (2019). First evidence of a therapeutic effect of miransertib in a teenager with Proteus syndrome and ovarian carcinoma. *American journal of medical genetics. Part A*, *179*(7), 1319–1324. https://doi.org/10.1002/ajmg.a.61160

Lewis, Messinger, Ginn, & Ford (1998). A hereditary disorder of cornification and multiple congenital defects in five Rottweiler dogs. *Veterinary dermatology*, *9*(1), 61–72. https://doi.org/10.1046/j.1365-3164.1998.00079.x

Ligresti, G., Militello, L., Steelman, L. S., Cavallaro, A., Basile, F., Nicoletti, F., Stivala, F., McCubrey, J. A., & Libra, M. (2009). PIK3CA mutations in human solid tumors: role in sensitivity to various therapeutic approaches. *Cell cycle (Georgetown, Tex.)*, *8*(9), 1352–1358. https://doi.org/10.4161/cc.8.9.8255

Lim, E. T., Uddin, M., De Rubeis, S., Chan, Y., Kamumbu, A. S., Zhang, X., D'Gama, A. M., Kim, S. N., Hill, R. S., Goldberg, A. P., Poultney, C., Minshew, N. J., Kushima, I., Aleksic, B., Ozaki, N., Parellada, M., Arango, C., Penzol, M. J., Carracedo, A., Kolevzon, A., … Walsh, C. A. (2017). Rates, distribution and implications of postzygotic mosaic mutations in autism spectrum disorder. *Nature neuroscience*, *20*(9), 1217–1224. https://doi.org/10.1038/nn.4598

Lim, J. S., Gopalappa, R., Kim, S. H., Ramakrishna, S., Lee, M., Kim, W. I., Kim, J., Park, S. M., Lee, J., Oh, J. H., Kim, H. D., Park, C. H., Lee, J. S., Kim, S., Kim, D. S., Han, J. M., Kang, H. C., Kim, H. H., & Lee, J. H. (2017). Somatic Mutations in TSC1 and TSC2 Cause Focal Cortical Dysplasia. *American journal of human genetics*, *100*(3), 454–472. https://doi.org/10.1016/j.ajhg.2017.01.030

Lin, S. M., Luk, H. M., Lo, I. F. M., Tam, W. K., Chan, K. Y. K., Tse, H. Y., Leung, W. C., Tang, M. H. Y., & Kan, A. S. Y. (2020). Prenatal diagnosis and long-term follow-up of a Chinese patient with mosaic variegated aneuploidy and its molecular analysis. *Clinical case reports*, *8*(8), 1369–1375. https://doi.org/10.1002/ccr3.2802

Lindhurst, M. J., Parker, V. E., Payne, F., Sapp, J. C., Rudge, S., Harris, J., Witkowski, A. M., Zhang, Q., Groeneveld, M. P., Scott, C. E., Daly, A., Huson, S. M., Tosi, L. L., Cunningham, M. L., Darling, T. N., Geer, J., Gucev, Z., Sutton, V. R., Tziotzios, C., Dixon, A. K., … Semple, R. K. (2012). Mosaic overgrowth with fibroadipose hyperplasia is caused by somatic activating mutations in PIK3CA. *Nature genetics*, *44*(8), 928–933. https://doi.org/10.1038/ng.2332

Lindhurst, M. J., Sapp, J. C., Teer, J. K., Johnston, J. J., Finn, E. M., Peters, K., Turner, J., Cannons, J. L., Bick, D., Blakemore, L., Blumhorst, C., Brockmann, K., Calder, P., Cherman, N., Deardorff, M. A., Everman, D. B., Golas, G., Greenstein, R. M., Kato, B. M., Keppler-Noreuil, K. M., … Biesecker, L. G. (2011). A mosaic activating mutation in AKT1 associated with the Proteus syndrome. *The New England journal of medicine*, *365*(7), 611–619. https://doi.org/10.1056/NEJMoa1104017

Lindner, A., Marbach, F., Tschernitz, S., Ortner, C., Berneburg, M., Felthaus, O., Prantl, L., Kye, M. J., Rappl, G., Altmüller, J., Thiele, H., Schreml, S., & Schreml, J. (2019). Calcyphosine-like (CAPSL) is regulated in Multiple Symmetric Lipomatosis and is involved in Adipogenesis. *Scientific reports*, *9*(1), 8444. https://doi.org/10.1038/s41598-019-44382-1

Ljungberg, M. C., Bhattacharjee, M. B., Lu, Y., Armstrong, D. L., Yoshor, D., Swann, J. W., Sheldon, M., & D'Arcangelo, G. (2006). Activation of mammalian target of rapamycin in cytomegalic neurons of human cortical dysplasia. *Annals of neurology*, *60*(4), 420–429. https://doi.org/10.1002/ana.20949

López Correa, C., Brems, H., Lázaro, C., Marynen, P., & Legius, E. (2000). Unequal meiotic crossover: a frequent cause of NF1 microdeletions. *American journal of human genetics*, *66*(6), 1969–1974. https://doi.org/10.1086/302920

Luks, V. L., Kamitaki, N., Vivero, M. P., Uller, W., Rab, R., Bovée, J. V., Rialon, K. L., Guevara, C. J., Alomari, A. I., Greene, A. K., Fishman, S. J., Kozakewich, H. P., Maclellan, R. A., Mulliken, J. B., Rahbar, R., Spencer, S. A., Trenor, C. C., 3rd, Upton, J., Zurakowski, D., Perkins, J. A., … Murillo, R. (2015). Lymphatic and other vascular malformative/overgrowth disorders are caused by somatic mutations in PIK3CA. *The Journal of pediatrics*, *166*(4), 1048–54.e545. https://doi.org/10.1016/j.jpeds.2014.12.069

Lyon M. F. (1962). Sex chromatin and gene action in the mammalian X-chromosome. *American journal of human genetics*, *14*(2), 135–148.

Ma, L., Guo, H., Zhao, Y., Liu, Z., Wang, C., Bu, J., Sun, T., & Wei, J. (2024). Liquid biopsy in cancer current: status, challenges and future prospects. *Signal transduction and targeted therapy*, *9*(1), 336. https://doi.org/10.1038/s41392-024-02021-w

Macdonald, R. H., & Sims, R. T. (1969). Linear lesions. *The British journal of dermatology*, *81*, 72–79. https://doi.org/10.1111/j.1365-2133.1969.tb12857.x

Macmurdo, C. F., Wooderchak-Donahue, W., Bayrak-Toydemir, P., Le, J., Wallenstein, M. B., Milla, C., Teng, J. M., Bernstein, J. A., & Stevenson, D. A. (2016). RASA1 somatic mutation and variable expressivity in capillary malformation/arteriovenous malformation (CM/AVM) syndrome. *American journal of medical genetics. Part A*, *170*(6), 1450–1454. https://doi.org/10.1002/ajmg.a.37613

Madsen, R. R., Vanhaesebroeck, B., & Semple, R. K. (2018). Cancer-Associated PIK3CA Mutations in Overgrowth Disorders. *Trends in molecular medicine*, *24*(10), 856–870. https://doi.org/10.1016/j.molmed.2018.08.003

Maertens, O., Brems, H., Vandesompele, J., De Raedt, T., Heyns, I., Rosenbaum, T., De Schepper, S., De Paepe, A., Mortier, G., Janssens, S., Speleman, F., Legius, E., & Messiaen, L. (2006). Comprehensive NF1 screening on cultured Schwann cells from neurofibromas. *Human mutation*, *27*(10), 1030–1040. https://doi.org/10.1002/humu.20389

Maertens, O., De Schepper, S., Vandesompele, J., Brems, H., Heyns, I., Janssens, S., Speleman, F., Legius, E., & Messiaen, L. (2007). Molecular dissection of isolated disease features in mosaic neurofibromatosis type 1. *American journal of human genetics*, *81*(2), 243–251. https://doi.org/10.1086/519562

Mahdaviani, K., Benador, I. Y., Su, S., Gharakhanian, R. A., Stiles, L., Trudeau, K. M., Cardamone, M., Enríquez-Zarralanga, V., Ritou, E., Aprahamian, T., Oliveira, M. F., Corkey, B. E., Perissi, V., Liesa, M., & Shirihai, O. S. (2017). Mfn2 deletion in brown adipose tissue protects from insulin resistance and impairs thermogenesis. *EMBO reports*, *18*(7), 1123–1138. https://doi.org/10.15252/embr.201643827

Mancini, G., Pirruccio, K., Yang, X., Blüher, M., Rodeheffer, M., & Horvath, T. L. (2019). Mitofusin 2 in Mature Adipocytes Controls Adiposity and Body Weight. *Cell reports*, *26*(11), 2849–2858.e4. https://doi.org/10.1016/j.celrep.2019.02.039

Mandl, J., Mészáros, T., Bánhegyi, G., Hunyady, L., & Csala, M. (2009). Endoplasmic reticulum: nutrient sensor in physiology and pathology. *Trends in endocrinology and metabolism: TEM*, *20*(4), 194–201. https://doi.org/10.1016/j.tem.2009.01.003

Mann, J. P., Duan, X., Patel, S., Tábara, L. C., Scurria, F., Alvarez-Guaita, A., Haider, A., Luijten, I., Page, M., Protasoni, M., Lim, K., Virtue, S., O'Rahilly, S., Armstrong, M., Prudent, J., Semple, R. K., & Savage, D. B. (2023). A mouse model of human mitofusin-2-related lipodystrophy exhibits adipose-specific mitochondrial stress and reduced leptin secretion. *eLife*, *12*, e82283. https://doi.org/10.7554/eLife.82283

Martínez-Glez, V., Tenorio, J., Nevado, J., Gordo, G., Rodríguez-Laguna, L., Feito, M., de Lucas, R., Pérez-Jurado, L. A., Ruiz Pérez, V. L., Torrelo, A., Spinner, N. B., Happle, R., Biesecker, L. G., & Lapunzina, P. (2020). A six-attribute classification of genetic mosaicism. *Genetics in medicine : official journal of the American College of Medical Genetics*, *22*(11), 1743–1757. https://doi.org/10.1038/s41436-020-0877-3

Martin-Giacalone, B. A., Weinstein, P. A., Plon, S. E., & Lupo, P. J. (2021). Pediatric Rhabdomyosarcoma: Epidemiology and Genetic Susceptibility. *Journal of clinical medicine*, *10*(9), 2028. https://doi.org/10.3390/jcm10092028

Mautner, V. F., Kluwe, L., Friedrich, R. E., Roehl, A. C., Bammert, S., Högel, J., Spöri, H., Cooper, D. N., & Kehrer-Sawatzki, H. (2010). Clinical characterisation of 29 neurofibromatosis type-1 patients with molecularly ascertained 1.4 Mb type-1 NF1 deletions. *Journal of medical genetics*, *47*(9), 623–630. https://doi.org/10.1136/jmg.2009.075937

McClintock, B. (1951). Chromosome organization and genic expression. *Cold Spring Harbor symposia on quantitative biology*, *16*, 13–47. https://doi.org/10.1101/sqb.1951.016.01.004

McCune, D. (1936). Osteitis fibrosa cystica: The case of a nine-year-old girl who also exhibits precocious puberty, multiple pigmentation of the skin and hyperthyroidism. *American Journal of Diseases of Children, 52*, 743–744.

McGowan-Jordan, J., Hastings, R. J., & Moore, S. (2020). ISCN 2020: an International system for cytogenetic nomenclature (2020). *Cytogenetic and Genome Research 2020, Vol. 160, No. 7-8.*

Messiaen, L., Vogt, J., Bengesser, K., Fu, C., Mikhail, F., Serra, E., Garcia-Linares, C., Cooper, D. N., Lazaro, C., & Kehrer-Sawatzki, H. (2011). Mosaic type-1 NF1 microdeletions as a cause of both generalized and segmental neurofibromatosis type-1 (NF1). *Human mutation*, *32*(2), 213–219. https://doi.org/10.1002/humu.21418

Michelangelo. (1501–1504). *David* [Marble sculpture]. Galleria dell'Accademia, Florence, Italy. Retrieved from http://www.museumsinflorence.com/musei/David_by_michelangelo.html

Miki, Y., Nishisho, I., Horii, A., Miyoshi, Y., Utsunomiya, J., Kinzler, K. W., Vogelstein, B., & Nakamura, Y. (1992). Disruption of the APC gene by a retrotransposal insertion of L1 sequence in a colon cancer. *Cancer research*, *52*(3), 643–645.

Miller, T. W., Rexer, B. N., Garrett, J. T., & Arteaga, C. L. (2011). Mutations in the phosphatidylinositol 3-kinase pathway: role in tumor progression and therapeutic implications in breast cancer. *Breast cancer research : BCR*, *13*(6), 224. https://doi.org/10.1186/bcr3039

Mirzaa, G. M., & Dobyns, W. B. (2013). The "megalencephaly-capillary malformation" (MCAP) syndrome: the nomenclature of a highly recognizable multiple congenital anomaly syndrome. *American journal of medical genetics. Part A*, *161A*(8), 2115–2116. https://doi.org/10.1002/ajmg.a.35940

Mirzaa, G. M., & Poduri, A. (2014). Megalencephaly and hemimegalencephaly: breakthroughs in molecular etiology. *American journal of medical genetics. Part C, Seminars in medical genetics*, *166C*(2), 156–172. https://doi.org/10.1002/ajmg.c.31401

Mirzaa, G. M., Campbell, C. D., Solovieff, N., Goold, C., Jansen, L. A., Menon, S., Timms, A. E., Conti, V., Biag, J. D., Adams, C., Boyle, E. A., Collins, S., Ishak, G., Poliachik, S., Girisha, K. M., Yeung, K. S., Chung, B. H. Y., Rahikkala, E., Gunter, S. A., McDaniel, S. S., … Dobyns, W. B. (2016). Association of MTOR Mutations With Developmental Brain Disorders, Including Megalencephaly, Focal Cortical Dysplasia, and Pigmentary Mosaicism. *JAMA neurology*, *73*(7), 836–845. https://doi.org/10.1001/jamaneurol.2016.0363

Mirzaa, G., Graham, J. M., Jr, & Keppler-Noreuil, K. (2023, April 6). *PIK3CA-Related Overgrowth Spectrum.* GeneReviews® - NCBI Bookshelf. https://ncbi.nlm.nih.gov/books/NBK153722/

Mirzaa, G., Timms, A. E., Conti, V., Boyle, E. A., Girisha, K. M., Martin, B., Kircher, M., Olds, C., Juusola, J., Collins, S., Park, K., Carter, M., Glass, I., Krägeloh-Mann, I., Chitayat, D., Parikh, A. S., Bradshaw, R., Torti, E., Braddock, S., Burke, L., … Dobyns, W. B. (2016). *PIK3CA*-associated developmental disorders exhibit distinct classes of mutations with variable expression and tissue distribution. *JCI insight*, *1*(9), e87623. https://doi.org/10.1172/jci.insight.87623

Moloney, D. M., Slaney, S. F., Oldridge, M., Wall, S. A., Sahlin, P., Stenman, G., & Wilkie, A. O. (1996). Exclusive paternal origin of new mutations in Apert syndrome. *Nature genetics*, *13*(1), 48–53. https://doi.org/10.1038/ng0596-48

Montgomery D. W. (2001). The cause of the streaks in nevus linearis. 1901. *Archives of dermatology*, *137*(10), 1291.

Moog, U., Felbor, U., Has, C., & Zirn, B. (2020). Disorders Caused by Genetic Mosaicism. *Deutsches Arzteblatt international*, *116*(8), 119–125. https://doi.org/10.3238/arztebl.2020.0119

Moosa, S., & Wollnik, B. (2016). Altered FGF signalling in congenital craniofacial and skeletal disorders. *Seminars in cell & developmental biology*, *53*, 115–125. https://doi.org/10.1016/j.semcdb.2015.12.005

Morgan, T. H. (1914). Mosaics and gynandromorphs in *Drosophila*. *Proceedings of the Society for Experimental Biology and Medicine*, 11(6), 169–170. https://doi.org/10.3181/00379727-11-105

Moss, C., & Savin, J. (1995). *Dermatology and the new Genetics*. Wiley-Blackwell.

Mukohara T. (2015). PI3K mutations in breast cancer: prognostic and therapeutic implications. *Breast cancer (Dove Medical Press)*, *7*, 111–123. https://doi.org/10.2147/BCTT.S60696

Munro, C. S., & Wilkie, A. O. (1998). Epidermal mosaicism producing localised acne: somatic mutation in FGFR2. *Lancet (London, England)*, *352*(9129), 704–705. https://doi.org/10.1016/S0140-6736(05)60820-3

Murgiano, L., Waluk, D. P., Towers, R., Wiedemar, N., Dietrich, J., Jagannathan, V., Drögemüller, M., Balmer, P., Druet, T., Galichet, A., Penedo, M. C., Müller, E. J., Roosje, P., Welle, M. M., & Leeb, T. (2016). An Intronic MBTPS2 Variant Results in a Splicing Defect in Horses with Brindle Coat Texture. *G3 (Bethesda, Md.)*, *6*(9), 2963–2970. https://doi.org/10.1534/g3.116.032433

Nakashima, M., Saitsu, H., Takei, N., Tohyama, J., Kato, M., Kitaura, H., Shiina, M., Shirozu, H., Masuda, H., Watanabe, K., Ohba, C., Tsurusaki, Y., Miyake, N., Zheng, Y., Sato, T., Takebayashi, H., Ogata, K., Kameyama, S., Kakita, A., & Matsumoto, N. (2015). Somatic Mutations in the MTOR gene cause focal cortical dysplasia type IIb. *Annals of neurology*, *78*(3), 375–386. https://doi.org/10.1002/ana.24444

Neilson, K. M., & Friesel, R. E. (1995). Constitutive activation of fibroblast growth factor receptor-2 by a point mutation associated with Crouzon syndrome. *The Journal of biological chemistry*, *270*(44), 26037–26040. https://doi.org/10.1074/jbc.270.44.26037

Nicholson, G. A., Magdelaine, C., Zhu, D., Grew, S., Ryan, M. M., Sturtz, F., Vallat, J. M., & Ouvrier, R. A. (2008). Severe early-onset axonal neuropathy with homozygous and compound heterozygous MFN2 mutations. *Neurology*, *70*(19), 1678–1681. https://doi.org/10.1212/01.wnl.0000311275.89032.22

Oldridge, M., Zackai, E. H., McDonald-McGinn, D. M., Iseki, S., Morriss-Kay, G. M., Twigg, S. R., Johnson, D., Wall, S. A., Jiang, W., Theda, C., Jabs, E. W., & Wilkie, A. O. (1999). De novo alu-element insertions in FGFR2 identify a distinct pathological

basis for Apert syndrome. *American journal of human genetics*, *64*(2), 446–461. https://doi.org/10.1086/302245

Online Mendelian Inheritance in Man, OMIM®. McKusick-Nathans Institute of Genetic Medicine, Johns Hopkins University (Baltimore, MD), {12.11.2024}. World Wide Web URL: https://omim.org/

Orloff, M. S., He, X., Peterson, C., Chen, F., Chen, J. L., Mester, J. L., & Eng, C. (2013). Germline PIK3CA and AKT1 mutations in Cowden and Cowden-like syndromes. *American journal of human genetics*, *92*(1), 76–80. https://doi.org/10.1016/j.ajhg.2012.10.021

Ornitz, D. M., Xu, J., Colvin, J. S., McEwen, D. G., MacArthur, C. A., Coulier, F., Gao, G., & Goldfarb, M. (1996). Receptor specificity of the fibroblast growth factor family. *The Journal of biological chemistry*, *271*(25), 15292–15297. https://doi.org/10.1074/jbc.271.25.15292

Ortonne, N., Wolkenstein, P., Blakeley, J. O., Korf, B., Plotkin, S. R., Riccardi, V. M., Miller, D. C., Huson, S., Peltonen, J., Rosenberg, A., Carroll, S. L., Verma, S. K., Mautner, V., Upadhyaya, M., & Stemmer-Rachamimov, A. (2018). Cutaneous neurofibromas: Current clinical and pathologic issues. *Neurology*, *91*(2 Suppl 1), S5–S13. https://doi.org/10.1212/WNL.0000000000005792

Oxford University Press. (n.d.). *mosaic*. In *Oxford Learner's Dictionaries*. Retrieved June 24, 2025, from https://www.oxfordlearnersdictionaries.com/definition/english/mosaic

Ozarslan, B., Russo, T., Argenziano, G., Santoro, C., & Piccolo, V. (2021). Cutaneous Findings in Neurofibromatosis Type 1. *Cancers*, *13*(3), 463. https://doi.org/10.3390/cancers13030463

Pacot, L., Vidaud, D., Sabbagh, A., Laurendeau, I., Briand-Suleau, A., Coustier, A., Maillard, T., Barbance, C., Morice-Picard, F., Sigaudy, S., Glazunova, O. O., Damaj, L., Layet, V., Quelin, C., Gilbert-Dussardier, B., Audic, F., Dollfus, H., Guerrot, A. M., Lespinasse, J., Julia, S., … Pasmant, E. (2021). Severe Phenotype in Patients with Large Deletions of *NF1*. *Cancers*, *13*(12), 2963. https://doi.org/10.3390/cancers13122963

Pagon, R. A., Hall, J. G., Davenport, S. L., Aase, J., Norwood, T. H., & Hoehn, H. W. (1979). Abnormal skin fibroblast cytogenetics in four dysmorphic patients with normal lymphocyte chromosomes. *American journal of human genetics*, *31*(1), 54–61.

Paller, A. S., Syder, A. J., Chan, Y. M., Yu, Q. C., Hutton, E., Tadini, G., & Fuchs, E. (1994). Genetic and clinical mosaicism in a type of epidermal nevus. *The New England journal of medicine*, *331*(21), 1408–1415. https://doi.org/10.1056/NEJM199411243312103

Pansuriya, T. C., van Eijk, R., d'Adamo, P., van Ruler, M. A., Kuijjer, M. L., Oosting, J., Cleton-Jansen, A. M., van Oosterwijk, J. G., Verbeke, S. L., Meijer, D., van Wezel,

T., Nord, K. H., Sangiorgi, L., Toker, B., Liegl-Atzwanger, B., San-Julian, M., Sciot, R., Limaye, N., Kindblom, L. G., Daugaard, S., … Bovée, J. V. (2011). Somatic mosaic IDH1 and IDH2 mutations are associated with enchondroma and spindle cell hemangioma in Ollier disease and Maffucci syndrome. *Nature genetics*, *43*(12), 1256–1261. https://doi.org/10.1038/ng.1004

Paplomata, E., & O'Regan, R. (2014). The PI3K/AKT/mTOR pathway in breast cancer: targets, trials and biomarkers. *Therapeutic advances in medical oncology*, *6*(4), 154–166. https://doi.org/10.1177/1758834014530023

Parker, V. E. R., Keppler-Noreuil, K. M., Faivre, L., Luu, M., Oden, N. L., De Silva, L., Sapp, J. C., Andrews, K., Bardou, M., Chen, K. Y., Darling, T. N., Gautier, E., Goldspiel, B. R., Hadj-Rabia, S., Harris, J., Kounidas, G., Kumar, P., Lindhurst, M. J., Loffroy, R., Martin, L., … Biesecker, L. G. (2019). Safety and efficacy of low-dose sirolimus in the PIK3CA-related overgrowth spectrum. *Genetics in medicine : official journal of the American College of Medical Genetics*, *21*(5), 1189–1198. https://doi.org/10.1038/s41436-018-0297-9

Pasmant, E., Sabbagh, A., Spurlock, G., Laurendeau, I., Grillo, E., Hamel, M. J., Martin, L., Barbarot, S., Leheup, B., Rodriguez, D., Lacombe, D., Dollfus, H., Pasquier, L., Isidor, B., Ferkal, S., Soulier, J., Sanson, M., Dieux-Coeslier, A., Bièche, I., Parfait, B., … members of the NF France Network (2010). NF1 microdeletions in neurofibromatosis type 1: from genotype to phenotype. *Human mutation*, *31*(6), E1506–E1518. https://doi.org/10.1002/humu.21271

Pavone, P., Pappalardo, X. G., Mustafa, N., Falsaperla, R., Marino, S. D., Corsello, G., Bianca, S., Parano, E., & Ruggieri, M. (2022). Pathogenic correlation between mosaic variegated aneuploidy 1 (MVA1) and a novel BUB1B variant: a reappraisal of a severe syndrome. *Neurological sciences : official journal of the Italian Neurological Society and of the Italian Society of Clinical Neurophysiology*, *43*(11), 6529–6538. https://doi.org/10.1007/s10072-022-06247-w

Pelorosso, C., Watrin, F., Conti, V., Buhler, E., Gelot, A., Yang, X., Mei, D., McEvoy-Venneri, J., Manent, J. B., Cetica, V., Ball, L. L., Buccoliero, A. M., Vinck, A., Barba, C., Gleeson, J. G., Guerrini, R., & Represa, A. (2019). Somatic double-hit in MTOR and RPS6 in hemimegalencephaly with intractable epilepsy. *Human molecular genetics*, *28*(22), 3755–3765. https://doi.org/10.1093/hmg/ddz194

Perera, U., Kennedy, B. A., & Hegele, R. A. (2018). Multiple Symmetric Lipomatosis (Madelung Disease) in a Large Canadian Family With the Mitochondrial *MTTK* c.8344A>G Variant. *Journal of investigative medicine high impact case reports*, *6*, 2324709618802867. https://doi.org/10.1177/2324709618802867

Pham, A. H., Meng, S., Chu, Q. N., & Chan, D. C. (2012). Loss of Mfn2 results in progressive, retrograde degeneration of dopaminergic neurons in the nigrostriatal

circuit. *Human molecular genetics*, *21*(22), 4817–4826. https://doi.org/10.1093/hmg/dds311

Pinto, C. I., Carvalho, P. J., & Correia, M. M. (2017). Madelung's Disease: Revision of 59 Surgical Cases. *Aesthetic plastic surgery*, *41*(2), 359–368. https://doi.org/10.1007/s00266-016-0759-x

Poduri, A., Evrony, G. D., Cai, X., Elhosary, P. C., Beroukhim, R., Lehtinen, M. K., Hills, L. B., Heinzen, E. L., Hill, A., Hill, R. S., Barry, B. J., Bourgeois, B. F., Riviello, J. J., Barkovich, A. J., Black, P. M., Ligon, K. L., & Walsh, C. A. (2012). Somatic activation of AKT3 causes hemispheric developmental brain malformations. *Neuron*, *74*(1), 41–48. https://doi.org/10.1016/j.neuron.2012.03.010

Qiagen. (2010, July). Isolation of genomic DNA from saliva and mouthwash using the QIAamp® DNA Blood Mini Kit; spin procedure - (EN). Retrieved from https://www.qiagen.com/us/resources/resourcedetail?id=bf32146a-77fd-40c2-8743-c28974f7935b&lang=en

Qiagen. (2017, February). QIAamp® DSP DNA FFPE Tissue Kit Handbook. Retrieved from https://www.qiagen.com/us/resources/resourcedetail?id=686d8542-3f16-48ad-b5d2-92275acaeedc&lang=en

Qiagen. (2019, October). QIAamp Circulating Nucleic Acid Handbook. Retrieved from https://www.qiagen.com/us/resources/resourcedetail?id=0c4b31ab-f4fb-425f-99bf-10ab9538c061&lang=en

Qiagen. (2020, August). AllPrep® DNA/RNA FFPE Handbook. Retrieved from https://www.qiagen.com/us/resources/resourcedetail?id=3ff86eb0-d95b-4941-95c3-252ad30fe3e6&lang=en

Qiagen. (2020, January). *therascreen* PIK3CA RGQ PCR Kit Handbook. Retrieved from https://www.qiagen.com/us/resources/resourcedetail?id=2d7ab465-a0e2-4311-8f90-1bea278aa47e&lang=en

Qiagen. (2023, June). QIAamp DNA Mini and Blood Mini Handbook. Retrieved from https://www.qiagen.com/us/resources/resourcedetail?id=62a200d6-faf4-469b-b50f-2b59cf738962&lang=en

Raedt, T. D., Stephens, M., Heyns, I., Brems, H., Thijs, D., Messiaen, L., Stephens, K., Lazaro, C., Wimmer, K., Kehrer-Sawatzki, H., Vidaud, D., Kluwe, L., Marynen, P., & Legius, E. (2006). Conservation of hotspots for recombination in low-copy repeats associated with the NF1 microdeletion. *Nature genetics*, *38*(12), 1419–1423. https://doi.org/10.1038/ng1920

Rancan, F., Rajes, K., Sidiropoulou, P., Hadam, S., Guo, X., Zabihi, F., Mirastschijski, U., Rühl, E., Haag, R., Blume-Peytavi, U., & Vogt, A. (2023). Efficacy of topically applied rapamycin-loaded redox-sensitive nanocarriers in a human skin/T cell co-

culture model. *International immunopharmacology*, *117*, 109903. https://doi.org/10.1016/j.intimp.2023.109903

Raymond, Y., Fernando, S., Menezes, M., Mol, B. W., McLennan, A., da Silva Costa, F., Hardy, T., & Rolnik, D. L. (2024). Placental, maternal, fetal, and technical origins of false-positive cell-free DNA screening results. *American journal of obstetrics and gynecology*, *230*(4), 381–389. https://doi.org/10.1016/j.ajog.2023.11.1240

Reilly, K., Doyle, S., Hamilton, S. J., Kilby, M. D., & Mone, F. (2023). Pitfalls of prenatal diagnosis associated with mosaicism. *The Obstetrician & Gynaecologist, 25*(1), 28–37. https://doi.org/10.1111/tog.12850

Reintjes, N., Li, Y., Becker, A., Rohmann, E., Schmutzler, R., & Wollnik, B. (2013). Activating somatic FGFR2 mutations in breast cancer. *PloS one*, *8*(3), e60264. https://doi.org/10.1371/journal.pone.0060264

Resta, N., Calabrese, O., Grossi, V., Lugli, L., Simone, C., Ranieri, C., Piglionica, M., Lepore Signorile, M., Rossi, K., Carli, D., & Mussa, A. (2021). Correspondence on "Clinical spectrum of MTOR-related hypomelanosis of Ito with neurodevelopmental abnormalities," by Carmignac et al. *Genetics in medicine : official journal of the American College of Medical Genetics*, *23*(11), 2223–2224. https://doi.org/10.1038/s41436-021-01256-0

Revencu, N., Boon, L. M., Mendola, A., Cordisco, M. R., Dubois, J., Clapuyt, P., Hammer, F., Amor, D. J., Irvine, A. D., Baselga, E., Dompmartin, A., Syed, S., Martin-Santiago, A., Ades, L., Collins, F., Smith, J., Sandaradura, S., Barrio, V. R., Burrows, P. E., Blei, F., … Vikkula, M. (2013). RASA1 mutations and associated phenotypes in 68 families with capillary malformation-arteriovenous malformation. *Human mutation*, *34*(12), 1632–1641. https://doi.org/10.1002/humu.22431

Revencu, N., Fastre, E., Ravoet, M., Helaers, R., Brouillard, P., Bisdorff-Bresson, A., Chung, C. W. T., Gerard, M., Dvorakova, V., Irvine, A. D., Boon, L. M., & Vikkula, M. (2020). RASA1 mosaic mutations in patients with capillary malformation-arteriovenous malformation. *Journal of medical genetics*, *57*(1), 48–52. https://doi.org/10.1136/jmedgenet-2019-106024

Richards, S., Aziz, N., Bale, S., Bick, D., Das, S., Gastier-Foster, J., Grody, W. W., Hegde, M., Lyon, E., Spector, E., Voelkerding, K., Rehm, H. L., & ACMG Laboratory Quality Assurance Committee (2015). Standards and guidelines for the interpretation of sequence variants: a joint consensus recommendation of the American College of Medical Genetics and Genomics and the Association for Molecular Pathology. *Genetics in medicine : official journal of the American College of Medical Genetics*, *17*(5), 405–424. https://doi.org/10.1038/gim.2015.30

Rivière, J. B., Mirzaa, G. M., O'Roak, B. J., Beddaoui, M., Alcantara, D., Conway, R. L., St-Onge, J., Schwartzentruber, J. A., Gripp, K. W., Nikkel, S. M., Worthylake, T., Sullivan, C. T., Ward, T. R., Butler, H. E., Kramer, N. A., Albrecht, B., Armour, C. M.,

Armstrong, L., Caluseriu, O., Cytrynbaum, C., … Dobyns, W. B. (2012). De novo germline and postzygotic mutations in AKT3, PIK3R2 and PIK3CA cause a spectrum of related megalencephaly syndromes. *Nature genetics*, *44*(8), 934–940. https://doi.org/10.1038/ng.2331

Robertson, S. C., Meyer, A. N., Hart, K. C., Galvin, B. D., Webster, M. K., & Donoghue, D. J. (1998). Activating mutations in the extracellular domain of the fibroblast growth factor receptor 2 function by disruption of the disulfide bond in the third immunoglobulin-like domain. *Proceedings of the National Academy of Sciences of the United States of America*, *95*(8), 4567–4572. https://doi.org/10.1073/pnas.95.8.4567

Rocha, N., Bulger, D. A., Frontini, A., Titheradge, H., Gribsholt, S. B., Knox, R., Page, M., Harris, J., Payne, F., Adams, C., Sleigh, A., Crawford, J., Gjesing, A. P., Bork-Jensen, J., Pedersen, O., Barroso, I., Hansen, T., Cox, H., Reilly, M., Rossor, A., … Semple, R. K. (2017). Human biallelic MFN2 mutations induce mitochondrial dysfunction, upper body adipose hyperplasia, and suppression of leptin expression. *eLife*, *6*, e23813. https://doi.org/10.7554/eLife.23813

Rodriguez-Laguna, L., Ibañez, K., Gordo, G., Garcia-Minaur, S., Santos-Simarro, F., Agra, N., Vallespín, E., Fernández-Montaño, V. E., Martín-Arenas, R., Del Pozo, Á., González-Pecellín, H., Mena, R., Rueda-Arenas, I., Gomez, M. V., Villaverde, C., Bustamante, A., Ayuso, C., Ruiz-Perez, V. L., Nevado, J., Lapunzina, P., … Martinez-Glez, V. (2018). CLAPO syndrome: identification of somatic activating PIK3CA mutations and delineation of the natural history and phenotype. *Genetics in medicine : official journal of the American College of Medical Genetics*, *20*(8), 882–889. https://doi.org/10.1038/gim.2017.200

Roehl, A. C., Mussotter, T., Cooper, D. N., Kluwe, L., Wimmer, K., Högel, J., Zetzmann, M., Vogt, J., Mautner, V. F., & Kehrer-Sawatzki, H. (2012). Tissue-specific differences in the proportion of mosaic large NF1 deletions are suggestive of a selective growth advantage of hematopoietic del(+/-) stem cells. *Human mutation*, *33*(3), 541–550. https://doi.org/10.1002/humu.22013

Rosato, B., Ranieri, D., Nanni, M., Torrisi, M. R., & Belleudi, F. (2018). Role of FGFR2b expression and signaling in keratinocyte differentiation: sequential involvement of PKCδ and PKCα. *Cell death & disease*, *9*(5), 565. https://doi.org/10.1038/s41419-018-0509-x

Roscioli, T., Flanagan, S., Mortimore, R. J., Kumar, P., Weedon, D., Masel, J., Lewandowski, R., Hyland, V., & Glass, I. A. (2001). Premature calvarial synostosis and epidermal hyperplasia (Beare-Stevenson syndrome-like anomalies) resulting from a P250R missense mutation in the gene encoding fibroblast growth factor receptor 3. *American journal of medical genetics*, *101*(3), 187–194. https://doi.org/10.1002/ajmg.1369

Ruggieri, M., & Huson, S. M. (2001). The clinical and diagnostic implications of mosaicism in the neurofibromatoses. *Neurology*, *56*(11), 1433–1443. https://doi.org/10.1212/wnl.56.11.1433

Sage-Schwaede, A., Engelstad, K., Salazar, R., Curcio, A., Khandji, A., Garvin, J. H., Jr, & De Vivo, D. C. (2019). Exploring mTOR inhibition as treatment for mitochondrial disease. *Annals of clinical and translational neurology*, *6*(9), 1877–1881. https://doi.org/10.1002/acn3.50846

Sapp, J. C., Turner, J. T., van de Kamp, J. M., van Dijk, F. S., Lowry, R. B., & Biesecker, L. G. (2007). Newly delineated syndrome of congenital lipomatous overgrowth, vascular malformations, and epidermal nevi (CLOVE syndrome) in seven patients. *American journal of medical genetics. Part A*, *143A*(24), 2944–2958. https://doi.org/10.1002/ajmg.a.32023

Sawyer, S. L., Cheuk-Him Ng, A., Innes, A. M., Wagner, J. D., Dyment, D. A., Tetreault, M., Care4Rare Canada Consortium, Majewski, J., Boycott, K. M., Screaton, R. A., & Nicholson, G. (2015). Homozygous mutations in MFN2 cause multiple symmetric lipomatosis associated with neuropathy. *Human molecular genetics*, *24*(18), 5109–5114. https://doi.org/10.1093/hmg/ddv229

Schiltz, D., Anker, A., Ortner, C., Tschernitz, S., Koller, M., Klein, S., Felthaus, O., Schreml, J., Schreml, S., & Prantl, L. (2018). Multiple Symmetric Lipomatosis: New Classification System Based on the Largest German Patient Cohort. *Plastic and reconstructive surgery. Global open*, *6*(4), e1722. https://doi.org/10.1097/GOX.0000000000001722

Schindler, O. (c. 1888–1910). *David und Goliath* [Painting]. Wikimedia Commons. https://commons.wikimedia.org/wiki/File:Osmar_Schindler_David_und_Goliath.jpg

Schinzel A. (1981). Incomplete trisomy 22. III. Mosaic-trisomy 22 and the problem of full trisomy 22. *Human genetics*, *56*(3), 269–273. https://doi.org/10.1007/BF00274677

Schmidt, J., Kaulfuß, S., Ott, H., Gaubert, M., Reintjes, N., Bremmer, F., Dreha-Kulaczewski, S., Stroebel, P., Yigit, G., & Wollnik, B. (2024). Expansion of the complex genotypic and phenotypic spectrum of FGFR2-associated neurocutaneous syndromes. *Human genetics*, *143*(2), 159–168. https://doi.org/10.1007/s00439-023-02634-1

Schneeberger, M., Dietrich, M. O., Sebastián, D., Imbernón, M., Castaño, C., Garcia, A., Esteban, Y., Gonzalez-Franquesa, A., Rodríguez, I. C., Bortolozzi, A., Garcia-Roves, P. M., Gomis, R., Nogueiras, R., Horvath, T. L., Zorzano, A., & Claret, M. (2013). Mitofusin 2 in POMC neurons connects ER stress with leptin resistance and energy imbalance. *Cell*, *155*(1), 172–187. https://doi.org/10.1016/j.cell.2013.09.003

Schwarzenbach, H., Hoon, D. S., & Pantel, K. (2011). Cell-free nucleic acids as biomarkers in cancer patients. *Nature reviews. Cancer*, *11*(6), 426–437. https://doi.org/10.1038/nrc3066

Sebastián, D., Sorianello, E., Segalés, J., Irazoki, A., Ruiz-Bonilla, V., Sala, D., Planet, E., Berenguer-Llergo, A., Muñoz, J. P., Sánchez-Feutrie, M., Plana, N., Hernández-Álvarez, M. I., Serrano, A. L., Palacín, M., & Zorzano, A. (2016). Mfn2 deficiency links age-related sarcopenia and impaired autophagy to activation of an adaptive mitophagy pathway. *The EMBO journal*, *35*(15), 1677–1693. https://doi.org/10.15252/embj.201593084

Serebrovsky, A. S. (1925). "Somatic segregation" in domestic fowl. *Journal of Genetics, 16*(1), 33–42. https://doi.org/10.1007/bf02983986

Shadrina, M., Kalay, Ö., Demirkaya-Budak, S., LeDuc, C. A., Chung, W. K., Turgut, D., Budak, G., Arslan, E., Semenyuk, V., Davis-Dusenbery, B., Seidman, C. E., Yost, H. J., Jain, A., & Gelb, B. D. (2025). Efficient identification of de novo mutations in family trios: a consensus-based informatic approach. *Life science alliance*, *8*(6), e202403039. https://doi.org/10.26508/lsa.202403039

Shirley, M. D., Tang, H., Gallione, C. J., Baugher, J. D., Frelin, L. P., Cohen, B., North, P. E., Marchuk, D. A., Comi, A. M., & Pevsner, J. (2013). Sturge-Weber syndrome and port-wine stains caused by somatic mutation in GNAQ. *The New England journal of medicine*, *368*(21), 1971–1979. https://doi.org/10.1056/NEJMoa1213507

Siemens, H. W. (1948). *Algemene dermatologie: Diagnostiek en therapie.* Amsterdam: Scheltema & Holtema's Boekhandel en Uitgeversmaatschappij.

Siemens, H. W. (1952). *Allgemeine Diagnostik und Therapie der Hautkrankheiten: als Einführung in die Dermatologie für Studierende und Praktiker*. Berlin: Springer.

Smyth, E. C., Babina, I. S., & Turner, N. C. (2017). Gatekeeper Mutations and Intratumoral Heterogeneity in *FGFR2*-Translocated Cholangiocarcinoma. *Cancer discovery*, *7*(3), 248–249. https://doi.org/10.1158/2159-8290.CD-17-0057

Stern, C. (1936). Somatic crossing-over and segregation in *Drosophila melanogaster*. *Genetics*, 21(6), 625–730. https://doi.org/10.1093/genetics/21.6.625

Stosser, M. B., Lindy, A. S., Butler, E., Retterer, K., Piccirillo-Stosser, C. M., Richard, G., & McKnight, D. A. (2018). High frequency of mosaic pathogenic variants in genes causing epilepsy-related neurodevelopmental disorders. *Genetics in medicine : official journal of the American College of Medical Genetics*, *20*(4), 403–410. https://doi.org/10.1038/gim.2017.114

Sturtevant, A. H. (1929). The claret mutant type of *Drosophila simulans*: A study of chromosome elimination and of cell-lineage. *Zeitschrift für Wissenschaftliche Zoologie*, 135, 323–356.

Sylvester, D. E., Chen, Y., Grima, N., Saletta, F., Padhye, B., Bennetts, B., Wright, D., Krivanek, M., Graf, N., Zhou, L., Catchpoole, D., Kirk, J., Latchoumanin, O., Qiao, L., Ballinger, M., Thomas, D., Jamieson, R., Dalla-Pozza, L., & Byrne, J. A. (2022). Rare germline variants in childhood cancer patients suspected of genetic predisposition to

cancer. *Genes, chromosomes & cancer*, *61*(2), 81–93. https://doi.org/10.1002/gcc.23006

Tanaka, R., Umegaki-Arao, N., Sasaki, T., Aoki, S., Yoshida, K., Niizeki, H., & Kubo, A. (2018). Linear keratinocytic epidermal nevi on trunk skin caused by a somatic FGFR2 p.C382R mutation. *The Journal of dermatology*, *45*(11), e302–e303. https://doi.org/10.1111/1346-8138.14344

Tavormina, P. L., Bellus, G. A., Webster, M. K., Bamshad, M. J., Fraley, A. E., McIntosh, I., Szabo, J., Jiang, W., Jabs, E. W., Wilcox, W. R., Wasmuth, J. J., Donoghue, D. J., Thompson, L. M., & Francomano, C. A. (1999). A novel skeletal dysplasia with developmental delay and acanthosis nigricans is caused by a Lys650Met mutation in the fibroblast growth factor receptor 3 gene. *American journal of human genetics*, *64*(3), 722–731. https://doi.org/10.1086/302275

Taylor, D. L., Wildin, R. S., & Morley, K. W. (2021). Novel neonatal presentation of megalencephaly-polymicrogyria-pigmentary mosaicism syndrome (MPPM) related to MTOR mutation: Report of a case. *Pediatric dermatology, 38*(2), 536–537. https://doi.org/10.1111/pde.14480

The "Elephant-Man." (1886). *The British Medical Journal*, *2*(1354), 1188–1189. http://www.jstor.org/stable/25270008

Theiler, M., Weibel, L., Christen-Zaech, S., Carmignac, V., Sorlin, A., Neuhaus, K., Chevarin, M., Thauvin-Robinet, C., Philippe, C., Faivre, L., Vabres, P., & Kuentz, P. (2021). Cerebriform sebaceous nevus: a subtype of organoid nevus due to specific postzygotic FGFR2 mutations. *Journal of the European Academy of Dermatology and Venereology : JEADV*, *35*(10), 2085–2090. https://doi.org/10.1111/jdv.17319

Tibbles, J. A., & Cohen, M. M., Jr (1986). The Proteus syndrome: the Elephant Man diagnosed. *British medical journal (Clinical research ed.)*, *293*(6548), 683–685. https://doi.org/10.1136/bmj.293.6548.683

Tjio, J. H., & Levan, A. (1956). The chromosome number of man. *Hereditas, 42*, 1-6. https://doi.org/10.1111/j.1601-5223.1956.tb03010.x

Toll, A., Fernández, L. C., Pons, T., Groesser, L., Sagrera, A., Carrillo-de Santa Pau, E., Vicente, A., Baselga, E., Vázquez, M., Beltrán, S., Pisano, D. G., Rueda, D., Gut, M., Pujol, R. M., Hafner, C., Gut, I., Valencia, A., & Real, F. X. (2016). Somatic Embryonic FGFR2 Mutations in Keratinocytic Epidermal Nevi. *The Journal of investigative dermatology*, *136*(8), 1718–1721. https://doi.org/10.1016/j.jid.2016.03.040

Töndury, G. (1964). Embryologie und Hauttopographie. *Archiv für klinische und experimentelle Dermatologie*, *219*, 12–24. https://doi.org/10.1007/BF00522849

Towers, R. E., Murgiano, L., Millar, D. S., Glen, E., Topf, A., Jagannathan, V., Drögemüller, C., Goodship, J. A., Clarke, A. J., & Leeb, T. (2013). A nonsense mutation

in the IKBKG gene in mares with incontinentia pigmenti. *PloS one*, *8*(12), e81625. https://doi.org/10.1371/journal.pone.0081625

Trevisan, V., Meroni, A., Leoni, C., Sirchia, F., Politano, D., Fiandrino, G., Giorgio, V., Rigante, D., Limongelli, D., Perri, L., Sforza, E., Leonardi, F., Viscogliosi, G., Contaldo, I., Orteschi, D., Proietti, L., Zampino, G., & Onesimo, R. (2024). Trisomy 22 Mosaicism from Prenatal to Postnatal Findings: A Case Series and Systematic Review of the Literature. *Genes*, *15*(3), 346. https://doi.org/10.3390/genes15030346

Trujillano, D., Bertoli-Avella, A. M., Kumar Kandaswamy, K., Weiss, M. E., Köster, J., Marais, A., Paknia, O., Schröder, R., Garcia-Aznar, J. M., Werber, M., Brandau, O., Calvo Del Castillo, M., Baldi, C., Wessel, K., Kishore, S., Nahavandi, N., Eyaid, W., Al Rifai, M. T., Al-Rumayyan, A., Al-Twaijri, W., … Abou Jamra, R. (2017). Clinical exome sequencing: results from 2819 samples reflecting 1000 families. *European journal of human genetics : EJHG*, *25*(2), 176–182. https://doi.org/10.1038/ejhg.2016.146

U.S. Food and Drug Administration. (2019, May 24). *FDA approves alpelisib for metastatic breast cancer* [Press release]. Retrieved July 5, 2025, from https://www.fda.gov/drugs/resources-information-approved-drugs/fda-approves-alpelisib-metastatic-breast-cancer

U.S. Food and Drug Administration. (2022, April 5). *FDA approves alpelisib for PIK3CA-related overgrowth spectrum* [Press release]. Retrieved May 5, 2025, from https://www.fda.gov/drugs/resources-information-approved-drugs/fda-approves-alpelisib-pik3ca-related-overgrowth-spectrum

van Dessel, L. F., Vitale, S. R., Helmijr, J. C. A., Wilting, S. M., van der Vlugt-Daane, M., Oomen-de Hoop, E., Sleijfer, S., Martens, J. W. M., Jansen, M. P. H. M., & Lolkema, M. P. (2019). High-throughput isolation of circulating tumor DNA: a comparison of automated platforms. *Molecular oncology*, *13*(2), 392–402. https://doi.org/10.1002/1878-0261.12415

Venot, Q., Blanc, T., Rabia, S. H., Berteloot, L., Ladraa, S., Duong, J. P., Blanc, E., Johnson, S. C., Hoguin, C., Boccara, O., Sarnacki, S., Boddaert, N., Pannier, S., Martinez, F., Magassa, S., Yamaguchi, J., Knebelmann, B., Merville, P., Grenier, N., Joly, D., … Canaud, G. (2018). Targeted therapy in patients with PIK3CA-related overgrowth syndrome. *Nature*, *558*(7711), 540–546. https://doi.org/10.1038/s41586-018-0217-9

Vogt, J., Mussotter, T., Bengesser, K., Claes, K., Högel, J., Chuzhanova, N., Fu, C., van den Ende, J., Mautner, V. F., Cooper, D. N., Messiaen, L., & Kehrer-Sawatzki, H. (2012). Identification of recurrent type-2 NF1 microdeletions reveals a mitotic nonallelic homologous recombination hotspot underlying a human genomic disorder. *Human mutation*, *33*(11), 1599–1609. https://doi.org/10.1002/humu.22171

Waldvogel, S. M., Posey, J. E., & Goodell, M. A. (2024). Human embryonic genetic mosaicism and its effects on development and disease. *Nature reviews. Genetics*, *25*(10), 698–714. https://doi.org/10.1038/s41576-024-00715-z

Wang, J. C., Dang, L., Mondal, T. K., & Khan, A. (2007). Prenatally diagnosed mosaic trisomy 22 in a fetus with left ventricular non-compaction cardiomyopathy. *American journal of medical genetics. Part A*, *143A*(22), 2744–2746. https://doi.org/10.1002/ajmg.a.32004

Wang, Y., Zhou, X., Oberoi, K., Phelps, R., Couwenhoven, R., Sun, M., Rezza, A., Holmes, G., Percival, C. J., Friedenthal, J., Krejci, P., Richtsmeier, J. T., Huso, D. L., Rendl, M., & Jabs, E. W. (2012). p38 Inhibition ameliorates skin and skull abnormalities in Fgfr2 Beare-Stevenson mice. *The Journal of clinical investigation*, *122*(6), 2153–2164. https://doi.org/10.1172/JCI62644

Warton, K., Graham, L. J., Yuwono, N., & Samimi, G. (2018). Comparison of 4 commercial kits for the extraction of circulating DNA from plasma. *Cancer genetics*, *228-229*, 143–150. https://doi.org/10.1016/j.cancergen.2018.02.004

Wataya-Kaneda, M., Tanaka, M., Yang, L., Yang, F., Tsuruta, D., Nakamura, A., Matsumoto, S., Hamasaki, T., Tanemura, A., & Katayama, I. (2015). Clinical and Histologic Analysis of the Efficacy of Topical Rapamycin Therapy Against Hypomelanotic Macules in Tuberous Sclerosis Complex. *JAMA dermatology*, *151*(7), 722–730. https://doi.org/10.1001/jamadermatol.2014.4298

Webster, M. K., & Donoghue, D. J. (1996). Constitutive activation of fibroblast growth factor receptor 3 by the transmembrane domain point mutation found in achondroplasia. *The EMBO journal*, *15*(3), 520–527.

Weinstein, L. S., Shenker, A., Gejman, P. V., Merino, M. J., Friedman, E., & Spiegel, A. M. (1991). Activating mutations of the stimulatory G protein in the McCune-Albright syndrome. *The New England journal of medicine*, *325*(24), 1688–1695. https://doi.org/10.1056/NEJM199112123252403

Wenger, T., Miller, D., & Evans, K. (2020, April 30). *FGFR Craniosynostosis Syndromes overview.* GeneReviews® - NCBI Bookshelf. https://www.ncbi.nlm.nih.gov/books/NBK1455/

White Horse Productions. (n.d.). *Equine coat color genetics basics: Blended & intermediate patterns*. Retrieved July 16, 2025, from http://www.whitehorseproductions.com/ecg_basics4.html

Wright, S., & Eaton, O. N. (1926). Mutational mosaic coat patterns of the guinea pig. *Genetics*, *11*(4), 333–351. https://doi.org/10.1093/genetics/11.4.333

Xie, Y., Su, N., Yang, J., Tan, Q., Huang, S., Jin, M., Ni, Z., Zhang, B., Zhang, D., Luo, F., Chen, H., Sun, X., Feng, J. Q., Qi, H., & Chen, L. (2020). FGF/FGFR signaling in

health and disease. *Signal transduction and targeted therapy*, *5*(1), 181. https://doi.org/10.1038/s41392-020-00222-7

Yang, F., Yang, L., Wataya-Kaneda, M., Hasegawa, J., Yoshimori, T., Tanemura, A., Tsuruta, D., & Katayama, I. (2018). Dysregulation of autophagy in melanocytes contributes to hypopigmented macules in tuberous sclerosis complex. *Journal of dermatological science*, *89*(2), 155–164. https://doi.org/10.1016/j.jdermsci.2017.11.002

Yang, F., Yang, L., Wataya-Kaneda, M., Yoshimura, T., Tanemura, A., & Katayama, I. (2018). Uncoupling of ER/Mitochondrial Oxidative Stress in mTORC1 Hyperactivation-Associated Skin Hypopigmentation. *The Journal of investigative dermatology*, *138*(3), 669–678. https://doi.org/10.1016/j.jid.2017.10.007

Yapijakis, C., Pachis, N., Sotiriadou, T., Vaila, C., Michopoulou, V., & Vassiliou, S. (2023). Molecular Mechanisms Involved in Craniosynostosis. *In vivo (Athens, Greece)*, *37*(1), 36–46. https://doi.org/10.21873/invivo.13052

Ye, J., Coulouris, G., Zaretskaya, I., Cutcutache, I., Rozen, S., & Madden, T. L. (2012). Primer-BLAST: a tool to design target-specific primers for polymerase chain reaction. *BMC bioinformatics*, *13*, 134. https://doi.org/10.1186/1471-2105-13-134

Yeung, K. S., Tso, W. W. Y., Ip, J. J. K., Mak, C. C. Y., Leung, G. K. C., Tsang, M. H. Y., Ying, D., Pei, S. L. C., Lee, S. L., Yang, W., & Chung, B. H. (2017). Identification of mutations in the PI3K-AKT-mTOR signalling pathway in patients with macrocephaly and developmental delay and/or autism. *Molecular autism*, *8*, 66. https://doi.org/10.1186/s13229-017-0182-4

Yu, K., Herr, A. B., Waksman, G., & Ornitz, D. M. (2000). Loss of fibroblast growth factor receptor 2 ligand-binding specificity in Apert syndrome. *Proceedings of the National Academy of Sciences of the United States of America*, *97*(26), 14536–14541. https://doi.org/10.1073/pnas.97.26.14536

Yung, D., Freeman, K., & Mirzaa, G. (2022). Pulmonary Vein Stenosis Associated with Germline *PIK3CA* Mutation. *Children (Basel, Switzerland)*, *9*(5), 671. https://doi.org/10.3390/children9050671

Zhang, C., Fu, L., Fu, J., Hu, L., Yang, H., Rong, T. H., Li, Y., Liu, H., Fu, S. B., Zeng, Y. X., & Guan, X. Y. (2009). Fibroblast growth factor receptor 2-positive fibroblasts provide a suitable microenvironment for tumor development and progression in esophageal carcinoma. *Clinical cancer research: an official journal of the American Association for Cancer Research*, *15*(12), 4017–4027. https://doi.org/10.1158/1078-0432.CCR-08-2824

Zhao, L., & Vogt, P. K. (2008). Class I PI3K in oncogenic cellular transformation. *Oncogene*, *27*(41), 5486–5496. https://doi.org/10.1038/onc.2008.244

Zlotnikoff, M. (1945). A human mosaic: bilaterally asymmetrical noevus pigmentosus pilosus et mollusciformis unilateralis. *Journal of Heredity*, *36*(6), 163-168. https://doi.org/10.1093/oxfordjournals.jhered.a105487

Zollino, M., Ranieri, C., Grossi, V., Leoni, C., Lattante, S., Mazzà, D., Simone, C., & Resta, N. (2019). Germline pathogenic variant in PIK3CA leading to symmetrical overgrowth with marked macrocephaly and mild global developmental delay. *Molecular genetics & genomic medicine*, *7*(8), e845. https://doi.org/10.1002/mgg3.845

Zolotov, S., Xing, C., Mahamid, R., Shalata, A., Sheikh-Ahmad, M., & Garg, A. (2017). Homozygous LIPE mutation in siblings with multiple symmetric lipomatosis, partial lipodystrophy, and myopathy. *American journal of medical genetics. Part A*, *173*(1), 190–194. https://doi.org/10.1002/ajmg.a.37880

APPENDIX

ΔCT cutoff values - *therascreen* PIK3CA RGQ PCR Kit

Plasma specimens

Assay	Cutoff value (ΔC_T)
C420R	≤6.0
E542K	≤4.8
E545A	≤10.0
E545D	≤7.0
E545G	≤9.5
E545K	≤10.0
Q546E	≤10.0
Q546R	≤7.0
H1047L	≤10.0
H1047R	≤9.0
H1047Y	≤6.2

Tissue specimens

Assay	Cutoff value (ΔC_T)
C420R	≤6.0
E542K	≤4.8
E545A	≤10.0
E545D	≤7.5
E545G	≤9.5
E545K	≤6.5
H1047L	≤10.0
H1047R	≤7.0
H1047Y	≤6.2
Q546E	≤10.0
Q546R	≤7.0